Research Insights

Solar Concentrating Modules With Louvered Heliostats

Emerging Research and Opportunities

Dmitry Strebkov, Natalya Filippchenkova, and Anatoly Irodionov

IGI Global
PUBLISHER of TIMELY KNOWLEDGE

Solar Concentrating Modules With Louvered Heliostats:

Emerging Research and Opportunities

Dmitry Strebkov
Federal State Budget Scientific Institution, Russia & Federal Scientific Agroengineering Center VIM, Russia

Natalya Filippchenkova
Federal State Budget Scientific Institution, Russia & Federal Scientific Agroengineering Center VIM, Russia

Anatoly Irodionov
Federal State Budget Scientific Institution, Russia & Federal Scientific Agroengineering Center VIM, Russia

A volume in the Advances in Environmental Engineering and Green Technologies (AEEGT) Book Series

Published in the United States of America by
IGI Global
Engineering Science Reference (an imprint of IGI Global)
701 E. Chocolate Avenue
Hershey PA, USA 17033
Tel: 717-533-8845
Fax: 717-533-8661
E-mail: cust@igi-global.com
Web site: http://www.igi-global.com

Library of Congress Cataloging-in-Publication Data

Names: Strebkov, D. S. (Dmitriĭ Semënovich), 1937- author. | Filippchenkova, Natalya, 1992- author. | Irodionov, Anatoly, 1950- author.
Title: Solar concentrating modules with louvered heliostats : emerging research and opportunities / by Dmitry Strebkov, Natalya Filippchenkova, Anatoly Irodionov.
Description: Hershey, PA : Engineering Science Reference, an imprint of IGI Global, 2020. | Includes bibliographical references and index. | Summary: "This book explores current trends in the development of energy supply systems associated with the use of concentrated solar radiation"-- Provided by publisher.
Identifiers: LCCN 2020001945 (print) | LCCN 2020001946 (ebook) | ISBN 9781799842767 (hardcover) | ISBN 9781799853008 (paperback) | ISBN 9781799842774 (ebook)
Subjects: LCSH: Solar collectors--Equipment and supplies. | Heliostat.
Classification: LCC TJ812 .S77 2020 (print) | LCC TJ812 (ebook) | DDC 621.47/2--dc23
LC record available at https://lccn.loc.gov/2020001945
LC ebook record available at https://lccn.loc.gov/2020001946

This book is published in the IGI Global book series Advances in Environmental Engineering and Green Technologies (AEEGT) (ISSN: 2326-9162; eISSN: 2326-9170)

British Cataloguing in Publication Data
A Cataloguing in Publication record for this book is available from the British Library.

All work contributed to this book is new, previously-unpublished material.
The views expressed in this book are those of the authors, but not necessarily of the publisher.

For electronic access to this publication, please contact: eresources@igi-global.com.

Advances in Environmental Engineering and Green Technologies (AEEGT) Book Series

ISSN:2326-9162
EISSN:2326-9170

MISSION

Growing awareness and an increased focus on environmental issues such as climate change, energy use, and loss of non-renewable resources have brought about a greater need for research that provides potential solutions to these problems. Research in environmental science and engineering continues to play a vital role in uncovering new opportunities for a "green" future.

The **Advances in Environmental Engineering and Green Technologies (AEEGT)** book series is a mouthpiece for research in all aspects of environmental science, earth science, and green initiatives. This series supports the ongoing research in this field through publishing books that discuss topics within environmental engineering or that deal with the interdisciplinary field of green technologies.

COVERAGE

- Air Quality
- Alternative Power Sources
- Policies Involving Green Technologies and Environmental Engineering
- Cleantech
- Renewable Energy
- Water Supply and Treatment
- Green Transportation
- Radioactive Waste Treatment
- Waste Management
- Biofilters and Biofiltration

IGI Global is currently accepting manuscripts for publication within this series. To submit a proposal for a volume in this series, please contact our Acquisition Editors at Acquisitions@igi-global.com or visit: http://www.igi-global.com/publish/.

The Advances in Environmental Engineering and Green Technologies (AEEGT) Book Series (ISSN 2326-9162) is published by IGI Global, 701 E. Chocolate Avenue, Hershey, PA 17033-1240, USA, www.igi-global.com. This series is composed of titles available for purchase individually; each title is edited to be contextually exclusive from any other title within the series. For pricing and ordering information please visit http://www.igi-global.com/book-series/advances-environmental-engineering-green-technologies/73679. Postmaster: Send all address changes to above address.

Titles in this Series

For a list of additional titles in this series, please visit:
https://www.igi-global.com/book-series/advances-environmental-engineering-green-technologies/73679

Energy-Efficient Underwater Wireless Communications and Networking
Nitin Goyal (Chitkara University Institute of Engineering and Technology, Chitkara University, Punjab, India) Luxmi Sapra (Chitkara University Institute of Engineering and Technology, Chitkara University, Punjab, India) and Jasminder Kaur Sandhu (Chitkara University Institute of Engineering and Technology, Chitkara University, Punjab, India)
Engineering Science Reference • © 2021 • 339pp • H/C (ISBN: 9781799836407) • US $195.00

Impacts of Climate Change on Agriculture and Aquaculture
Ahmed Karmaoui (Southern Center for Culture and Sciences, Morocco) Kirby Barrick (University of Florida, USA) Michael Reed (University of Kentucky, USA) and Mirza Barjees Baig (King Saud University, Saudi Arabia)
Engineering Science Reference • © 2021 • 333pp • H/C (ISBN: 9781799833437) • US $195.00

Development Challenges and Strategies in Global Arid Regions
Umar Garba Benna (Benna Associates, Nigeria)
Engineering Science Reference • © 2021 • 300pp • H/C (ISBN: 9781799837930) • US $195.00

Molecular Plant Breeding and Genome Editing Tools for Crop Improvement
Pradip Chandra Deka (Sir Padampat Singhania University, India)
Engineering Science Reference • © 2021 • 489pp • H/C (ISBN: 9781799843122) • US $195.00

Recent Advancements in Bioremediation of Metal Contaminants
Satarupa Dey (Shyampur Siddheswari Mahavidyalaya, India) and Biswaranjan Acharya (School of Computer Engineering, KIIT University (Deemed), India)
Engineering Science Reference • © 2021 • 363pp • H/C (ISBN: 9781799848882) • US $195.00

701 East Chocolate Avenue, Hershey, PA 17033, USA
Tel: 717-533-8845 x100 • Fax: 717-533-8661
E-Mail: cust@igi-global.com • www.igi-global.com

Table of Contents

Preface

RELEVANCE OF THE TOPIC OF WORK

The development of solar energy is becoming increasingly widespread in many countries of the world. One of the main ways to reduce the cost of energy generated by solar modules, as well as reduce the need for centralized energy supply, is the use of non-tracking concentrator solar modules integrated into the building structure.

The theme of the work, chosen by the authors, lies in line with current trends in the development of energy supply systems associated with the use of concentrated solar radiation. In this regard, work aimed at increasing productivity and extending the time interval of non-tracking solar concentrator modules by installing a system of louvered heliostats on the input surface of the concentrator is of interest and is relevant.

In the introduction the authors substantiate the relevance of the research direction.

The first chapter analyzes the current state and prospects of using concentrated solar radiation in solar power plants with various types of photodetectors, the development of BIPV technologies in the framework of the Smart City concept.

The second chapter shows that the use of a louvered heliostat with a constant lamella pitch and a relatively simple control algorithm is equivalent to increasing the angular aperture of the concentrator without decreasing the concentration coefficient. An algorithm for controlling a louvered heliostat has been developed to prevent blocking and shading effects that reduce the optical efficiency of the heliostat. Based on the consideration of an practically important three-dimensional problem, an algorithm for calculating the solar radiation flux on the receiving surface of a non-tracking parabolic cylindrical concentrator with louvered heliostats has been developed.

The functional dependences of the minimum necessary relative steps of the lamellas are obtained to prevent blocking and shading that relate the position of the Sun and the angle of inclination of the mirror lamellas. An analytical form of the dependence connecting the height of the Sun and the angle of inclination of the mirror lamellas is presented.

The third chapter shows the developed and patented designs of solar modules with non-tracking concentrators and louvered heliostats that have zero blocking and shading losses. The design of a compact PVT receiver for a non-tracking parabolic cylindrical solar concentrator has been developed and patented, providing a thermal efficiency of the module at the level of 60..70% with a service life of at least 25 years. Thermal calculations of solar concentrator modules with photoelectric, thermal and PVT receivers are carried out.

The fourth chapter presents the results of an experimental study of concentrator solar modules with a louvered heliostat.

The presented experimental data array was obtained using an automatic registration system for the main parameters, which allows obtaining information on the short circuit current, open circuit voltage of the solar concentrator module, insolation (total and direct), ambient temperature, and the temperature at the input and output of the module (temperature sensors).

An analysis of the electrical and thermal parameters of the PVT receiver of the concentrator solar module is carried out. The thermal efficiency of the PVT receiver is in the range of 60 ... 70%. With equal values of insolation and ambient temperature, electricity production by the PVT panel's photoelectric panel is on average 10-25% higher than that of a PV receiver. The conducted experiment confirms the developed algorithm for calculating the passage of sunlight on the mirror surface of the lamellas and parabolic cylinder, which allows to calculate the flux of solar radiation on the receiving surface of the solar concentrator (relative error of not more than 5%).

In the fifth chapter, a feasibility study is carried out and the main areas of application of non-tracking solar concentrator modules with louvered heliostats are determined. Calculations confirm the high efficiency of using louvered heliostats. The maximum annual energy production of non-tracking solar concentrator modules is achieved with the vertical orientation of the concentrator, which is very important when placing solar modules on the southern facades of buildings. The annual amount of insolation at the receiver for concentrators with a louvered heliostat with an angular aperture of 26 ° and 18 °, respectively, is on average 2 and 3.4 times higher than the total insolation on a flat surface and 1.6 and 2.2 times higher than the insolation

on the receiving surface of the concentrator modules without shutters with similar angular aperture values. The use of non-tracking concentrator modules with a louvered heliostat allows to reduce the cost of electricity produced in comparison with concentrator modules without blinds by 40-60%, thermal energy - by 50%.

In the sixth chapter are identified the basic requirements for solar power plants with concentrators integrated into buildings. The designs of a solar house containing solar concentrator modules have been developed. The result of the development of solar house designs is an increase in the efficiency of using solar energy and a reduction in the cost of electricity and heat, as well as the creation of efficient solar systems built into the facades and roofs of buildings to provide them with electricity and heat. The design of a roofing solar panel with high optical efficiency and low consumption of semiconductor material and low cost has been developed and patented. As a result of using a roofing solar panel, the efficiency of using solar energy is increased and the cost of generating electric energy and heat is reduced. With the cost of semi-parabolic cylindrical reflectors 4, 5 30 $/m^2$, a concentration of 4.92, an optical efficiency of 0.8 and an electrical efficiency of 15%, the cost of a roofing solar panel will be $ 12, or $ 1/W, at an existing cost of $ 3 / W, those it will decrease by 2.5 times, while the costs of the composite hub and receiver will be approximately equal and amount to 50% of the cost of the roofing solar panel.

The integrated concentrated PVT system of the building, designed for applying a solar-grid shading system to the blinds, is considered. In this way, the concentrator takes advantage of tracking the shading of the blinds at a sunny height and thus increases the optical efficiency. The optical efficiency for DIW is 73.5% and for IPA 76.5%. The refractive system shows potential to be cost-effective due to the use of standard silicon solar cells and low-accuracy trackers to partially cover electricity and heat energy demands of buildings. As reflectors can fulfill a building function the cost of the concentrator could be split and then the part corresponding to the concentrating system itself would be diminished.

The most promising areas in the field of integration of solar modules (planar and concentrating) in the construction of buildings are: development of BIPV technologies (roofing, film, facade materials); the integration of solar energy concentrators that do not require biaxial tracking (medium and low concentrations) on the facades and roofs of buildings (parabolic concentrators, lenses and Fresnel mirrors); integration of highly concentrated modules on the roofs of buildings.

The seventh chapter presents, developed in VIESH, a solar roofing panel (solar shingles), which combines the functions of a roof and a solar module.

Unlike foreign samples, built-in stationary solar concentrators are used in the solar shingles, which made it possible to reduce the area of silicon solar cells by 4 times and receive electric energy and hot water from the solar roof. The solar tile has a protective anti-vandal coating of tempered glass and a cable for connecting to the adjacent solar tile.

The life of the SPP is determined mainly by the durability of the solar modules, which depends on the technology and materials used to seal the solar modules. Sealing standard modules by laminating an ethylene vinyl acetate (EVA) film provides an SPP service life of 25 years in cold climates and 20 years in tropical climates. Sealing the modules with polysiloxane gel extends the service life of the SPP to 40-50 years.

More energy is produced by tracking the solar panel to remain aligned to the sun at a right angle to the rays of light. Now-a-days various artificial techniques are introduced into photovoltaic (PV) system for utilisation of renewable energy. It is essential to track the generated power of the PV system and utilise the collected solar energy optimally. Artificial Neural Network (ANN) is initially used to forecast the solar insolation level and followed by the Particle Swarm Optimisation to optimise the power generation of the PV system based on the solar insolation level, cell temperature, efficiency of PV panel and output voltage requirements.

Genetic Algorithm is a general purpose optimization algorithm that is distinguished from conventional optimization techniques by the use of concepts of population genetics to guide the optimization search. Tabu Search Algorithms is a conceptually simple and an elegant iterative technique for finding good solutions to optimization problems. Simulated Annealing Algorithms appeared as a promising heuristic algorithm for handling the combinatorial optimization problems. Fuzzy logic Algorithms set theory can be considered as a generation of the classical set theory.

The ANN based solar insolation forecast has shown satisfactory results with minimal error and the generated PV power can be optimised significantly with the aids of the PSO algorithm.

In the eighth chapter are considered the prospects of using artificial intelligence algorithms in solar energy, projects of regional, global solar energy systems.

Artificial intelligence algorithms make it possible to effectively determine the cause and types of damage and emergency situations, adapt to a specific type of electrical equipment.

Artificial intelligence algorithms are a powerful tool for recognizing and predicting signals, and their ability to learn makes it possible to develop adaptive systems for protecting and diagnosing electrical equipment in solar energy.

The basic requirements for solar power plants connected to the Unified Energy System of Russia are considered. Artificial intelligence algorithms can find wide application in the field of dispatching solar power systems. The "new" infrastructure and ideology of solar energy of the 21st century are called upon to be "intelligent" energy-information networks built as multi-agent systems based on artificial intelligence algorithms.

THE SIGNIFICANCE OF THE RESEARCH RESULTS OBTAINED IN THE WORK

The research results presented in the work can be used in the development of technological schemes and designs of photovoltaic, thermal and cogeneration power plants with solar energy concentrators.

The scientific and practical significance of the work consists in the formation of a scientifically based approach to the development of non-tracking solar modules with a system of linear louvered heliostats and the selection of the operating mode of the developed modules depending on various requirements of the consumer of thermal or electric energy; the proposed design of solar concentrator modules with louvered heliostats with increased duration of work installed on the facades of buildings can solve the problem of the lack of space for placing solar energy facilities in the city, as well as provide heat and electricity to consumers in the residential and public sectors, as well as agricultural enterprises.

Materials of work can be used in organizations and departments related to the design, construction and operation of solar power plants.

The validity of scientific provisions, conclusions and recommendations given in the work are confirmed by the correctness of the goals and objectives, using statistical methods of data processing. The results and conclusions are characterized by internal unity, are in a logical relationship.

The reliability of the results is confirmed by the high convergence of the theoretically calculated data and the data obtained as a result of experimental studies.

The personal contribution of the authors lies in the development of optical schemes and designs of various types of solar modules with louvered heliostats and concentrators having zero loss due to shading and blocking of solar radiation; development of an algorithm for controlling a louvered heliostat, which excludes blocking and shading of sunlight by adjacent lamellas; development of an algorithm for calculating the flux of solar radiation on the receiving surface of a non-tracking parabolic-cylindrical concentrator with a louvered heliostat; development of a design, manufacture of a prototype and an experimental study of a non-tracking solar concentrator module with louvered heliostats; development of a system for automatic measurement of key parameters; a feasibility study on the use of non-tracking solar concentrator modules with louvered heliostats.

Introduction

The development of environmentally friendly renewable energy sources (RES) is a strategic task that determines the prospects for sustainable and energy-independent development of many countries in the context of the gradual depletion of cheap reserves of fossil fuels and the threat of increasing anthropogenic pollution. Many renewable energy technologies have already reached the level of competitiveness with existing energy sources and are gradually entering the market, including the Russian one.

The use of concentrating systems is one of the main ways to reduce the cost of energy produced by solar modules. Since in many areas with centralized energy supply there is an acute issue of energy efficiency of urban development, the use of concentrator solar modules that are integrated into buildings will reduce the need for centralized electricity and heat supply. The integrability of traditional concentrating modules into the roofs and facades of buildings is significantly hampered, since their work requires constant orientation to the Sun. Non-tracking concentrators are of greater interest for integration, since their relatively large angular aperture allows operation without tracking the sun. However, the duration of their work in the summer period is reduced to 2-4 hours per day, in other periods of the year the sun's rays may not fall at all within the angular aperture of the concentrator. It is possible to extend the time interval during which the sun rays arriving at the input surface of the concentrator reach the radiation receiver using a louvered heliostat concentrator located on the entrance surface. The device is a parallel rows of synchronously working narrow mirror strips - lamellae. The lamellaes of the louvered heliostat are installed at such an angle to the entrance surface so that the sun rays, as a result of daily or annual sun movement beyond the angular aperture, after reflection from the mirror lamellae again fall within the aperture of the solar concentrator.

Thus, the use of louvered heliostats can significantly increase the efficiency of non- tracking solar concentrators, including modules installed on the facades of administrative and residential buildings, which is especially important in the southern regions with a large proportion of direct solar radiation.

The book outlines the basics of using solar concentrating modules with louvered heliostats. The analysis of the current state and prospects for the use of concentrated solar radiation in solar power plants with various types of photodetectors has been carried out. The control algorithm of a linear louvered heliostat is considered to increase the efficiency of a non-tracking parabolic cylindrical concentrator; the algorithm for calculating the solar radiation flux on the receiving surface of a non-tracking parabolic-cylinder concentrator with a louvered heliostat is considered. Also considered are various designs, the results of an experimental study of non-tracking solar concentrating modules with a louvered heliostat. Prospective areas of application are considered and a feasibility study on the use of non-tracking solar concentrating modules with louvered heliostats is given.

The materials presented in the book are intended for scientists, engineers, graduate students and students of the specialties Unconventional and Renewable Energy Sources and Electric Power Industry, as well as other areas related to one way or another to solving the problems of energy saving environment.

The materials of the book can be used in organizations and departments related to the design, construction and operation of solar power plants.

Section 1

Chapter 1
The Overview of Basic Types and Characteristics of Solar Concentrating Modules With Louvered Heliostats

ABSTRACT

The principles of construction and operation of the main concentrating systems, including non-followable modules, are reviewed, and the work of the concentrators is analyzed. An analytical review of modern facade-integrated photovoltaic technologies was carried out, and their classification was given. The known methods for calculating a flat (two-dimensional) scheme for passing the sun's rays through a louvered heliostat make it impossible to assess the real effectiveness of using louvered heliostats with non-tracking solar concentrators, which makes it necessary to consider the practically important three-dimensional problem of calculating the solar radiation flux on the receiving surface of an unfollowing parabolic-cylindrical solar concentrator with louver heliostat.

INTRODUCTION

Currently, solar photovoltaic modules based on planar solar cells are widely used in the world. Along with photovoltaic systems, thermal solar collectors of flat and tubular vacuum structures have become widespread. Guided by the

DOI: 10.4018/978-1-7998-4276-7.ch001

possibility of combining, cheapening and optimizing these systems, research is being conducted all over the world to combine these two systems into one hybrid system, preserving the positive sides of each of them and fighting the negative ones. Research in this area is mainly aimed at improving the design, optimization of the gap gaps between solar cells and glazing, as well as between the back side of the absorber (radiator of solar cells) and module insulation. Much attention is paid to the thickness of all components, the layout of the systems (natural, forced circulation; single, double heating circuit), module durability and service life and, accordingly, the payback period.

The use of solar concentrators allows to increase the temperature of the coolant in the case of thermal energy conversion. With photoelectric conversion, concentrators allow increasing the flux density of solar radiation at the receiving surface and reducing the area of solar cells used. Concentrating systems operating at medium and high concentrations should have a tracking system, this leads to an increase in the cost of the whole structure, complication of operation and reduction of reliability. The use of non-tracking concentrators with systems of secondary reflectors in the form of louvered heliostats allows to improve the technical and economic indicators of the solar concentrating module.

PHOTOVOLTAIC MODULES

The efficiency of modern solar cells (SC) of silicon is 14–22%. Theoretical studies have shown that by using energy levels in the forbidden zone, it is possible to expand the range of spectral sensitivity and increase the efficiency to 44% for silicon (Arbuzov, Evdokimov, 2007; Poulek, Libra, Strebkov et al., 2013). For solar radiation, the efficiency of solar cells from silicon in the laboratory reaches 25%; in industrial conditions, 16–20%. For cascade heterostructures based on gallium arsenide, the maximum efficiency achieved in the laboratory is 42%, in industry 36%, in the composition of concentrating modules 23.5–26% (Strebkov, Pendzhiev, Mamedsakhatov, 2012).

Solar modules based on gallium arsenide GaAs have high efficiency (for single junction solar cells about 28% (Green, Emery, Hishikawa et al., 2012), increased ability to absorb solar radiation (SR), stability of characteristics at high operating temperatures and a number of other important features. Among thin-film solar cells, a high absorptivity of SR has a solar cell based on copper indium diselenide ($CuInSe_2$) - up to 99% of light is absorbed in the first micron of this material, the band gap of this semiconductor is 1.0 eV

(Gremenok, Tivanov, Zalessky, 2007). Solar modules are made for voltages of 12, 24, 36 V and higher voltage, they are not afraid of short circuits, but are very sensitive to shading a part of the surface. With a series connection, the current of the module is determined by the current of the least illuminated SC. When combining a solar cell into a module having *n* parallel rows, each of which is connected in series with *m* elements, the output voltage and current of the system will be respectively $V_{\text{out}} = V_0 \cdot m$, $I_{\text{out}} = I_0 \cdot n$.

THERMAL SOLAR MODULES

The main structural element of a thermal solar installation is a solar collector, in which solar energy is converted into heat and heat water, air or some other coolant. The basis of the flat collector is a light-absorbing surface, which must have reliable contact with a number of pipes or channels for the movement of the heated coolant. The combination of a flat radiation-absorbing surface and pipes forms a single structural element - the absorber. For better absorption of solar energy, the upper part of the absorber should have a special absorbing selective coating. Reducing heat loss from the absorber into the surrounding space is achieved through the use of thermal insulation, which covers the lower surface of the absorber, and translucent insulation placed above the absorber at a certain distance from it. All of these elements are placed in the housing, and sealing of the transparent insulation - glazing (Dufflie, Beckman, 1991) is performed. Among the principal advantages of a flat collector compared to other types of collectors is its ability to capture both direct and diffuse solar radiation. This allows you to install a collector stationary without the need for tracking the sun.

In solar collectors with concentrators, optical systems (mirrors or lenses) are used to increase the flux density of solar radiation on the surface, which absorbs energy, it is possible to achieve higher temperatures than in flat collectors. In general, focusing devices effectively concentrate only direct radiation. However, systems operating at low degrees of concentration may also focus on the receiver and some of the scattered radiation. Therefore, for focusing systems, the orientation of the concentrator and receiver, which requires tracking the Sun, is of great importance.

COMBINED PHOTOVOLTAIC THERMAL MODULES

The efficiency of a solar photovoltaic system depends on the material of the solar cell and its design. The main reasons for the decrease in the efficiency of photovoltaic converters are the deposition of dust on their surface and the heating of the material under the influence of radiation in the daytime. As a result, increasing the temperature reduces the amount of electricity generated. For example, increasing the temperature of silicon solar modules by 1 ° C reduces the efficiency of the module by 0,4 ... 0,5% (Hybrid solar collectors PVT, 2017). The search for ways to overcome the above negative factors led to the integration of photoelectric converters with flat solar collectors and the creation on their basis of a new type of installation, the so-called cogeneration photoelectric thermal modules (PVT). In Zakharchenko et al., (2004), a PVT module with a tubular-sheet heat exchanger is considered in detail.

The main disadvantage of this type of PVT module is the low efficiency of converting solar energy into heat due to the ineffective thermal contact of the heat exchanger channels with solar elements and large heat losses. The main disadvantage of the PVT system presented in (Bergene, Lovvik, 1995). The disadvantage is the short lifetime of the module using ethylene vinyl acetate as a filler (Florschuetz, 1979). It should also be noted the large heat loss due to ineffective facial insulation from the external environment. The main task of optimizing the design presented in (Sandnes, Rekstad, 2002) is to optimize the size of the gaps with a thermally conductive layer and coolant.

By improving the design of the thermal photovoltaic module (Ibrahim, Jin, Daghigh et al., 2009), where the absorber is made in the form of a rectangle in cross section, it is possible to manufacture an absorber in the form of a V-shaped triangle, which is shown in (Othman, Ruslan, Sopian et al., 2009). Due to this design change, heat losses are reduced, and it is also possible to manufacture a thermal photovoltaic module with both air and liquid heat transfer media.

Using all the positive aspects of the structures mentioned above, it is possible to increase the overall efficiency of the PVT module, however, in cases where the coolant temperature is insufficient for any reason, it is advisable to use concentrator parabolic systems of low concentration (Alfegi, Sopian, Othman et al., 2007; Strebkov, Mayorov, Panchenko, 2013).

The work (Sevela, Olesen, 2013) presents the development and research of the heating, ventilation and air conditioning system for an individual dwelling house. The authors of the project used a hybrid solar collector as the main

solar energy converter. According to the results of an experimental study, the efficiency of obtaining thermal energy was 42% (Sevela, Olesen, 2013).

In Tikhonov (2014), the methodology for calculating the energy balance distribution of a photoelectric thermal module is considered in detail. The disadvantages of the known installations are also low efficiency, high consumption of materials, so the issue of increasing the efficiency of solar energy conversion in the PVT-module and, consequently, reducing the unit cost of generating electricity and heat is relevant. You should also reduce the cost, simplify and optimize the very design of thermal photovoltaic modules, which will reduce the payback period.

SOLAR CONCENTRATING SYSTEMS

Concentration systems by the method of collecting radiant energy can be divided into:

- refracting (lenses and prism concentrators);
- reflecting, i.e. mirrors with generators of various shapes;
- concentrators using holograms, which are obtained by registering in the layer of photosensitive material an interference pattern from two coherent radiation beams;
- luminescent solar concentrators, which are a translucent plate of luminescent material. The luminous flux, falling into the plane of the plate, is reemitted due to the luminescence of the dye to the side face, which is the focal surface.

According to the degree of concentration can be divided into three groups:

- Strongly concentrating - concentration of more than 100 times (parabolic concentrators, lenses, Fresnel lenses)
- average concentration from 10 to 100 times (highly concentrating high degree of defocusing, as well as some prismatic and cylindrical concentrators)
- slightly concentrating - less than 10 times (quasi-stationary and stationary, luminescent and holographic concentrators).

Refractive Concentrating Systems

Refractive concentrators include (Strebkov & Tver'yanovich, 2007):

1. Concentric Fresnel lenses made in the form of concentric refractive elements with straight / curved lines forming working surfaces;
2. Linear (cylindrical) Fresnel lenses with refractive elements in the form of triangular prisms;
3. Dispersion Fresnel lenses;
4. Holographic concentrators.

In (Andreev, Davidyuk, Ionova et al., 2010), a solar concentrating module with three-stage nanohetero-structured photoelectric receivers (FEP) was considered, as well as the conditions for effective concentration of radiation by Fresnel lenses and heat removal from the FEP. Measured under natural conditions, the efficiency of a concentrating module with an entrance aperture of 0.5 x 0.5 m was 24.3%, which is twice as high as the efficiency of planar modules based on silicon. In the test modules of a smaller size, with the introduction of a correction for the standard temperature (25 ° C), the FEP temperature and the efficiency value reached 26.5%. In the module design in question, circular Fresnel lenses with conic microprisms of constant width are used. The focal spot increases by this value. The profile pitch was chosen to be 0.25 mm based on the limitations imposed by the technology of manufacturing precision matrices for Fresnel lenses. In this case, the size of the focal spot increases mainly due to chromatic aberration.

The advantages of Fresnel lenses include high structural quality, ease of installation in supporting structures with a high degree of filling of the occupied area, the required accuracy of tracking systems for the Sun may be lower than for mirror concentrators, which greatly simplifies the design and increases the reliability of the solar module with a tracking concentrator . Along with the advantages of concentrating systems based on Fresnel lenses have a number of features. First of all, this is the presence of chromatic aberrations (Summer, 1961). The disadvantages of Fresnel lenses include Fresnel reflection losses, which exceed the losses on glass reflectors, limiting the opening angle to 45 °, associated with increased energy losses due to the mutual shading of the refractive scratches, while the total losses from shading and Fresnel reflection can be about 15% (Lidorenko, Zhukov, Nabiullin et al., 1977; Lidorenko, Evdokimov, Strebkov, 1988).

One of the promising areas of development of concentrating systems is the use of holographic concentrators. For use with photoelectric receivers, a holographic device must have high efficiency (at least 90%) and ensure the decomposition of radiation in a fairly wide range of operating frequencies at which photoelectric energy conversion is possible. The ratio of the limiting frequencies of solar radiation corresponding to the energy-significant range for photoelectric conversion is about 2: 1. In the known experimental samples of holographic photoelectric converters, an efficiency of about 30% has now been achieved (two-dimensional holograms), and for three-dimensional holograms - 93 ... 97% (Uvarov, Zhabo, Rogankov, 1984).

Prismatic Concentrating Systems

Prismatic concentrators (Strebkov, Filippchenkova, 2014; Mills, Guitranich, 1978) represent in cross section a prism having a front receiving face, a rear face with a reflective coating located at an angle α to the front face, and the surface of the exit of concentrated radiation. The concentrator works as follows: the radiation hits the front face at an angle i, refracts, reflects from the back face and comes to the front face at an angle $r_3 > r_m$, where r_m is the angle of total internal reflection for the prism material with refractive index n (Tver'yanovich, 1981).

The main disadvantages of prismatic concentrators are large light losses in the transparent material of prisms, high consumption of transparent material (glass or organic glass), relatively high weight characteristics, low specific power of the solar cells.

Reflecting Concentrating Systems

Reflecting concentrators include focons, foclines, cylindrical, parabolic-cylindrical, paraboloid, hyperboloid, louvered heliostats, Cassegrain, Newton systems, etc. (Figure 1)

In (Edmonds, 2017), a solar photovoltaic module with a semi-cylindrical solar energy concentrator was considered, containing two-sided solar elements in the form of strips perpendicular to the module base, connected and installed between two glass sheets. The actual concentration factor, taking into account the optical efficiency of reflection is 1.56. The disadvantage of this type of photovoltaic module is the low coefficient of concentration and the high cost of the module.

Figure 1. Solar module with a parabolic concentrator and a solar power station based on it

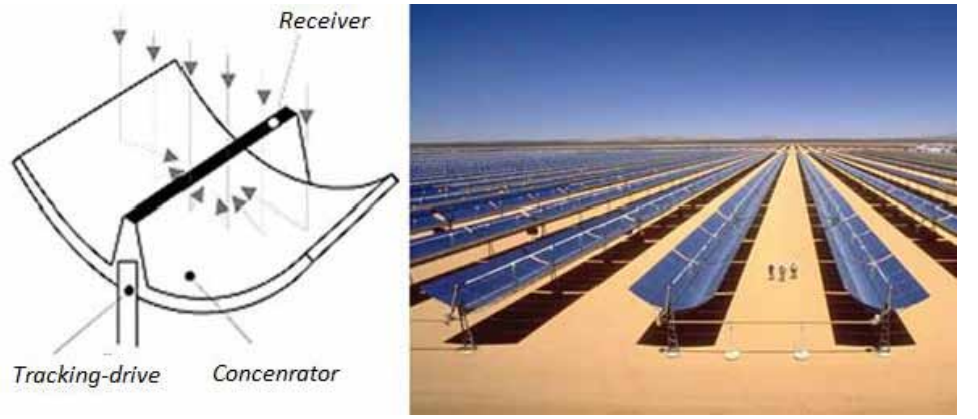

The solar module with a solar energy concentrator, considered in (Strebkov, Tver'yanovich, Irodionov et al., 2001), contains a flat protective transparent enclosure, the normal to the surface of which is in the meridional plane, and a radiation receiver in the form of a strip mounted on a protective transparent enclosure in the focus of the linearly focusing cylindrical concentrator (Figure 2). To ensure the continuous operation of the solar module during the year, an additional protective transparent barrier was installed parallel to the protective transparent fencing parallel to it, and remotely controlled horizontal jalousies with facets were installed in the gap between the two fences, which had a mirror coating on both sides, and the width the facet is 3-4 times longer than the distance between the facets.

The disadvantages of the considered solar module are large cosine radiation losses associated with the deviation of the plane of symmetry of a parabolic-cylinder reflector from the normal to the working surface of the module, and optical transmission losses in horizontal louvers with facets. Also at stationary installation the module does not work at high azimuth angles in the morning and evening hours. To use solar radiation in the morning and evening hours, you must use a tracking system. When installing the tracking system, the concentrator starts to work when the Sun deviates by 30 ° from the East-West axis, which corresponds to 8 hours of work per day.

In (Sodnomov, Strebkov, Tyukhov et al., 2005), a solar module with a concentrator containing a mirror reflector in the form of a main branch of a parabolic-cylinder concentrator with a second semi-cylindrical mirror reflector, a receiver with a two-sided working surface in the focal plane of said

Figure 2. General view of the solar module with a concentrator
**1 – protective transparent fencing; 2 – cylindrical reflector; 3 – parabolic cylindrical reflector; 4 – circular cylindrical reflector; 5 – the plane of symmetry; 6 – focal axis; 7 – radiation receiver; 8 – battery tank; 9 – double-glazed window; 10 – solar cells; 11 – horizontal surface*

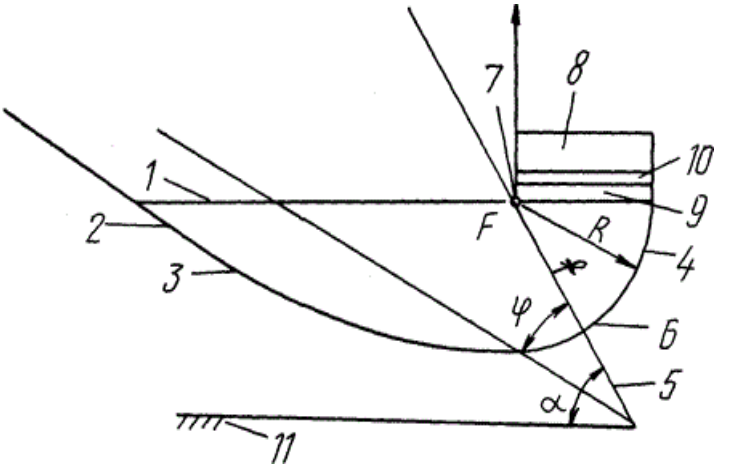

concentrator (Figure 3) was considered. The mirror reflector, the circulation circuit, the hot water storage tank are the bearing body, since made in the form of a one-volume construction of metal or polymer material, and one of the sides of the tank is a receiving element, which allows to increase the range of working angles of the concentrator.

The disadvantages of the developed solar module are low efficiency, high consumption of materials, low efficiency of conversion of solar energy into heat due to insufficient thermal contact of solar cells with heat exchanger channels in the cogeneration module.

Concentrating Systems Based on Louver Heliostats

It is possible to extend the time interval during which the sun rays entering the input surface of the concentrator reach the radiation receiver using the louvered heliostat concentrator (Kivalov, Zakhidov, 2001; Strebkov, Tver'yanovich, Tyukhov et al., 2002; Evdokimov, Kivalov, Strebkov et al., 2001) located on the input surface of the concentrator.

The use of louver heliostats is considered in the works of D.I. Teplyakov and E.V. Tveryanovich (Teplyakov, Tver'yanovich, 1993) and later monograph D.S. Strebkov and E.V. Tveryanovich (Strebkov, Tver'yanovich, 2007). In the above works, the features of this type of heliostats were investigated, including

Figure 3. General view of the solar module with a concentrator
**1 – focusing mirror reflector, 2 – protective glass coating; 3 – receiver of solar radiation; 4 – adjustable mounting brackets for the receiver of solar radiation; 5 – electric circuit of photoelectric converters of a solar radiation receiver; 6 – circulation circuit; 7 – crane; 8 – battery tank; 9 – a jellied mouth with a cover*

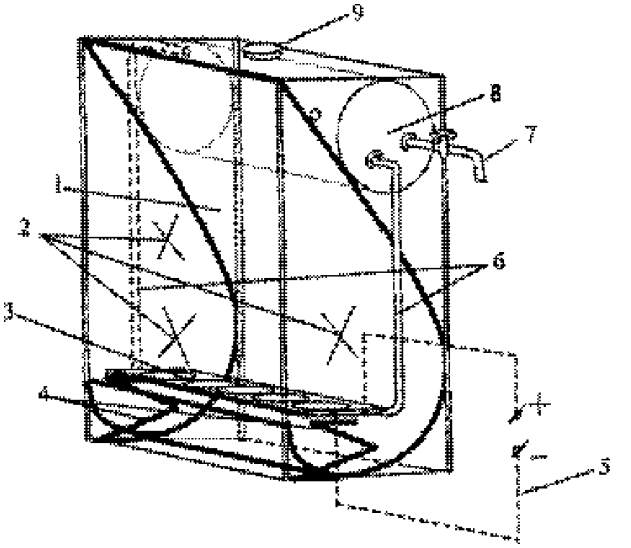

effects that affect the optical efficiency of the system, and the energy losses during characteristic days of different periods of the year were calculated. Considered a bounded flat (two-dimensional) scheme for the passage of sunlight through a louvered heliostat, as it was supposed to track the sun in azimuth – the sun rays are always in a plane perpendicular to the lamellae.

In (Bezrukikh, Strebkov, Tveryanovich et al., 1999), a solar module containing an energy concentrator having a working surface on which solar radiation is incident was considered, miniature mirror screens made in the form of louvres made of flat mirror facets were installed on the working surface of the prism; in the form of two symmetrically arranged prisms having a common solar cells, and a miniat is installed on the working surface of the concentrator in the zone of one or both prisms mirror screens (Figure 4).

The disadvantage of the photovoltaic module are low power density of the photovoltaic converter. In (Strebkov, Bazarova, Tarasov, 2007; Bazarova, 2008) a solar module was considered, containing a non-tracking parabolic-cylindrical solar energy concentrator with a receiver installed in the focal plane, on the input surface of the mid-section of the concentrator on a common frame along the East-West axis, a system of angular heliostats made in the form

Figure 4. Solar photovoltaic module with a composite concentrator in the form of a prism installed on the working surface of the jalousies from the flat mirror facets

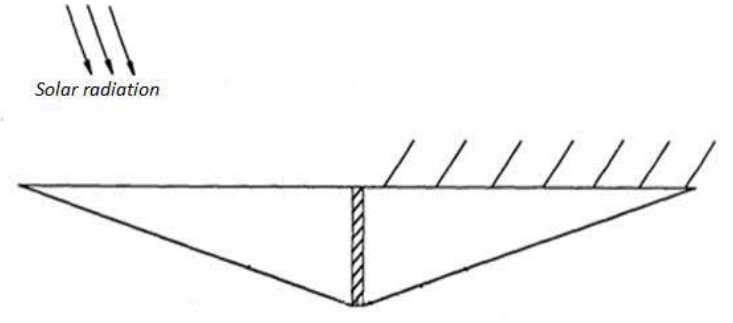

of flat curtains mirror facets, the planes of which are at an angle of 120° to each other and set at an angle of $\mu=114-\varphi+\delta$ to the plane of the mid-section, where φ is the geographical latitude of the location of the concentrator, δ is the declination of the sun's rays (Figure 5).

Figure 5. A general view of a non-tracking power plant with a concentrator and a radiation receiver in the form of a strip and a system of angular louvered heliostats
**1 –parabolic cylindrical concentrator; 2 – asymmetrical cylindrical reflector; 3 – circular cylindrical reflector; 4 – the plane of symmetry; 5 – focal axis; 6 – radiation receiver; 7 – entrance surface; 8 – total frame; 9 – system of angular heliostats; 10 – jalousies; 11 – mirror plate jalousies*

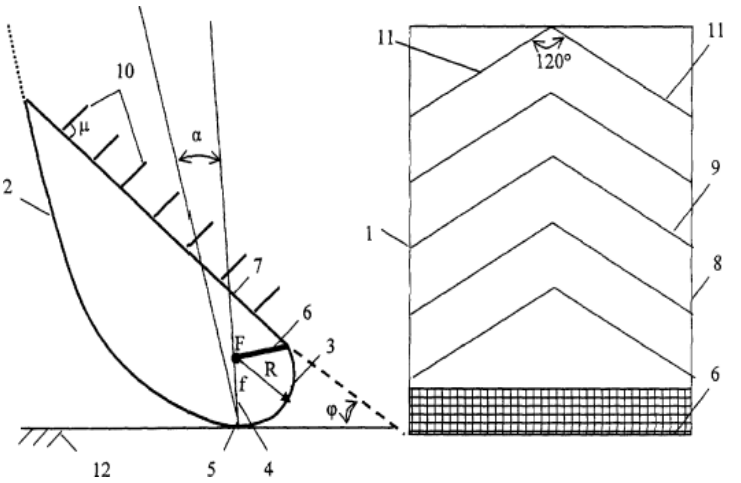

The disadvantages of the developed solar module are shading of the light-receiving surfaces, reducing the duration of the concentrator to 2-4 hours per day in the summer.

ANALYSIS OF SOLAR CONCENTRATORS

An important value for comparing solar concentrating modules of various geometric shapes is the concentration coefficient *k*, which is defined as the ratio of the midship area of the concentrator to the total spot area in the focal plane. For paraboloid (Strebkov, Irodionov, Filippchenkova, 2015):

$$k = \left(\frac{\sin 2\Theta_m}{\alpha} \right)^2 \tag{1.1}$$

where α – angle of the sun, α = 0,0093 rad.; Θ_m – opening angle equal to the angle between the optical axis of the paraboloid and the reflected beam (Figure 6).

Figure 6. Composite parabolic concentrator and opening angle

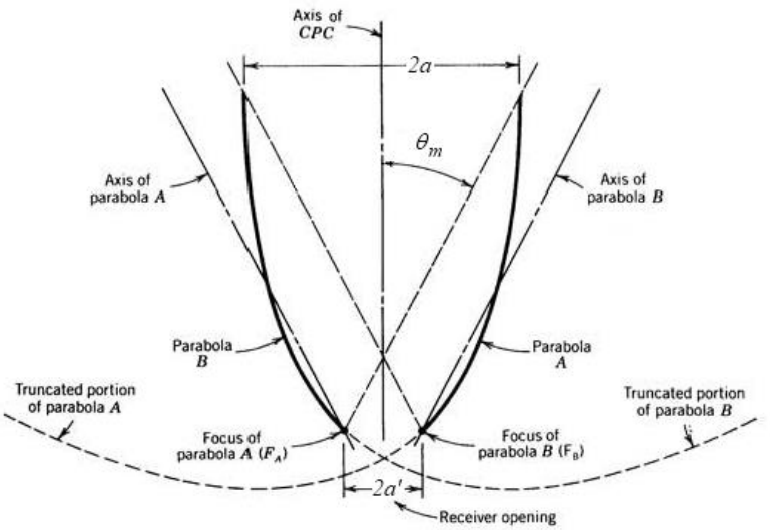

The expression for the degree of concentration k of the simplified Fresnel mirror as a function of the opening angle Θ_m and the number of rings m has the form:

$$k = \frac{\sin^2 2\Theta_m}{\left[\alpha + \frac{\sin 2\Theta_m}{2m}\right]^2} \tag{1.2}$$

The main disadvantage of the Fresnel mirror is the incomplete use of the area due to the presence of non-operating zones.

Figure 7 shows the optical layout of a solar module with Fresnel mirrors.

Figure 7. Diagram of a solar photovoltaic system with Fresnel mirrors

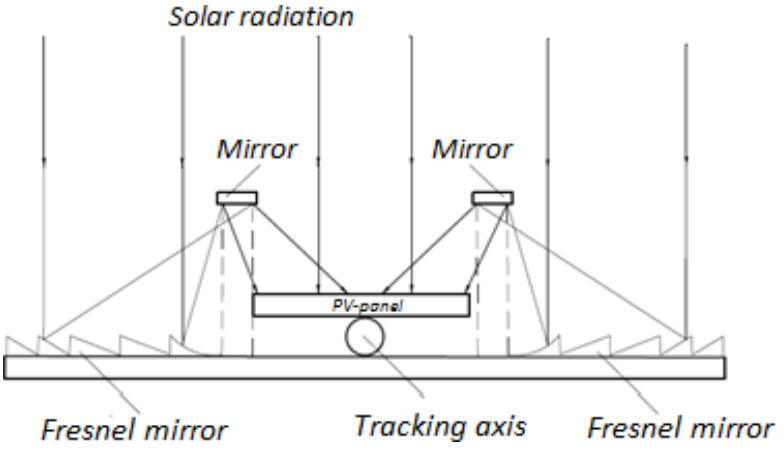

If a concentrator with a flat or hollow receiver located in the focal plane is considered, then the concentration coefficient:

$$k = \frac{\sin 2\Theta_m}{\left\{\frac{\alpha\left(\cos\Theta_m - \frac{1}{2}\right)}{2\cos^2(2\Theta_m)} + tg2\Theta_m\left(\frac{\sin\Theta_m}{\sin 2\Theta_m} - \frac{1}{2}\right)\right\}^2} \tag{1.3}$$

Concentration coefficient for a parabolic cylinder is:

$$k = \frac{\sin\left(2\Theta_m\right)}{\alpha} \tag{1.4}$$

For a circular cylinder, the concentration coefficient is equal to the square root of the expression for the concentration of the hemisphere:

$$k = \frac{\sin\Theta_m}{\dfrac{\alpha\left(\cos\Theta_m - \dfrac{1}{2}\right)}{2\cos^2(2\Theta_m)} + tg2\Theta_m\left(\dfrac{\sin\Theta_m}{\sin 2\Theta_m} - \dfrac{1}{2}\right)} \tag{1.5}$$

Figure 8 presents a general view of the solar module with a concentrator, where the main mirror reflector is made as one branch of a parabolic-cylinder concentrator with an aperture angle of 36° and two cylindrical mirror reflectors with radii *R* and *d*, and the edges of the radiation receiver band coincide with the optical axis and the third branch mirror reflector.

Figure 8. Solar module with an asymmetric concentrator with an aperture angle of 36° and a vertical receiver

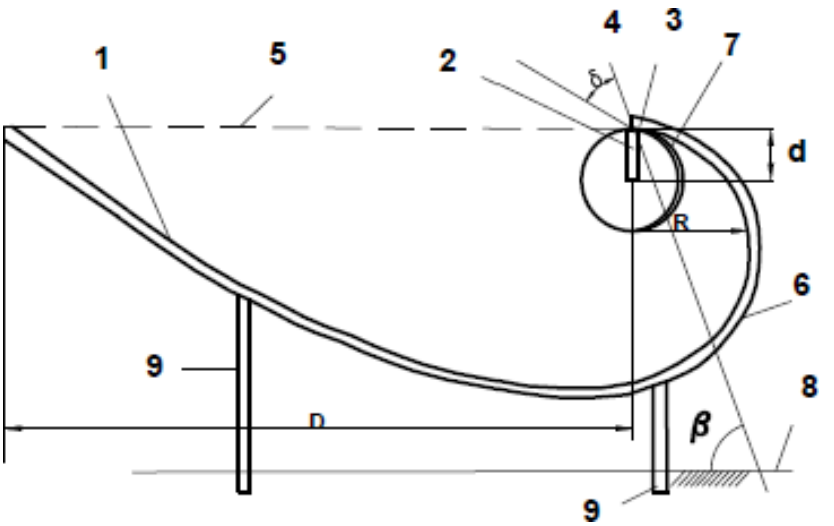

The solar module with a concentrator contains the main focusing parabolic-cylinder mirror reflector 1 with an aperture angle δ, a receiver with a two-sided working surface 2, a focal axis 3 and a reflector focal plane 4. The width of the solar module in the horizontal plane is equal to the width D of the module 5 of the concentrator plus radius R of the second semi-cylindrical reflector 6. Receiver 2 with an optical width d is installed perpendicular to the plane of the module 5 between the focal axis 3 and the axis of the third semi-cylindrical mirror image 7. The focal plane 3 is inclined to the horizontal plane 8 at an angle β.

The solar module with a concentrator 1 is attached to the horizontal plane 8 by means of supports 9. The angle β can vary from $\beta_1=113,75°–\varphi$ to $\beta_2=66,25°–\varphi+\delta$. In the first case, β_1, the focal plane 4 of parabolic-cylinder concentrator 1 is directed to the position of the Sun on June 22 (summer solstice), in the second case, β_2 – branch of parabolic-cylinder concentrator 1 is directed to the position of the Sun on December 22 (winter solstice).

The coefficient of geometric concentration for the module in Figure 1.17 is:

$$K_{geom} = D/d = 8/(1 - cos(2\delta)) \quad (1.6)$$

For $\delta°$=24, 32, 36° the value of the geometric concentration are 24.2, 14.2 and 11.6, respectively, i.e. the introduction of the second 6 and third 7 mirror concentrator increases the concentration ratio by 4 times.

When using double-sided receivers 2, it is possible to simplify the design of the non-tracking concentrator using one branch of the parabola, reduce the focal length of the module, increase the degree of concentration of radiation, and reduce the cost of the solar module by reducing the receiver area.

The main requirements for concentrating systems are:

1. Minimal energy loss during concentration;
2. The ability to sustainably provide the necessary distribution of the radiation density on the SC;
3. Manufacturability of manufacturing and installation;
4. Resistance to external factors;
5. Convenience and ease of operation;
6. The ability to repair and replace individual items;
7. Low cost.

SUN TRACKING SYSTEMS

One of the constructive elements of solar power plants is the Sun Tracking System (STS). STS can be clock and continuous, single-axis and two-axis, with a clockwork and sun position sensors, etc. Sun tracking systems can increase the efficiency of modules with single-sided silicon modules by 30-40% and by 50-60% with double-sided (Vorobiev, Horley, Gonzalez-Hernandez, 2005).

The company Seltek (Swing tracking device for the Sun, 2018) is one of the manufacturers of turning devices, representing a computer system that provides automatic tracking of the sun. The main control of the device is carried out using a microprocessor, which implements the programmed algorithm based on the trajectory of the Sun. The disadvantage of such devices is that without taking into account clouds in the daytime, the computer continuously sends control signals to the actuator.

Figure 9 shows the rotator made by Seltek.

Figure 9. Rotary device for tracking the Sun produced by Seltek

In (Prokopov, Yarmukhametov, 2007), a solar power station containing a vertical shaft with an azimuthal rotation drive was considered, at the upper end of which there is a horizontal shaft with symmetric eccentric leads mounted at its ends in contact with a sinusoidal groove of a rigidly fixed horizontal ring. A solar photodetector with azimuthal rotation automatic control system is rigidly fixed on a horizontal shaft. During azimuthal rotation of the shaft, the horizontal shaft with its drivers interacting with the sinusoidal groove of the horizontal ring, rotates by 45 ° in one or the other direction when moving along the groove, respectively morning-noon-evening, which ensures the zenithal tracking of the station's photodetector. The disadvantages of a solar power plant are its limited use only in conjunction with photovoltaic modules, which limits the potential for using its slewing bearing structure, as well as the fact that the zenithal rotation of the frame is always ensured along the same trajectory, which does not provide high precision tracking of the installation. as the angle of elevation of the sun varies throughout the year.

In (Nikitin, Tikhonov, Kharchenko et al., 2013), an installation was proposed that monitors the Sun of its receiving panel by azimuthal and zenithal (declination) parameters during daylight for different dates of the year using a single electric motor in accordance with the calculated data for a certain latitude of use of the installation and ensuring the reorientation of the positioned object at dawn (turn from west to east).

Figure 10 shows the ED-3500 Dual dual tracker solar tracker (Solar tracker ED-2000 Dual., 2016) (the tracker is oriented in two planes: up and down: from -10° to 75°; left-right: from -120° to 120°). When using the Energy Tracks XY solar trackers, the sun is always perpendicular to the module.

Automatic systems of orientation to the Sun were also considered in (Omar, Shaari, Omar, & Yahaya, 2006; Chun-Sheng, Yi-Bo, Si-yang et al., 2008; Li, G., Shi, Fu, & Zhou, 2008). In the article (Omar, Shaari, Omar et al., 2006), the authors show the possibility of using systems developed for space satellites in ground-based solar power plants.

In the works (Pshennov, 2009; Sorokin, 2005), the dependence of the efficiency of the orientation system on the Sun on the motor step size is investigated. It is shown that with increasing step size, the amount of energy expended for orientation rapidly decreases, but the photodetector often goes beyond the boundaries of the light spot, which creates the need to reduce the geometric dimensions of the photodetector and, consequently, the electrical power at a constant solar radiation flux density. The values of the optimal step of the orientation system in the considered works are 0.5 ... 2° (Sorokin, 2005). Economic efficiency is maximum at a step size of 1° (Pshennov, 2009).

Figure 10. Biaxial solar tracker ED-3500 Dual

In (Thein, 2010), the creation of a system of orientation to the sun using the angle error sensor and the method of total differential determination of directivity is considered. In the conditions of long-term shading, such a system requires special measures to ensure the alignment of the rotation of the tracking system with the movement of the Sun. In (Ovsyannikov, 2003) the use of similar tracking systems for solar furnaces and other power plants is considered.

Orientation devices based on solar radiation sensors (i.e., without the need to enter position and time data) do not prove to be reliable and often fail, especially with heavy clouds and high albedo of the earth's surface, dusting, and contamination of the light-receiving surfaces of the sensors. In this connection, orientation methods based on program methods are becoming more attractive. In such orientation systems, the sun is tracked thanks to a stepping motor or servomotor.

The main advantage of servo drives is the availability of feedback, due to which such a system can maintain positioning accuracy at high speeds and high moments. Also, the system is distinguished by high overload capacity, low inertia, high dynamic performance, no effect of losing steps (as in a stepper motor). The disadvantages of servo drives in comparison with stepper motors is the higher price (on average, 15-20% higher than that of stepper (Comparison of servo and stepper motors. KIP-Service. Industrial automation, 2014).

THE OVERVIEW OF BUILDING-INTEGRATED SOLAR MODULES

In the 70s-80s of the 20th century, along with the usual installation of photovoltaic modules to generate electricity, two new concepts in architecture emerged, describing two main approaches to integrating solar panels into building construction:

BAPV (Building Applied Photovoltaics): Adding photovoltaic modules on top of the building envelope (facade or roof);

BIPV (Building Integrated Photovoltaics): Replacement of part (or completely) of building envelopes with photovoltaic modules specially created for this project. Figure 11 shows options for the location of photovoltaic panels.

Figure 11. Variants of integration of photovoltaic modules BAPV, BIPV
**A— pitched roof, B— flat roof, C — skylight (lamp), D —facade cladding, E — facade glazing, F— external devices*

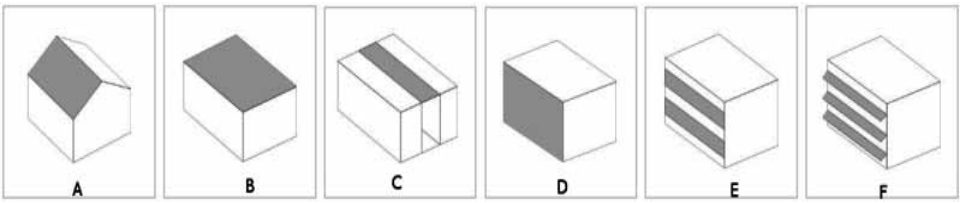

BAPV systems are installed on the building after construction is completed, therefore their installation does not directly relate to the building structure. However, in some cases, in accordance with local legislation, the placement of equipment on the front facade of historic buildings that change its appearance may be prohibited. In this context, the use of **BIPV** systems is a more appropriate solution.

Building Integrated Photovoltaics (BIPV-systems) refer to the use of solar energy as part of building structures (roofs and facades) (Herig, & Perez, Wenger et al., 2015; Herig, Thomas, Perez et al., 1999). As a replacement for an alternative building material, BIPV is more cost-effective compared to conventional PV systems, which require additional areas and support structures to be installed. The global installation of BIPV-systems increased at an increased rate from 2006 to 2010, by 121% annually from 29 MW in 2006 to 682 MW in 2010 (GlobalData, Primary Research Research and Markets,

Building Integrated Photovoltaic (BIPV) - Global Market Size, Technology Road-Map, Regulations and Pricing Analysis to 2015, 2011).

The amount of solar radiation falling on the building's surface depends on the orientation of this surface and on the geographical latitude of the terrain. It is believed that the optimum angle of inclination to the horizon is close to the geographical latitude and directed clearly to the south, for example, for Moscow 56 ° to the horizon (Econet.ru: BAPV and BIPV-solar panels, 2015). Small deviations from this optimum angle of inclination and direction lead only to small losses in the development. If this optimal angle and direction is taken as 100%, then the output signal from the remaining surfaces of the building (Econet.ru: BAPV and BIPV-solar panels, 2015).

Figures 12-13 show the appearance of the outer wall of the building with solar panels (USA, California) and Herz-Jesu Kirche (Plauen, Germany, 2002).

Currently, the use of solar concentrator systems is limited in scale and most of the existing installations use devices of considerable size. Despite the current economic situation, there is a tendency to a rapid increase in production (Kurtz, 2009).

Figure 12. The exterior of the outer wall of the building with solar panels (USA, California)

Figure 13. Herz-Jesu Kirche (Plauen, Germany, 2002).
**Photovoltaic modules were added using a hidden mounting system. Solarwatt's black, matte modules are perfectly combined with the existing architecture, while at the same time adding a high-tech element slightly. Installation area: 160 m². Installed peak power: 24 kW. Power generation: 21,000 kWh / year*

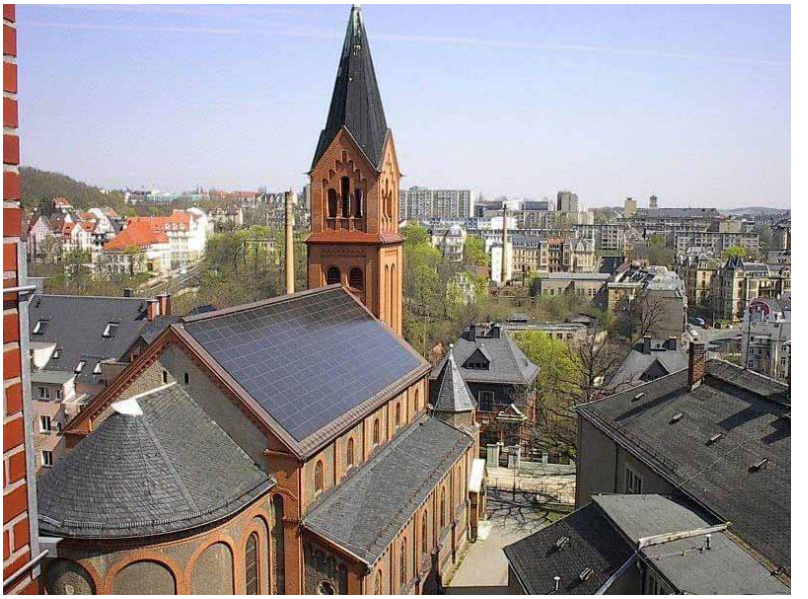

The main requirements for solar concentrators that are integrated into buildings are (Reijenga, 2000):

1. Natural integration;
2. Pleasant architectural design;
3. A good composition of colors and materials;
4. Dimensions, corresponding harmony and composition;
5. Compliance with the context of the building;
6. Well thought out and innovative design.

Of particular interest for integration are solar concentrators with a low concentration ratio (less than 10 times), since they have a linear geometry and for their effective operation it is enough to follow only one axis (Tripanagnostopoulos, 2008).

High system concentration requires two-axis tracking with high accuracy (tolerances below 0.28). The integrability of such a system will be greatly hampered. Inclusion is best achieved on the roof of a building (particularly for flat roofs), where the system is invisible from the outside. The problem

of integrating highly concentrating systems can be solved if the tracking is ensured by the movement of the receiver while the concentrator itself is stationary. However, installation on the facades of such systems presents certain problems: mirrors make it difficult for light to enter the building and the mobile receiver must protrude out of the building, which creates an additional load on the building structure.

In (Chemisana, Rosell, 2016) proposed a solution for the integration of concentrator solar modules into the facades of a building. The proposed concentrator is based on the Fresnel reflecting system. The concentration of solar radiation on a static receiver is achieved using a variety of mirrors that rotate together. All axes of rotation are in the same plane and parallel. This allows the use of a single engine, which provides important mechanical and economic advantages.

The maximum achieved concentration ratio of the module is 20.42 times. The installation can be used for heating or air conditioning the building.

Lleida State University (Spain) has developed a concentrator technology that uses reflection in the same way as in the systems developed by Chemizan and Rossell (Chemisana, Rosell, 2016), but with a design whose priority is architectural integrability. The system consists of linear Fresnel reflectors that focus the radiation in the same way as a lens. The receiver remains stationary and tracking the Sun is achieved in a simple and efficient way by turning individual mirrors. Thus, the overall movement is minimized, which facilitates integration into buildings and offers various possibilities to meet the diverse requirements of specific installations.

A new step in architecture are buildings with all-glass facades. TATPROF company produces a system of sun blades that provide such an arrangement and inclination of its elements in order to reduce the influence of solar radiation in summer and increase its access in winter time (Tatprof, 2016).

Thus, the most promising areas in the integration of solar modules (planar and concentrating) into the construction of buildings:

- development of BIPV technologies (roofing, film, facade materials);
- Integration of solar concentrators that do not require biaxial tracking (medium and low concentrations) on facades and roofs of buildings (parabolic concentrators, lenses and Fresnel mirrors);
- integration of high concentrating modules on the roofs of buildings.

In this regard, the issue of the integration of non-observant solar concentrating modules with louvered heliostats with an increased duration

of work on the facades of buildings becomes relevant. Installation of non-monitored solar concentrating modules with louvered heliostats on the facades of buildings can solve the problem of lack of space to accommodate solar energy facilities in the city, and also provide residential and public consumers with heat and electricity.

HISTORY AND STATUS OF THE DEVELOPMENT AND IMPLEMENTATION OF BIPV-TECHNOLOGIES

In the late 1970s, the US Department of Energy (DOE) began to sponsor projects to promote distributed photovoltaic systems, including working with industry to integrate photovoltaic systems with building materials. By the 1980s, companies such as General Electric, Solarex, and Sanyo developed prototype photovoltaic shingles, but technical problems and high costs slowed the commercialization of these products (Goodrich, Woodhouse, Margolis et al., 2011). As photovoltaic technologies became more and more efficient and reliable in the following years, more and more interested parties sought to combine photovoltaic devices with building materials. In 1993, DOE developed a program called Building Opportunities in the USA for photovoltaic systems (PV: Bonus), which was developed, in particular, for the commercialization of innovative BIPV products (Goodrich, Woodhouse, Margolis et al., 2011). Similar programs were created by groups in Europe and Japan around the same time (Goodrich, Woodhouse, Margolis et al., 2011). In 2008, partnerships between PV manufacturers, architects, and building materials suppliers are proposing to introduce barriers and bring new economically competitive products to the market (Goodrich, Woodhouse, Margolis et al., 2011).

One of the first homes in the USA with BIPV was built in 1980 (Goodrich, Woodhouse, Margolis et al., 2011), and the systems were subsequently incorporated into commercial structures, such as 4 Times Square Building in New York in 2001, where about 15 were installed kW of amorphous silicon (a-Si) BIPV (before 2001). Larger BIPV systems were installed not long ago, including the DC 6.5-MWp system at Hongqiao Railway Station in China, completed before the 2010 Shanghai World Expo (Goodrich, Woodhouse, Margolis et al., 2011). At the simplest level, BIPV systems are derived from the general constructions of the PV module and installation methods; early product designs were often customized for specific buildings and architectural features. Today, BIPV products have more unified designs that are designed

to integrate with many building materials. Although market prices for BIPV are still higher than for rack-mounted PV modules, the new products offer lower prices and better performance than previous BIPV systems.

Overall, the global development of BIPV technologies is small compared to standard PV modules. According to some estimates, the total installed capacity of BIPV (and associated semi-integrated photovoltaic products) throughout the world by the end of 2009 was 250–300 MW (Goodrich, Woodhouse, Margolis et al., 2011). This represented about 1% of the total installed power of distributed photovoltaic systems of the time (Goodrich, Woodhouse, Margolis et al., 2011). A portion of this limited market share can be attributed to the BIPV price premium relative to standard PV modules, as well as to quality factors.

ANALYSIS OF THE COST STRUCTURE OF BIPV-MODULES

The National Renewable Energy Laboratory (NREL), in collaboration with industry, has developed a methodology for analyzing system costs (Goodrich, A., Woodhouse, M., Margolis, R., & Ong, S., 2011. This method is similar to the approach used by many developers of solar projects to approximate the book value of solar assets, characterizing the unsubsidized cash purchase price for systems under construction. The analysis includes all materials, labor, regulatory costs, as well as overhead and profits (O & P) for installed residential systems. Costs are in US dollars per peak watt of DC power ($ / W or $ / Wp DC).

BIPV modules often include additional materials to protect a building from a wide range of weather conditions. On the other hand, most BIPV modules reduce installation costs by eliminating common installation equipment of PV modules, such as spacers, z-channels, clamps, and associated labor costs. BIPV modules can also be installed faster than existing PV modules. In addition, it is important to consider the potential benefits of compensating for the costs of using traditional building materials (for example, shingles) in areas where a BIPV module is installed.

The cost structure of the BIPV module includes overhead costs and profit margins and sales taxes as part of the installation cost category, and these factors are determined as a percentage of the total system costs.

The resulting share of indirect capital costs in system costs is a function of system power, which is different for each case. Therefore, large systems have smaller indirect capital costs in terms of $ / W.

Additionally, the costs of inverters, meters, system monitors, junction boxes, fuses and holders, conductors should be considered.

The debate continues about the value of flexible photovoltaic and BIPV modules, but it is clear that the BIPV technology does not require flexible form factors. Among the BIPV currently installed BIPV and integrated PV structures, the most widely used are PV-moles based on crystalline silicon cSi technology (Goodrich, Woodhouse, Margolis et al., 2011).

If BIPV-modules completely replace traditional building materials, then the system cost reflects a proportionate cost offset. The development of multifunctional products is a central task for designers of BIPV modules, since building materials often require higher resistance than PV modules have, and BIPV technologies must meet standards for both PV and building.

The analysis in (Goodrich, Woodhouse, Margolis et al., 2011) shows that the effective cost in the case of BIPV-modules is $ 0.69 / W lower than the price of the basic version of PV-modules, the difference is more than 10%. A cost reduction of $ 0.18 / W occurs, as it is assumed that in this case the BIPV-modules replaces shingles. Excluding support structures and the associated labor costs are estimated to reduce BIPV's total costs by $ 0.55 / W ($ 0.27 / W for labor and $ 0.27 / W for materials). However, not all differences reduce costs in the case of BIPV modules. Smaller module sizes in the case of BIPV modules lead to an increase in total labor costs for installing the module by $ 0.08 / V, and a BIPV module margin of 10% adds $ 0.22 / W.

Indirect capital costs are also slightly lower in the case of a BIPV module, because its system power is greater than in the case of PV (5.0 kW).

The context of the illustrated cost advantages of BIPV modules is crucial for understanding the overall capabilities and challenges for BIPV products.

The effective prices of the BIPV and the thin-film BIPV module are about the same, with prices more than 10% lower than in the base case of PV. The effective price in the case of a BIPV thin film is about 1% cheaper than in the case of a PV module.

PERFORMANCE STUDIES OF BIPV MODULES

The work (Fan1, Khaing, & Liang, 2012) presents the results of a study of the effectiveness of BIPV-modules under shadow conditions. Two identical

BIPV systems were installed on the connecting line between educational buildings T12 and T14. The PV array of each system has two parallel PV branches, each of which consists of fourteen Uni-Solar PVL-128 triple-film photovoltaic modules of amorphous silicon (a-Si).

The output of the PV array is connected to an SMA 1.7 kW mains inverter (SB1700). The triple joints of the photovoltaic module on three layers are arranged in such a way that the upper layer of the junction absorbs blue light, the middle layer of the compound has green light, and the lower layer of the compound has red light. This spectral separation ability helps achieve higher conversion efficiencies. Compared to other types of silicon photovoltaic modules, photovoltaic module based on amorphous silicon a-Si has a lower temperature coefficient of the module Pmax. As a result, a-Si photovoltaic modules can provide better performance in a hot zone, such as in a tropical region.

The site position for the BIPV system is one of the most important factors to consider when designing, since any partial shading on photovoltaic modules will significantly reduce the energy output of the system.

It can be noted that out of 12 months, System 1 generated more power for the network than System 2 in 7 months (April, May, June, July, August, September and October), System 1 produced less energy than System 2 in 4 months (November, December, January and February), and the output of the two systems are very close in March.

As a result, it has been shown that a partial shadow from surrounding objects really impairs the performance of the BIPV system. In order to avoid the problem of partial shading and improving the performance of the BIPV system, solar access on the spot should be calculated by the system developers based on information on obstacle heights and solar energy profile.

In most cases, photovoltaic panels are combined with the second layer of the building structure, for example, for roof insulation. If they are integrated directly into the second layer without an air gap, the photovoltaic panel heats up and its efficiency drops. It also increases the temperature of the building and increases the load on the cooling system. Consequently, an air gap is formed between the photovoltaic panel and the building layer, which provides airflow behind the photovoltaic panels, prevents overheating of the photovoltaic panels and, consequently, the loss of their efficiency, and also leads to excessive heat. Sometimes, excess heat can be used for space heating, and therefore this system is called Building Integrated Photovoltaic / Thermal (BIPV / T).

In (Agathokleousa, Kalogiroua, & Pierretb, 2013) showed that the air gap can be ventilated naturally or mechanically using a fan, which depends on the climatic conditions and the needs of the building. Sometimes natural ventilation may be sufficient to move the system's excess heat, but in very hot climates, using a fan to supply air into the air gap may be more efficient. However, natural ventilation has several advantages compared to a mechanically ventilated system, such as the cost of the fan, the noise from the fan, special installation space, the difficulty of maintaining the fans after installation, etc.

The size of the air gap, to be effective, depends on the amount of heat that is generated due to the hot surface of the photovoltaic panel, which depends on the location of the system and weather conditions (ambient temperature and amount of radiation) angle of inclination of the system, height of the system, holes.

Mirzaei, Paterna, Carmeliet, 2014 conducted a study of the role of air flow in the cavity on the performance of BIPV panels. It was concluded that the surface temperature of the photovoltaic panel is lower when there is an open cavity. In addition, it is mentioned that the flow passing below the PV panel was almost twice as large as the flow above PV. In addition to flat panels, stepped also tested. It is concluded that the stepped device creates greater turbulence in the air gap and thus has a significant advantage in PV cooling than a flat device.

The work (Agathokleousa, Kalogiroua, & Pierretb, 2013) presents the simulation results and the monitoring data of the roofing BIPV panel. The PV module has dimensions of 905x1395x59 mm and a weight of 7.3 kg. This is an opaque module, which is later painted black to reproduce the natural color of the roof.

Demonstration Building is a new residential building located in Mons, Belgium. The orientation of the building from south to west is 10°. The BIPV system is installed on the southern roof of a building with a 40° slope.

The photovoltaic panels used are produced in the framework of the BFIRST project with a new sealing method using fiber-reinforced composite materials.

The study (Agathokleousa, Kalogiroua, & Pierretb, 2013) established the following. Roof photo-electric modules, although they are significantly lighter than other photo-electric modules for integrating buildings on the market, fit perfectly into the design of a building and look like ordinary tiles.

The photovoltaic panels in the bottom row of the roof are cooler than the panels in the top row because of the air intake at the bottom. The maximum measured temperature from August to October was 52 ° C below and 62 ° C

above. Energy production has no decline in the period with high temperature PV. Increasing the surface temperature of the upper PV row to 63 ° C did not affect the total energy production in the system.

The natural ventilation air gap is sufficient to maintain the temperature of the photovoltaic panels below 62 ° C, even in August, when the ambient temperature and solar radiation were maximum.

In the modernization project (Edward, 2015), in which photovoltaic panels with a total area of 25 m × 4 m (H × W) were installed on the southwest side of the vertical facade of the building at the University of Hong Kong. The location of the building on a hillside in the western region of the island of Hong Kong. The system also acts as a heat buffer to reduce the building's heat gain from sunlight during the sunset period. The system was composed of two types of thin-film photovoltaic panels; each type of panel occupied 25 m × 2 m vertically. The thin film panel has its advantages: low cost, the look is similar to normal glass curtain wall panels. In fact, the installation of these panels in the project was exactly the same as for ordinary glass panels and the concept of a modular structure is used in the assembly process.

The total peak power is about 4.3 kW, and the average annual electricity generation of the system is about 3200 kWh.

ENERGY EFFICIENCY AND ENERGY SAVING AS THE MAIN TREND OF MODERN ARCHITECTURAL PRACTICE WITHIN THE FRAMEWORK OF THE SMART CITY-CONCEPT

Energy efficiency of buildings plays a significant, sometimes decisive role in modern architecture. The complex of architectural-technical and energy-saving measures to improve the energy efficiency of buildings involves the development of heat-efficient structures, engineering systems, the use of alternative sources of heat and electricity, including in the structure of distributed generation.

At the moment there are certain indicators by which buildings and structures can be assigned to different groups according to the degree of energy efficiency. Energy efficiency class depends on the climatic characteristics of the region of the designed building, on the possibility of using those or other natural resources. Depending on the geographical location of the design and construction site, various architectural solutions are used.

In a general overview of the architectural standards for energy saving, three fundamentally different energy efficiency groups can be distinguished (Stamenkovich, 2011):

- buildings producing energy;
- partially volatile buildings;
- completely non-volatile buildings.

A low energy house compared to a standard house is a partly volatile building (Low Energy House, Passive House, Ultra-Low Energy House). The houses of this type use increased thermal insulation, energy-saving windows, low level of air penetration from the outside, fresh air ventilation with heat recovery, as well as more stringent heating and cooling requirements. In addition, in such homes is monitored for compliance with the minimum water consumption.

The concept of a building with zero energy balance is based on the fact that a building can satisfy all of its energy needs through geographically accessible renewable energy sources. Buildings with zero energy balance and zero CO_2 emissions (Zeroenergy House or Net Zero Energy House) can be independent of urban energy networks in the event of complete autonomy of facilities. At the same time, the amount of energy generated from renewable energy sources should be equal to the annual energy consumption of the building (Brodach, 2010). In practice, this solution is implemented in such a way that periodically energy is consumed from the centralized network and returns back to the city network.

Energy Plus House buildings consume much less energy than they receive. In such buildings, renewable energy sources are used. Efficiency is achieved through architectural solutions with passive and active use of solar energy, proper location of the construction site, as well as with the help of additional technological installations that produce energy.

With the wider distribution of the above categories energy efficiency of buildings on urban buildings, they can have a significant beneficial effect on the environmental situation of large cities.

The building with zero energy balance or the so-called passive house in the European classification of energy-efficient houses occupies a special place. The emphasis in the construction and operation of such a house is put on active thermal insulation, as well as on the availability of renewable energy sources that complement the classical heating system: solar panels, heat pumps, etc.

The main activities for the formation of zero energy balance of the building (About buildings with a zero energy balance and plans for zeroing abroad, 2019):

1. Reducing energy consumption through the use of architectural and engineering solutions: orientation of the building, daylight, natural ventilation, evaporative cooling, etc.
2. The use of renewable energy sources located in the building: solar panels, solar water heating systems and wind power plants located directly on the building.
3. The use of renewable energy sources located on the territory adjacent to the building: solar panels, solar water heating systems, hydro and wind power plants located on the territory adjacent to the building.
4. The use of renewable energy sources located outside the territory adjacent to the building: biomass, wood pellets, ethanol or biodiesel.
5. Purchase of energy from third-party renewable sources: purchase of energy from solar, wind power installations of third-party specialized systems or the use of other schemes for the purchase of energy.
6. Sale or storage of surplus electricity: surplus electricity is exported to the external power grid or local storage is organized.

The concept of Smart City is the development of socially oriented infrastructure, including smart power supply (smart grid Smart Grid system), smart environment, smart transport, smart home, smart management. The concept of a smart city is first of all:

1. Using the latest information and communication technology.
2. The introduction of innovative technologies of energy, transport and construction.
3. Social, business and cultural self-sufficiency of the city.
4. Development of standards for green building.
5. Quarters, houses and areas as urban planning and energy levels-units (Bushuev, Livinsky, 2015).

Smart city systems are being actively developed in world practice for the power supply of local facilities and territories. Their introduction was caused by the need to harmonize the conditions and modes of distributed generation, mainly with the help of renewable energy sources, in the general grid structure. Decentralized systems are not autonomous, and their connection to a common

power grid structure requires a sufficiently developed information and control network built according to the Smart Grid methodology.

According to the study of Smart Cities, conducted by Juniper Re-search in 2015, Barcelona ranked first in the world in the ranking of smart cities. LED flashlights reduce lighting costs and optimize energy supply. They work depending not only on the time of day, but also on weather conditions: humidity, temperature and air pollution level. In 2000, Barcelona became the first European city to set up a solar collector system on the buildings of new hotels, hospitals, fitness centers and swimming pools. At the same time, urban heating systems use steam from waste incineration, and cooling systems use seawater.

In Japan, not far from Yokohama, the smart city of Tsunashima officially opened. A multifunctional administrative building, an eco-friendly residential complex, an intelligent shopping and entertainment center, an Apple research laboratory, Keio University Student Campus, a hydrogen charging station and other futuristic objects are located on its territory (Figure 14).

Figure 14. The smart city of Tsunashima

San Francisco uses innovative communication tools for transportation infrastructures that calculate estimated arrival times. And the roofs of buses equipped with photovoltaic panels produce energy.

Because of the policy pursued by the government, Germany is the world leader in introducing and investing in solar technology. In Berlin, solar panels are installed on the building of the office of the German Chancellor, the main station, on the roofs of shopping centers.

In Paris, solar panels are also actively used for the electricity supply of eco-quarters (Figure 15).

In Moscow, work on the implementation of the Smart city began with the development in 2014 of the concept of an energy-efficient metropolis - New Moscow, performed on the instructions of the Department of the fuel and energy economy of the city of Moscow by the efforts of the JSC State Institute of Energy Strategy involving a wide range of specialists from other organizations (Electronic resource, 2018).

Figure 15. Solar panels on the roof of the Galeries Lafayette shopping center in Berlin

The annexed territories of New Moscow can become an important step on the way of turning the capital into a green, favorable for life metropolis. This requires mass development and introduction of new organizational and high-tech solutions that ensure the quality of life of the population, the socially oriented development of the economy and the requirements of the functions of the capital status of the city.

In connection with the development of new territories, as well as the reconstruction of the residential and industrial sphere in the old city borders, the smart city becomes the key object of Smart City. A vivid example of such an object is the high-energy quarter Moscow-City. New Smart-objects will be able to provide high reliability of energy supply of high-rise buildings, saturated with various kinds of communications. To do this, they themselves must have not only a developed network of external power supply, but also their own power sources. Thus, the Moscow-City project provides for cogeneration plants located on the common territory with the Expocentre Fairgrounds, a wind power cluster on the right bank of the Moscow River, solar panels (on the roof of the IQ-guater building) (Figure 16).

Figure 16. High-energy-intensive quarter Moscow-City

The solar energy in Moscow is currently represented by the following objects (Figure 17):

- Wi-Fi stations in the parks (Izmailovsky Park, Sokolniki, Tsaritsyno);
- Parking meters new;
- City bike rental stations;
- Traffic lights at pedestrian crossings;
- Public transport stops (Timiryazevskaya street);
- Street lights (eco paths laid on the slope of Sparrow Hills) (Electronic resource, 2017).

Figure 17. Solar energy in Moscow

The main advantages of renewable energy are their inexhaustibility as opposed to fossil fuels, environmental friendliness - using and extracting energy from renewable energy does not pose an environmental threat, reducing costs for transporting electricity and dispatching due to the possibility of locating generation in close proximity to the consumer, energy independence from a centralized network. Also, the use of renewable energy allows to reduce the consumption of fossil fuels.

The main problems in the implementation of renewable energy facilities in the metropolis are low concentration of renewable energy, as a result, the need for large-scale power installations, the relatively high cost of production, lack of government support and regulatory framework, instability, generation dependence on weather conditions, lack of space to accommodate objects RES in the city.

Legislative Framework for RES

The Federal Law on Energy Saving (Federal Law On Energy Saving and On Increasing Energy Efficiency and On Amending Certain Legislative Acts of the Russian Federation, 2009) provides for the creation of legal, economic, and organizational bases to stimulate energy saving and increase energy efficiency.

The energy strategy of Russia for the period up to 2030, approved by the Order of the Government of the Russian Federation of November 13, 2009 No. 1715-p, notes the insufficient development of small energy and low involvement in the energy balance of local energy sources of regional and local importance (Order of the Government of the Russian Federation, 2009).

Order of the Government of the Russian Federation No. 1-p dated January 8, 2009 On Approval of the Main Directions of the State Policy in the Field of Increasing the Energy Efficiency of the Electric Power Industry Based on the Use of Renewable Energy Sources for the Period up to 2024 (Amended on May 15, 2018) the volume of production and consumption of electric energy using renewable energy sources (except for hydropower plants with an installed capacity of more than 25 MW) for the period up to 2024, 4.5% (On Approving the Main Directions of the State Policy in the Field of Increasing the Energy Efficiency of the Electric Power Industry Based on the Use of Renewable Energy Sources for the Period up to 2024 (as amended on May 15, 2018).

According to the Order of the Ministry of Energy of Russia No. 121 of February 28, 2018 "On Approval of the Scheme and Program for the Development of the Unified Energy System of Russia for 2018-2024", in the structure of the UES of Russia generating capacity, the share of WEC and SES will increase from 0.3% in 2017 to 1,8% in 2024 ("On approval of the scheme and development program of the UES of Russia for 2017–2023").

At the level of an individual consumer, the Smart infrastructure can be represented as an integrated power supply system of a smart house.

A smart house or an intelligent building is a brand new object in terms of infrastructure support. It integrates various life support systems (electricity, heat, gas, water supply) into a common engineering infrastructure complex; focused on large-scale consumer saturation with telecommunications and information services; as a mandatory element of development, it takes into account the availability of individual passenger transport, incl. and electric car. At the same time, the key features of a smart house are in a developed system of monitoring and control over compliance with climatic parameters, lighting, security, energy saving and effective (automatic) energy consumption. The advantages of a smart house: energy conservation - control over the consumption of electricity, water and other resources, security, optimal microclimate, beautiful design, ease of management.

The prospects for energy-saving technologies and the concept of Smart City on the territory of the megalopolis are enormous.

Applying the smart city approach to the power supply system of Moscow and the Trotsky and Novomoskovsk (TINAO) administrative districts involves the use of the following solutions:

1. Intellectualization of residential buildings and urban lighting systems;

2. Development of distributed generation, including using renewable energy sources;
3. The introduction of intelligent energy accounting systems;
4. Development of infrastructure for public and private electric transport.

The structure of the territories of TINAO, which is a decentralized set of foci-clusters, is the most optimal for applying the Smart City model in terms of the development of distributed generation. The implementation of the Smart City approach is justified primarily on the territory of TINAO, while in areas with existing buildings in the old city boundaries, emphasis should be placed on maintaining the existing electricity and heat supply systems, optimizing their structure and maximizing energy efficiency (Bushuev, Livinsky, 2015).

CONCLUSION

The principles of construction and operation of the main concentrating systems, including non-followable modules, are reviewed, and the work of the concentrators is analyzed. An analytical review of modern facade-integrated photovoltaic technologies was carried out, their classification was given.

When developing existing designs of non-glare parabolic cylindrical concentrators with fixed linear and angular mirror lamellae, the possibilities of increasing the duration of the concentrator operation due to rotation of the mirror lamellaee system following the solar rays and, as a result, increasing the annual productivity of solar concentrating modules were not considered.

The known methods for calculating a flat (two-dimensional) scheme for passing the sun's rays through a louvered heliostat make it impossible to assess the real effectiveness of using louvered heliostats with non-tracking solar concentrators, which makes it necessary to consider the practically important three-dimensional problem of calculating the solar radiation flux on the receiving surface of an unfollowing parabolic-cylindrical solar concentrator with louver heliostat.

REFERENCES

About buildings with a zero energy balance and plans for zeroing abroad. (2019). Retrieved from: http:// http://portal-energo.ru/articles/details/id/493

Agathokleousa, R. A., Kalogiroua, S.A., & Pierretb, S. (2013). *A Building Integrated Photovoltaic (BIPV) demonstration building in Belgium with new Fibre Reinforced Solar Technology PV modules: Analysis with Simulation and Monitoring data*. Academic Press.

Alfegi, M. E. A., Sopian, K., Othman, M. Y. H., & Yatim, B. B. (2007). Transient mathematical model of both side single pass photovoltaic thermal air collector. *Journal of Engineering and Applied Sciences (Asian Research Publishing Network)*, *2*, 22–26.

Andreev, V. M., Davidyuk, N. Yu., Ionova, Ye. A., Pokrovsky, P. V., Rumyantsev, V. D., & Sadchikov, N. A. (2010). Optimization of parameters of solar modules based on lens radiation concentrators and cascade photoelectric converters. *Journal of Technical Physics*, *80*(2), 118–125.

Arbuzov, Yu. D., & Evdokimov, V. M. (2007). Fundamentals of photoelectricity. Ed. GNU VIESH, 289.

Bazarova, E. G. (2008). *Improving the efficiency of solar energy in power plants with concentrators* (Doctoral dissertation).

Bergene, T., & Lovvik, O. (1995). Model calculations on a flat-plate solar heat collector with integrated solar cells. *Solar Energy*, *55*(6), 453–462. doi:10.1016/0038-092X(95)00072-Y

Bezrukikh, P.P., Strebkov, D.S., Tveryanovich, E.V., & Irodionov, A.E. (1999). *Solar photovoltaic module (options).* The patent for the invention Nº 2133415 of the Russian Federation, IPC F24J 2/42, F24J 2/08, H02N 6/00. No. 98108658/06; publ. 20/07/1999.

Brodach, M.M. (2010). Buildings with zero energy balance - myth or reality? *AVOK*, 8.

Bushuev, V.V., & Livinsky, P.A. (2015). *Energy Efficient Metropolis - Smart City New Moscow.* Publishing House Energy.

Chemisana, D., & Rosell, J. I. (2016). Design and optical performance of a nonimaging Fresnel reflective concentrator for building integration applications. *Energy Conversion and Management*. *Renewable Energy*, *85*, 564–572. doi:10.1016/j.renene.2015.07.009

Chun-Sheng, W., Yi-Bo, W., Si-yang, L., & Yanchang, P. (2008). Study on automatic sun-tracking technology in PV generation. *Electric Utility Deregulation and Restructuring and Power Technologies*, *Third International Conference*, 2586 - 2591.

Comparison of servo and stepper motors. KIP-Service. Industrial automation. (2014). Retrieved from: http://kipservis.ru/kipia_primenenie/servoprivod_i_shagovie_dvigateli.htm

Dufflie, J. A., & Beckman, W. A. (1991). *Solar engineering of Thermal Processes* (2nd ed.). John Wiley and Sons Inc.

Econet.ru. BAPV and BIPV-solar panels. (2015). *What is the difference*. Retrieved from: https://econet.ru/articles/81109-bapv-i-bipv-solnechnye-paneli-v-chyom-raznitsa

Edmonds, I. (2017). *Solar Energy Materials*. Retrieved from: https://www.sciencedirect.com/journal/solar-energy-materials

Edward, W. C. L. O. (2015). *Overview of Building Integrated Photovoltaic (BIPV).* Systems in Hong Kong.

Electronic Resource. (2017). Retrieved from: https://yandex.ru/collections/card/5a2655492a6f93d3c407f8d0/

Electronic Resource. (2018). Retrieved from: http://smart-energy.msk.ru/

Evdokimov, V. M., Kivalov, S. N., Strebkov, D. S., & Tveryanovich, E. V. (2001). Improving the energy performance of modules with stationary concentrators. *Heliotechnics*, *4*, 38–44.

Fan, J., Khaing, H. H., & Liang, Y. J. (2012). Performance of BIPV Systems under Shadows. *2012 International Congress on Informatics, Environment, Energy and Applications-IEEA 2012*, 38.

Federal Law On Energy Saving and On Increasing Energy Efficiency and On Amending Certain Legislative Acts of the Russian Federation. (2009). 261-FL.

Florschuetz, L. W. (1979). Extension of the Hottel–Whiller model to the analysis of combined photovoltaic/thermal flat plate collectors. *Solar Energy*, *22*(4), 361–366. doi:10.1016/0038-092X(79)90190-7

GlobalData. (2011). *Primary Research and Markets, Building Integrated Photovoltaic (BIPV) - Global Market Size, Technology Road-Map, Regulations and Pricing Analysis to 2015*. Retrieved from: https://www.researchandmarkets.com/research/4d746b/building_integrate

Goodrich, A., Woodhouse, M., Margolis, R., & Ong, S. (2011). Building-Integrated Photovoltaics (BIPV) in the Residential Sector: An Analysis of Installed Rooftop System Prices Ted James. National Renewable Energy Laboratory.

Green, M., Emery, K., Hishikawa, Y., Warta, W., & Dunlop, E. (2012). Solar cell efficiency tables. *Progress in Photovoltaics: Research and Applications*, *20*(1), 12–20. doi:10.1002/pip.2163

Gremenok, V. F., Tivanov, M. S., & Zalessky, V. B. (2007). Solar cells based on semiconductor. Center of BSU, 222.

Herig, C., Thomas, H., Perez, R., & Wenger, H. (1999). Residential Customer Sited Photovoltaics Niche Markets. *Proceedings ASES Annual Meeting*.

Herig, C. R., & Perez, H. W. (2015). *Commercial Buildings and PV, a Natural Match*. NREL Brochure DOE/GO-1998 NREL. https://www.nrel.gov/ncpv/pdfs/pv_com_bldgs.pdf

Hybrid solar collectors PVT. (2017). Retrieved from: https://ecology.md/page/gibridnye-solnechnye-kollektory-pvt

Ibrahim, A., Jin, G. L., Daghigh, R., Salleh, M. H. M., Othman, M. Y., Ruslan, M. H., Mat, S., & Sopian, K. (2009). Hybrid photovoltaic thermal (PV/T) air and water based solar collectors suitable for building integrated applications. *American Journal of Environmental Sciences*, *5*(5), 618–624. doi:10.3844/ajessp.2009.618.624

Kivalov, S. N., & Zakhidov, R. A. (2001). The use of concentrating systems for photoelectric conversion of solar radiation. *Heliotekhnika*, *3*, 66–78.

Kurtz, S. (2009). Opportunities for development of a mature concentrating photovoltaic power industry. CS MANTECH Conference.

Li, G., Shi, X., Fu, C., & Zhou, G. (2008). Design and implementation of a novel MPPT controller based on sun tracking technology. *Electrical Machines and Systems, ICEMS 2008. International Conference*, 2611 - 2615.

Lidorenko, N.S., Evdokimov, V.M., Strebkov, D.S. (1988). The development of photovoltaic energy. *Informelectro*, 50.

Lidorenko, N. S., Zhukov, K. V., Nabiullin, F. Kh., & Tver'yanovich, E. V. (1977). Prospects of using Fresnel lenses for concentrating systems of solar installations. *Heliotekhnika*, *4*, 22–25.

Mills, D. R., & Guitranich, I. E. (1978). Ideal prism solar concentrators. *Solar Energy*, *21*(5), 430–432. doi:10.1016/0038-092X(78)90175-5

Mirzaei, P. A., Paterna, E., & Carmeliet, J. (2014). Investigation of the role of cavity airflow on the performance of building-integrated photovoltaic panels. *Solar Energy*, *107*, 510–522. doi:10.1016/j.solener.2014.05.003

Nikitin, B.A., Tikhonov, P.V., Kharchenko, V.V., & Tikhonov, A.V. (2013). *Installation of automatic tracking of the receiving panel for the sun.* The patent for the invention Nº2482401 of the Russian Federation, IPC F24J 2/54. No 2011121234/06; publ. 20/05/2013.

Omar, A. M., Shaari, S., Omar, A. R., & Yahaya, M. R. Y. (2006). An Automated Solar Photovoltaic Biaxial Tracking System: SolT2A. *Power and Energy Conference, IEEE International*, 44-47. 10.1109/PECON.2006.346616

Order of the Government of the Russian Federation. (2009). 1715-p. Russia's energy strategy for the period until 2030.

Order of the Government of the Russian Federation No. 1-p dated January 8, 2009 On Approving the Main Directions of the State Policy in the Field of Increasing the Energy Efficiency of the Electric Power Industry Based on the Use of Renewable Energy Sources for the Period up to 2024 (as amended on May 15, 2018)

Order of the Ministry of Energy of Russia No. 143 dated 03/01/2017 On approval of the scheme and development program of the UES of Russia for 2017–2023

Othman, M. Y. H., Ruslan, H., Sopian, K., & Jin, G. L. (2009). Performance study of photovoltaic-thermal (PV/T) solar collector with V-grooved absorber plate. *Sains Malaysiana*, *38*, 537–541.

Ovsyannikov, E. M. (2003). *Electric drives for ground-based and space-based solar systems. Theory and practice* (Doctoral dissertation).

Poulek, V., Libra, M., Strebkov, D., & Kharchenko, V. (2013). Photoelectric conversion of solar energy. Theory and practice of using solar energy. Ed. GNU VIESH, 321.

Prokopov, O.I., & Yarmukhametov, U.R. (2007). *Solar power station*. The patent for the invention Nº 2298860 RF, IPC H01L 31/042, F24J 2/54. No. 2005105145/28; publ. 10/05/2007.

Pshennov, V. B. (2009). Method of determining the energy efficiency of solar power drives with the concentration of the flow of radiant energy. *Dissertation abstract*, 12.

Reijenga, T. (2000). Photovoltaic building integration concepts – what do architects need. *Proc. IEA PVPS Task 7 workshop Lausanne featuring a review of PV products, IEA PVPS Task 7*.

Reijenga, T. (2000). Photovoltaics in the built environment. *Proc. 2nd world solar electric buildings conference*.

Sandnes, B., & Rekstad, J. (2002). A photovoltaic/thermal (PV/T) collector with a polymer absorber plate: Experimental study and analytic model. *Solar Energy*, *72*(1), 63–73. doi:10.1016/S0038-092X(01)00091-3

Sevela, P., Olesen, B. (2013). Hybrid solar collector. *Sustainable Building Technologies*, 90-97

Sodnomov, B., Strebkov, D.S., & Tyukhov, I. I. (2005). *Solar module with a concentrator*. The patent for the invention Nº 2252371 of the Russian Federation, IPC F24J 2/14, F24J 2/34. / No. 2003120707/06; publ. 20.05.2005.

Solar tracker ED-2000 Dual. (2016). Retrieved from: http://energy-ds.ru/catalog/generating/solnecnye-trakery/ed2000d.html

Sorokin, G. A. (2005). Electric drives of power solar power plants without concentration of radiation. *Dissertation abstract*, 15.

Stamenkovich, M.Z. (2011). Modern trends in the design of energy efficient and environmentally friendly buildings. *Architecture and Modern Information Technology*, *3*(16).

Strebkov, D. S., & Filippchenkova, N. S. (2014). Development of solar modules with prism concentrators and deflecting optical systems. *Theoretical*. *Scientific and Practical Journal Innovations in Agriculture*, *3*(8), 149–153.

Strebkov, D.S., Irodionov, A.E., & Filippchenkova, N.S. (2015). Analysis of the characteristics of solar modules with concentrators. *Mechanization and Electrification of Agriculture*, *12*, 21-23.

Strebkov, D.S., Mayorov, V.A., & Panchenko, V.A. (2013). Solar heat-photoelectric module with a parabotor concentrator. *Alternative Energy and Ecology*, *1/2*, 35-39.

Strebkov, D.S., Tver'yanovich, E.V., Irodionov, A.E., Kidyashev, Yu.K., Semenenko, V.F., Ananenkov, A.G., Neelov, Yu.V., Yakupov, Z. G., Isaeva, A.N., & Danko, E.M. (2001). *Solar module with concentrator.* The patent for the invention Nº 2172903 of the Russian Federation, IPC F24J2 / 26. No. 2000108561/06; publ. 27.08.2001.

Strebkov, D. S., Tver'yanovich, E. V., Tyukhov, I. I., Irodionov, A. E., & Yartsev, N. V. (2002). Solar concentrator technologies for energy supply of buildings. *Soil Technology*, *3*, 64–68.

Strebkov, D.S., & Tver'yanovich, E.V. (2007). Solar concentrators. *GNU VIESH*, 315.

Strebkov, D.S., Bazarova, E.G., & Tarasov, V.P. (2007). *Solar power plant (options).* The patent for the invention Nº2303205 of the Russian Federation, IPC F24J 2/42, F24J2 / 14. No. 2006109214/06; publ. 20/07/2007.

Strebkov, D.S., Pendzhiev, A.M., & Mamedsakhatov, B.D. (2012). The development of solar energy in Turkmenistan. *GNU VIESH*, 496.

Summer, V. (1961). Photo cells in industry. *Gosenergoizdat*, 568.

Swing tracking device for the Sun. (2018). Retrieved from: http://selteq.com

Tatprof. (2016). Retrieved from: https://tatprof.ru

Teplyakov, D. I., & Tver'yanovich, E. V. (1993a). Linear louver heliostats of SPS: Cosine and inter-luster effects. *Heliotechnics*, *4*, 54–58.

Teplyakov, D. I., & Tver'yanovich, E. V. (1993b). Linear louver heliostats of SES: Radiation losses. *Heliotechnics*, *5*, 54–57.

Teplyakov, D. I., & Tver'yanovich, E. V. (1993c). Linear louver heliostats of SES: Loss of energy production. *Heliotechnics*, *6*, 63–70.

Thein, L. W. (2010). *Research and development of automatic control systems for mobile solar energy power plants under prolonged shading conditions: abstract of a thesis*. Candidate of Technical Sciences: 05.13.06. Moscow.

Tikhonov, P. V. (2014). *Justification of parameters of a photoelectric thermal module* (Doctoral dissertation).

Tripanagnostopoulos, Y. (2008). Building integrated concentrating PV and PV/T systems. *Proceedings of the Eurosun*.

Tver'yanovich, E. V. (1981). Selection of design parameters of prism concentrators of solar radiation. *Heliotechnics*, *6*, 16–19.

Uvarov, V. V., Zhabo, V. V., & Rogankov, M. P. (1984). *Agricultural Heat Energy and the Environment*. Kolos.

Vorobiev, Y., Horley, P., & Gonzalez-Hernandez, J. (2005). Experimental and Theoretical Evaluation of the Solar Energy Collection by Tracking and Non-Tracking Photovoltaic Panel. *ISES 2005 Solar World Congress*, 6-12.

Zakharchenko, R., Licea-Jime'nez, L., Pe'rez-Garci'a, S. A., Vorobeiv, P., Carrasco, D. U., Pe'rez-Robels, J. F., & ... . (2004). Photovoltaic solar panel for a hybrid PV/thermal system. *Solar Energy Materials and Solar Cells*, *82*(1-2), 253–261. doi:10.1016/j.solmat.2004.01.022

Chapter 2
Theoretical Bases of the Use of Solar Concentrating Modules With Louvered Heliostats

ABSTRACT

A functional relationship was obtained linking the position of the Sun, the step of the mirror lamellae of the heliostat, and their orientation to ensure zero blocking and shading losses in the louvered heliostat. Based on the consideration of a three-dimensional problem, the algorithm for calculating the passage of sunlight through the mirror surface of the lamellae and parabolic cylinder allows calculating the flux of solar radiation on the receiving surface of the solar concentrator. An algorithm for controlling lamellar heliostat mirror lamellas has been developed that significantly increases the efficiency of a solar concentrator—using a louvre heliostat with a constant lamella pitch is equivalent to increasing the angular aperture of the concentrator from 26° to 70° without reducing the concentration ratio.

BAR-TO-BAR EFFECTS IN NON-TRACKING SOLAR CONCENTRATORS WITH LOUVERED HELIOSTATS

This section discusses the use of louvered heliostats in conjunction with non-tracking solar concentrators (Figure 2). The specificity of the non-tracking concentrator – a large angular aperture – allows you to freely change the direction of sunlight reflected from the lamellae within the limits specified by the aperture, which greatly expands the possibilities for controlling the geometry of the louvered heliostats.

DOI: 10.4018/978-1-7998-4276-7.ch002

Figure 1. Louver heliostat above the input surface of a solar concentrator

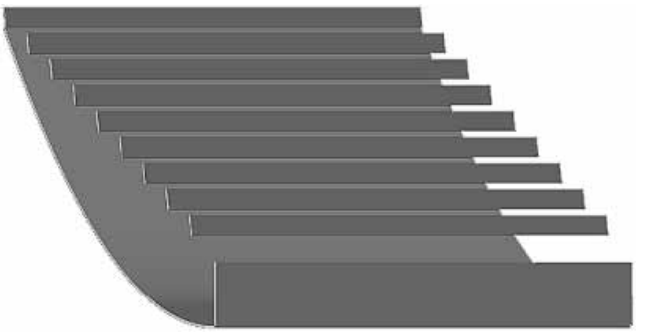

The control system must correct the inclination tilt and, perhaps, the distance between the mirror lamellae behind the movement of the Sun across the sky to minimize unwanted bar-to-bar effects, which lead to a loss of energy. The main results of the bar-to-bar effects are presented in (Strebkov, Irodionov, Filippchenkova, 2015).

Blocking and Shading

The profile of a non-tracking cylindrical solar concentrator with an angular aperture of 26°, a geometric concentration factor of 4.3, and the louver heliostat on the input surface is presented in Figure 2.2. All the numerical results below, including the graphs, are received for this solar concentrator.

Sunlight can potentially arrive on an input of the concentrator from any point of a hemisphere on its surface. The section of this hemisphere by the mirror plane of the concentrator is given in Figure 2, along with the section of the dihedral angle, which defines the aperture of the cylindrical solar concentrator. A part of the potential directions will be cut by the horizon plane during the inclined installation of the concentrator.

The correction of the direction by the mirror lamellae is required for the sunlight, the projections of which lie in zones *I* and *II*, i.e., outside the aperture of the concentrator. Sunlight from zone *I* arrives on the surface of the concentrator on the smaller dip angles, the solar radiant flux density at the input surface of the concentrator in these directions is higher and, therefore, the solar concentrator can be used more efficiently. The work of the louver heliostat will be considered in relation to the directions of sunlight from zone

Figure 2. Profile of the non-tracking solar concentrator with a louver heliostat

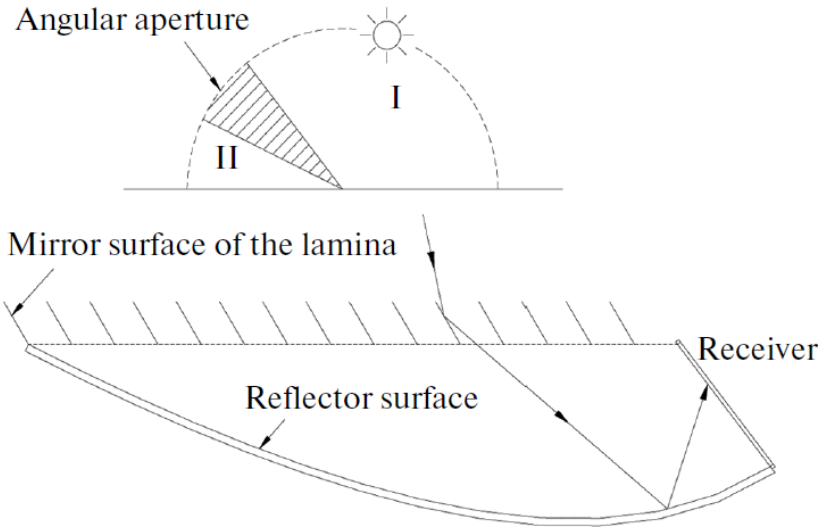

I; thus, the heliostat is oriented so that the mirror surface of the lamellae are turned towards the radiation receiver.

Using the louver heliostats is connected to the possible manifestation of a number of undesirable bar-to-bar effects, with the main ones being blocking, shading and the breakthrough of solar radiation.

The blocking effect is that a part of the reflected beams falls on the back side of the next lamina (Figure 2.3, 2.4). It is important for the prevention of this effect that the step between the next lamellae is not less than t_b (Figure 2.3, a).

By the sine law of:

$$\frac{b}{\sin\gamma} = \frac{t_b}{\sin\varepsilon}, \tag{2.1}$$

where b is the lamina width; t_b is the lamella step, which prevents blocking; γ is the descent angle of a reflected flux relative to the plane OO' (Figure 2.3 a) (the basic plane).

In turn, the angle ε can be presented as follows:

$$\varepsilon = 180 - \alpha - \gamma \tag{2.2}$$

or

$$\varepsilon = 90 - z - \gamma \tag{2.3}$$

where α is the angle between the mirror surface of the lamellae and the basic plane; and z *i*s the elevation angle of the normal to the mirror surface of the lamellae relative to the basic plane.

Then,

$$\frac{t_b}{b} = \frac{\cos\left(z+\gamma\right)}{\sin\gamma} \tag{2.4}$$

The shading effect of lamellae is manifested in the fact that each lamella obscures a part of the mirror surface of the adjacent lamella (Figure 3, 4). The minimum step between lamellae t_s (Figure 3 b), which allows to avoid shading, is determined as follows.

Similar to the previous one:

$$\frac{b}{\sin h} = \frac{t_s}{\sin\varphi}, \tag{2.5}$$

where h is the projection on the plane of symmetry of the heliostat angle between the direction to the Sun and the base plane, while $0 \le h \le 180°$.

Express the angle φ through the angles h and z

$$\varphi = 180 - \mathrm{h} - \theta \tag{2.6}$$

or

$$\varphi = 90 + (\mathrm{z} - h) \tag{2.7}$$

Then,

$$\frac{t_s}{b} = \frac{\cos\left(z-h\right)}{\sin h}. \tag{2.8}$$

From consideration of Figure 2.3 a it follows that

$$h = 2z + \gamma \tag{2.9}$$

The values of z are taken based on the sign.

Figure 3. Minimum admissible step of the lamellae for the prevention of the blocking (a) and shading effect (b) in the reflected radiation

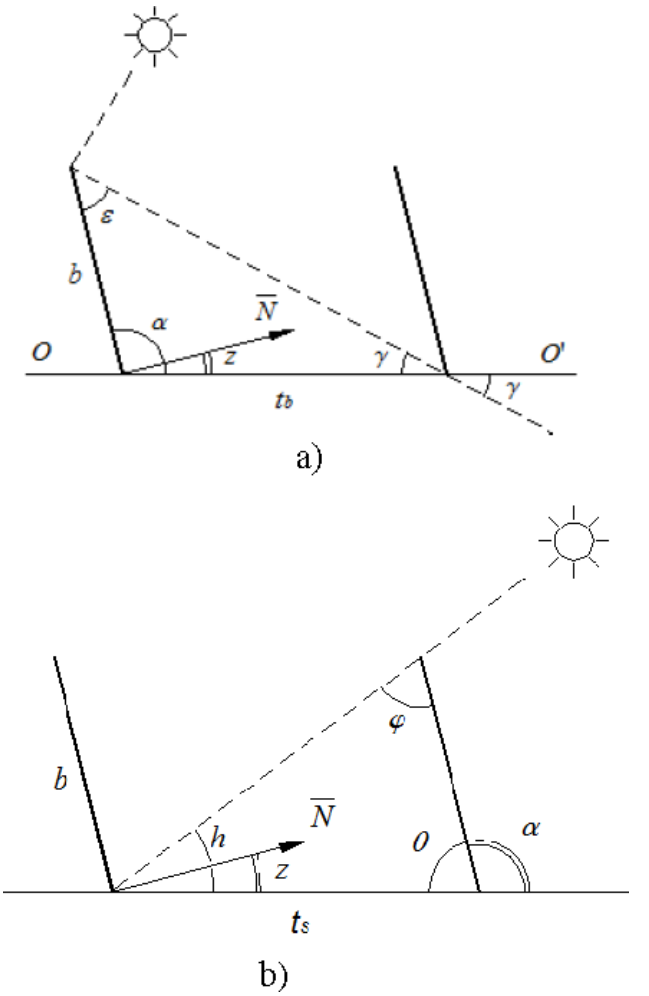

Then the minimum distance between the lamella to prevent shading of the mirror surfaces

$$t_s = b\frac{\cos(h-z)}{\sin h}, \tag{2.10}$$

and to prevent blocking

$$t_b = b\frac{\cos(h-z)}{\sin \gamma}. \tag{2.11}$$

The functional dependences of the minimum required relative steps of the lamellae $t/b = f(h,z)$ to prevent blocking and shading are presented in Figure 2.5, taking into account the allowable range of the angle γ. In this case, for the profile in Figure 2.2, the angle of decline of the rays γ reflected from the mirror lamellae should be within 26 ... 52 ° relative to the entrance surface of the concentrator. The sun rays from these directions after reflection on the main mirror surface of the concentrator fall on the receiver.

Analytical view of the dependence $h=f(z)$, connecting the height of the Sun h and the angle of inclination of the slats z to simultaneously prevent the effects of blocking and shading:

$$h = 2z + arctg\left(\frac{\cos z}{t_b / b + \sin z}\right) \tag{2.12}$$

Figure 4. The pattern of the passage of the rays in a solar concentrator with a louvered heliostat during shading (1) and blocking (2) mirror lamellas

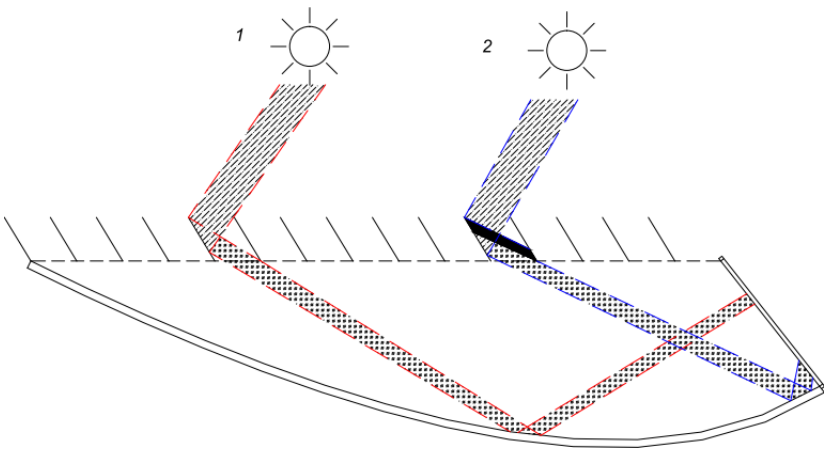

Figure 5. Relative lamella pitch to prevent blocking (a) and shading (b): t/b – relative lamella pitch, z – elevation angle normal to the mirror surface of the lamella relative to the base plane, h – projection of the angle between the direction to the Sun and the base plane

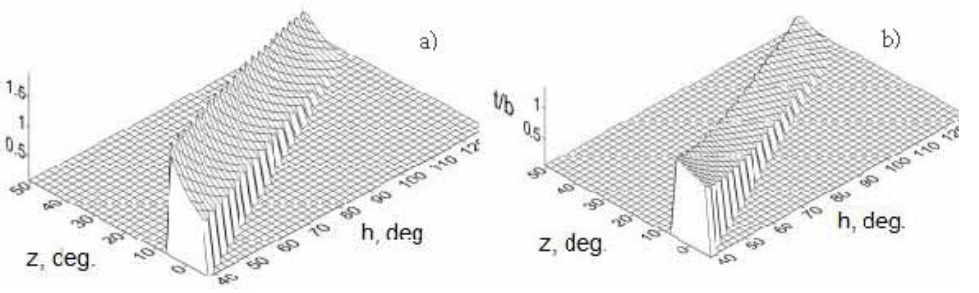

It is obvious that in order to simultaneously prevent blocking and shading, the actual lamella pitch at each of the set of points (h, z) should be equal to the largest of the corresponding t_b and t_s values. In this case, only at negative z angles the lamella pitch, which prevents shading t_s, is greater than the t_b pitch necessary to prevent blocking. The combined graph of the relative step of the lamellae – contour for ease of analysis – is shown in Figure 2.6. From consideration of Figure 2.6 it follows that the isoline 0,5 covers the range of angles h, characterizing the position of the Sun relative to the concentrator, from 84° to 128°. This means that in the specified range, in order to prevent blocking and shading, there is no need to change the lamella pitch, it is enough to correct only their tilt angle with a constant relative lamella pitch

The angle of 128° is of particular importance in this case - it is the boundary of zone *I* (Figure 2.2) at the junction with the dihedral angle of the concentrator aperture. In the range of 128°£ h £ 154°, the sun's rays directly fall within the angular aperture. The task of the heliostat in this case is not to hinder the passage of light to the entrance surface of the concentrator, for which the lamellae should be oriented parallel to the sun's rays, i.e. $z=h-90$.

Thus, the use of a louvered heliostat with a constant lamella pitch and with a relatively simple control algorithm is equivalent to an increase in the angular aperture of the concentrator from 26° to 70°.

If necessary, the heliostat with a variable pitch of mirror lamellae should be used to further extend the active work time of the concentrator. To prevent blocking and shading at angles h smaller than 84° it is necessary to increase the lamella pitch. For example, go to contour 1,0 (Figure 6), covering the interval 44°£ h £ 98°.

Figure 6. Relative lamella pitch to simultaneously prevent shading and blocking effects

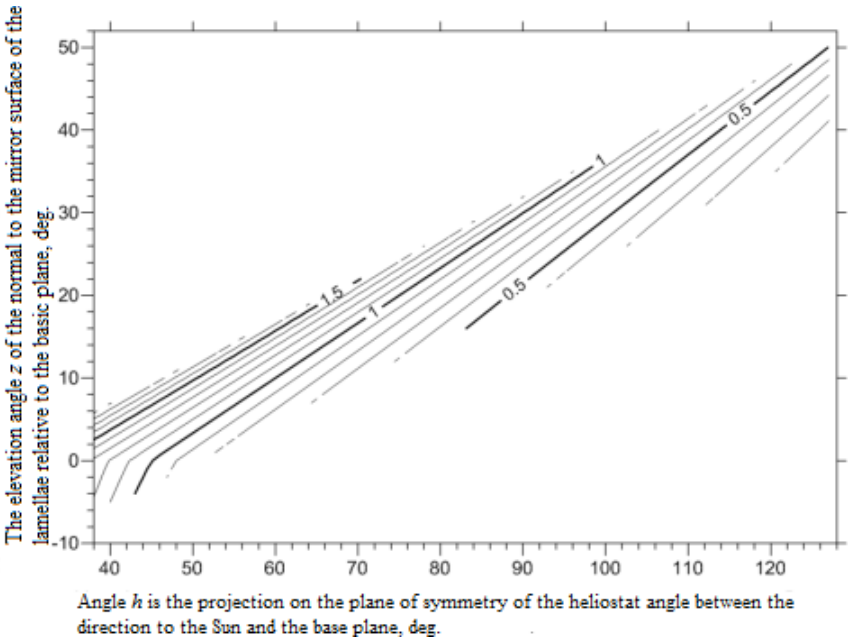

Breakthrough of Solar Radiation

It is obvious that the breakthrough of solar radiation past the lamellae of the louvered heliostat (strip *AB* in Figure 7) can only be in the absence of shading of the lamellae, i.e. at the lamella step $t>t_s$. The result is a desire to simultaneously prevent blocking and shading of the lamellae at $t_b>t_s$. As the analysis shows, in practically important cases, the condition $z>0$ is sufficient to satisfy this inequality.

If $z<0$, then $t_s>t_b$ and then there is no shading, blocking and «breakthrough» of radiation, but unlit *BC* bands appear on the surface of the concentrator input (Figure 8). The appearance of unlit bands may cause a decrease in the output power of the module as a result of greater irregularity of solar radiation on the surface of the receiver.

The simultaneous absence of all bar-to-bar effects: shading, blocking, breakthrough of solar radiation and unlit bands can be only if $t_s=t_b$ and, therefore, for $z=0$, i.e. when turning the plates along the normal to the surface of the concentrator inlet.

Figure 7. The effect of breakthrough of solar radiation past the lamellas of a louvered heliostat

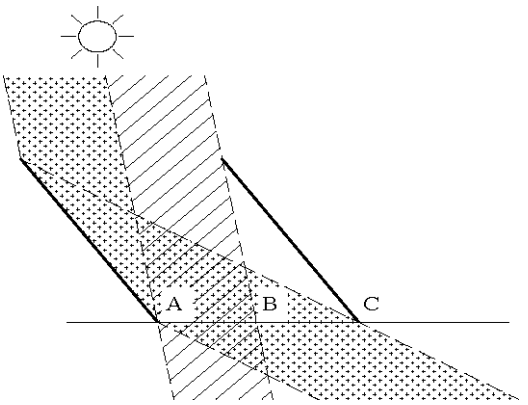

Figure 8. Unlit bands on the entrance surface of a solar concentrator with a louvered heliostat

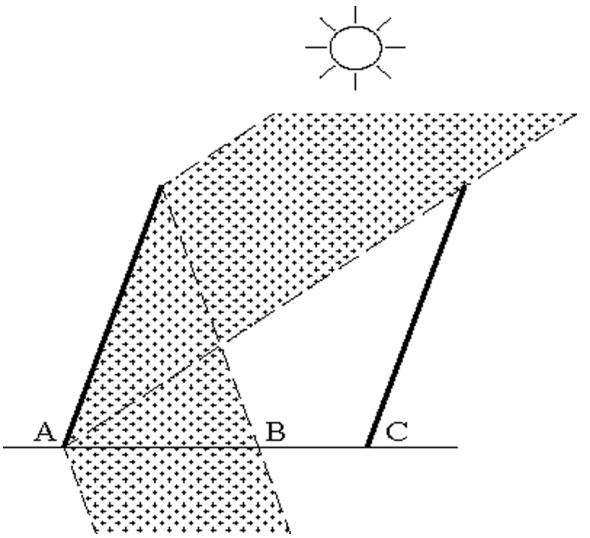

The sun rays passing through the *AB* band (Figure 7) do not change their original direction and, as a result, are scattered by the mirror system of the concentrator without falling on the receiver.

The minimum, in the absence of other bar-to-bar effects, the width of the solar radiation transmission band at the entrance surface $\Delta = AB$ (Figure 7) is equal to:

$$\Delta = t_b - t_s = b\cos(h-z)\left(\frac{1}{\sin\gamma} - \frac{1}{\sin h}\right). \tag{2.13}$$

It is obvious that energy losses due to the effect breakthrough of solar radiation are proportional to Δ and depend on the position of the Sun and the relative step of the lamellae. The calculation results are shown in Figure 9.

Possible energy losses are considerable, especially with increasing angle values. h.

Figure 9. Energy loss due to the effect of transmission of solar radiation

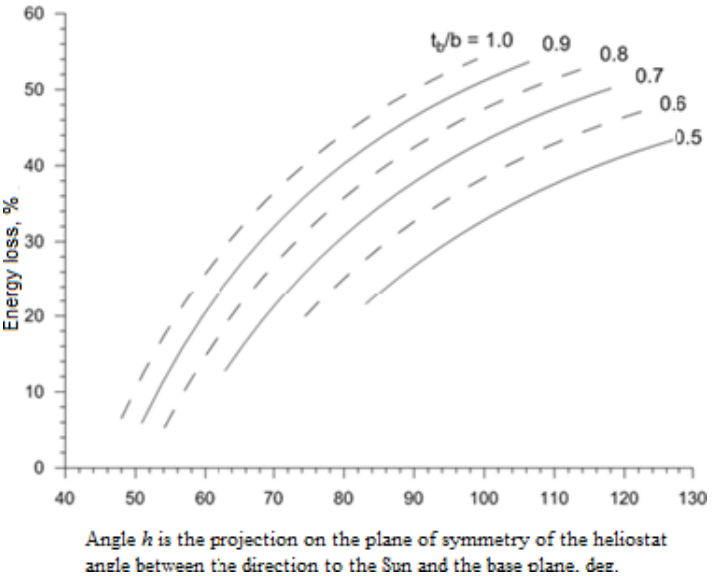

AN ALGORITHM FOR CALCULATING THE SOLAR RADIATION FLUX ON THE RECEIVING SURFACE OF A NON-TRACKING PARABOLIC-CYLINDER CONCENTRATOR WITH A LOUVERED HELIOSTAT

In this section, based on the consideration of a practically important three-dimensional problem, an algorithm is developed for calculating the solar radiation flux on the receiving surface of a non-tracking parabolic cylindrical solar concentrator with a louvered heliostat, presented in (Strebkov, Irodionov, Filippchenkova, 2017).

Coordinate Systems and Directional Vectors of Solar Rays

If the *XOY* plane of the coordinate system coincides with the plane of the celestial equator, and the *OY* axis is directed to the south (Figure 10), the coordinates of the unit vector $\bar{L}$ that specifies the direction of solar rays are written as:

$$X = -\cos\delta \sin\omega;\ Y = -\cos\delta \cos\omega;\ Z = -\sin\delta, \tag{2.14}$$

where δ is the solar declination and ω is the hour angle.

Figure 10. Equatorial coordinates of the Sun and the directional vector of solar rays

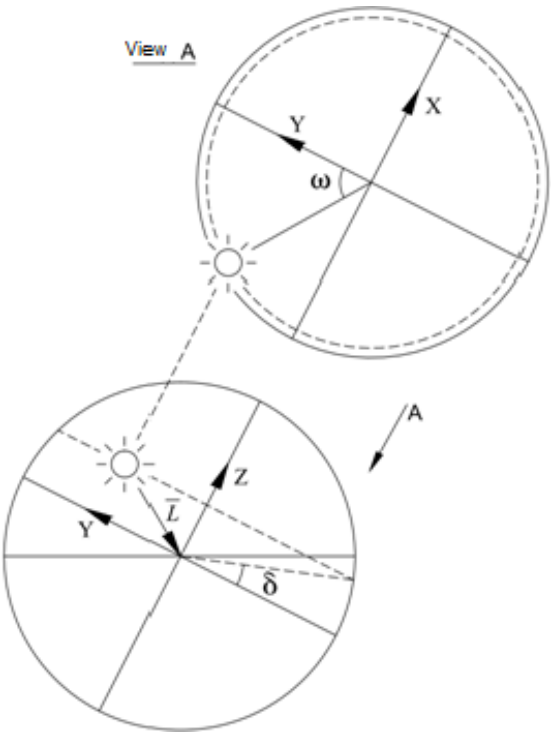

In turn,

$$\omega = 15(ts\_h\_12), \tag{2.15}$$

where ts_h is the true solar time, hours.

Relations between vectors that determine the direction of incident and specularly reflected solar radiation are determined.

Figure 11 shows a unit circle that is found in the same plane with the vectors $\bar{L}$ (the incident solar ray) and $\bar{N}$ (the normal to the mirror surface).

It follows from Figure 2.11 that the reflected ray vector $\bar{L}_r$ is calculated as

$$\bar{L}_r = \bar{L} + \bar{D}. \tag{2.16}$$

In turn,

$$\bar{D} = 2\sin(\vartheta - 90)\bar{N}. \tag{2.17}$$

And finally there is

$$\bar{L}_r = \bar{L} - 2\bar{N}\cos\vartheta. \tag{2.18}$$

Figure 11. Determination of the direction of a specularly reflected ray

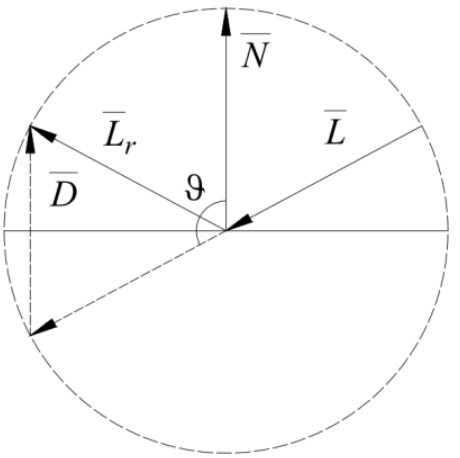

According to (Korn & Korn, 1973), the cosine of the angle between the unit vectors $\bar{L}$ and $\bar{N}$ is equal to

$$\cos\vartheta = XL_X N + YL_Y N + ZL_Z N, \tag{2.19}$$

where X_L, Y_L, Z_L, X_N, Y_N, Z_N – respectively coordinates of unit vectors $\bar{L}$ and $\bar{N}$.

It is noted that the surface with the normal $\bar{N}$ is lighted by solar rays along the direction $\bar{L}$ if $\cos\vartheta<0$.

It is considered the path of the rays reflected from the mirror surface of the parabolic trough concentrator (Figure 2.12).

In the coordinate system (Figure 2.12), the equation of a parabola with the focal parameter p has the following form:

$$z^2 = 2py \tag{2.20}$$

Differentiating expression (2.20), is obtained:

$$y' = z / p. \tag{2.21}$$

It is represented the coordinates of the normal vector $\bar{N}_p$ to the reflecting surface of the concentrator as:

$$X_{Np} = 0;\ Y_{Np} = \cos\varepsilon = \frac{1}{\sqrt{1+\mathrm{tg}^2\varepsilon}};\ Z_{Np} = -\sin\varepsilon = -\frac{\mathrm{tg}\varepsilon}{\sqrt{1+\mathrm{tg}^2\varepsilon}}, \tag{2.22}$$

where X_{Np}, Y_{Np}, Z_{Np} –respectively coordinates of unit vector $\bar{N}_p$.

Since $\mathrm{tg}\varepsilon = y'$, finally:

$$X_{Np} = 0;\ Y_{Np} = \frac{p}{\sqrt{p^2+z^2}};\ Z_{Np} = -\frac{z}{\sqrt{p^2+z^2}}. \tag{2.23}$$

The coordinate systems for which is derived expressions (2.14) and (2.23) do not coincide in the general case. They are most frequently turned through the angle ξ (Figure 13) around the *OX* axis relative to each other.

In figure 13 marked: β – angle of inclination of the inlet surface of the concentrator to the horizon, deg., φ – latitude, deg., μ – edge angle of parabolic-cylinder concentrator, deg., $OY_K Z_K$ – coordinate system associated with parabolic-cylinder concentrator.

Figure 12. Profile of a parabolic cylindrical reflector

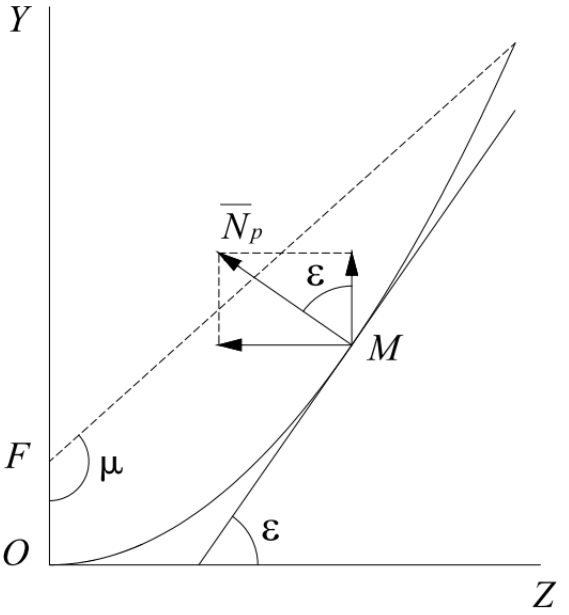

Figure 13. Determination of the angle of rotation of the coordinate system associated with a parabolic-cylinder concentrator

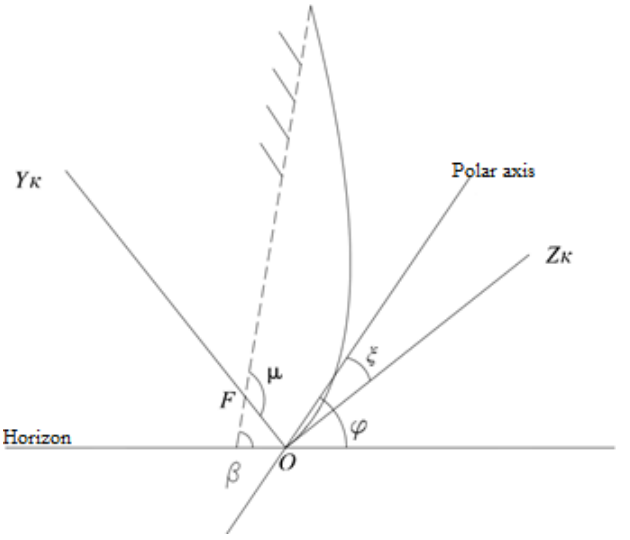

The transformation of the coordinates during the rotation of the axes may be expressed as the following (Korn, Korn, 1973):

$$\begin{pmatrix} x \\ y \\ z \end{pmatrix} = \begin{pmatrix} i\tilde{i} & \tilde{ij} & i\tilde{k} \\ j\tilde{i} & \tilde{jj} & j\tilde{k} \\ k\tilde{i} & \tilde{kj} & k\tilde{k} \end{pmatrix} \begin{pmatrix} \tilde{x} \\ \tilde{y} \\ \tilde{z} \end{pmatrix}, \tag{2.24}$$

where nine scalar products express the cosines of the angles between the coordinate axes. If the coordinate systems are turned through the angle ξ around the common *OX* axis, the cosine matrix can be written as:

$$\begin{pmatrix} 1 & 0 & 0 \\ 0 & \cos\xi & \sin\xi \\ 0 & -\sin\xi & \cos\xi \end{pmatrix}. \tag{2.25}$$

Then, the coordinates of the solar ray vector in the coordinate system associated with the parabolic trough concentrator will be the following:

$$\begin{cases} X_L = -\cos\delta \sin\omega, \\ Y_L = -\cos\delta \cos\omega \cos\xi - \sin\delta \sin\xi, \\ Z_L = \cos\delta \cos\omega \sin\xi - \sin\delta \cos\xi. \end{cases} \tag{2.26}$$

According to expression (2.19), for the cosine of the angle between the vectors $\overline{N}_p$ and $\overline{L}$, writed the expression:

$$\cos\vartheta_p = \frac{pY_L - zZ_L}{\sqrt{p^2 + z^2}} \tag{2.27}$$

In this case, the directional vector of the reflected solar ray $\overline{L}_r$ has the coordinates (see expression (2.18)):

$$\begin{cases} X_{rp} = X_L, \\ Y_{rp} = Y_L - \dfrac{2p}{\sqrt{p^2 + z^2}} \cos\vartheta_p, \\ Z_{rp} = Z_L + \dfrac{2z}{\sqrt{p^2 + z^2}} \cos\vartheta_p \end{cases} \tag{2.28}$$

Trajectories of Solar Rays Reflected From the Lamellae

It is studied the operation of a louvered heliostat, representing a system of flat mirrors, lamellae, sized $l \times b$ (length × breadth), which are mounted on the entry surface of the concentrator with the step t at the angle α to the entry surface (Figure 14).

The normal vector to the mirror surface of the lamella (the heliostat) has the following coordinates:

$$X_{Nh}=0;\ Y_{Nh}= -\sin(\mu-\alpha);\ \mathrm{ZN}h_{=} -\cos(\mu-\alpha), \tag{2.29}$$

where μ is the boundary angle of the parabolic trough concentrator (Figure 14).

Figure 14. Louvered heliostat at the entry surface of the concentrator

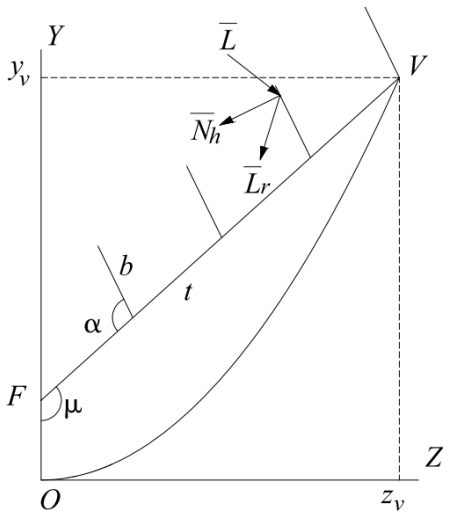

Then, in accordance with expression (2.19) for the cosine of the angle between the normal vector to the heliostat surface $\bar{N}_h$ and the solar ray $\bar{L}$, is writed:

$$\cos\vartheta = -YL_s\text{in}(\mu-\alpha) - \text{ZLco}_s(\mu-\alpha) \tag{2.30}$$

Consequently, the solar ray reflected from the lamella has the following coordinates:

$$\begin{cases} X_{rh} = X_L; \\ Y_{rh} = Y_L + 2\cos\vartheta_h \sin\left(\mu-\alpha\right); \\ Z_{rh} = Z_L + 2\cos\vartheta_h \cos\left(\mu-\alpha\right), \end{cases} \tag{2.31}$$

where $\text{X}r_{h,}$ $\text{Y}r_{h,}$ $\text{Z}r_h$–respectively coordinates of unit vector $\bar{N}_h$.

According to (Vygodskii, 1963), the equation of the straight line passing through any point *D* in the direction of the reflected ray $\bar{L}_r$ is expressed as:

$$\frac{x-x_D}{X_{rp}} = \frac{y-y_D}{Y_{rp}} = \frac{z-z_D}{Z_{rp}} = k. \tag{2.32}$$

At the point of intersection of the straight line (2.32) with the parabolic trough concentrator (2.20), parameter *k* is equal to:

$$k = \frac{p}{Z_{rp}}\left[\frac{Y_{rp}}{Z_{rp}} \mp \sqrt{\left(\frac{Y_{rp}}{Z_{rp}}\right)^2 - \frac{2}{p}\left(z_D\frac{Y_{rp}}{Z_{rp}} - y_D\right)}\right] - \frac{z_D}{Z_{rp}}. \tag{2.33}$$

If the point *D* is found on the surface of the parabolic trough concentrator, $k = 2(pY_{rp}/Z_{rp} - z_D)/Z_{rp}$, taking into account the relationships between the coordinates y_D and z_D; if in point *D* lies on the lamella surface, the sign in expression (2.33) is determined from the condition that the coordinate of the point of intersection of the ray and the parabolic trough is $z<z_D$.

When this straight line intersects the focal plane of the parabolic trough concentrator ($z=0$), the expression is strongly simplified and takes the form

$$k = -\frac{z_D}{Z_{rp}}. \tag{2.34}$$

In the given coordinate system, the shape of the trajectory of the solar ray passing over the mirror surface of the parabolic trough concentrator is invariant relative to the X coordinate of the initial point of the trajectory. Such geometry makes it possible to increase the computational efficiency of the method if is considered that the light passes across the concentrator as whole bands in parallel to the generator of the parabolic trough. If is assumed that the lateral (narrow) sides of the band are also the segments of the straight lines, the position and the shape of the lighted band on the receiver surface are fully determined by the coordinates of the two apices on one of its lateral sides. In turn, the coordinates of these apices are determined by the trajectories of two solar rays from their first reflection on the lighted edge of the mirror surface (the edge $x = 0$ or $x = l$, which depends on the Sun's position) and to the receiver surface. The distance between the initial points of these trajectories is chosen arbitrarily on the basis of the required calculation accuracy.

For trajectories 1 and 2, the coordinates of the points of intersection of the reflected rays and the concentrator surfaces are calculated by the following recurrence relations ($i \geq 0$):

$$\begin{cases} {}^1x_{i+1} = {}^1k_i\left({}^1X_r\right)_i + {}^1x_i; \\ {}^1y_{i+1} = {}^1k_i\left({}^1Y_r\right)_i + {}^1y_i; \\ {}^1z_{i+1} = {}^1k_i\left({}^1Z_r\right)_i + {}^1z_i. \end{cases}$$

$$\begin{cases} {}^2x_{i+1} = {}^2k_i\left({}^2X_r\right)_i + {}^2x_i; \\ {}^2y_{i+1} = {}^2k_i\left({}^2Y_r\right)_i + {}^2y_i; \\ {}^2z_{i+1} = {}^2k_i\left({}^2Z_r\right)_i + {}^2z_i. \end{cases} \tag{2.35}$$

The calculation is performed consecutively, starting from the lamella which is farthest from the receiver.

The calculation is continued by the recurrent formulas (2.35) until the both rays reach the receiver surface. If at a certain calculation step a light

band simultaneously illuminates the receiver and the reflector, it is required to find an initial point of the trajectory that leads to the point with the coordinates $\{z,0,0\}$ at this step using the interpolation and then to consider two independent light bands.

If after the i th reflection the light band is incident on the plane Z=0, according to [2.4], at this moment, its area (an unoriented quadrangle) is equal to:

$$S_b = \frac{1}{2}\left\| \begin{vmatrix} {}^1x_i & {}^1y_i \\ {}^2x_i & {}^2y_i \end{vmatrix} + \begin{vmatrix} {}^2x_i & {}^2y_i \\ {}^2x_i + l & {}^2y_i \end{vmatrix} + \begin{vmatrix} {}^2x_i + l & {}^2y_i \\ {}^1x_i + l & {}^1y_i \end{vmatrix} + \begin{vmatrix} {}^1x_i + l & {}^1y_i \\ {}^1x_i & {}^1y_i \end{vmatrix} \right\|. \tag{2.36}$$

The Sun is outside the plane of the concentrator midsection most of the time; as a result, the light band is displaced along the OX axis and a part of the solar flux passes by the receiver. The area of the lighted band on the receiver surface is expressed as

$$S_t = \frac{1}{2}\left\| \begin{vmatrix} {}^1x_i & {}^1y_i \\ {}^2x_i & {}^2y_i \end{vmatrix} + \begin{vmatrix} {}^2x_i & {}^2y_i \\ l & {}^2y_i \end{vmatrix} + \begin{vmatrix} l & {}^2y_i \\ l & {}^1y_i \end{vmatrix} + \begin{vmatrix} l & {}^1y_i \\ {}^1x_i & {}^1y_i \end{vmatrix} \right\|. \tag{2.37}$$

The solar radiation flux on each lamella is

$$w_h = -El(b/m_h)\cos\vartheta\mathrm{h}, \tag{2.38}$$

where E is the density of the solar radiation flux across the surface perpendicular to the ray; m_h – quantity of the initial bands fit in the width of the mirror lamella.

Then, the solar radiation flux on the receiver surface has the form:

$$w_t = w_h \frac{S_t}{S_b}\rho^i, \tag{2.39}$$

where ρ is the coefficient of solar light reflection from the mirror surface.

In some cases, a light band can degenerate into a triangle or can be completely displaced beyond the receiving surface of the module.

It is evident that the total flux of solar energy on the receiver surface is equal to the sum of the fluxes from the lighted bands on all of the lamellae $W_t = \sum_{n,m} w_t$.

Figure 15 shows the block diagram for calculating the flux of solar radiation on the receiving surface of the concentrator.

Figure 15. A block diagram of the algorithm for calculating the flux of solar radiation on the receiving surface of the concentrator

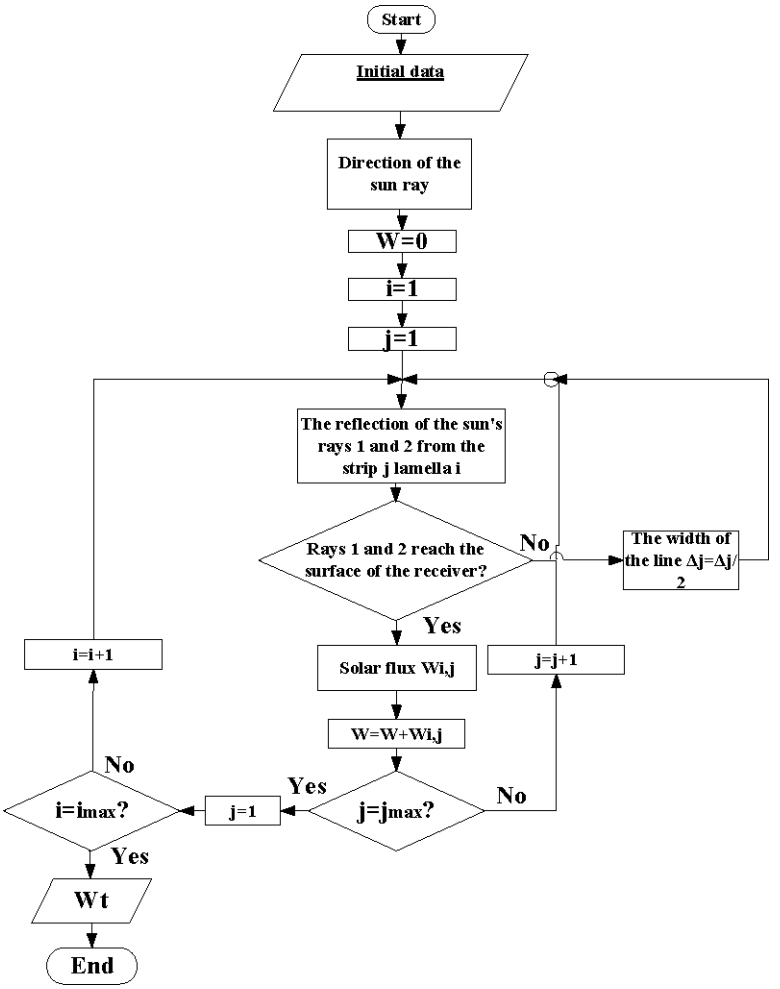

Direct Passage of Solar Rays to the Mirror Surface of the Parabolic Trough

If solar rays are incident directly within the angular aperture, a heliostat must not interfere with the passage of light to the entry surface of the concentrator; for this purpose, the lamellae should be oriented in parallel to solar rays. In this case, a solar ray is first reflected on the mirror surface of the parabolic trough.

The length of the directrix of the parabolic trough is expressed by the curvilinear integral (Korn, Korn, 1973).

$$S = \int_0^{z_v} \sqrt{1+\left(y'\right)^2}\,dz = \frac{1}{p}\int_0^{z_v} \sqrt{p^2+z^2}\,dz = \frac{z_v}{2p}\sqrt{p^2+z_v^2} + \frac{p}{2}\ln\left(\frac{z_v+\sqrt{p^2+z_v^2}}{p}\right). \tag{2.40}$$

If it is splited the directrix of the parabolic trough into m_p equal arcs with the length $\Delta s = S/m_p$ and start from $\left({}^1z_{m=1}\right)_0 = 0$, then the boundaries of the bands, which are the initial points of the trajectories, are determined from the following equation:

$$\left({}^2z_m\right)_0\sqrt{p^2+\left({}^2z_m\right)_0^2} + p^2\ln\left[\left({}^2z_m\right)_0 + \sqrt{p^2+\left({}^2z_m\right)_0^2}\right] = C, \tag{2.41}$$

where

$$C = 2p\Delta s + \left({}^1z_m\right)_0\sqrt{p^2+\left({}^1z_m\right)_0^2} + p^2\ln\left[\left({}^1z_m\right)_0 + \sqrt{p^2+\left({}^1z_m\right)_0^2}\right]. \tag{2.42}$$

It is evident that the X coordinates of the initial points of the trajectories of the reflected solar rays are equal to zero or the width of the parabolic trough l with respect to the Sun's position, and the Y coordinates are calculated by the equation of a parabola (2.20).

The solar radiation flux that is incident on the surface of the parabolic trough is described by the equation:

$$w_p = -El\int\limits_{(\Gamma)} \cos\vartheta_p ds \tag{2.43}$$

By substituting the value of cosϑp from (2.27) into expression (2.43), after elementary transformations for the band m on the surface of the parabolic trough, it is obtained

$$\left(w_p\right)_m = -\frac{El}{p}\int\limits_{\left({}^1z_m\right)_0}^{\left({}^2z_m\right)_0}\left(pY_L - zZ_L\right)dz = El\left\{\frac{Z_L}{2p}\left[\left({}^2z_m\right)_0^2 - \left({}^1z_m\right)_0^2\right] - Y_L\left[\left({}^2z_m\right)_0 - \left({}^1z_m\right)_0\right]\right\}. \tag{2.44}$$

In other respects, the procedure for calculating the passage of a light band across the mirror surface of the solar concentrator is the same as for the light reflected from the heliostat lamellae in the previous sections.

In addition, under the above conditions, a part of the solar rays may hit the receiving surface of the module, creating a radiation flux on it without additional reflections:

$$w_{td} = -El\frac{p}{2}Z_L. \tag{2.45}$$

ORIENTATION OF NON-TRACKING SOLAR CONCENTRATOR WITH LOUVERED HELIOSTAT

One of the most important criteria for the optimal design and efficient use of a non-tracking solar concentrator with a louvered heliostat is the daily duration of its operation during a year.

In (Bazarova, Strebkov, Irodionov et al., 2008), the duration of the daily operation of a non-tracking parabolic-cylindrical solar concentrator with angular parameters 48x24 is determined, which is set so that the angle of inclination of the entrance surface is equal to the latitude of the installation site. Without adjusting the position of the concentrator, the duration of its work in the summer period will be 2-4 hours, which is clearly not enough. Also in (Bazarova, Strebkov, Irodionov et al., 2008) it was shown that to ensure the duration of the concentrator operation in the summer period up to 8-10 hours

and 4-6 hours in the winter, an adjustment of the angle of inclination of the entrance surface to the horizon in the summer and winter season is necessary.

Determination of the Duration of the Solar Module with a Parabolic-Cylinder Concentrator and a Deflecting Optical System Based on Louvered Heliostats

Figure 15 presents the cross section of the celestial sphere and the diurnal course of the sun with a certain declination (Filippchenkova, Strebkov, 2016).

Whether the sun beam hits the receiver is determined by the projection of the vector $\vec{CL}$ (Figure 15), which sets the direction of the sun's rays, onto the transverse plane of the concentrator. At the southern orientation, the transverse plane of the concentrator coincides with the plane of the celestial meridian.

There is the following relationship:

$$tg\delta = tg\alpha \cos \vartheta, \tag{2.46}$$

where ϑ – the angle between the circle of declination of the sun and the celestial meridian, deg.; α – the angle between the desired vector $\vec{CL}$ projection and the celestial equator, deg.; δ – declination, deg.

$$\vartheta = 15 \bullet (12 - t), \tag{2.47}$$

where t – true solar time, hour.

Declination can be found from the Cooper equation:

$$\delta = 23,45 \cdot \sin\left(360 \cdot \frac{284 + n}{365}\right), \tag{2.48}$$

where n – day number of the year.

In Figure 16a, the aperture angle of an unwalking solar concentrator with a louvered heliostat is plotted on the plane of the celestial meridian. The concentrator is set at an angle equal to the local latitude - the plane of the receiver coincides with the plane of the celestial equator (summer position).

In order for the sunlight to be concentrated on the receiver, the projection of the vector defining the direction to the Sun must fall into the shaded sector

(aperture angle of the concentrator). In accordance with the expression (2.46) on the day of the summer solstice ($\delta = 23{,}45°$, $\alpha = 24°$) the sun rays will fall on the receiver from 6 h 37 m to 17 h 22 m (true solar time).

In the period from March 22 to September 18 ($\delta > 0°$) the duration of the concentrator operation is at least 10 hours / day. From September 19 to March 21 ($\delta 0°$) to ensure the duration of the concentrator at least 10 hours / day, an adjustment of the angle of inclination of the entrance surface is necessary. Figure 16b shows the movement of the Sun relative to the concentrator for the winter position.

Development of a Control Algorithm for Louver Heliostat

Previously it was shown that the duration of operation of a non-tracking solar concentrator with a louvered heliostat installed on the entrance surface, with seasonal adjustment of the angle of inclination of the entrance surface of the concentrator to the horizon β will be at least 10 hours / day. Let us determine the dependence of the angle of inclination of the lamellas of the louvered heliostat on the angle of inclination of the surface of the concentrator entrance.

Figure 16. The cross section of the celestial sphere and the daily path of the sun

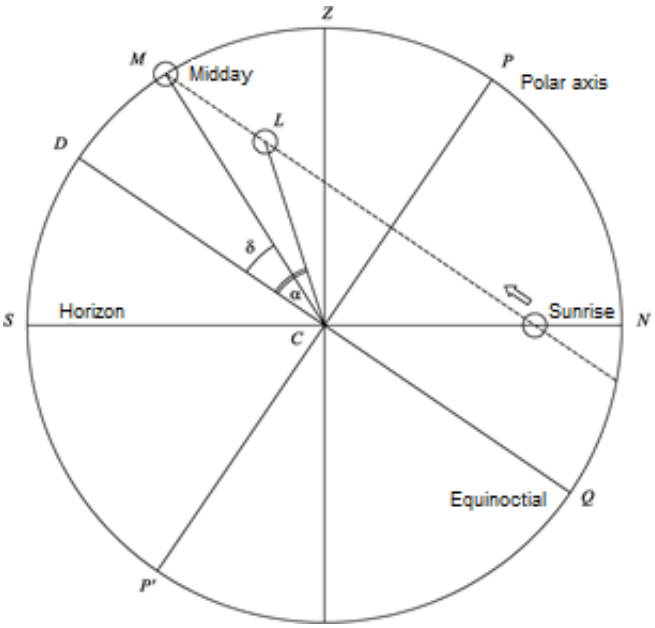

Recall that *h* denotes the projection of the angle onto the plane of symmetry of the heliostat between the direction to the Sun and the reference plane (Figure 2.3). Figure 2.17 shows a diagram of the passage of sunlight for the three possible directions of the vector $\bar{L}$.

Based on Figure 2.17, the angle *h*:

$$h = \mu + arctg\left(\frac{Z_L}{Y_L}\right) \tag{2.49}$$

where μ is the boundary angle of the parabolic trough concentrator.

Figure 17. Heavenly meridian and aperture angle of the solar concentrator with louvered heliostat (a - summer position, b - winter position)

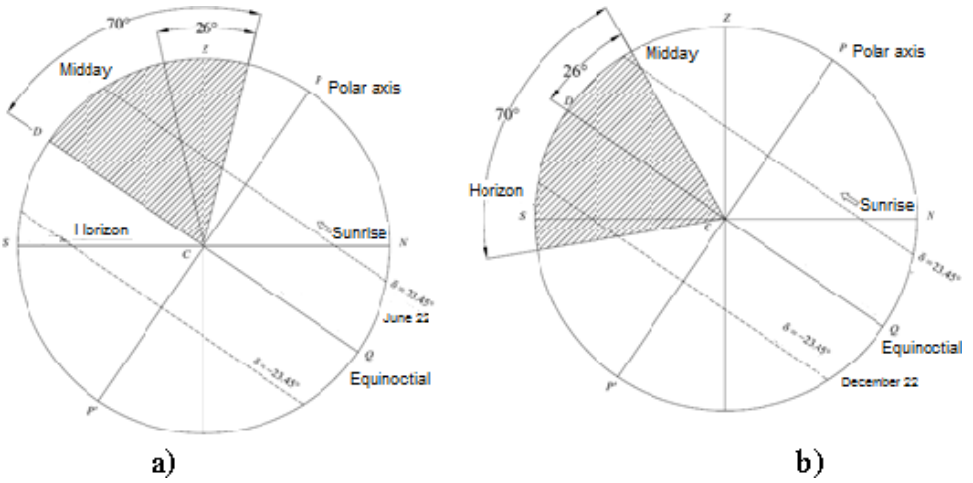

As shown in Figure 13, the angle of rotation of the coordinate system associated with a parabolic-cylinder concentrator can be found as follows:

$$\xi = \mu - \beta - 90° + \phi \tag{2.50}$$

where β– *a*ngle of inclination of the inlet surface of the concentrator to the horizon, deg.;φ – latitude, deg.

Knowing the angle h, according to the dependences of the relative pitch of the slats obtained in Section 2.1 to simultaneously prevent the effects

of shading and blocking, it is easy to determine the angle of inclination of the mirror slats for a specific time of day. A program for calculating the coordinates of the sunbeam and, accordingly, the angle of inclination of the lamellae depending on the day of the year, time of day, latitude / longitude of the terrain, contact angle and angle of inclination of the surface of the entrance of the concentrator, has been implemented to develop an algorithm for managing the louver heliostat system.

Figure 19 provides a flowchart of a program for calculating schedules for controlling the angle of inclination of the heliostat slats to prevent blocking and shading.

Figure 18. Diagram of the passage of rays through the louvered heliostat

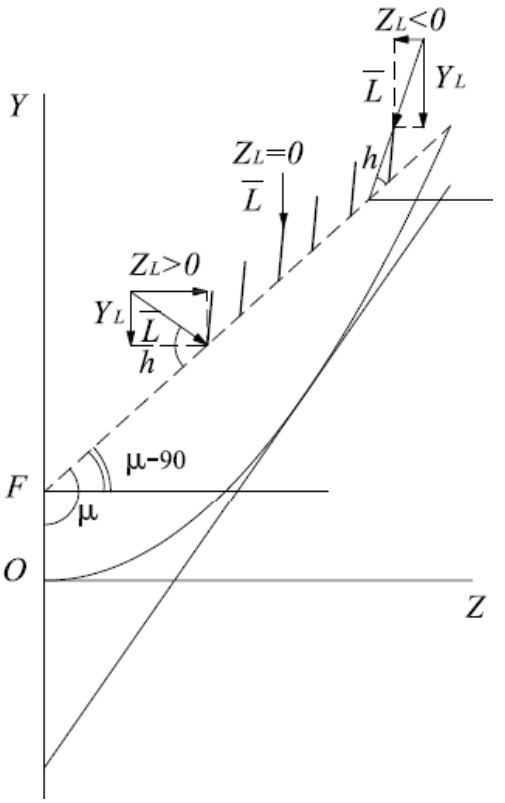

To illustrate the work of the program, Figure 20-23 presents calculated graphs for a parabolic-cylinder concentrator with an angular aperture of 18° and 26°, set at an angle of 90° to the horizon (Moscow latitude).

Figure 19. The block diagram of the program for calculating the graphs of regulation of the angle of inclination of the heliostat slats

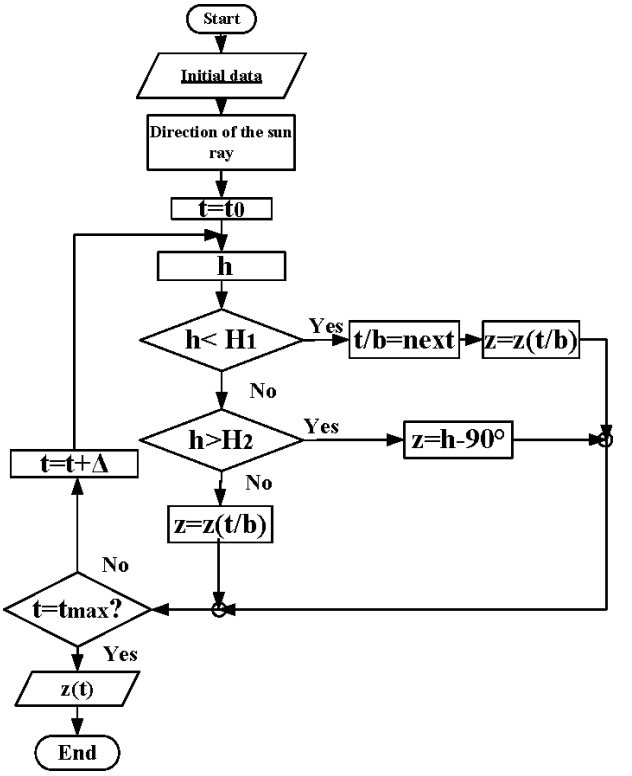

Figure 20. Dependence of the angle of inclination of lamellar lamellas of a heliostat on the time of day for a parabolic-cylinder concentrator with an angular aperture of 26° (data for the periods October-March)

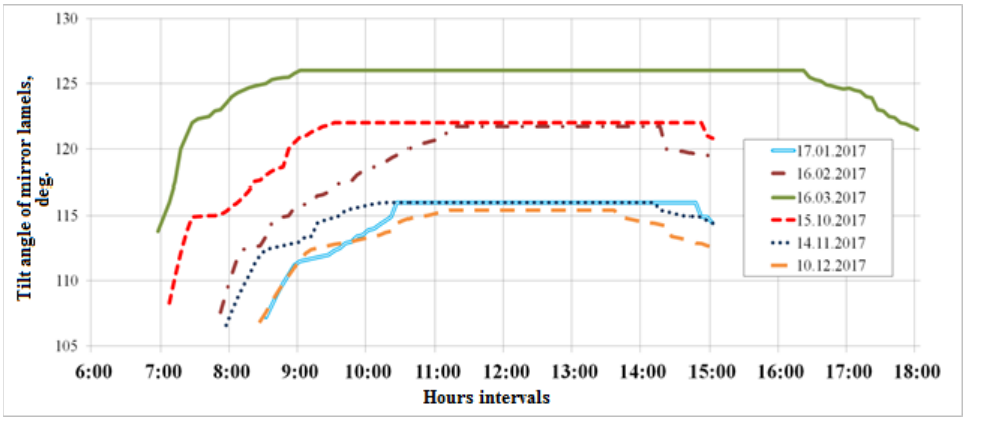

It should be noted that in buildings designed for construction in areas with an average monthly temperature of July 21° C and above (such areas include the entire South of Russia), in premises with a permanent stay of people and rooms where, according to technological and hygienic requirements, solar rays or overheating, light openings with orientation within 130–315° should be equipped with a sun shade. To protect window openings oriented to the southern sector of the horizon from excessive insolation, it is recommended to arrange external horizontal blinds, awnings, awnings, canopies and other sun-protection elements (Shevchenko, 1998). For the designed construction of the concentrating module, it is possible to install it on the facade of the building at an angle of 90° («vertical wall»), which will make it possible to more harmoniously fit the concentrator into the architectural concept of the building without deteriorating its appearance (Strebkov, Irodionov, Filippchenkova, 2017).

CONCLUSION

A functional relationship was obtained linking the position of the Sun, the step of the mirror lamellae of the heliostat and their orientation to ensure zero blocking and shading losses in the louvered heliostat.

Figure 21. Dependence of the angle of inclination of lamellar lamellae of the heliostat on the time of day for a parabolic-cylinder concentrator with an angular aperture of 26 ° (data for the periods April-September)

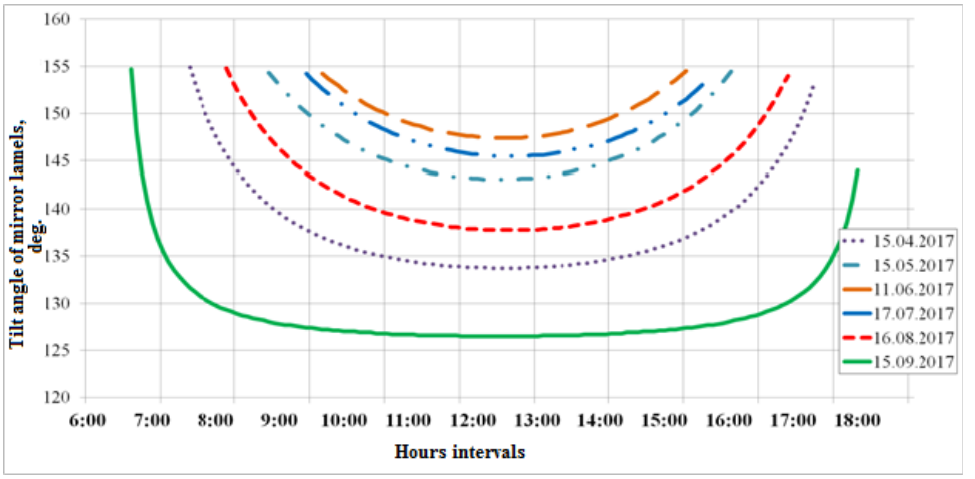

Figure 22. Dependence of the angle of inclination of lamellar lamellas of the heliostat on the time of day for a parabolic-cylinder concentrator with an angular aperture of 18 ° (data for the periods October-March)

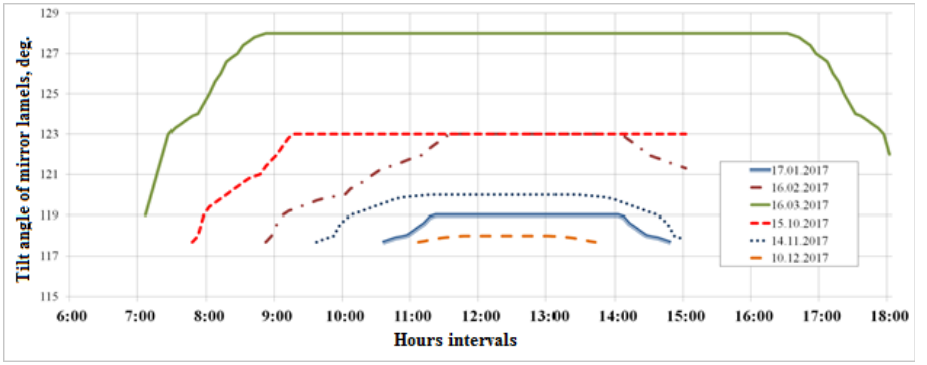

Figure 23. Dependence of the angle of inclination of the lamellar lamellae of the heliostat on the time of day for a parabolic-cylinder concentrator with an angular aperture of 18 °

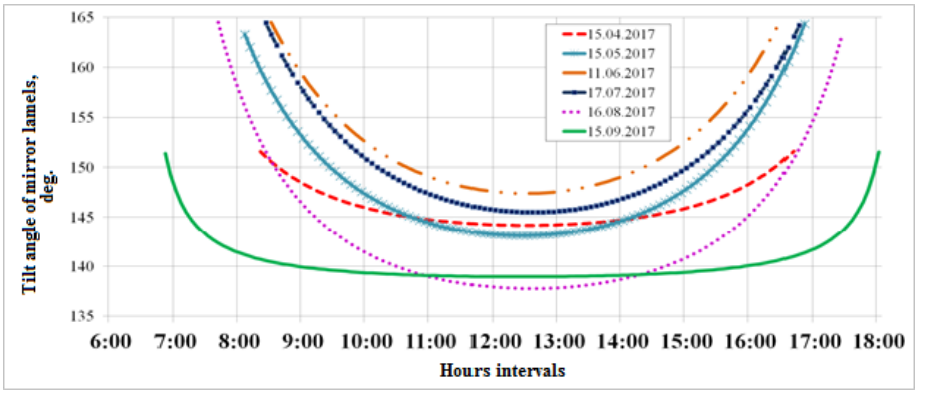

Based on the consideration of a three-dimensional problem, the algorithm for calculating the passage of sunlight through the mirror surface of the lamellae and parabolic cylinder allows calculating the flux of solar radiation on the receiving surface of the solar concentrator.

An algorithm for controlling lamellar heliostat mirror lamellas has been developed that significantly increases the efficiency of a solar concentrator — using a louvre heliostat with a constant lamella pitch is equivalent to increasing the angular aperture of the concentrator from 26° to 70° without reducing the concentration ratio.

REFERENCES

Bazarova, E. G., Strebkov, D. S., Irodionov, A. E., & Tarasov, V. P. (2008). Optimal orientation of non-tracking solar concentrator. *Thermal Engineering*, *12*, 9–12.

Filippchenkova, N. S., & Strebkov, D. S. (2016). Non-tracking solar concentrating modules with louvered heliostats. Renewable energy sources: Materials of the All-Russian Scientific Conference with International Participation and the X Scientific Youth School, 335-341.

Korn, G., & Korn, T. (1973). Mathematics Handbook (for scientists and engineers). *Science*, 832.

Shevchenko, L. P. (1998). Architecture and climate of the South-Russian region. Textbook. manual for universities, Growth. state arch. Inst., 183.

Strebkov, D. S., Irodionov, A. E., & Filippchenkova, N. S. (2015). Non-tracking solar concentrators with louvered heliostats: Bar-to-bar effects. *Heliotechnics*, *4*, 72–78.

Strebkov, D. S., Irodionov, A. E., & Filippchenkova, N. S. (2017). Non-tracking solar concentrators with louvered heliostats: A calculation algorithm. *Heliotechnics*, *1*, 43–47.

Strebkov, D. S., Irodionov, A. E., & Filippchenkova, N. S. (2017). Development of a control algorithm for a louvered heliostat of a non-tracking solar concentrator. *Fundamental and Applied Problems of Physics: Proceedings of the International Conference June 13-14, 2017*, *Academy of Sciences of the Republic of Uzbekistan NPO «Physics-Sun»,* 162-166.

Vygodskii, M. Ya. (1963). Analiticheskaya geometriya (Analytical Geometry). *Fizmatgiz*, 528.

Chapter 3
Development of Modules With Different Types of Concentrators and Receivers of Solar Radiation

ABSTRACT

Optical schemes and designs of four types of solar modules with louvered heliostats and concentrators with zero shading losses and blocking of solar radiation have been developed. The design of a compact thermal photovoltaic solar radiation detector for a non-tracking parabolic-cylindrical solar concentrator provides the thermal efficiency of the module in the range of 0,6–0,7, the service life of at least 25 years due to the sealing of the photoelectric elements using a two-component polysiloxane gel.

DEVELOPMENT OF CONCENTRATOR DESIGNS AND LOUVERED HELIOSTATS SYSTEMS

In the laboratory of solar power plants VIESH, a sample design of a parabolic-cylindrical facet concentrator was developed (Figures 1-3, where n is the number of mirror facets) with an angular aperture of 26 ° and a concentration of 4.3. The width of the mirror facets is 50 mm, the number - 12 pieces.

DOI: 10.4018/978-1-7998-4276-7.ch003

Figure 1. The frame of the cylindrical facet concentrator (angular aperture of 26 °): Concentrator Tie Bar

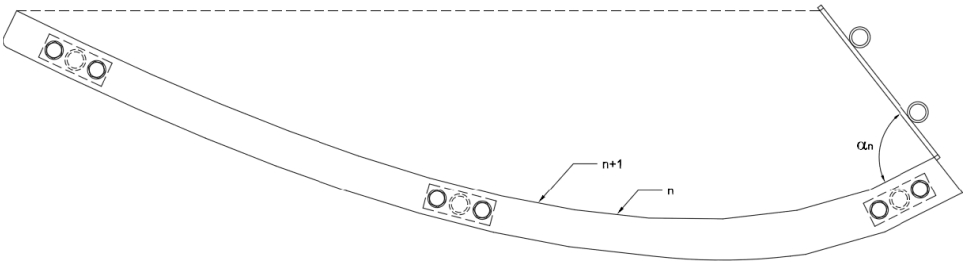

Figure 2. The frame of the cylindrical facet concentrator (angular aperture of 26 °): General form

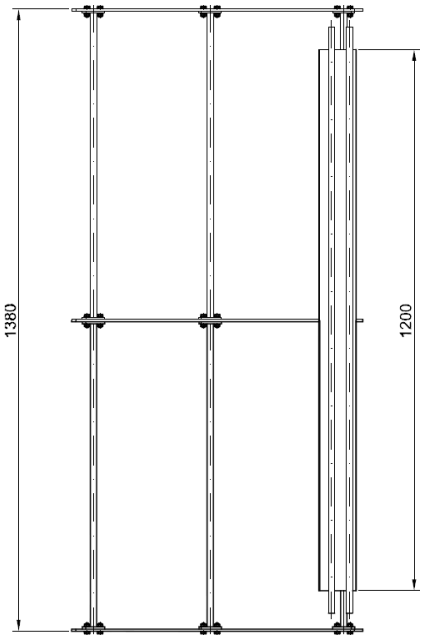

Figure 3. The frame of the cylindrical facet concentrator (angular aperture of 26 °)

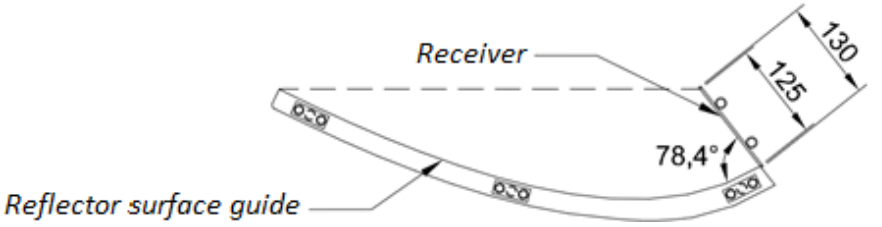

The authors have developed options for the construction of solar modules with various types of concentrators and deflecting optical systems based on louver heliostats, presented in the figures 4-10 (Strebkov, Irodionov, Filippchenkova, 2016; Strebkov, Irodionov, Nikitin et al., 2016; Strebkov, Irodionov, Panchenko et al., 2016; Strebkov, Irodionov, Filippchenkova, 2016).

The solar module with a concentrator in Figure 4 contains a working surface 1 on which radiation 2 is incident, deflecting the optical system 3 with the surface of entrance 4 and exit 5 of the rays, consisting of the main mirror reflectors. The deflecting optical system 3 of width $B = QO$ creates on the surface of output 5 a stream of parallel rays with angles β_1 and β_2, which arrive at receiver 6 of width $A = OO_1$, mounted along the rays β_1 and β_2 on the OO_1, plane perpendicular to the working surface 1 and passing through the side edge 7 of the deflecting optical system 3.

From triangle QOO_1:

$$A = OO_1 = QO \cdot \text{ctg}\ \beta_1 = B\ \text{ctg}\ \beta_1.$$

The concentration coefficient for the deflecting optical system 3 QOO_1, taking into account the cosine loss at $\beta_0 \neq 0$, will be:

$$k_1 = \frac{QO\cos\beta_0}{OO_1} = \frac{B\cos\beta_0}{A} = tg\beta_1 \cdot \cos\beta_0 \qquad (3.1)$$

Figure 4. Solar module with concentrator and one-way receiver (Strebkov, Irodionov, Filippchenkova, 2016)

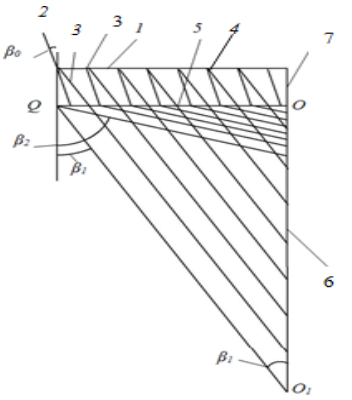

In Figure 5, a flat mirror reflector 8 is installed along the midline I_1I_2 Δ QO_1O parallel to the 5 QO ray exit surface in such a way that the beam QI_1 after reflection from the mirror reflector 8 falls into point O. A one-way receiver 9 of size $A = OI_2$ is installed in the OI_2 plane. The concentration coefficient of the solar module in Figure 3.2, taking into account the cosine loss is:

$$k_2 = \frac{QO \cdot \cos\beta_0}{OI_1} \tag{3.2}$$

$A = OI_1 = IG = QG \cdot \text{ctg}\ \beta_1.$

$QO = 2\ QG.$

$$k_2 = \frac{2QG \cdot \cos\beta_0}{QG \cdot ctg\beta_1} = 2tg\beta_1 \cdot \cos\beta_0 \tag{3.3}$$

Figure 5. Solar module with a concentrator containing a flat mirror reflector parallel to the working surface of the module (Strebkov, Irodionov, Filippchenkova, 2016)

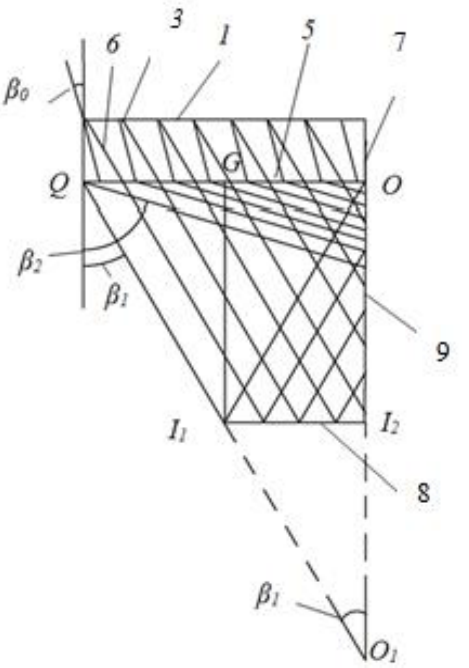

In Figure 6, one mirror reflector 10 is installed along the Y_1Y_2 line, and the second mirror reflector 11 is installed in the 5 QO beam exit plane so that the beam QY_1 after reflection from the mirror reflector 10 enters the X_2 point of the mirror reflector 11 and after reflection from the mirror reflector 11 hit the point Y_2. Points X_1 and X_2 choose from the condition:

$$QX_1 = X_1X_2 = X_2O,$$

$$QO = QX_1 + X_1X_2 + X_2O = 3\ X_2O.$$

The receiver 11 is installed in the plane OY_2. Receiver width is:

$$OY_2 = X_1Y_1 = QX_1 \cdot \text{ctg}\ \beta_1 = X_2O\ \text{ctg}\ \beta_1.$$

Figure 6. Solar module with a concentrator containing a flat mirror reflector parallel to the plane of the mid-section, as well as an additional flat mirror reflector mounted on the exit surface (Strebkov, Irodionov, Filippchenkova, 2016)

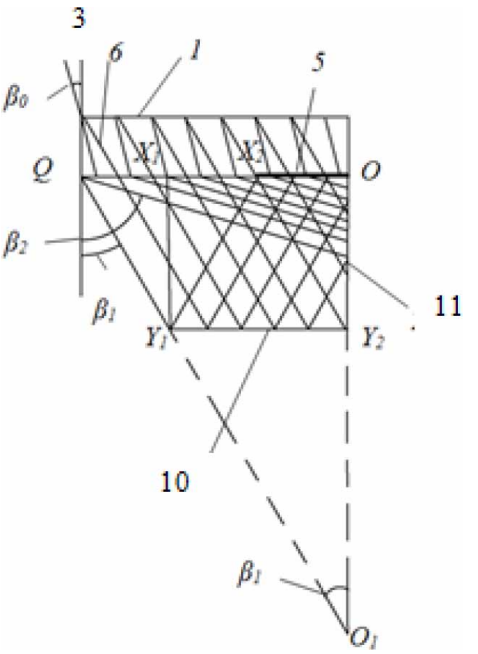

Concentration coefficient taking into account cosine losses:

$$k_3 = \frac{(QO - X_2O) \cdot \cos\beta_0}{OY_2} = 2tg\beta_1 \cdot \cos\beta_0 \tag{3.4}$$

Concentration coefficient for a solar module with two deflecting optical systems and a two-way receiver:

$$k_4 = 4\ tg\ \beta_1 \tag{3.5}$$

In Figure 7, the solar module with a concentrator contains a cylindrical mirror reflector 12 with a radius $R = OS = OO_5 = B\ cos\ \beta_1$ with an axis located at the point O on touching the output surface of the deflecting optical system 3 and the receiver 13 with a width of receiver OO_5.

Figure 7. Solar module with a concentrator containing a mirrored cylindrical reflector (Strebkov, Irodionov, Filippchenkova, 2016)

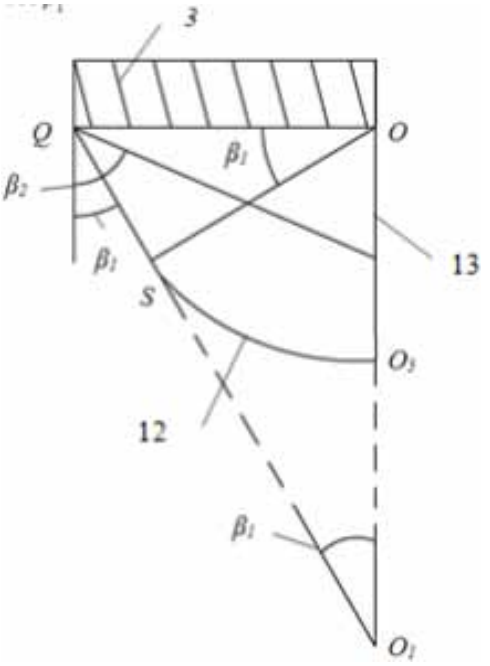

Receiver width 13:

$$A = R = OQ \cdot \cos \beta_1.$$

Concentration coefficient taking into account cosine losses:

$$k_5 = \frac{QO \cdot \cos \beta_0}{OO_5} = \frac{\cos \beta_0}{\cos \beta_1} \tag{3.6}$$

In Figure 8, the mirror reflector 14 with an angle ψ to the normal to the surface of output 5 is connected at point Z*1* with a mirror reflector 15 $Z1_o7$ parallel to the plane of output 5 of the Q*O* rays β*1* and β*2*. Point Z*1* is chosen from the condition that the beam with an angle β*1* after reflection from the reflector 15 $Z1_o7$ falls into the point O of the receiver 16.

Figure 8. Solar module with a concentrator containing a flat mirror reflector with an angle Ψ to the normal to the plane of the ray exit, connected to another mirror reflector parallel to the ray exit plane (Strebkov, Irodionov, Filippchenkova, 2016)

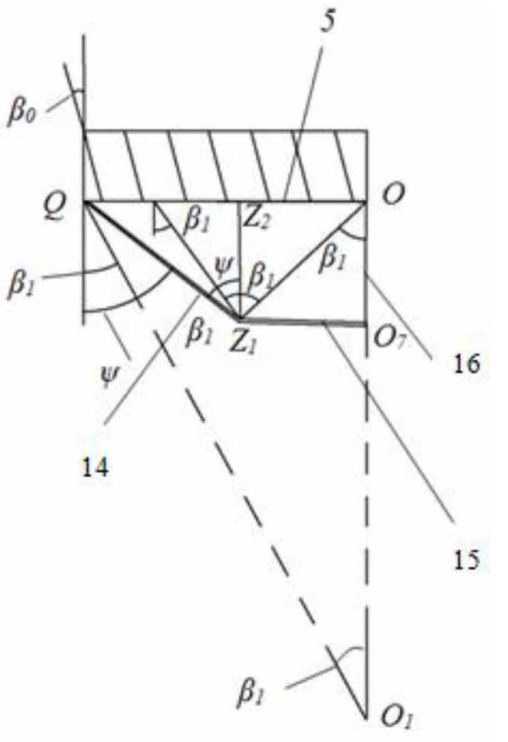

Reflector 15 width:

$Z_1O_7 = OO_7 \cdot \text{tg}\ \beta_1 = A\ \text{tg}\ \beta_1.$

Reflector 14 width:

$QZ_2 = OO_7 \bullet tg\psi.$

Output surface width 5:

$B = QO = QZ_2 + OZ_2 = OO_7(tg\psi + tg\beta 1).$

Receiver width 16:

$$A = OO_7 = \frac{QO}{tg\psi + tg\beta_1} = \frac{B}{tg\psi + tg\beta_1}.$$

Concentration coefficient taking into account cosine losses:

$$k_6 = \frac{QO \cdot \cos\beta_0}{OO_7} = (tg\psi + tg\beta_1) \cdot \cos\beta_0 \tag{3.7}$$

Unlike solar modules with concentrators based on Fresnel lenses, the proposed modules with a concentrator use a parallel beam of rays on the receiver, which ensures the absence of optical losses typical of prism concentrators and Fresnel lenses. A solar module with a deflecting optical system based on louvered heliostats can be used to transmit a parallel flow of solar energy to radiation detectors in greenhouses, buildings, and underground structures.

In the solar module in Figure 3.9, parabolic-cylindrical concentrator 4 with parametric angle δ, focal axis F and vertex O receiver 6 is installed between focal axis F and vertex O of parabolic cylindrical concentrator 4. The deflection optical system 3 of width $B = QO_1$ creates a parallel flow on parabolic-cylindrical concentrator 4 rays with angles β_1 and β_2.

Concentration coefficient taking into account cosine losses:

$$k_7 = \frac{QO_1 \cdot \cos\beta_0}{OF} = \frac{2\cos\beta_0}{1 - \cos(2\delta)} \tag{3.8}$$

Figure 9. Solar module with a deflecting optical system with one parabolic cylindrical concentrator (Strebkov, Irodionov, Nikitin et al., 2016)

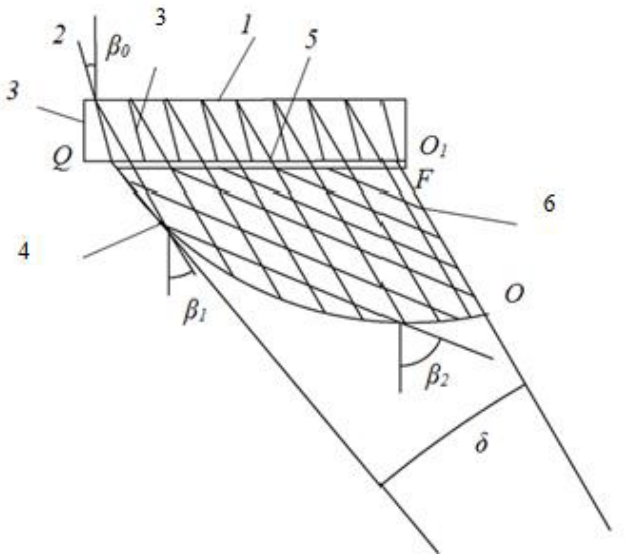

In Figure 3.10, a solar module with a concentrator contains two deflecting rays of counter-optical systems, in which the angle between the main mirror reflectors 7 and 8 of the two deflecting optical systems is $Q_1 = 2\varphi 0\_2\beta 0$, and the angle between the surfaces of the inlet 9 and 10 is Q2= 180°–2β0. The solar module contains two parabolic cylindrical concentrators 11 and 12 with a common focal axis F, *a* common two-way receiver 13, in which the entrance surfaces 14 and 15 form an angle Q3= $_{Q}2= {}_{1}80°–2\beta 0$. Lines 16 and 17, which are tangent to the surface of parabolic-cylinder concentrators 11 and 12, form an angle between themselves at the entrance surfaces 14 and 15 and the outer edges of the aperture angles Q4= $1_{8}0°–2(\delta+\beta 0)$. The concentration coefficient of the solar module with a concentrator in Figure 3.10 is equal to

$$k_8 = \frac{4\cos\beta_0}{1-\cos(2\delta)} \tag{3.9}$$

In the considered designs of solar modules with a system of louvered heliostats, the concentrator can also be made in the form of a prism of total internal reflection (Strebkov, Irodionov, Filippchenkova, 2016).

Figure 10. Solar module with a concentrator, consisting of two deflecting optical systems and two parabolic cylindrical concentrators (Strebkov, Irodionov, Panchenko et al., 2016)

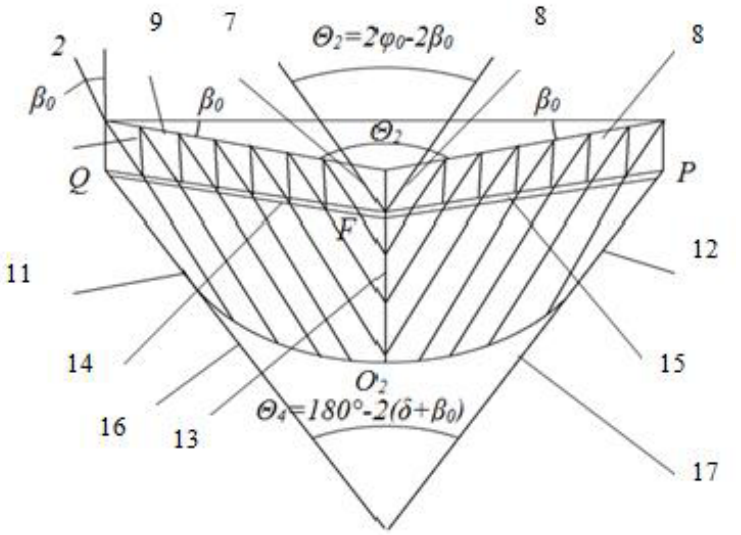

Compared to the considered solar module (Strebkov, Tver'yanovich, Irodionov et al., 2001), solar modules with a concentrator (Strebkov, Irodionov, Nikitin et al., 2016; Strebkov, Irodionov, Panchenko et al., 2016; Strebkov, Irodionov, Filippchenkova, 2016) have zero blocking and shading losses. The solar receiver can be made with a heat removal device to generate electricity and (or) hot water.

As was already shown in Section 1, photoelectric, thermal-photoelectric and thermal receivers can be used as a radiation detector in low-concentration concentrator solar modules. The use of each of these options has its own characteristics. In the first case, the parameters characterizing the efficiency of the module, are the temperature of the photodetectors, power generation; in the second variant, the coolant temperature, the thermal and electrical power output of the module, is added to the monitored parameters; in the third - the temperature of the coolant, thermal power.

THERMAL PHOTOELECTRIC RECEIVER OF THE SOLAR CONCENTRATING MODULE (PVT-MODULE)

Theoretical evaluations of the performance of the main structures and configurations of PVT modules were carried out in (Zondag, de Vries, van Helden et al., 2003).

The importance of having a good heat-conducting contact between solar cells and a heat absorber in photovoltaic thermal modules was determined in (Zakharchenko, Licea-Jime'nez, Pe'rez-Garci'a et al., 2004).

This section shows the method for calculating the thermal characteristics of the receiver of the concentrating module using the example of the developed design.

Figure 11 shows the PVT receiver of a solar concentrating module developed and patented at VIESH (Strebkov, Irodionov, Persits et al., 2015).

Figure 11. 3D-model (a) and cross-section (b) and PVT-receiver of the solar concentrating module

**1– vacuum glazing, 2 – heat carrier channel, 3 – cellular polycarbonate, 4 – layer of polysiloxane gel, 5 – rubber cord, 6 – solar cells, 7– pipe*

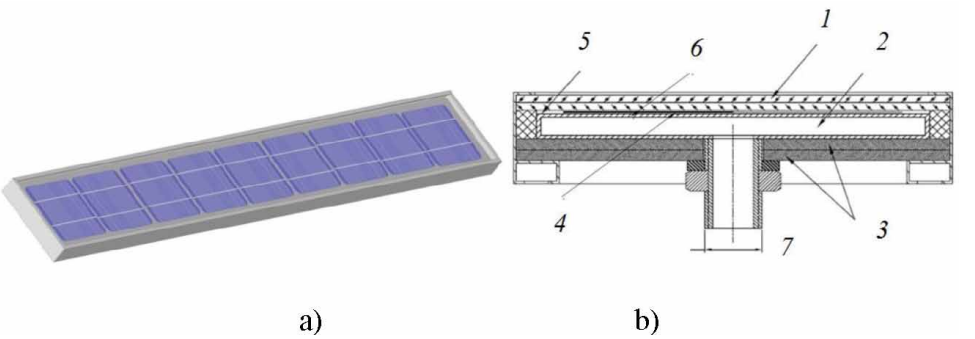

Since the manufacture of a vacuum glass unit in Russia is difficult due to the lack of production sites and the high cost of the product, it is possible to replace it with a single-chamber glass unit with an air gap for the manufacture of a PVT receiver of a solar concentrating module. Table 1 for comparison presents the heat transfer resistances of various materials and structures.

From the point of view of heat engineering, the simplest single-chamber double-glazed window is a closed air gap of small thickness compared to the area of the glazing bounding surfaces.

Table 1. Heat transfer resistance of various materials and structures (Mitina, Strebkov, Trushevsky et al., 2010)

Nomination	Thickness, мм	Resistance to heat transfer, $m^2 \cdot °K/W$
Two sheets of glass with a gap of 16 mm	30	0,37
Vacuum glass unit	6	0,44
Vacuum glass unit with IR coating on one glass	6	0,85
Double vacuum glass unit with IR coating on two glasses	12	2,0
2.5 brick brick wall	64	1,2

Heat transfer through the air gap is carried out by radiation, convection and thermal conductivity. The insulating capacity of glass units is estimated by the value of thermal resistance R_{gl}. The higher the thermal resistance, the better the heat-shielding properties of the glazing. The value of R_{gl} can be determined by the formula:

$$R_{gl} = R_{in} + R_g + R_{air} + R_{out}, \tag{3.10}$$

where $R_{in} = 0,12$, $R_{out} = 0,04$ $m^2 \cdot K/W$ – respectively, resistance to heat transfer from the inner and outer surfaces of the glazing (GOST R 54858-2011, 2012); R_g – thermal resistance of glass, $m^2 \cdot K/W$; R_{air} – thermal resistance of the air gap, $m^2 \cdot K/W$.

The thermal resistance of glass in a glass unit is defined as

$$R_g = \Sigma \delta_i / \lambda_i, \tag{3.11}$$

where δi – thickness of each glass, m; λi – thermal conductivity coefficient of glass, equal to silicate glass 0,76 (W/(m·K)).

With a glass thickness of 3 – 6 mm (0,003 – 0,006 m), the value of R_g will be 0,004 – 0,01 $m^2 \cdot K/W$.

Such components of heat exchange as radiation and convection play a large role in the heat-shielding properties of a glass unit (Figure 3.12).

The heat transfer resistance of one air gap is defined as:

$$R_{air} = 1/K_{air} = 1/(K_1 + K_2), \tag{3.12}$$

Figure 12. Heat transfer through the glazing design, where 1 – radiation, 2 – convection, 3 – thermal conductivity; λ –coefficient of thermal conductivity; μ –dynamic viscosity; ε – radiative absorption

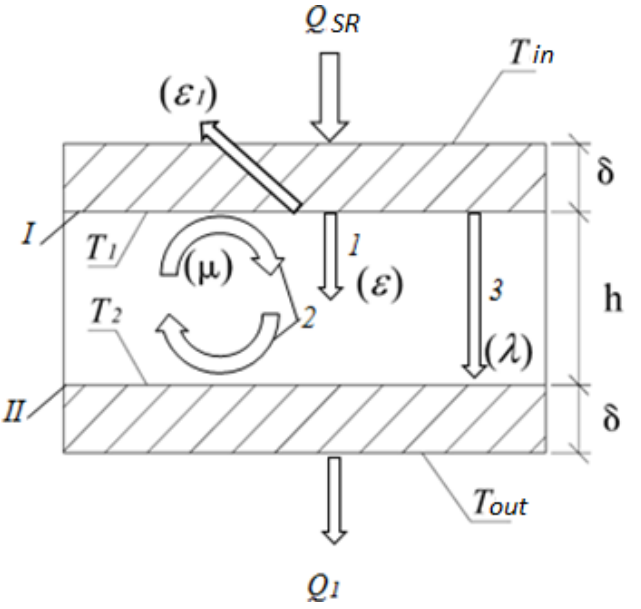

where K_{air} is the heat transfer coefficient of the air gap; K_1 is the heat transfer coefficient of the air gap due to convection and thermal conductivity of the gas filling the layer; K_2 – heat transfer coefficient of the air gap due to radiation.

The heat transfer coefficient of the air gap due to convection and thermal conductivity of the gas filling the layer can be defined as:

$$K_1 = Nu \bullet (\delta/\lambda) , \tag{3.13}$$

where N*u* is the Nusselt number, which determines the nature of heat exchange within the air layer (convective or conductive (due to thermal conductivity) heat transfer). If N*u* = 1, then the heat transfer in the interlayer is determined only by thermal conductivity, that is, K*1* = δ/λ.

Heat transfer coefficient due to radiation is defined as:

$$K2 = qS_R\Delta t, \tag{3.14}$$

where q_{SR} – the heat flux passing through the glass unit due to radiation when the temperature difference on its surfaces is Δt. In this case, q_{SR} value can be defined as:

$$q_{SR} = \sigma \varepsilon_1 \varepsilon_2 \left| \left(\frac{T_1}{100} \right)^4 - \left(\frac{T_2}{100} \right)^4 \right| \tag{3.15}$$

where σ = 5,67 W/m^2·K^4 – Stefan - Boltzmann constant; T_1 and T_2 – absolute temperatures of heat exchanging surfaces, K;ε_1 and ε_2 – respectively, radiative - absorption properties of surfaces I and II (Figure 3.12).

The coefficient K_2 depends on the temperature of the surfaces between which the heat exchange occurs by radiation. However, for practical calculations, it is sufficient to determine the dependence of K_2 on the emissivity of the glass inner glass, that is, ε_1, according to Table 2. (Aizenberg, 1983).

Table 2. Dependence of the K_2 value on the emissivity of the inner glass pane

ε_1	0,1	0,2	0,3	0,4	0,5	0,6	0,7	0,8
K_2, [W/m^2 ·K]	0,5	1	1,46	1,9	2,34	2,76	3,17	3,55

When the thickness of the air gap to 8 mm, convection of air will be difficult. The nature of the change in thermal resistance of the glass R_{gl} depending on the thickness of the air gap is shown in Figure 13. From the graph it can be seen that with the thickness of the interlayer up to 8 mm, the total resistance of the glass unit increases in proportion to the increase in its thickness. At the same time K_1 (formula 13) is determined based purely on the conditions of thermal conductivity $K_1 = \delta / \lambda \text{air}_{is}$ where λair_{is} the coefficient of thermal conductivity of air. For clean glass, the emissivity ε is 0,8 (Aizenberg, 1983).

Figure 14 shows a section of a PVT receiver with an air glass unit (8 mm gap). Further, all calculations will be carried out for this receiver design.

Figure 15 shows a diagram of the cross-section of a PVT receiver with an air glass unit with an indication of the thickness of all layers.

Figure 13. Change in thermal resistance of the glass R_{gl} depending on the thickness of the air gap

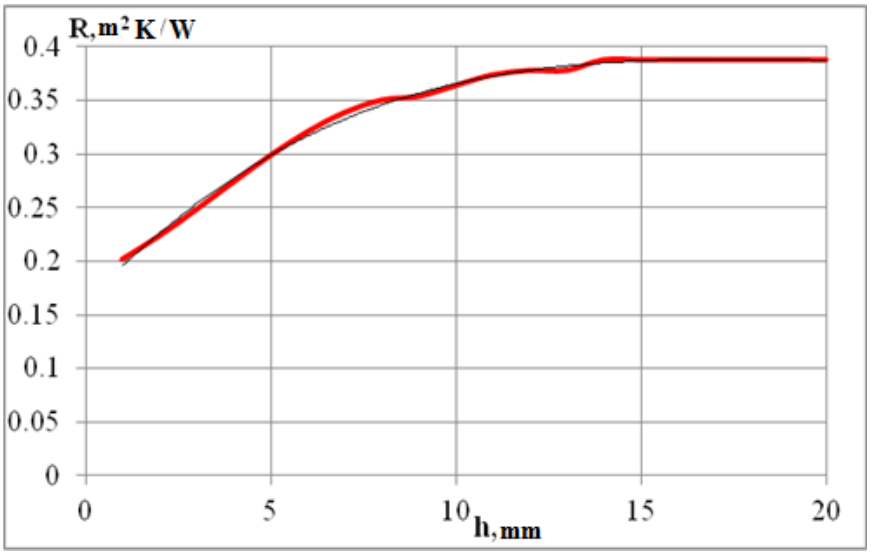

Figure 14. PVT-receiver with an air glass unit

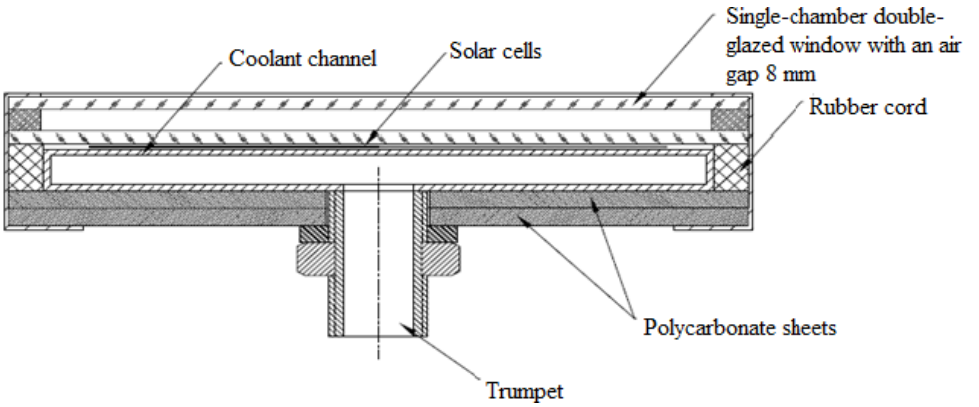

A polysiloxane two-component silicone optically transparent low-modulus gel with a thermal conductivity coefficient $\lambda g = 0{,}2$ W/(m·K) was used as an electrically insulating material with a thickness of 0,1 ... 2 mm (Strebkov, Persits, Panchenko, 2014; Panchenko, Strebkov, Persits, 2015). The tank-absorber (coolant channel) in which the coolant is heated is made of steel. The walls of the coolant channel are steel sheets with a thickness of 1,5 mm over the entire area with a coefficient of thermal conductivity $\lambda ta_{nk=}$ 52 W/(m·K)

Figure 15. Cross-section of a PVT receiver
**1 – double-glazed window with an air gap of 8 mm (glass thickness of 4 mm); 2 – a layer of polysiloxane gel; 3 – photo-receiver; 4 – coolant channel wall (steel 1,5 mm thick); 5 – heat carrier (water, layer thickness 7 mm); 6 – two sheets of cellular polycarbonate 4 mm thick*

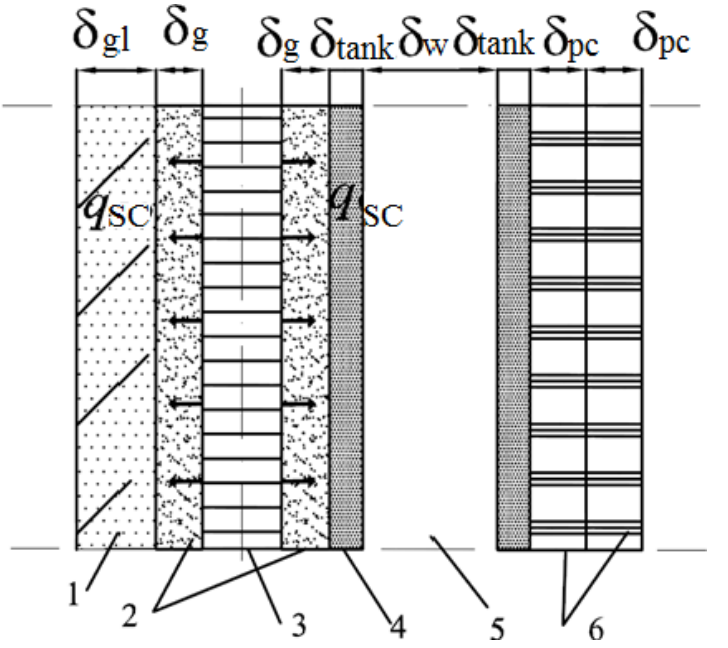

(thermal conductivity of steel) (Heat transfer coefficients of various materials, 2016). As an insulating material, two sheets of transparent polycarbonate are used with a thickness of 4 mm each with a thermal conductivity coefficient

λpc$_{=}$ 0,2 W/(m·K) (The main properties of polycarbonate, 2016).

In the first approximation, it is assumed that the heat flux propagates symmetrically, i.e. q$S_{C=}$1402,5 W/m2·

From the side of the photo-receiver, the heat flux passes through the layer of polysiloxane gel and the steel channel of the module, equal to:

$$q_{SC} = \frac{t_{SC} - t_{\text{tank}}}{\frac{\delta_{\text{g}}}{\lambda_{\text{g}}} + \frac{\delta_{\text{tank}}}{\lambda_{\text{tank}}}}, \tag{3.16}$$

where t_{sc},t_{tank}– the temperature of the photo-receiver and the wall of the coolant channel in this section, °C; λg_ thermal conductivity coefficient of the polysiloxane gel layer, W/m·°C, is taken equal to 0,2 W/m·°C; λta$_{nk_}$ the coefficient of thermal conductivity of steel, W/m·°C, is assumed to be 52 W/m·°C.

The same amount of heat is transferred to the coolant from the channel surface:

$$q_{SC} = \alpha f_{.}(t t_{ank} - t W_{)}, \tag{3.17}$$

where t_W– canal water temperature, °C; αf_ fluid heat transfer coefficient.

Coolant temperature will change due to heat flow:

$$q_W = q_{SC} - c_p \bullet \rho \bullet v \cdot (t i_n - to_{ut)}, \tag{3.18}$$

where c_p – heat capacity of the coolant, J/kg·°C (for water it is taken equal 4179 J/kg·°C); ρ– water density, kg/m3 (for water it is taken equal 991 kg/m3); v– coolant speed, m/c; t$i_{n_}$ water inlet temperature, °C (is assumed to be equal 25°C); t$o_{ut_}$ duct outlet water temperature, °C.

To determine αf it is used the formula to find the Nusselt number:

$$\nu = \alpha \ell / \lambda W, \tag{3.19}$$

where l – characteristic size (channel width 7 mm), m; λW– thermal conductivity of water, W/m·°C, taken equal 0,634 W/m·°C.

To find the Nusselt number, it is used simplified formulas for the calculation in the case of forced flow of coolant in the channels (calculation error ±4%) (Ovchinnikov, 2015).

Through the cover glass to the ambient air from the surface of the photo-receiver the heat flux is transmitted (in the first approximation it is assumed to be equal to qS_C=1402,5 W/m2):

$$q_{SC} = \frac{t_{SC} - t_{gl}}{\frac{\delta_g}{\lambda_g} + R_{gl}}, \tag{3.20}$$

where t_{gl}– glass temperature, °C; R_{gl}– previously calculated thermal resistance of the glass unit, m^2·K/W.

In turn, the same flow spreads from glass to the environment:

$$q_{SC} = \frac{t_{\text{gl}} - t_{\text{am}}}{\dfrac{1}{h_k + h_{\text{r}}}}, \tag{3.21}$$

where t_{am} – ambient temperature, °C (accept 25°C); h_k, h_t – respectively, the heat transfer coefficients to the environment by convection and radiation, W/m^2·°C.

The coefficient of heat transfer by convection into the environment depends on the wind speed and is determined by the Mc Adams formula (Duffie, Beckman, 1991):

$$h^k = 5.7 + 3.8 \bullet v \tag{3.22}$$

where v – wind speed, m/c.

The heat transfer coefficient of radiation from glass to the environment is according to the formula:

$$h^r_{b.in-am.} = \frac{\sigma \cdot (T^2_{gl} + T^2_{am.}) \cdot (T_{gl} + T_{am.})}{\dfrac{1}{\varepsilon_{gl}} + \dfrac{1}{\varepsilon_{soil}} - 1} \tag{3.23}$$

where σ = W/m^2·K^4 – Stefan-Boltzmann constant; T_{am} – ambient temperature, K; T_{gl} – glass temperature, K; ε_r – glass emissivity; ε_{soil} – soil blackness 0,9.

Next, using the method of successive approximations, it is finded the temperature of the photodetector and adjust the flow distribution.

Figures 16-18 show the calculation results (insolation on the input surface of a concentrator 1000 W/m^2).

As can be seen from Figures 16–18, with a water consumption of 11 *l*/*h*, the temperature of the photovoltaic converters does not exceed 60 ºC. The rated thermal power of the module is 348 W at a water temperature of 53 ºC.

Figure 16. Temperature distribution along the length of the heat sink channel

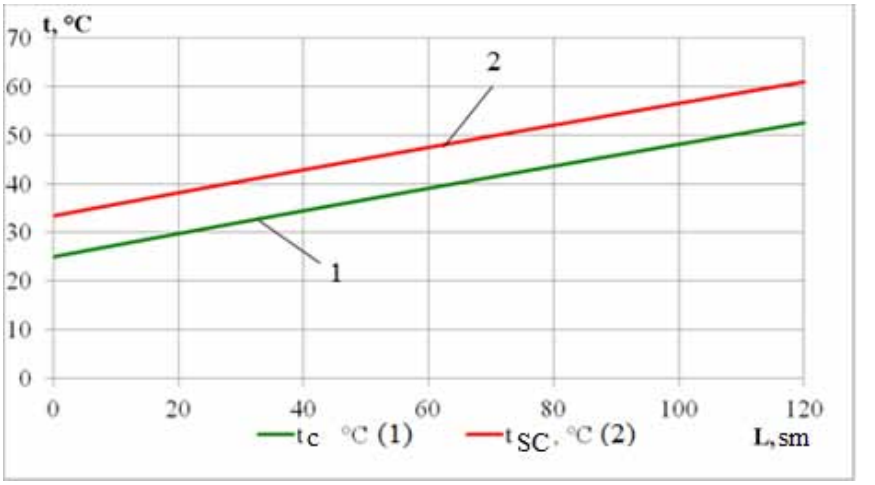

Figure 17. The dependence of the temperature of the photodetector and the outlet temperature of the coolant flow

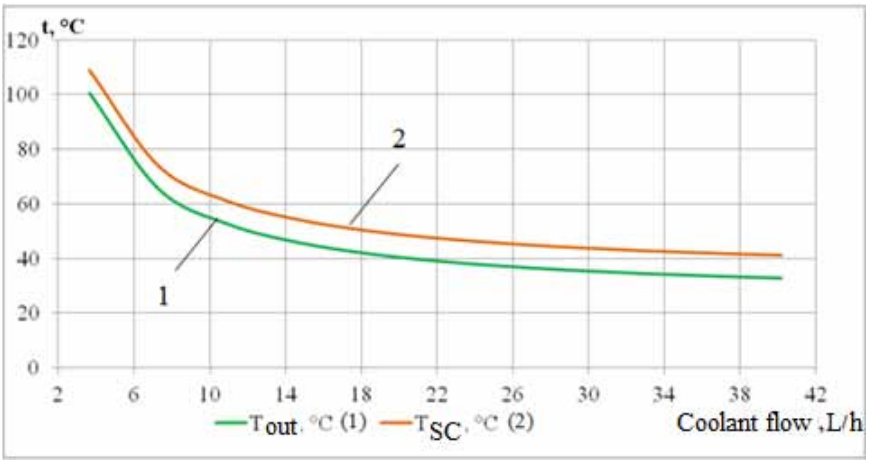

PHOTOVOLTAIC RECEIVER OF THE SOLAR CONCENTRATOR MODULE (PV-MODULE)

The energy of the light flux entering the surface of the photodetector is converted in the surface layer into electrical energy (efficiency of the photodetector 15%) and heat (85%). It is determined the density of the heat flux on the surface of the photoconverter under the assumption that the

concentration coefficient of the optical system is 5.5 (angular aperture 18 °), the optical efficiency is 75%, the insolation at the surface of the inlet of the concentrator 1000 W/m^2 at 80% direct component content. In this instance q_{SC} =1000·5,5·0,8·0,75·0,85=2805 W/m^2. In a first approximation, it is assumed that the heat flux propagates symmetrically, i.e. q_{SC} =1402,5 W/m^2.

Figure 18. The dependence of the nominal heat output from the coolant flow

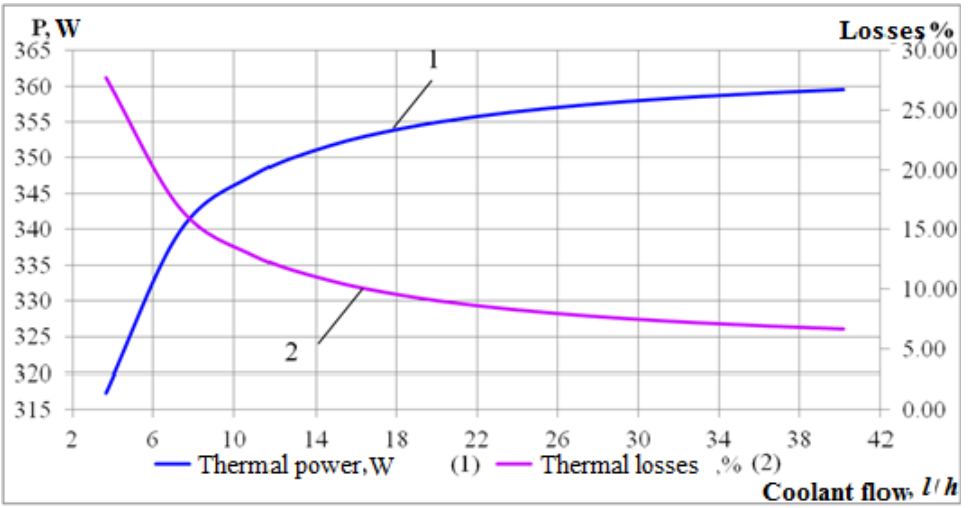

It is composed the heat balance equations on one side of the solar cells.

From the photodetector side, heat flux passes through the ethylene vinyl acetate film (EVA) of the module q_{SC}, equal:

$$q_{SC} = \frac{t_{SC} - t_{EVA}}{\frac{\delta_{EVA}}{\lambda_{EVA}} + \frac{\delta_{PET}}{\lambda_{PET}}}, \tag{3.24}$$

where t_{SC},t_{EVA} – solar cells and EVA temperatures in this section, °C; λE_{VA} – EVA thermal conductivity, W/m·°C; $\lambda PE_{T\_}$ PET thermal conductivity, Вт/м·°C.

The same amount of heat is transferred to the surrounding air from the surface of the ethylene vinyl acetate film:

$$q_{SC} = k(t_{EVA} - t_{am}), \tag{3.25}$$

where t_{am} – ambient temperature, °C; k– heat transfer coefficient.

Heat transfer coefficient

$$k = \frac{1}{\frac{1}{h_{.}} + \frac{1}{h_{r}}}, \tag{3.26}$$

where h_k,h_t– respectively, the heat transfer coefficients to the environment by convection and radiation, W/m^2·°C.

The heat transfer coefficient of radiation from the film material into the environment is found similarly by the formula 3.23.

In the same way, the equations of heat balance from the side of solar cells through glass are compiled.

The heat transfer coefficient is determined similarly. Next, using the method of successive approximations, it is determined the temperature of the photodetector and adjust the flow distribution. It is more convenient to carry out calculations in the Mathcad environment. The calculation was carried out for an ambient temperature of 25 °C, the thermal conductivity of the EVA is 0,35 W/m·°C, PET 0,24 W/m·°C, glass 0,76 W/m·°C. According to the calculation results, the temperature of the photodetector under given conditions does not exceed 80 °C, which is included in the operating temperature range of standard PV modules (from –40 °C to + 85 °C).

SOLAR CONCENTRATING MODULE WITH THERMAL RECEIVER

Figure 19 shows a cross-sectional diagram of a thermal receiver of a solar concentrator module with an indication of the thicknesses of all layers. The design of the receiver is similar to the above.

Similarly, to a first approximation, it is assumed that the heat flux propagates symmetrically from the absorber channel, i.e. q_{ab}=1402,5 W/m^2.

The heat flow passes from the absorber q_{ab}, equal:

$$q_{ab} = \frac{t_{ab} - t_w}{\frac{\delta_{\tan k}}{\lambda_{\tan k}} + \frac{1}{\alpha_w}}, \tag{3.27}$$

Figure 19. Cross-section of a thermal receiver
**1 – 3 mm thick glass; 2 – air gap; 3 – coolant channel wall (steel 1,5 mm thick); 4 – heat carrier (water, layer thickness 7 mm); 5 – two sheets of cellular polycarbonate 4 mm thick*

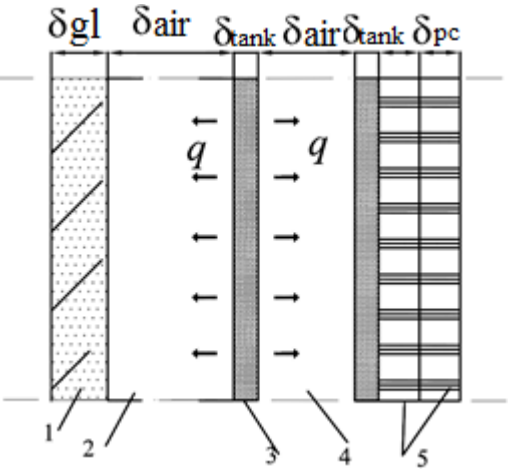

where t_{ab},t_w – temperature of the absorber (wall of the coolant channel) and water in this section, °C; $\lambda t_{ank–}$ thermal conductivity of steel, W/m·°C, accept equal 52 W/m·°C; $\alpha w–$ heat transfer coefficient of liquid.

The same amount of heat is transferred from the coolant to the layer of cellular polycarbonate:

$$q_{ab} = \frac{t_w - t_{PC}}{\frac{1}{\alpha_w} + \frac{\delta_{\tan k}}{\lambda_{\tan k}} + \frac{\delta_{PC}}{\lambda_{PC}}}, \tag{3.28}$$

where t_{PC} – cell polycarbonate temperature, °C; $\lambda P_{C–}$ thermal conductivity coefficient of cellular polycarbonate, W/m·°C, accept equal 0,2 W/m·°C.

The heat flux is transmitted through the coverslip to the ambient air from the surface of the absorber (in the first approximation, it is taken equal to q_{ab}=1402,5 W/m^2):

$$q_{ab} = \frac{t_{ab} - t_{gl}}{\frac{1}{h_k^{ab-gl} + h_r^{ab-gl}} + R_{gl}}, \tag{3.29}$$

where t_{gl} – glass temperature, °C; h_k^{ab-gl}, h_r^{ab-gl} – respectively, the heat transfer coefficients of convective heat transfer and heat transfer by radiation in the gap between the absorber and the glazing, W/m^2·°C; R_{gl} – thermal resistance of glass calculated earlier.

The heat transfer coefficient of convective heat transfer is calculated by the Nusselt formula (3.19), the heat transfer coefficient by radiation is similar to formula (3.23).

To find the Nusselt number, it is used the dependence on the Rayleigh number Ra, which was obtained experimentally by Hollands:

$$\nu = 1 + 1,44 \cdot \left(1 - \frac{1708 \cdot (\sin 1,8\alpha)^{1,6}}{Ra \cdot \cos\alpha}\right) \cdot \left(1 - \frac{1708}{Ra \cdot \cos\alpha}\right)^{+} + \left(\left(\frac{Ra \cdot \cos\alpha}{5830}\right)^{1/3} - 1\right)^{+} \tag{3.30}$$

where α – the angle of inclination of the module to the horizontal plane, deg.

The «+» sign after the bracket means that only positive values are taken into account, with negative values 0 is taken.

The Rayleigh number is calculated according to the formula:

$$Ra = \frac{g \cdot \beta_{air} \cdot \left(T_{ab} - T_{gl}\right) \cdot L^3}{\nu_{air} \cdot a_{air}}, \tag{3.31}$$

where β_{air} – volume expansion coefficient of air, for ideal gas $\beta = 1/T$, K^{-1}; T_{ab} – absorber temperature, K; T_{gl} – glass temperature, K; ν_{air} – kinematic viscosity coefficient of air, m^2/s; a_{air} – thermal diffusivity, m^2/s; L – the thickness of the air gap between the absorber and the glass, m (taken equal to 5 mm).

In turn, the same flow propagates from glass to the environment:

$$q_{ab} = \frac{t_{gl} - t_{am}}{\frac{1}{h_k + h_r}}, \tag{3.32}$$

where t_{am} – ambient temperature, °C (accept 25°C); h_k,h_t – accordingly, the coefficients of heat transfer to the environment by convection and radiation.

Next, using the method of successive approximations, it is determined the temperature of the absorber and adjust the flow distribution. It is more

convenient to carry out calculations in the Mathcad environment. Figures 3.20 - 3.22 show the calculation results.

As can be seen from Figures 20-22, at a water flow rate of 11 l / h, the temperature of the coolant at the outlet does not exceed 60 ºC. The nominal thermal power of the module is 394 W, which corresponds to a water temperature of 56 ° C.

DRIVING SYSTEM OF LOUVERED HELIOSTAT

The task of controlling the rotation of a louvered heliostat is to monitor the Sun by its zenithal (elevation angle *h*) parameter during the daylight hours using one electric motor (all axes of rotation of the mirror lamellae are in the same plane and parallel, which allows using one servo motor).

The proposed system for controlling the rotation of a louvered heliostat may include a servo drive, an Atmega328-PU microcontroller (MC) from Atmel, an RTC (Real time clock) module with a built-in backup power source, and a light sensor as main components.

Figure 20. Temperature distribution along the length of the heat sink channel

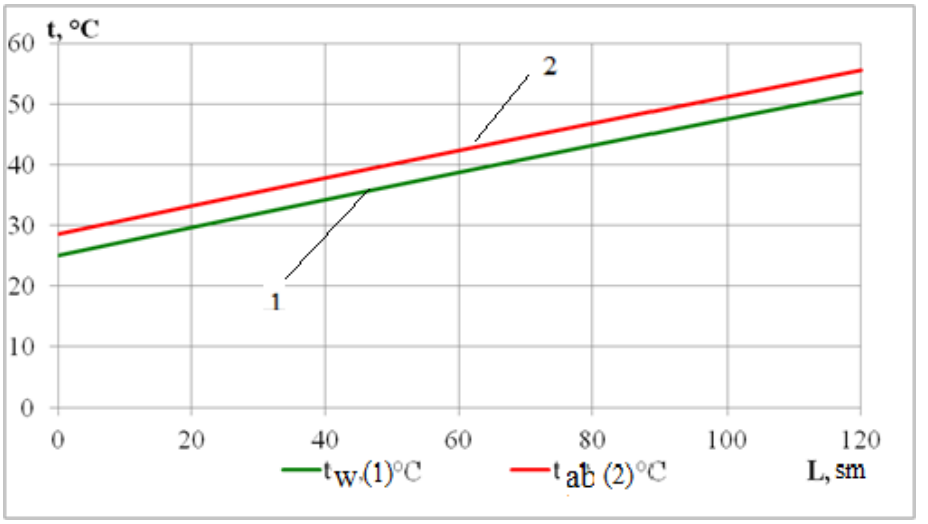

Figure 21. Dependence of absorber temperature and outlet temperature on coolant flow rate

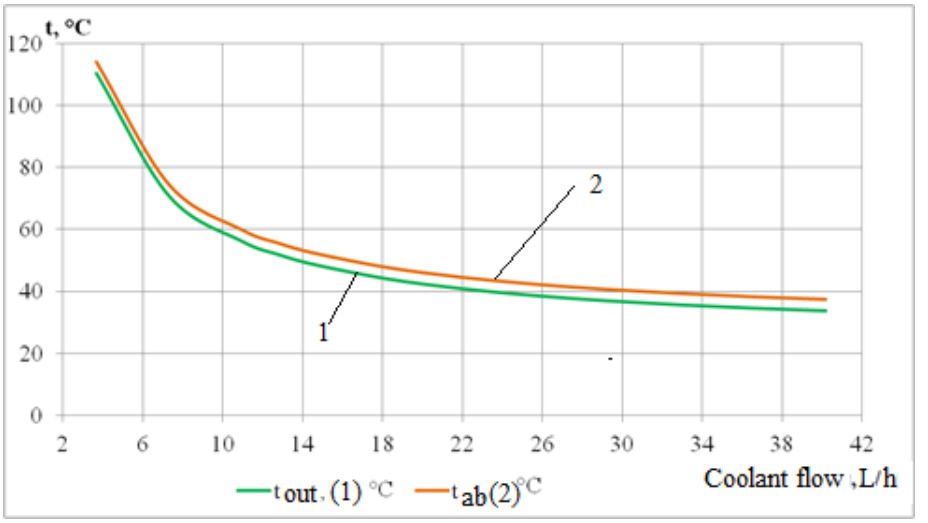

Figure 22. The dependence of the rated thermal power on the flow rate

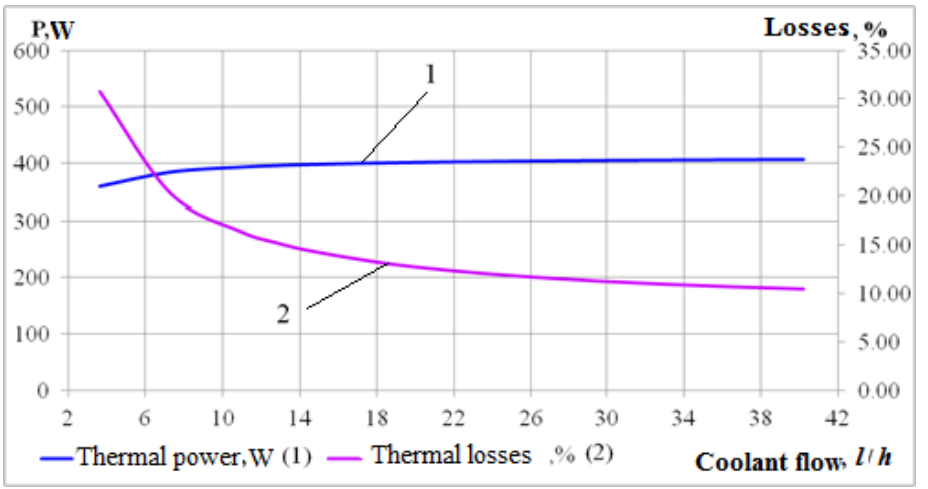

The program code for this system can be developed on the Arduino platform –an electronic designer and a convenient platform for the rapid development of electronic devices. The built-in library of Servo functions allows for software control of servos with the help of MCs. Let us consider in more detail the principle of operation of the system for controlling the

rotation of a louvered heliostat. At the beginning of the cycle, the MC reads readings from the RTC real-time clock module (date, time), then, if it is night time (for example, from 10:00 pm to 5:00 am, it is set in advance in the program code depending on the latitude of the terrain, sunrise time and sunset), the MC goes into sleep mode, and the built-in Watch dog timer will bring the MC out of sleep mode, for example, at 5:01 (time of sunrise). During the daytime, when the sun rays illuminate the elements of the light sensor located on the input surface of the concentrator, the signals from it are sent to the automatic control unit: if the SR level is within the limits that allow the concentrating module to start working (previously set in the program in accordance with the energy calculations of the module), the data from the RTC is read again and in accordance with the information of the database of the schedules for the regulation of the angle of inclination of the slats (also specified in the memory of the MC) motors ourselves to the desired angle. Then the cycle repeats.

For comparison, Table 3 presents the specific weight and cost parameters of a glass mirror and mirror aluminum (Alanod) used as a material for the heliostat mirror lamellaees, and also shows the change in these parameters depending on the width of the lamellae for a concentrator with an aperture angle of 26 ° and geometric parameters 1500x540 mm, relative lamellae pitch 0,5. As can be seen from table 3.3, the mass of the louvered heliostat (specular aluminum) does not exceed 2 kg. To ensure the rotation of the louvered heliostat system, a servo drive with a minimum power of 0.4 kW and a torque of at least 2 N·m is sufficient.

Figure 23 shows for clarity that according to weight and cost characteristics (with a slight discrepancy between the reflection coefficient of materials - no more than 3%), mirror anodized aluminum Alanod is significantly ahead of the mirror: for the considered concentrator with lamellae width $b = 100$ mm, the mass of the louver heliostats system from the mirror is 8.1 times higher than that of mirror aluminum, while the cost of such a system (only the cost of the slats is taken into account) is 10,6% lower than that of the louvered system of heliostats from the mirror.

CONCLUSION

Optical schemes and designs of four types of solar modules with louvered heliostats and concentrators with zero shading losses and blocking of solar radiation have been developed.

Table 3. Specific weight and cost indicators of Alanod mirror aluminum and glass mirror

Material	Specific indicators		$k_{refl.}$	b=30 mm				b=40 mm			
	Macca, kg/ m^2	Cost, rub./m^2		N, pieces	S, m^2	Mass, kg	Cost, rub.	N, pieces	S, m^2	Mass, kg	Cost, rub.
Mirror aluminum (0.4 mm thick)	1,27	960	0,95	35	1,578	2,0	1515	26	1,588	2,017	1524
Mirror (4 mm thick)	11	1150	0,98	28	1,279	14,068	1471	23	1,35	14,85	1553
Material	Specific indicators		$k_{refl.}$	b=50 mm				b=100 mm			
	Mass, kg/m^2	Cost, rub./m^2		N, pieces	S, m^2	Mass, kg	Cost, rub.	N, pieces	S, m^2	Mass, kg	Cost, rub.
Mirror aluminum (0.4 mm thick)	1,27	960	0,95	21	1,594	2,025	1530	11	1,607	2,041	1543
Mirror (4 mm thick)	11	1150	0,98	19	1,397	15,362	1607	10	1,5	16,5	1725

Figure 23. Comparison of the weight and price characteristics of various materials for the manufacture of mirror lamellae

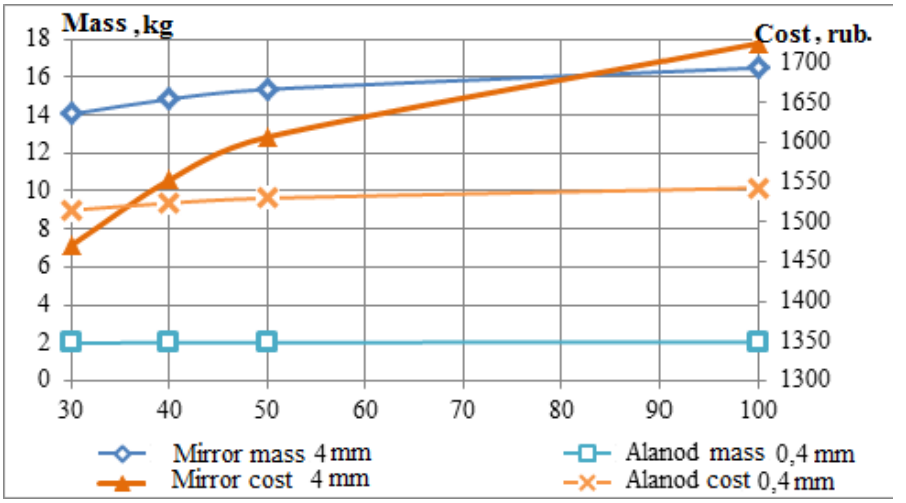

The design of a compact thermal photovoltaic solar radiation detector for a non-tracking parabolic-cylindrical solar concentrator provides the thermal efficiency of the module in the range of 0,6–0,7, the service life of at least 25 years due to the sealing of the photoelectric elements using a two-component polysiloxane gel.

The thermal calculation of the PVT receiver of the solar concentrating module showed that with a water flow rate of 11 *l/h*, the temperature of the photovoltaic cells does not exceed 60 ºC. Rated thermal power of the module is 348 W at a temperature of 53ºC.

REFERENCES

Aizenberg, Yu.B. (1983). Reference book on lighting: ed. Yu. B. Eisenberg. *Energoatomizdat*, 472.

Duffie, J. A., & Beckman, W. A. (1991). *Solar engineering of Thermal Processes* (2nd ed.). John Wiley and Sons Inc.

GOST R 54858-2011. (2012). *Front facade translucent structures. Method for determining reduced heat transfer resistance.* Moscow: Standardinform.

Heat transfer coefficients of various materials. (2016). Retrieved from http://www.xiron.ru/content/view/58/28/

Mitina, I.V., Strebkov, D.S., Trushevsky, S.N., Alekhina, M.B., & Anurov, S.A. (2010). *Vacuum glass unit with indicator.* Patent for invention Nº 2382162 of the Russian Federation, IPC E06B 3/66. No. 2008151043/03; publ. 20.02.2010.

Ovchinnikov, S.V. (2015). *Convective heat transfer. Techniques for the engineering calculation of the convective heat transfer coefficient: proc. Method. manual for students of the Faculty of Physics areas of training 03.03.02 «Physics» (bachelor) and 03.04.02 «Physics» (magistracy) [Electronic Edition].* SSU named after N.G. Chernyshevsky.

Panchenko, V.A., Strebkov, D.S., & Persits, I.S. (2015). Solar modules with increased service life at the level of nominal power. *Alternative Energy and Ecology*, *19*(183), 55 - 60.

Strebkov, D.S., Irodionov, A.E., & Filippchenkova, N.S. (2016). *Solar module with a concentrator.* The patent for the invention Nº 2576742 of the Russian Federation, IPC H02S 10/00, F24J 2/42, F24J 2/18. No. 2014118543/06; publ. 10.03.2016.

Strebkov, D.S., Irodionov, A.E., & Filippchenkova, N.S. (2016). *Solar module with a concentrator.* The patent for the invention Nº2576739 of the Russian Federation, IPC H02S 10/30, F24J 2/42. No. 2014119842/06; publ. 10.03.2016.

Strebkov, D.S., Irodionov, A.E., Nikitin, M.A., & Filippchenkova, N.S. (2016). *Solar module with a concentrator.* The patent for the invention Nº 2580462 RF, IPC F24J 2/42, F24J 2/18. No. 2015104574/06; publ. 10.04.2016.

Strebkov D.S., Irodionov A.E., Panchenko V.A., & Filippchenkova N.S. (2016). *Solar module with a concentrator.* The patent for the invention Nº2576752 of the Russian Federation, IPC H02S 10/30, F24J 2/42. No. 2014119843/06; publ. 10.03.2016.

Strebkov, D.S., Persits, I.S., & Panchenko, V.A. (2014). Solar modules with increased service life. *Innovations in agriculture. Theoretical and Scientific Journal. Innovations in Renewable Energy*, *3*(8), 154 - 158.

Strebkov, D.S., Tver'yanovich, E.V., Irodionov, A.E., Kidyashev, Yu.K., Semenenko, V.F., Ananenkov, AG, Neelov, Yu.V., Yakupov, Z. G., Isaeva, A.N., & Danko, E.M. (2001). *Solar module with a concentrator.* The patent for the invention Nº 2172903 of the Russian Federation, IPC F24J2 / 26. No. 2000108561/06; publ. 27.08.2001.

Strebkov, D.S., Irodionov, A.E., Persits, I.S., & Filippchenkova, N.S. (2015). *Guy-brid photovoltaic module*. The patent for the invention Nº 2546332 of the Russian Federation, IPC H02S 10/00, H01L 31/042. 2013154732/07; publ. 10.04.2015.

The main properties of polycarbonate. (2016). Retrieved from https://www.policarbon.ru/monolitnyiy-polikarbonat/svoystva-polikarbonata

Zakharchenko, R., Licea-Jime'nez, L., Pe'rez-Garci'a, S. A., Vorobeiv, P., Dehesa Carrasco, U., & Pe'rez-Robels, J. F. (2004). Photovoltaic solar panel for a hybrid PV/thermal system. *Solar Energy Materials and Solar Cells*, *82*(1-2), 253–261. doi:10.1016/j.solmat.2004.01.022

Zondag, H. A., de Vries, D. W., van Helden, W. G. J., van Zolengen, R. J. C., & Steenhoven, A. A. (2003). The yield of different combined PV-thermal collector designs. *Solar Energy*, *74*(3), 253–269. doi:10.1016/S0038-092X(03)00121-X

Chapter 4
Results of an Experimental Research of a Solar Concentrating Module With Louvered Heliostats

ABSTRACT

The developed system of automatic measurement of the main parameters of a solar concentrating module with PV, PVT, and heat receivers allows you to save time during information processing, to obtain data on the dynamics of the processes in the solar concentrating module with the required measurement periodicity. The developed algorithm for calculating the passage of sunlight through the mirror surface of the lamellae and the parabolic cylinder, implemented as a computer program, allows calculating the flow of solar radiation on the receiving surface of the solar concentrator with a relative error of not more than 5%, which is confirmed by experimental data.

INTRODUCTION

When conducting experimental studies of solar concentrator plants, the radiation source is of great importance. The use of artificial light sources during the experiment allows to conduct it indoors and at any time of the day. But at the same time, such sources in varying degrees correspond to the natural spectrum of solar radiation (Strebkov, Kharchenko, Nikitin et

DOI: 10.4018/978-1-7998-4276-7.ch004

al., 2013). Field experiments allow us to more qualitatively investigate the work of the solar concentrator facility, as well as the scheme of its operation, identify problems and solve them at the stage of research work, and thereby confirm the validity of theoretical propositions.

To verify the adopted scientific and technical solutions and to compare the theoretical and experimental data in the VIESH, a solar module with a parabolic cylindrical concentrator and a system of louvered heliostats was designed and manufactured, studies of the processes occurring in various structures of the module were carried out in order to evaluate its work.

THE DESIGN OF THE EXPERIMENTAL SAMPLE CONCENTRATOR SOLAR MODULE WITH LOUVERED HELIOSTATS SYSTEM

Figure 1 shows a 3D model of a parabolic-cylinder concentrator with a louvered heliostat.

An array of experimental data was obtained on the existing maket of a parabolic-cylinder concentrator with an angular aperture of 36°. Experimental studies were conducted at the test site VIESH. The test period is summer 2016, summer 2017. In the proposed design of the system louvered heliostats ratio t/b=1. The height of the mirror slat is 40 mm, length 1240 mm, thickness 4 mm, the number of 12 pcs. The main parameters of the developed concentrator

Figure 1. 3D model of a parabolic-cylinder concentrator with a louvered heliostat

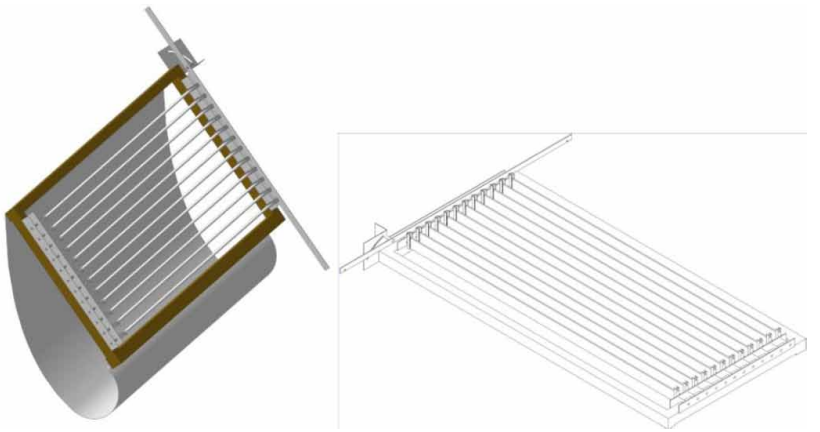

solar module with a system of louvered heliostats will be presented in tabular form below.

The height of the mirror slat is 40 mm, length 1240 mm, thickness 4 mm, the number of 12 pcs. The main parameters of the developed concentrator solar module with a system of louvered heliostats will be presented in tabular form below.

DESIGN AND PRODUCTION OF THERMAL PHOTOELECTRIC RECEIVER

In the production of solar thermal photovoltaic modules for insulation can be used energy-saving vacuum glazing (Filippchenkova, Panchenko, 2016; Mitina, Strebkov, Trushevsky et al., 2010). For the production of a solar thermal photovoltaic concentrating module, it was decided to replace it with an ordinary double-glazed window with an air gap.

An experimental thermal photovoltaic receiver of the concentrating module was made according to the designed sketches (Figure 2). The sealing of photovoltaic cells was carried out using a two-component polysiloxane compound, which provides the best characteristics of solar cells with concentrated solar radiation and high temperature (Strebkov, Persits, Panchenko, 2014; Panchenko, Strebkov, Persits, 2015).

The thermal insulation of the bottom surface of the module is made of two sheets of cellular polycarbonate 4 mm thick each, the side walls are insulated with rubber cords 10x12 mm. The frame of the receiver is made of aluminum profile (thickness 2 mm).

Solar cells are located on a blackened water radiator.

Figure 2. Producted thermal photovoltaic receiver concentrator solar installation

One of the main elements of the PVT-receiver layout is the coolant channel for a fluid, which has a rectangular cross-section in cross section, on the face (illuminated) side of which there is an ESS. The liquid is poured into the tank by means of a flexible liner and a pipe located at the base of the experimental PVT receiver, and the drainage is carried out using similar elements located on the opposite side of the module.

Table 1 presents the main technical characteristics of the developed concentrator solar module with a system of louvered heliostats.

Table 1. Main technical characteristics of a concentrator solar module with a system of louvered heliostats

Parameter	Value
Concentrator type	Parabolo cylindrical
Electric power (E=1000 W/m^2), W	13,736
Open circuit voltage, V	10,233
Short circuit current, A	1,773
Fil-factor (FF), %	75,73
Area of solar cells, m^2	0,141
Type of colar cells	Si
Geometric concentration coefficient	2,6
Overall dimensions of the thermal photoelectric receiver, m	1,227 x 0,162 x 0,034
Electric efficiency (η_{el}), %	10,175
Thermal efficiency (η_t), %	60
Optical efficiency (η_{opt}), %	75
Heat carrier	Water
Overall dimensions of the parabolic-cylinder concentrator, m	1,3 x 0,6 x 0,2
Heliostat mirror lamella area, m^2	0,6
Concentrator weight, kg	5
Heliostat mass, kg	5
Receiver weight, kg	8

PROGRAM AND METHODS OF FIELD, LABORATORY TESTS

The greatest influence on the efficiency of solar photovoltaic and thermal modules is provided by meteorological parameters: the intensity of solar

radiation, the temperature of the surrounding air. Existing standards (ANSI/ ASHRAE 92-1986 (RA91), 1986; ISO 9806-1:1994, 1994; AS 2535-1896; AS/NZS 2535.1:1999, 1999; DIN 4757/4, 1982) and methods for testing solar thermal modules allow experimental studies to be carried out both in situ and in laboratory conditions. When conducting experimental tests of thermal modules using stationary techniques, the most important factor is the constancy of meteorological conditions for a long time. According to the method (ASHRAE Standard 93-77, 1977), tests are conducted at around midday hours on clear days. According to the requirements of standards, the coolant flow rate must be maintained during the experiment within ± 1 ... 5%, the temperature of the coolant at the inlet must be maintained with an accuracy of ± 0,1 ... 0,5 ° C.

Field test targets:

1. Confirmation of the developed program for calculating the flux of solar radiation on the receiving surface of the solar module with a non-tracking parabolic cylindrical concentrator and a system of linear louvered heliostats.
2. Determination of energy characteristics:

photovoltaic module - measured parameters:
short circuit current (I_{sc}), open-circuit voltage (V_{oc}), obtaining current-voltage characteristics, ambient temperature (t_{am}), insolation (direct, total);
photovoltaic thermal module - measured parameters:
short circuit current (I_{sc}), open-circuit voltage (V_{oc}), obtaining current-voltage characteristics; water consumption L, ambient temperature t_{am}, inlet temperature to the receiver t_{in}, temperature at the outlet from the receiver t_{out}, insolation (direct, total).

The experimental research methodology includes the following steps:

1. Installation of the experimental module at the calculated angle of inclination of the surface of the entrance of the concentrator to the horizon with orientation to the geographical South.
2. The choice of the schedule for adjusting the angle of inclination of the louvre slats of the heliostat in accordance with the date of the test day.
3. Determination of the level of solar radiation incident on the radiation receiver for a parabolic-cylindrical concentrator during the day at a given angle of inclination of the surface of the concentrator entrance to the horizon.

4. Investigation of the energy characteristics of the solar module with a non-tracking parabolic cylindrical concentrator and a system of linear louvered heliostats in accordance with the set of variable parameters for testing purposes (see above)
5. Saving the obtained experimental data for further processing.

INSTRUMENTS AND EQUIPMENT USED FOR TESTING AN EXPERIMENTAL CONCENTRATOR SOLAR MODULE WITH A LOUVERED HELIOSTAT

In the course of the pilot study, the equipment of the laboratory laboratory was used at the VIESH, and a system for automatic data recording was also developed.

When conducting full-scale studies of solar modules, it is often difficult to quickly determine some parameters, for example, current-voltage characteristics. For this reason, other quantities are measured, which also determine the photoelectric parameters, such as the open circuit voltage V_{oc} and short circuit current I_{sc}. To check and adjust the angle of inclination of the surface of the entrance of the concentrator to the horizon, as well as the angle of inclination of the heliostat lamellae, two protractors were installed on the frame of the louvre heliostats system (Figure 3a).

To measure the intensity of solar radiation, the pyranometer «PELENG SF-61» was used by the single-channel company «Peleng» OJSC Republic of Belarus (Figure 4).

Temperature Sensors and Automatic Experimental Data Recording System

When conducting full-scale tests of an experimental sample of a solar concentrating module, it is necessary to ensure the accuracy and comparability of the results obtained, for which purpose it is desirable to monitor the processes in dynamics. In this regard, a system was created to automatically register the main parameters of the solar concentrating module in the course of field studies (Filippchenkova, Kharchenko, 2017).

Figure 5 shows the block diagram of the system for automatic registration of solar concentrating module parameters.

Figure 3. Photos of the experimental concentrating module under study with a PVT receiver: a) side view, b) front view

a)

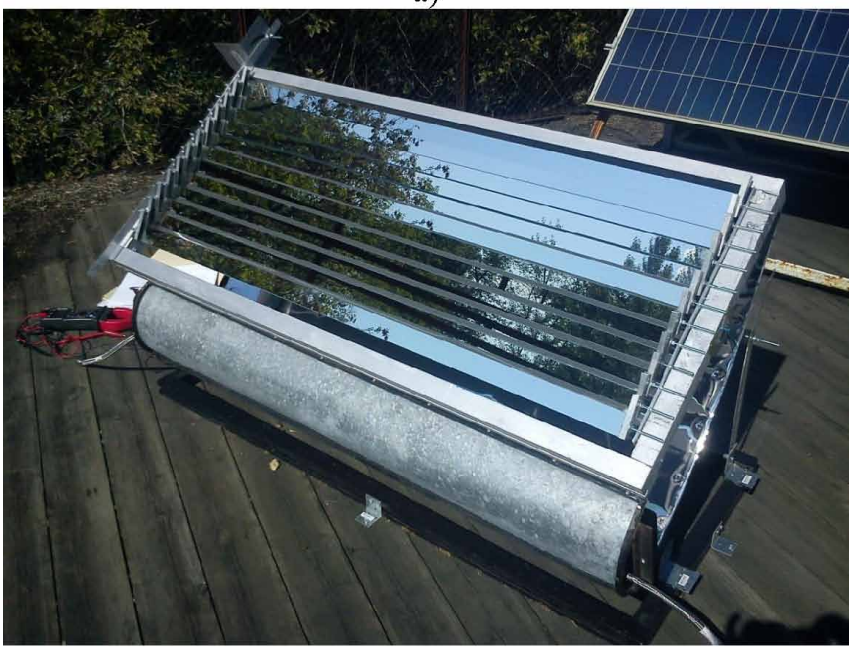

b)

Figure 4. Pyranometer "PELENG SF -61"

Figure 5. Block diagram of the system of automatic registration of parameters of the solar concentrating module

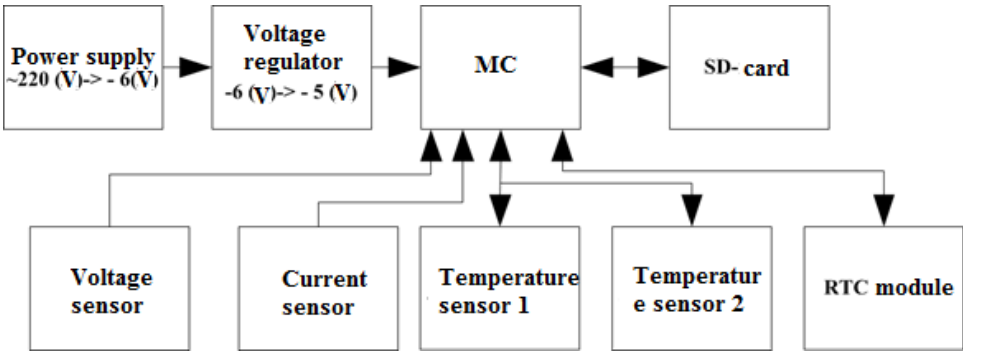

The proposed complex of automatic registration of the main parameters of the solar concentrating module was developed on the basis of the ATmega328-PU microcontroller (MC) from Atmel. This microcontroller was chosen for economic reasons. is not expensive and contains a sufficient amount of non-volatile FLASH, RAM SRAM memory for the execution of the program code. The software code developed on the Arduino platform is an electronic designer and a convenient platform for the rapid development of electronic devices. The platform has become popular all over the world due to the convenience of a programming language (based on C / C ++), as well as an open architecture and program code. Programmed via USB without

Figure 6. The appearance of the platform Arduino Uno (вид сверху)

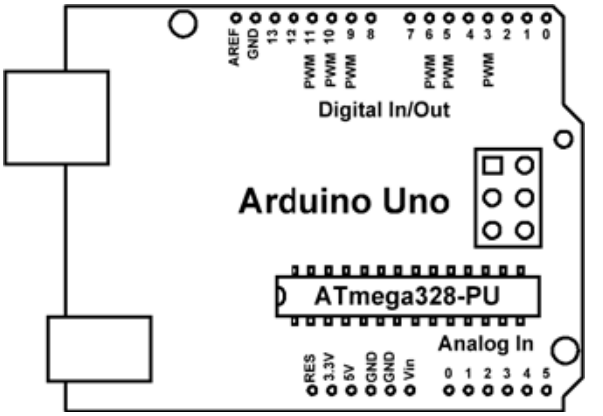

using programmers (Petin, V.A., 2016). Figure 6 shows the appearance of the ATmega328-PU platform.

A DS18B20 digital temperature sensor (Bloom, 2015) was used as a temperature sensor. Digital sensors are much more accurate than analog sensors, with the DS18B20 temperature sensor, the error is only 1%, and the resolution is 12 bits, which allows for more accurate temperature measurement.

Figure 7 shows the connection of the temperature sensor to the MC. The sensor is connected as follows: the GND pin with DS18B20 is connected to GND on the MC, the Vdd pin from the DS18B20 is connected to + 5V on the MK, the Data contact from the DS18B20 is connected to any digital pin on the MC. The only thing that needs to be added from the external additional strapping is a 4,7 kΩ pull-up resistor. You can connect several DS18B20 digital temperature sensors in parallel, but for a large number of sensors (more than 10), you need to use resistors with less resistance (for example, 1,6 kΩ or even less).

In this data logging system, reliable time control without interruption is required. If the power of the microcontroller disappears, the time counter will be lost. Therefore, the developed system uses an external real-time clock module RTC (Real time clock) with an integrated backup power source (lithium battery type - CR1225) (Technical description of the chip ACS712, 2017). A standard CR1225 battery produces a voltage of 3 V and has a capacity of 47 mAh. The RTC module contains a DS1307 chip, the current consumption of which is 300 (nA), then when powered from a lithium cell type CR1225, the module can work for about 17 years without external power (47mAh / 300nA = 156666, 67 hours = 6527, 78 days = 17, 87 years old). The data

Figure 7. Connection scheme DS18B20 to MC located on the board Arduino Uno

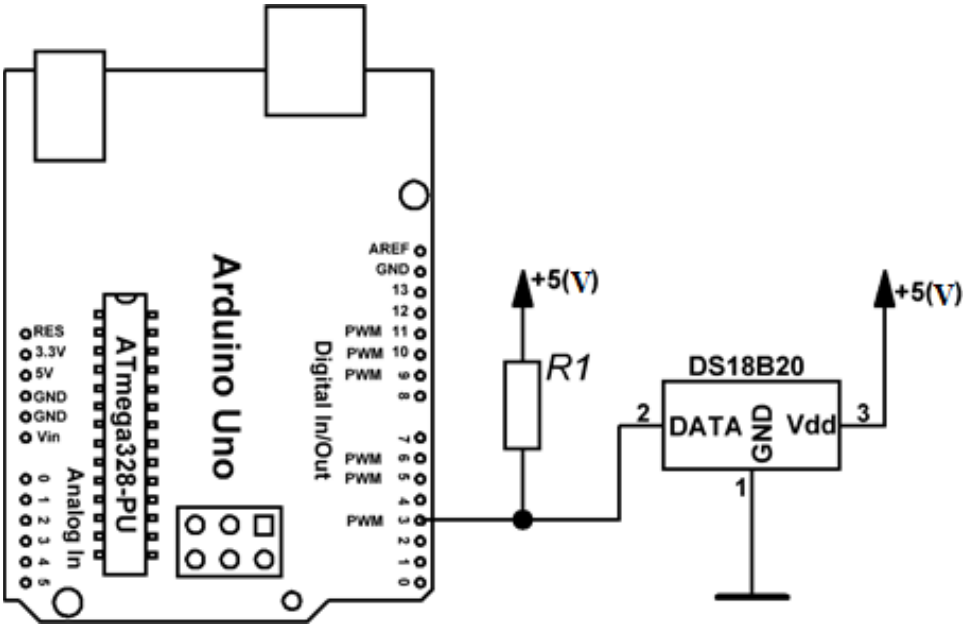

logging step is set in the program depending on the required periodicity of measurements; therefore, data can be recorded both hourly and at a higher frequency.

Since experimental studies should be carried out over a long period of time, for convenience, a universal high-speed module of SD + MicroSD card reader and an SD card was used, on which a CSV file was created containing a set of collected experimental data (Technical description of the chip ACS712, 2017).

To measure the short circuit current is used current sensor ACS712. The sensor determines the current value in the DC and AC circuits in the range up to 20 A. The ACS712 sensor error is 1.5%, and the measured current range is from –20 to +20 A (Technical description of the chip ACS712, 2017). The range of measurement and accuracy of the devices included in the complex are presented in the final table 2.

It should be noted that the current and voltage sensors used were calibrated using a calibrated laboratory power supply unit HY3005-3, while the average deviation of the readings was 1.15%, which corresponds to the measurement accuracy claimed by the manufacturer (Table 2).

Table 2. Measurement range and accuracy of instruments included in the measuring complex

Device name	Measured parameter	Measurement range	Measurement accuracy
Pyranometer Peleng SF -61	Solar radiation	10 ÷ 1600 W/m^2	2%
Multimeter MASTECH MY68	Open circuit voltage	326 mV÷1000 V	±0,5%
	Short circuit current	0,326 mA÷10 A	±2%
Digital temperature sensor DS18B20	Temperature	-55 °C ÷ +125 °C	0,5°C
Analog current sensor ACS712	Short circuit current	−20÷ +20 A	1,5%
Analog voltage sensor VDC 25V	Open circuit voltage	0 ÷25 V	1%

The wiring diagram is presented in Appendix B. All operations performed by the microcontroller are specified in the text of the written firmware.

RESULTS OF FIELD TESTS OF AN EXPERIMENTAL CONCENTRATOR SOLAR MODULE

Volt-Ampere Characteristic of a PV (T) Solar Concentrator Receiver Module

The VA-characteristic, measured under natural conditions, allows us to estimate the actual efficiency of the PV (T) receiver of the concentrator solar module. Figure 4.8 shows the IVC of a PV (T) receiver measured using a solar simulator with a single long-pulse flash PICOSOLAR.

As can be seen from figure 8, the PV (T) receiver (photovoltaic panel) with a SR intensity of 1000 W/m^2 and a working temperature of 25 ºC has a power of 13.7 W, and the electrical efficiency 10,175%.

Analysis of the Electrical Parameters of the PV Receiver of the Concentrator Solar Module

The first stage of experimental research was to study the electrical parameters of a solar concentrating module with a PV-receiver. To illustrate the operation of the measuring unit of the automatic recording system of experimental data, Figures 9-10 show time diagrams of characteristic days for a short-

Figure 8. VA-characteristic (1) and power curve (2) a PV (T) receiver of a solar concentrating module developed at an SR intensity of 1000 W/m² and an operating temperature 25 ºC

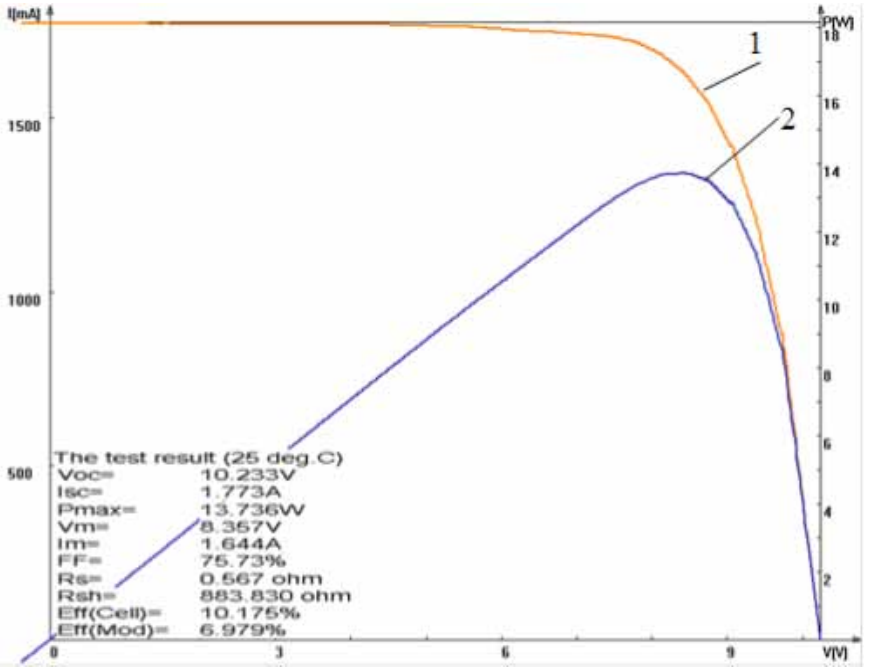

circuit current I_{sc}. PV receiver, insolation: total E_{Σ} and direct E_{dr}, as well as the ambient air temperature values t_{am} taken from the temperature sensor.

Graphs are obtained on the measuring unit with a recording interval of 1 s. Also, Figures 4.11–4.12, 4.14–4.15 show time diagrams for the short-circuit current I_{sc}, the open-circuit voltage of the V_{oc} PV-receiver, the insolation: the total E_{Σ} and the direct E_{dr}, as well as the values of the ambient air temperature t_{am} obtained for characteristic days on the measuring unit.

Figure 13 shows the IVC and the power curve of the PV receiver of the solar concentrating module with a total insolation on the surface perpendicular to the beam of 818 W/m² and the temperature of the solar cells 29 ºC.

As can be seen from Figure 13, the PV receiver with a total insolation of 818 W/m² and a solar cells temperature of 29 ºC has a peak power of 18,5 W.

Figure 16 graph of electrical power 12.08.2017 based on experimental data.

Figure 9. Module performance graphs, the angle of inclination of the concentrator inlet surface to the horizon β=10°, slant angle lamellae α=104°: I_{sc} (1), t_{am} (2), E_{Σ} (3), E_{dr} (4)

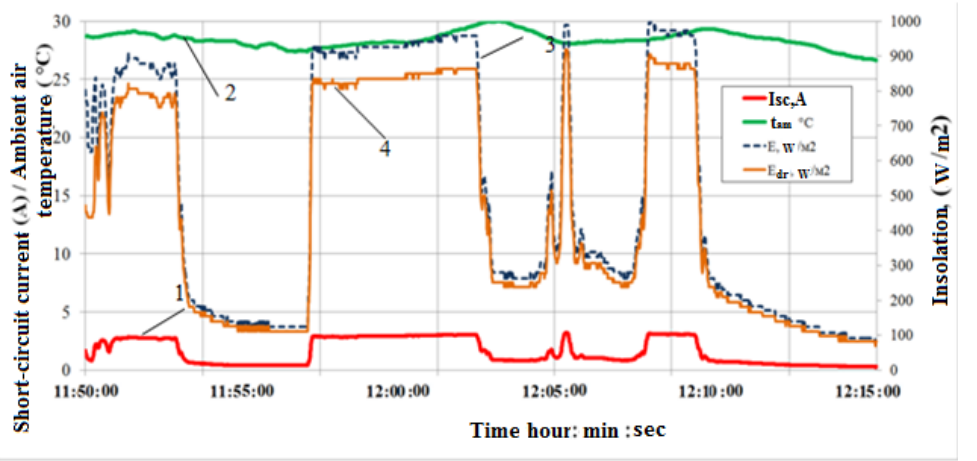

Figure 10. Module performance graphs, the angle of inclination of the concentrator inlet surface to the horizon β=15°, slant angle lamellae α=104°: I_{sc} (1), t_{am} (2), E_{Σ} (3), E_{dr} (4)

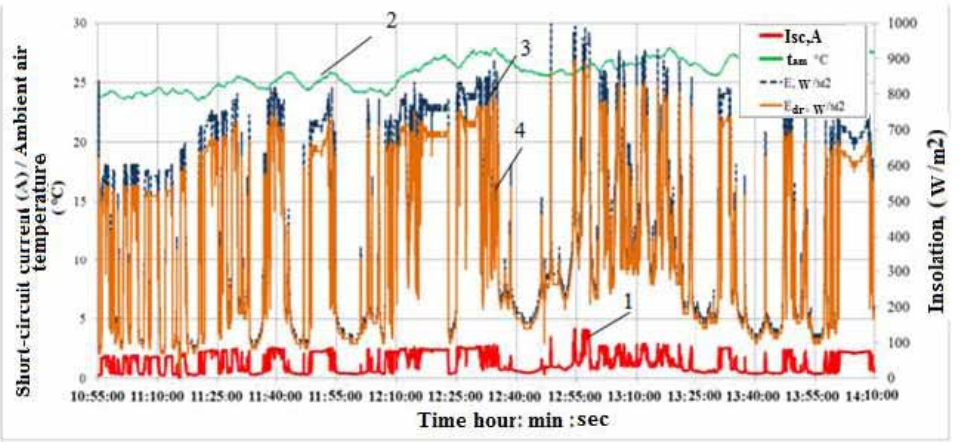

The effect of temperature on the efficiency of solar cells is calculated based on the dependences of the open-circuit voltage, short-circuit current, summarized in the works (Kharchenko, Nikitin, Tikhonov, 2010; Buresch, 1983).

Figure 11. Change insolation and ambient temperature: t_{am} (1), E_{Σ} (2), E_{dr} (3)

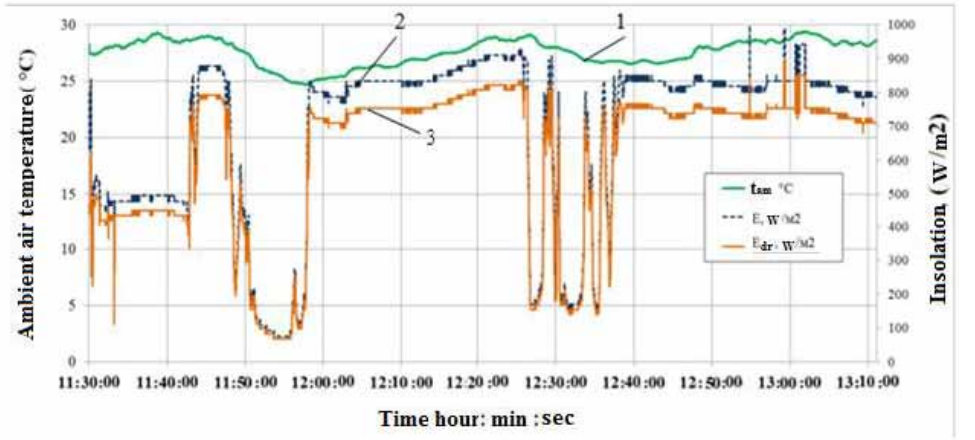

Figure 12. Graphs of performance of the module, the angle of inclination of the surface of the concentrator entrance to the horizon β=10°, slant angle lamellae α=100°: I_{sc} (4), V_{oc} (5)

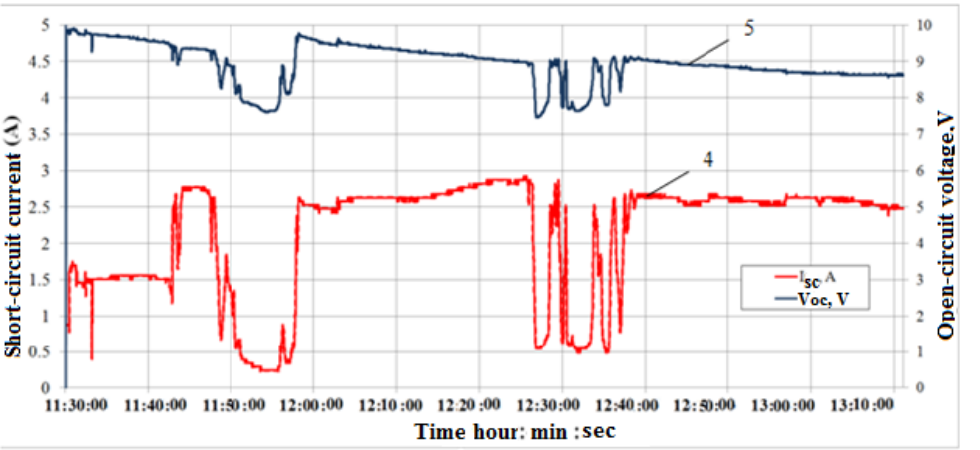

As can be seen from Figure 4.16, the effect of insolation on the production of electric energy is very significant, the indicators are reduced by several times.

Figure 13. VA-characteristic (1) and power curve (2) PV-receiver of a solar concentrating module with total insolation of 818 W/m² and temperature of solar cells 29 ºC

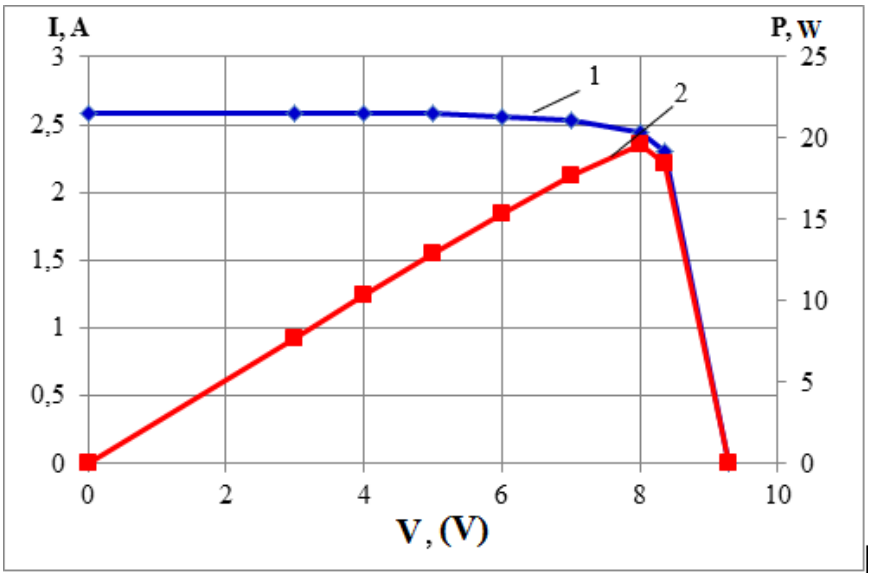

Figure 14. Change insolation and ambient temperature: t_{am} (1), E_{Σ} (2), E_{dr} (3)

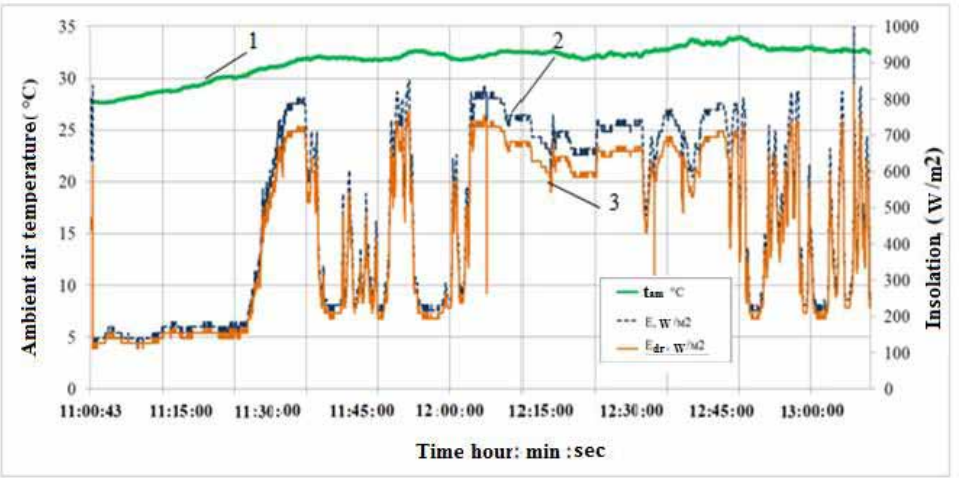

Figure 15. Module performance graphs, the angle of inclination of the concentrator inlet surface to the horizon β=10°, slant angle lamellae α=98°: I_{sc} (4), V_{oc} (5)

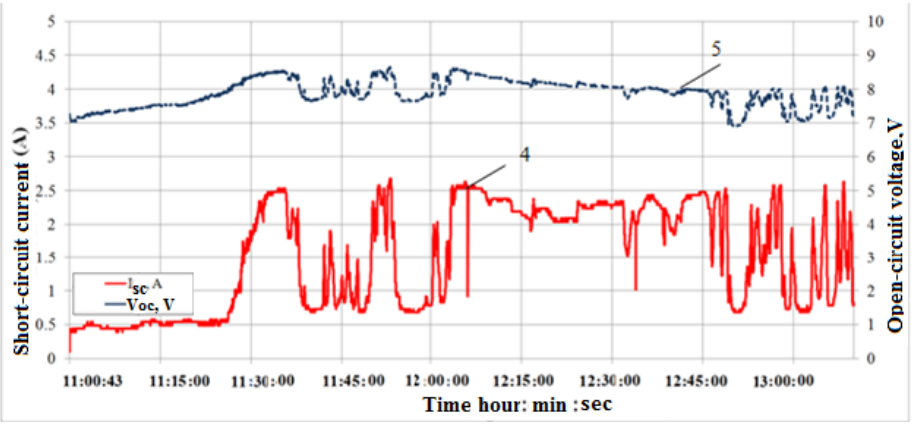

Figure 16. Graph of electrical power, the angle of inclination of the surface of the concentrator inlet to the horizon β=10°, slant angle lamellae α=100°: P_{el} (1), E_{Σ} (2), E_{dr} (3)

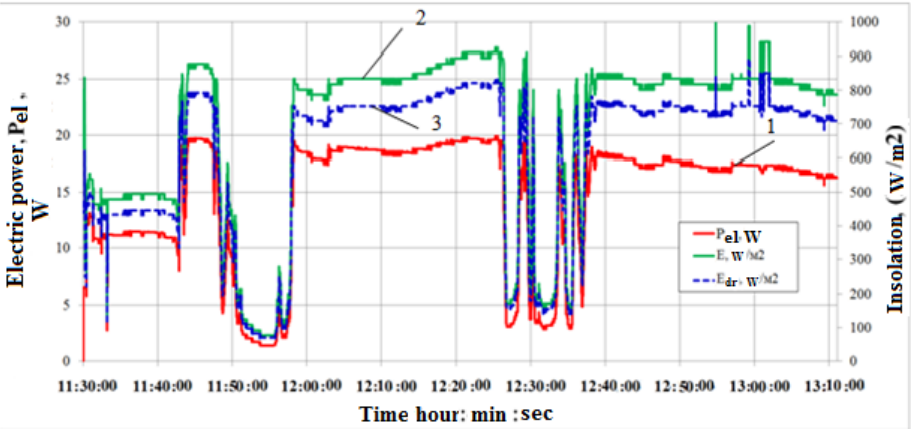

Analysis of Electrical and Thermal Parameters of a PVT Receiver of a Concentrator Solar Module

To illustrate the operation of the measuring unit of the automatic recording of experimental data for the characteristic days, Figures 17-18 show time diagrams for the short-circuit current I_{sc} PVT-receiver, insolation: total E_{Σ} and direct E_{dr}, as well as values of ambient air temperature t_{am}, inlet temperature t_{in}

and receiver output t_{out}, taken from temperature sensors. Graphs are obtained on the measuring unit with a recording interval of 1 s.

To illustrate the operation of the measuring unit of the automatic recording of experimental data, Figures 19-20 provide time diagrams for the short-circuit current I_{sc} PVT-receiver, insolation: total E_{Σ} and direct E_{dr}, as well as values of ambient air temperature t_{am}, inlet temperature t_{in} and receiver output t_{out}, taken from temperature sensors, *L*–coolant flow. The graphs are obtained on the measuring unit with a recording interval of 1 s.

Figure 17. Module performance graphs, the angle of inclination of the concentrator inlet surface to the horizon β=15°, slant angle lamellae α=106°: I_{sc} (1), E_{Σ} (2), E_{dr} (3)

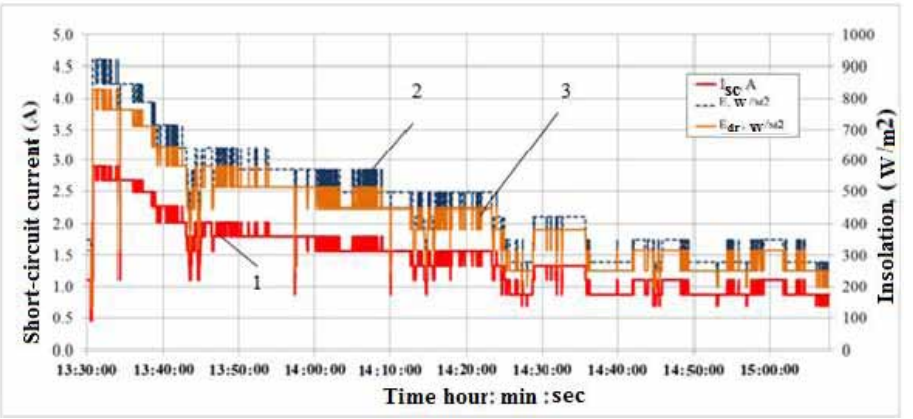

Figure 18. Module performance charts
**t_{am} (1), t_{in} (2), t_{out} (3), obtained by the measuring unit, the angle of inclination of the surface of the inlet of the concentrator to the horizon β = 15 °, slant angle lamellae α = 106 °, the flow rate of the coolant was: from 13:37 to 14:03 L=8,1 l/h, c 14:03 ∂o 14:34 L=9,6 l/h*

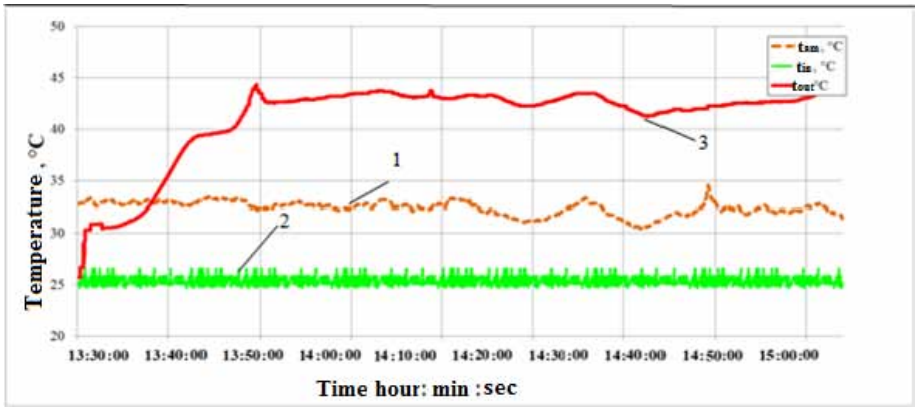

Figure 19. Module performance graphs, the angle of inclination of the concentrator inlet surface to the horizon β=15°, slant angle lamellae α=108°: I_{sc} (1), E_{Σ} (2), E_{dr} (3), V_{oc} (4)

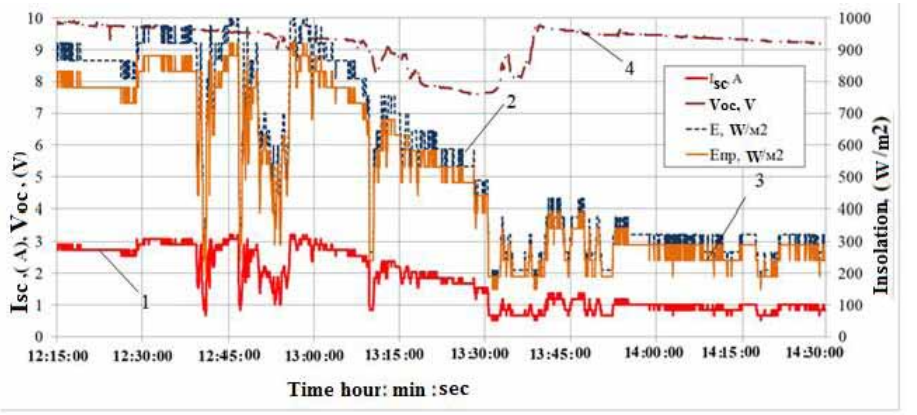

Figure 20. Module performance graphs: t_{am} (5), t_{in} (6), t_{out} (7), L (8), received by the measuring unit, the angle of inclination of the concentrator inlet surface to the horizon β=15°, slant angle lamellae α=108°

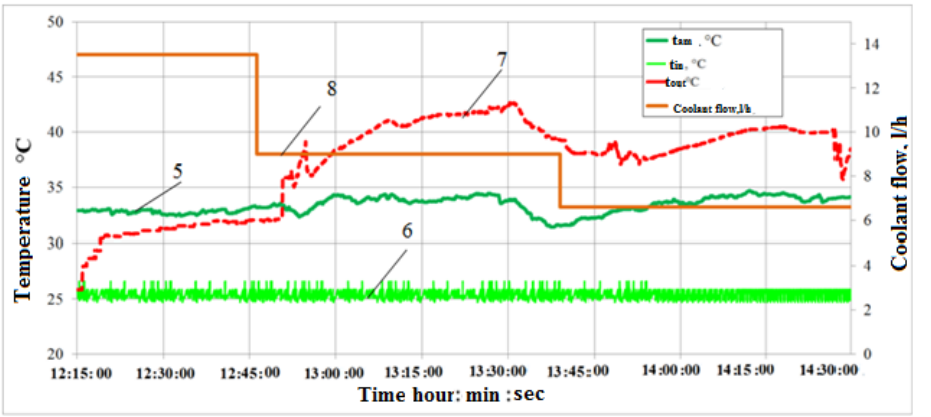

Figure 21 shows the dependence of the coolant temperature at the exit from the receiver on the flow rate (the value of the total insolation on the surface perpendicular to the beam is 866 W/m^2).

Figure 22 shows the IVC and the power curve of the photovoltaic panel of the PVT receiver of the solar concentrating module with total insolation of 976,7 W/m^2 (water consumption 13,5 l/h).

Figure 21. The dependence of the temperature of the coolant at the outlet of the receiver from the flow

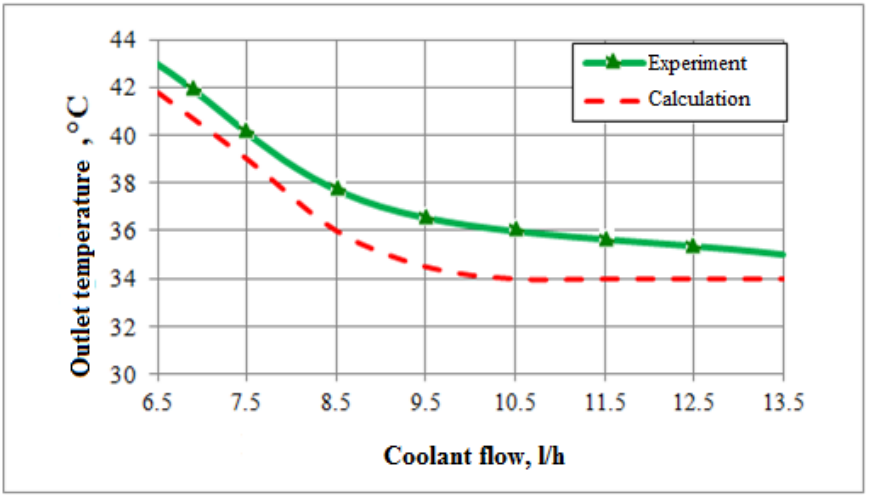

Figure 22. IVC and power curve of a PVT receiver of a solar concentrating module with total insolation 976,7 W/m² (water consumption 13,5 l/h)

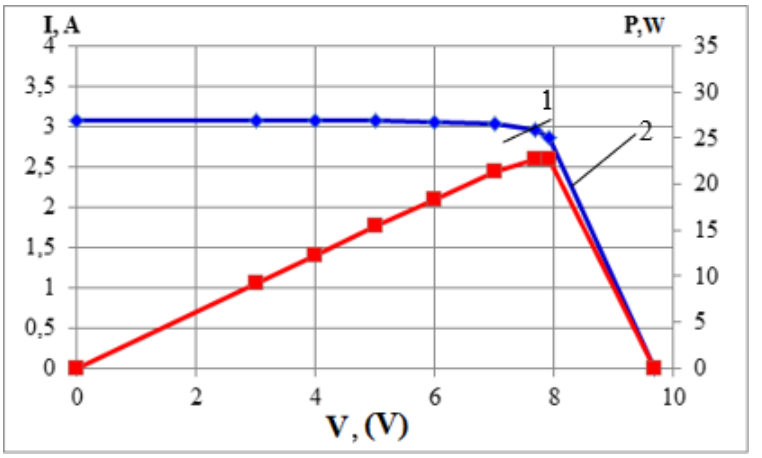

Along with the temperature of the coolant at the output of the PVT-receiver, an important parameter determining the efficiency of the concentrating module is thermal power. Figure 23 shows the plot of heat and electric power on 27.07.2017 based on experimental data and a calculation model.

Figure 23. Graph of heat and electric power angle of inclination of the inlet surface of the concentrator to the horizon β=15°, slant angle lamellae α=108°: $P_{m.}$ (1), E_{dr} (2), P_{el} (3)

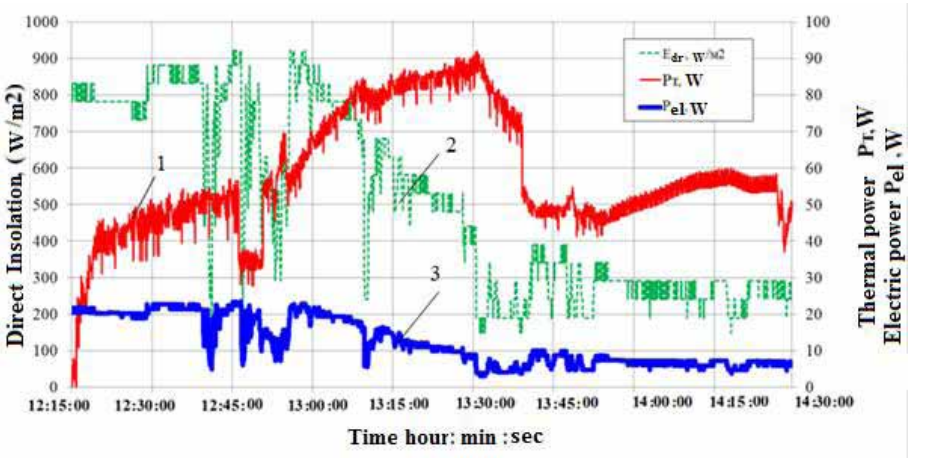

Thermal power of the PV (T) -module is based on the expression:

$$P_m = c \bullet \rho \bullet L \cdot (t i_n - to_{ut}), \tag{4.1}$$

where c– specific heat of water, J/kg·°C; ρ – water density, kg/m^3; L – water flow, m^3/c; t_{in}, t_{out} – water temperature at the inlet and outlet channels, respectively, °C.

COMPARISON OF EXPERIMENTAL AND CALCULATED DATA

During the tests, the date, time, direct solar radiation on the normal to the beam surface B_{ne} and short-circuit current I_e of the pre-calibrated photoelectric radiation receiver (0,00314 A / (W/m^2)) were recorded. The computer model allows for any given point in time to calculate the average density of the solar radiation flux on the surface of the receiver B_{tm}, and, consequently, the short circuit current of the module. Since the program works with a meteorological database containing average long-term insolation values, for comparison with actually measured values it is necessary to correct the calculated values obtained.

Rated short circuit current corresponding to the test conditions of the module:

$$I_m = 0.00314 B_{tm} \frac{B_{ne}}{B_{nm}}, \tag{4.2}$$

where B_{nm} – the average long-term value of direct solar radiation on the surface normal to the beam, W/m^2.

The relative error of the computer model:

$$\Delta = \frac{I_m - I_e}{I_e} 100, \% \tag{4.3}$$

A sample of experimental data and computer simulation results for the same points in time are shown in Table 3, Moscow time.

Table 3. Comparison of calculated and experimental results

Date	Time	Experiment		Computer model			Error, %
		B_{ne}	I_e, A	B_{nm},	B_{tm}	I_m, A	
11.07.2017	12:05	846	3.02	354	396	2.97	-1.7
05.08.2017	12:30	748.3	2.63	327	382	2.74	4.2
12.08.2017	11:46	723.95	2.45	340	367	2.45	-3

CONCLUSION

The developed system of automatic measurement of the main parameters of a solar concentrating module with PV, PVT and heat receivers allows you to save time during information processing, to obtain data on the dynamics of the processes in the solar concentrating module with the required measurement periodicity.

During the experimental study of a concentrating module with a PVT receiver, it was found that the ratio of the thermal power of the PVT receiver to the electric one with direct insolation values of 800 ± 100 W/m^2 is in the range from 1:1 to 5:1 with a thermal efficiency of 0,6– 0,7. With equal values of insolation and ambient temperature, the production of electricity

by the PVT-receiver photovoltaic panel is on average 10–25% higher than that of the PV-receiver.

The developed algorithm for calculating the passage of sunlight through the mirror surface of the lamellae and the parabolic cylinder, implemented as a computer program, allows calculating the flow of solar radiation on the receiving surface of the solar concentrator with a relative error of not more than 5%, which is confirmed by experimental data.

REFERENCES

ANSI/ASHRAE 92-1986 (RA91). (1986). Methods of testing to determine the thermal performance of solar collectors.

AS 2535-1896. Solar collectors with liquid as the heat-transfer fluid – Method for testing thermal performance.

ASHRAE Standard 93-77. (1977). New York: American Soc of Heating, Refrigerating and Air-Conditioning Engineers.

AS/NZS 2535.1:1999. (1999). Test method for solar collectors including pressure drop.

Bloom, J. (2015). *We study Arduino: tools and techniques of technical magic*. BVH – Petersburg.

Buresch, M. (1983). *Photovoltaic Energy Systems: Design and Installation*. McGraw-Hill.

DIN 4757/4. (1982). Determination of Efficiency, Thermal capacity and pressure drop of solar collectors. W. Berlin: Beuth Verlag.

Filippchenkova, N. S., & Kharchenko, A. V. (2017). Development of an automatic system for registering the main parameters of a solar concentrator plant. *Fundamental and applied problems of physics: Proceedings of the international conference June 13-14, 2017*, *Academy of Sciences of the Republic of Uzbekistan Scientific and Production Association «Physics-Sun»*, 192-195.

Filippchenkova, N.S., & Panchenko, V.A. (2016). Development and research of solar thermal photovoltaic modules. *Theoretical and Scientific-Practical Journal «Innovations in Agriculture», 5*(20), 136-141.

ISO 9806-1:1994. (1994). Test methods for solar collectors: Thermal performance of glazed liquid heating collectors including pressure drop.

Kharchenko, V., Nikitin, B., & Tikhonov, P. (2010). Utmost efficiency coefficient of solar cells versus forbidden gap of used semiconductor. *Adomavicius the 5th International Conference on Electrical and Control Technologies*, 289-294.

Mitina, I.V., Strebkov, D.S., Trushevsky, S.N., Alekhina, M.B., & Anurov, S.A. (2010). *Vacuum glass unit with indicator.* Patent for invention Nº 2382162 of the Russian Federation, IPC E06B 3/66. No. 2008151043/03; publ. 20.02.2010.

Panchenko, V.A., Strebkov, D.S., & Persits, I.S. (2015). Solar modules with extended service life at the level of nominal power. *Alternative Energy and Ecology*, *19*(183), 55 – 60.

Petin, V.A. (2016). Arduino and Raspberry Pi in Internet of Things projects. *BVH – Petersburg*, 320.

Strebkov, D. S., Kharchenko, V. V., Nikitin, B. A., Tikhonov, P. V., & Gusarov, V. A. (2013). Determination of conformity of the spectra of artificial light sources of the spectrums of standard solar radiation. *Moldavian Journal of the Physical Sciences*, *12*, 82–86.

Strebkov, D.S., Persits, I.S., & Panchenko, V.A. (2014). Solar modules with extended service life. Innovations in agriculture. Theoretical and scientific journal. *Innovations in Renewable Energy*, *3*(8), 154 – 158.

Technical description of the chip ACS712. (2017). Retrieved from http://files.amperka.ru/store-media/products/troyka-current-sensor/media/acs712.pdf

Chapter 5
Technical and Economic Characteristics of Solar Concentrating Modules With Louvered Heliostats

ABSTRACT

The calculations confirm the high efficiency of using louvered heliostats. The maximum annual energy production by non-tracking solar concentrating modules is achieved with a vertical orientation of the concentrator, which is very important when placing solar modules on the southern facades of buildings. The annual amounts of insolation at the receiver for concentrators with a louvered heliostat with an angular aperture of 26° and 18°, respectively, are on average 2 and 3.4 times higher than the total insolation on a flat surface and 1,6 and 2,2 times higher than insolation by blind surface receiving concentrating modules with similar angular aperture values. The cost of electricity produced when using non-glare concentrating modules with louvre is reduced by 40–60% compared to concentrating modules without louver, and thermal energy by 50%.

DOI: 10.4018/978-1-7998-4276-7.ch005

INTRODUCTION

The main factors hindering the development of solar energy in Russia are the lack of state support, as well as high competition from China, Japan, the USA, and Germany. However, there is a potential for the use of solar energy in Russia, especially in the Krasnodar Territory and Stavropol Territory, the eastern regions: Yakutia, the Magadan Region.

According to the Scheme and Development Program of the Unified Energy System of Russia for 2017–2023 the share of facilities based on renewable energy in the power balance of the UES of Russia will increase from 0,04% in 2016 to 0,9% by 2023, while the commissioning of new generating capacities (with a high probability of implementation) based on renewable energy sources in the UES of Russia in the period 2017–2023 are provided in the amount of 1875 MW.

GENERAL PROVISIONS FOR ASSESSING THE ECONOMIC EFFICIENCY OF SOLAR CONCENTRATING MODULES WITH DEFLECTING OPTICAL SYSTEMS BASED ON LINEAR LOUVERED HELIOSTATS

The methodological basis for evaluating the effectiveness of investments adopted in the work is the income-cost approach (Fomina, 2005). The design interval of the project covers the entire life cycle of the module operation – from the start of investment to the end of its operation. For economic evaluation, the estimated period is assumed to be equal to the life of the module – 25 years. The calculated interval is divided into time periods – steps whose duration is equal to one year. The moment of the end of the zero step is taken as the base moment of time, i.e. the year the module began operating.

The cost approach to evaluating the effectiveness of investments is an effective tool for the rapid preliminary comparison and ranking of alternative projects based on total discounted costs with preliminary fulfillment of the conditions of energy and economic comparability or on the basis of specific discounted costs per unit of useful product (Fomina, 2005).

Discounted costs reflect the year-specific costs, including capital investments in the project, the cost of production of products (electricity and heat) throughout the project life cycle, tax payments. Considering the instability of the Russian tax policy, in order to avoid distortion of the

calculation results, sometimes it is necessary to refuse to take into account taxes, which leads to an underestimation of project costs.

The effectiveness of investment is determined by comparing the discounted inflows and outflows of funds for the investment period. The criterion indicator here is net present value (NPV), defined as the difference between the amounts discounted to the beginning of the investment period of inflows and outflows of real money under the project for the entire investment period.

$$NPV = \sum_{t=0}^{T} P_t(1+d)^{-t} - \sum_{t=0}^{T} O_t(1+d)^{-t} \tag{5.1}$$

where P_t — real money inflow per year *t,* rub.; O_t — real money outflow per year *t,* rub.; d — rate of discount.

In fact, the difference between inflows and outflows of real money is an element of the flow of real money, that is:

$$R_t = P_t - O_t \tag{5.2}$$

As a result, NPV will be determined as the sum of the discounted elements of the flow of real money using the formula:

$$NPV = \sum_{t=0}^{T} R_t(1+d)^{-t} \tag{5.3}$$

If the NPV is greater than zero, this indicates that the discounted inflows are greater than the discounted outflows of real money for the entire investment period, which means investing in this project is cost-effective.

When NPV is equal to zero, the discounted inflows are equal to the discounted outflows of real money, the project's profitability is zero.

If NPV <0, the discounted outflows exceed the discounted inflows of real money for the entire investment period, which means investing in this project is economically inefficient, and therefore the project should be abandoned.

Discounted payback period (PBP – Pay-Back Period) – the period of time during which due to the inflow of real money the invested capital pays off (returns).

Determination of the payback period involves the calculation of the discounted elements of the flow of real money, followed by summing them on an accrual basis, taking into account the signs, until the sum of the

discounted elements of the flow of real money changes the sign from minus to plus, that is, if:

$$NPV_t = \sum_{t=0}^{t} R_t (1+d)^{-t} < 0,$$

$$NPV_{(t+1)} = \sum_{t=0}^{t} R_{(t+1)} (1+d)^{-(t+1)} > 0,$$

this means that the invested capital pays off in the period between the year t and the year (t + 1) of the investment period and the payback period is determined by the formula or graphically:

$$PBP = t \frac{NPV_t}{NPV_{(t+1)} - NPV_t} \tag{5.4}$$

In the framework of the calculation of economic efficiency as the main indicators are determined: net present value (*NPV*); discounted payback period (*PBP*); investment profitability index (*PI* – Profitability Index).

When assessing the economic efficiency of the implementation of renewable energy projects, the most complete economic indicator is the full present value of electricity / thermal energy (*LCOE – Levelized Cost of Energy*) – this is the ratio of the total reduced capital and operating costs to the volume of generated energy over the entire project implementation period. The indicator is used to estimate the minimum market price at which electricity (thermal energy) is to be sold, to ensure the payback of all types of project costs during the implementation period. The main calculation formula of the LCOE method is (Executive Summary - Projected Costs of Generating Electricity – 2015 Edition, 2017)

$$LCOE = \frac{\sum_{t=1}^{n} \frac{Kt + K\text{-}xpt}{(1+d)^t}}{\sum_{t=1}^{n} \frac{Wt}{(1+d)^t}}, \tag{5.5}$$

where W_t – energy production.

The LCOE method is universal and convenient for a comparative analysis of different types of energy production technologies, is used by many authoritative organizations (in particular, the International Energy Agency IEA) and fully meets the requirements for methods of preliminary economic comparisons of options (versatility, simplicity of the estimation algorithm, transparency of setting initial data).

ESTIMATION OF CAPITAL COSTS FOR THE INSTALLATION OF SOLAR CONCENTRATING MODULES WITH LINEAR LOUVERED HELIOSTATS

In general, the capital costs of all components and the installation of a standard photovoltaic system integrated into the facade of a building (flat modules without a concentrator) can be calculated using the following formula (Petrov, 2015):

$$K_{SPS}=K_{SC}+K_{ak}+K_{in}+ K_{eq}+K_{\text{inst}}, \tag{5.6}$$

where K_{SPS} – total investment, rub.; K_{SC} – investments due to solar cells, rub.; K_{ak} – investments due to batteries, rub.; K_{in} – investments due to inverters, rub.; K_{eq} – investments due to additional equipment, rub.; K_{inst} – investments due to the installation and installation of system elements, rub.

When calculating the capital costs of a photovoltaic system with concentrators and with louvered heliostats, it is necessary to add capital investments to the general investments due to the concentrating system and the tracking system:

$$K_{con\Sigma}= K_{SPS}+K_{con}+K_{track}, \tag{5.7}$$

where K_{con} – the investment due to the concentrator, the concentrator frame and the system of louvered heliostats, as well as the assembly of the concentrating module, rub.; K_{track} – investment, due to the tracking system, including tracking sensors, automation units, etc., rub.

Description of the Income and Expenditure Parts

The operating costs of maintaining the systems in question are insignificant in the first place because there is no need for fuel to generate electricity. The surface of the modules can be cleaned together with the adjacent glass surfaces of the facade, so no additional measures are required.

The only item of operating costs is the periodic monitoring of the health of the rotation control system of a louvered heliostat.

Since the lifetime of the servo drive (8 years) is less than the estimated service life of the system of concentrating modules with louvered heliostat, it is necessary to periodically replace the equipment that has served its life. At the same time, these periodic costs should be taken into account with regard to inflation. Then the cost of the servo in the year t is determined on the basis of the expression:

$$K_{drt} = K_{dr} \bullet (1 + i/100)^t \tag{5.8}$$

where K_{dr} – the cost of the servo at the start of the project, rub.; i – annual inflation, %.

The cost of annual maintenance and technical inspections of the servo was taken as 0,5% of the cost of the servo.

The values of electricity generation (heat energy) are a key factor in determining the economic efficiency of the implementation of investment projects for the design and modernization of building facades using photovoltaic systems. Revenues at the t-th project step are calculated by the formula:

$$P_t = W_t \bullet C_3, \tag{5.9}$$

where P_t – the inflow of real money in year t, rub.; W_t – the energy production of the system of modules (flat and with concentrators) per year t taking into account the degradation of the modules and the power consumption for the own needs of the system, kWh; C_e – tariff for electricity (thermal energy), rub./kWh.

The tariff is taken taking into account the projected growth for the region in which the project will be implemented.

In this section, the prospects of using a system of solar concentrating modules with deflecting optical systems based on louver heliostats will be estimated using the example of three geographical points: s. Perovo (Crimea), Sochi,

Dubai (United Arab Emirates). A detailed calculation of the characteristics produced by the example with. Perovo (Crimea).

For 2018, the single-rate tariff differentiated in three zones in the peak zone for electricity in the Republic of Crimea is 9,09 rub./kWh (Electricity tariffs for the city of Sevastopol from January 1, 2018, 2017). From 01.07.2018, the tariff for thermal energy for the Simferopol region of the Republic of Crimea will be 2483,65 rub./Gcal or 2,14 rub./kWh (Tariffs from January 1, 2018 in the Republic of Crimea: for hot, cold water and drainage, 2017). According to the forecast of the Ministry of Economic Development of the Russian Federation, the final prices for electricity in the retail market will increase for all categories of consumers in 2018 by 5,4–5,9% per year, in 2019 the rise in prices for electricity will be 5,1–5,6%, the tariffs for thermal energy were indexed from July 2017 by 4,1%, from July 2018 – by 3,9% and from July 2019 – by 3,7 percent (Electronic resource, 2017). According to Rosstat, inflation in 2017 was 7%, in the long-term, given the forecast of the Ministry of Economic Development, the annual average inflation rate in Russia should be 5% (The real inflation in Russia… 2017).

ESTIMATION OF ECONOMIC EFFICIENCY OF SOLAR CONCENTRATING MODULES WITH LOUVERED HELIOSTATS

The assessment of the economic efficiency of solar concentrating modules with louvered heliostats is made on the basis of calculations of the annual production of electrical and / or thermal energy by the system.

For the year, the specific energy output is determined by summing the monthly output values, found in turn, based on the hourly calculation of energy production for each specific day of the month.

Evaluation of Projected Energy Production by Solar Concentrating Modules with Louvered Heliostats

For a preliminary assessment, consider several options for solar modules integrated into the facade of the building at an angle of 90° («vertical wall»):

- flat module;

- concentrating module with an angular aperture of 26° (geometric coefficient of concentration 4.3) without louvered heliostats;
- concentrating module with an angular aperture of 26° (geometric coefficient of concentration 4.3) with a system of louvered heliostats;
- concentrating module with an angular aperture of 18° (geometric coefficient of concentration 5.5) without louvered heliostats;
- concentrating module with an angular aperture of 18° (geometric coefficient of concentration 5.5) with a system of louvered heliostats.

In the first approximation, the criterion of the performance of solar modules will be the annual amounts of insolation on the receiving surface. The calculation is given by the example of three geographical points: s. Perovo (Crimea), Sochi, Dubai (United Arab Emirates). The results of the calculations are shown in the figures 1-3.

Figure 1. Annual amounts of insolation on the receiver (s. Perovo, Crimea)

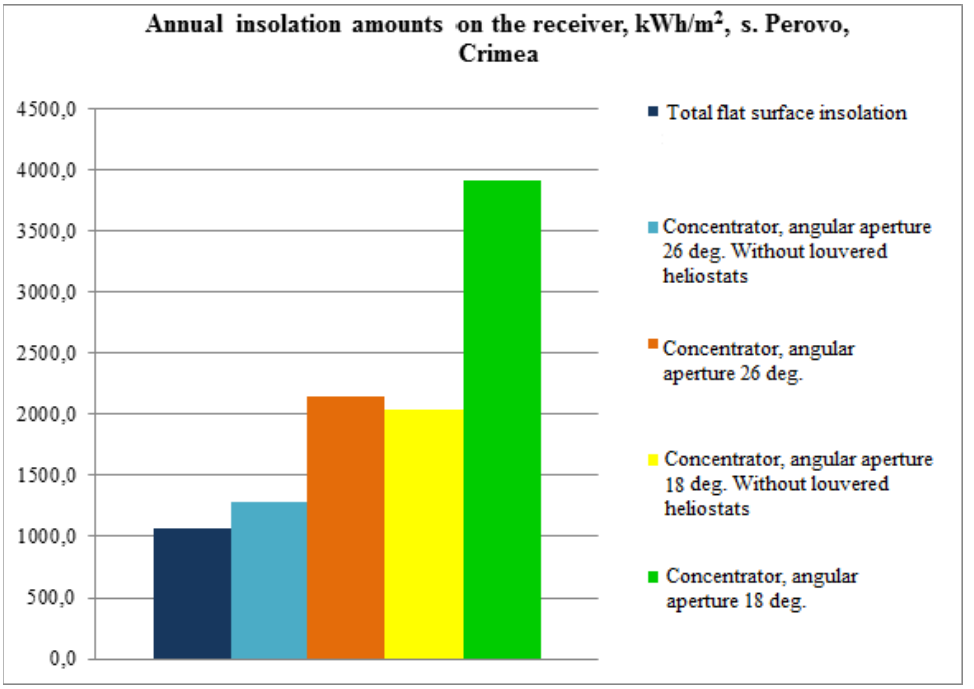

Figure 2. Annual amounts of insolation on the receiver (Sochi)

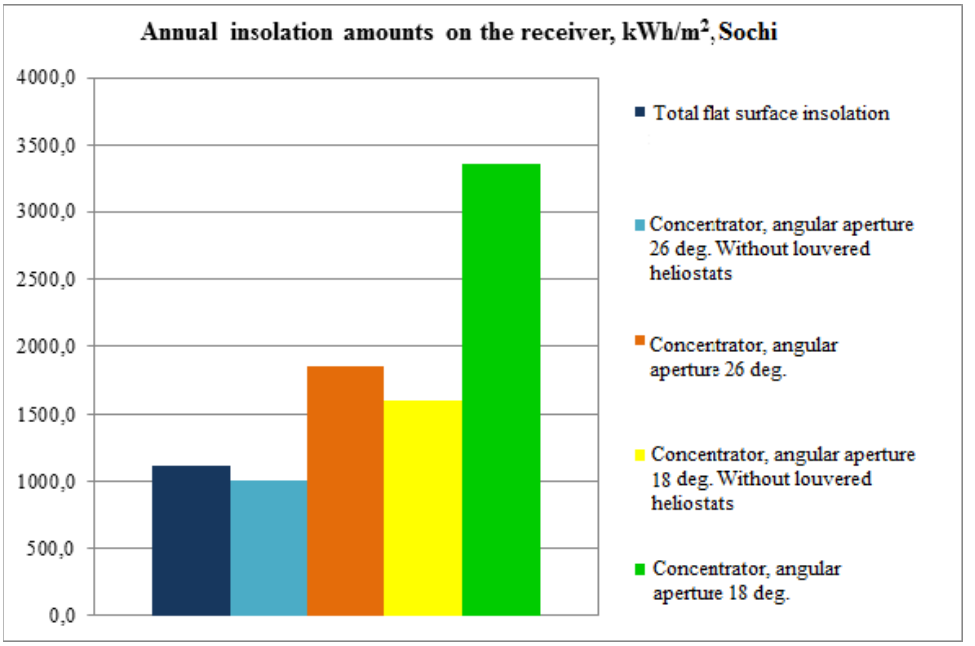

Figure 3. Annual insolation amounts on the receiver (Dubai, United Arab Emirates)

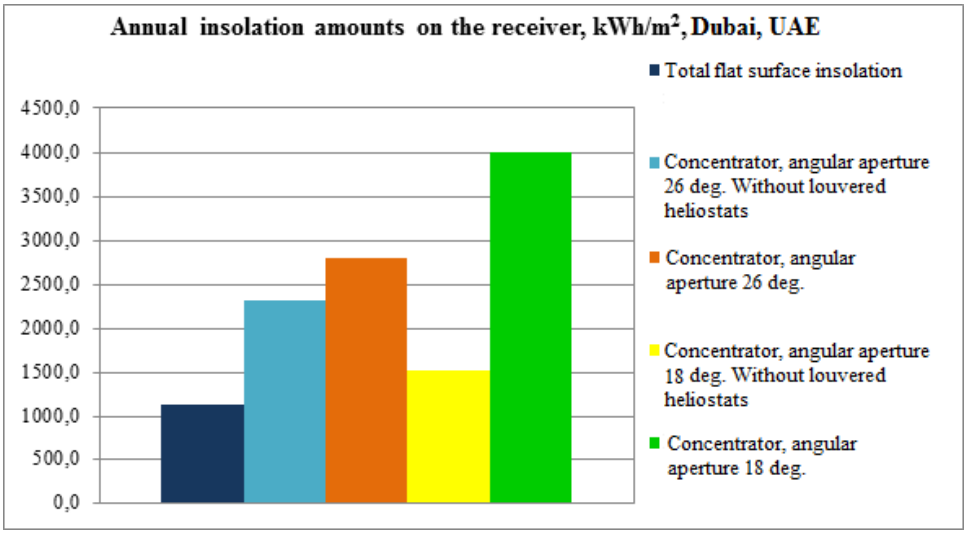

As can be seen from Figures 1-3, the annual sums of insolation at the receiver for the considered geographical points for concentrators with louvered heliostats with an angular aperture of 26 ° and 18 °, on average, are 2 and 3.4 times higher than the total insolation on a flat surface and in 1,6 and 2,2 times higher than insolation on the receiving surface of concentrating modules without louvers with similar values of the angular aperture. Figure 4 shows the annual sums of solar radiation on the surface of the receiver, the angular aperture of the concentrators 18° (Sochi).

Figure 4. Annual sums of solar radiation on the surface of the receiver. Angle aperture of 18° concentrators (Sochi)

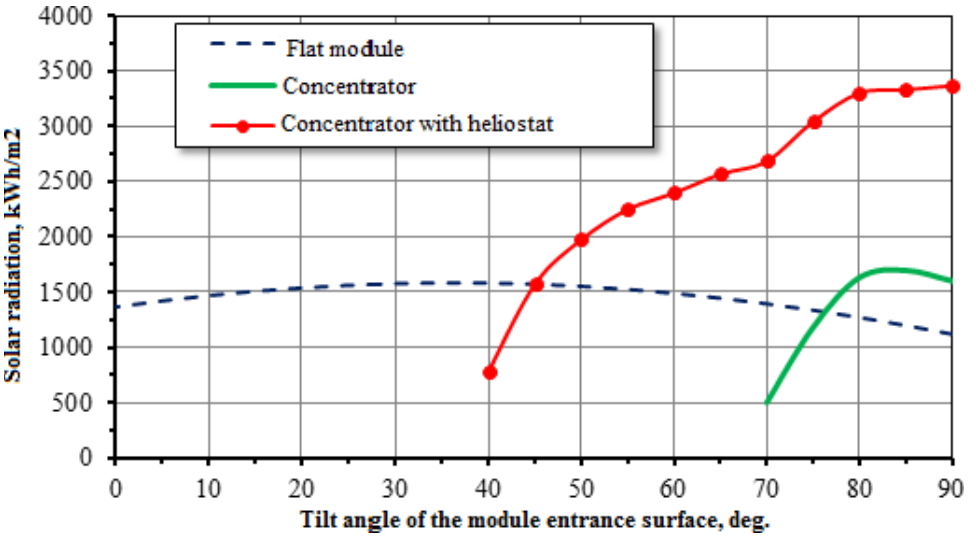

The calculations confirm the high efficiency of using louvered heliostats and significant differences in the optimal orientation of «flat» and non-tracking concentrating modules. The maximum annual output is achieved with a vertical orientation of the concentrator, which is very important when placing solar modules on the southern facades of buildings. At the same time, the average annual concentration coefficient of a module with a louvered heliostat is 5,4, without a heliostat – 2,6.

The definition of predicted energy production is implemented using a specially developed program, the mathematical model presented in Section 2 is part of it. Based on the data of the arrival of solar radiation, the program

calculates the arrival of insolation on the receiver of a concentrating module with a louvered heliostat.

In view of the temporal irregularity of the arrival of solar radiation (daily, seasonal), if solar concentrating modules (PV, thermal and PVT) cannot guarantee 100% of the load coverage, the uncovered part of the load must be provided either by other installations based on renewable energy sources or by traditional energy sources.

Electrical Loads

When considering a system of concentrating modules with photoelectric receivers, i.e. For electricity generation, the most acceptable option is to operate in parallel with the network: the grid solar power plant will operate in parallel with the centralized power supply system, while the unused power is sent to the common power grid, and in case of a shortage of generated electricity, the inverter compensates for the need from the common power grid In areas with centralized power supply, electric batteries are not used, as they double the cost with The systems, solar modules are equipped with network inverters, switching modules to the power station is not on the networks of 12-24 V DC, and 220-380 V AC).

Heat Load

Since the developed design of a concentrator with a louvered heliostat allows harmoniously inscribing modules into the facade of buildings, the thermal load of the solar concentrator thermal and PVT modules system is determined by the hot water consumption by the administrative building according to (*Internal piping*…2016). The norms of hot water consumption for administrative buildings are given in (*Internal piping*…2016) and on average days are 5 liters per 1 worker; let the number of workers in the building be 200 people, the number of working days per year is on average 250, then the required volume of hot water per year will be $G_g = 250000$ *l*/year. It follows that the required amount of thermal energy for hot water supply of the administrative building Q_t (kWh/year) will be equal to:

$$Q_t = \frac{G_g \cdot c_p \cdot (t_{out} - t_{in})}{3600} \tag{5.10}$$

where c_p – the specific heat capacity of water, kJ/kg·°C (4,2 kJ/kg·°C); t_{out} – the temperature of hot water at the outlet of the system of thermal/PVT-modules, is assumed to be 60 °C (Internal piping…2016); t_{in} – water temperature at the system inlet, is assumed to be equal to the ambient temperature.

Table 1 presents data on the arrival of solar insolation on a flat surface and on a receiver of a concentrating module with a louvered heliostat with an angular aperture of 18°, inclined at an angle of 85° to the horizon, as well as an average daily ambient temperature (Surface meteorology and Solar Energy, 2017) for s. Perovo (Crimea).

Figure 5 shows the daily course of insolation on the surface of the receiver for two characteristic months in a year, calculated on the basis of the data of ("Scientific and applied reference book", 1990). When calculating the daily course of insolation, a previously developed algorithm for controlling a louvered heliostat for the geographic point under consideration was taken into account. Figure 6 shows the annual course of insolation on the surface of the receiver – flat and concentrating modules with a louvered heliostat. Monthly amounts of insolation were calculated on the basis of data on the daily course of insolation for characteristic days in a year ("Scientific and applied reference book", 1990).

Figure 5. s. Perovo, Crimea. Daily insolation course on the surface of the solar module receiver with a louvered heliostat (18° angular aperture): March

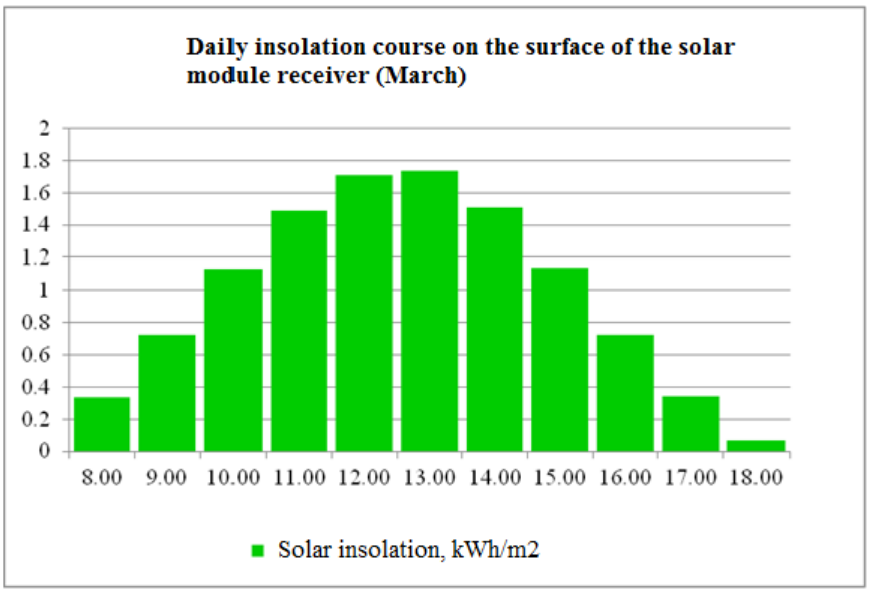

Table 1. Data on the arrival of solar insolation on a flat module and on a receiver of a concentrating module with a louvered heliostat with an angular aperture of 18° (Crimea, s. Perovo. The angle of inclination of the input surface of the module is 85°)

Name	Monthly sums of solar radiation, kWh/m²												Year
	Month												
	1	2	3	4	5	6	7	8	9	10	11	12	
1. 18 ° concentrator with louvered heliostat	2.7	224.3	331.7	382.1	510.9	411.3	545	697	478.8	438.4	43.9	0	4066
1.1. Average concentration coefficient	0.05	3.9	5	6.1	9.1	8.4	8.7	7.5	5.1	4.6	0.7	0	4.9
2. Flat module	68.2	84.3	103.5	102.8	98.4	86.7	98.9	119.4	132.5	130.7	84.8	61.8	1172
3. 18 ° concentrator without jalousie	0.9	72.3	114.3	115.7	182.4	137.1	188.5	232.3	159.6	152.7	14.7	0	1371
Average ambient temperature, °C													
Indicator	3.7	3.2	5.9	10.8	16.1	20.8	24.6	24.5	19.9	14.7	8.7	4.6	13.1

Figure 6. s. Perovo, Crimea. Daily insolation course on the surface of the solar module receiver with a louvered heliostat (18° angular aperture): August

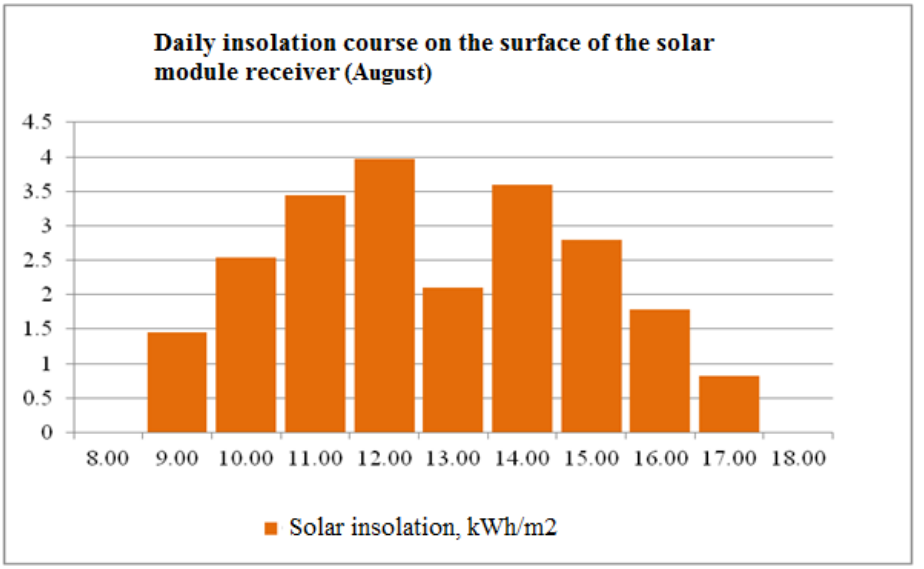

Electricity Generation

For the economic evaluation of investment options when generating electricity, two photovoltaic systems with an installed capacity of 10 kW each were selected based on flat modules SF-M672 (Export PV 340 W panel, 2017) and concentrating modules with louvered heliostats. Figure 5.7 presents the results of calculations of the generation of electrical energy during the year (p. Perovo, Crimea). The efficiency of solar cells is assumed to be 15%. When calculating the generation of electricity by photovoltaic modules, the effect of elevated temperature at a concentration was taken into account, the method for determining which is given in Section 3. Electricity generated by a photovoltaic panel is determined by:

$$W_{el}=\eta_{sc}\cdot F_{rec.sc}\cdot E_{SR}\cdot k_{\eta(T)}, \quad (5.11)$$

where η_{SC} – the efficiency of solar cells at a temperature of 25°C; $F_{rec.sc}$ – the receiving surface area of solar cells, m^2; E_{SR} – insolation on the receiver, kWh/m^2; $k_{\eta(T)}$ – the coefficient of influence of the working temperature of the solar cells on the efficiency.

Figure 7. s. Perovo, Crimea. The annual course of insolation on the surface of the receiver – flat and concentrator with louvered heliostat

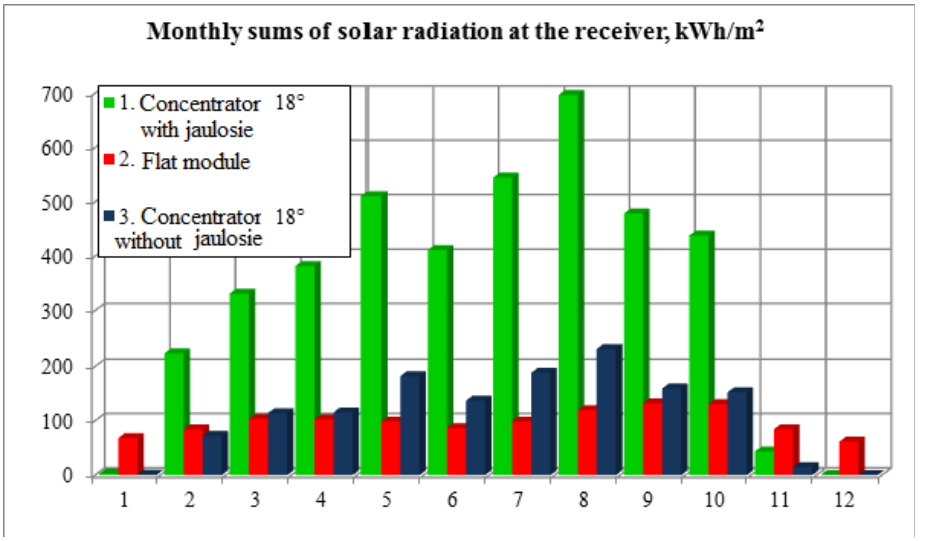

The coefficient $k_{\eta(T)}$ is determined by the expression (Diaf, Diaf, Belhamel et al., 2007):

$$k_{\eta(T)}=1-\beta_t\cdot(T_{op}-T_{nom}), \tag{5.12}$$

where T_p – the operating temperature of the solar cells, K; $T_{ном}$ – the temperature corresponding to the standard conditions for measuring the characteristics of solar cells (298 K or 25 °C); β_t – the coefficient of change in the efficiency of solar cells, is assumed to be 0,005 K^{-1}.

As can be seen from Figure 7, the annual power generation by a flat module system with an installed capacity of 10 kW will be 10 MWh/year, a system with concentrating modules with louvered heliostats –10,165 MWh/year, which is almost 3 times higher than that of concentrating modules without louver heliostats (3,43 MWh / year).

Heat Energy Generation

The choice of the number of flat and concentrator collectors for the power supply of a typical administrative building was made on the basis of the need to cover the share of heat load. Vitosol 100-f flat collectors (Solar collector

Viessmann Vitosol 100-F, 2017) with an absorber area of 2,3 m^2 in the amount of 7 pcs., As well as thermal concentrator solar modules with louvered heliostats with a receiver area of 1.25 m2 in the amount of 5 pcs. Figure 5.8 presents the results of calculations of heat generation during the year (s. Perovo, Crimea). As can be seen from Figure 5.8, the annual heat generation by the Vitosol 100-f flat collector system will be 11,3 MWh/year, the system with concentrator heat modules with louvered heliostats – 15,5 MWh/year (1,4 times above), concentrating modules without louvered heliostats – 5,5 MWh/year (2,8 times lower than those of modules with louvered heliostats).

Figure 8. s. Perovo, Crimea. Annual power generation by the system based on flat and concentrator (without and with louvered heliostat) modules. Installation angle 85°

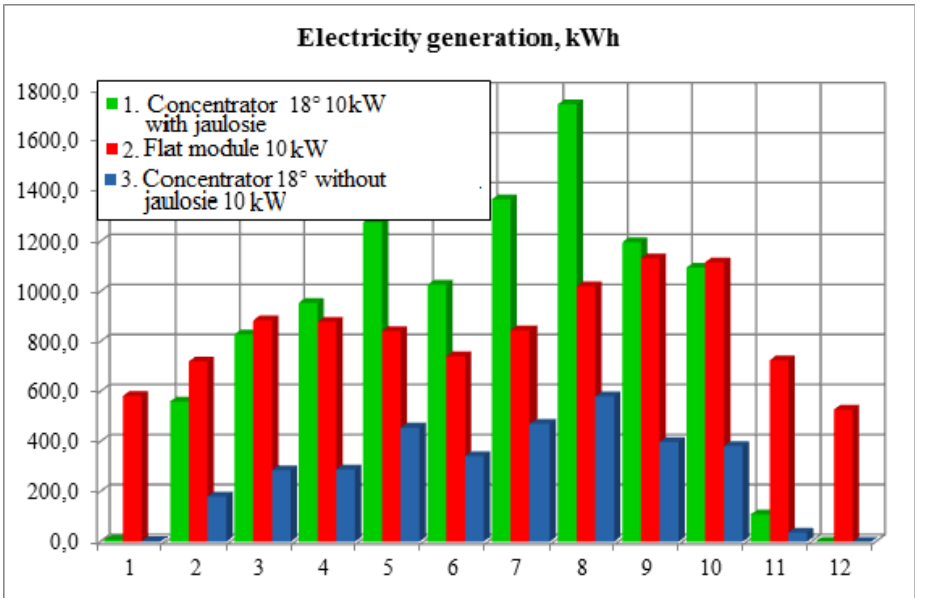

Cogeneration PVT Modules

Based on earlier calculations of the production of electrical and thermal energy, it can be concluded that in cogeneration modules (PVT), the generation of thermal energy will be predominant. The choice of the number of flat and concentrator PVT-modules for energy supply of a typical administrative building was made based on the need to cover the share of heat load. Flat PVT-modules POWERTHERM M 180/750 (Flat Hybrid Solar Collector,

2017). with an absorber area of 1,4 m^2 in an amount of 12 pcs., As well as PVT modules with louvered heliostats with a receiver area of 1,25 m^2 in an amount of 5 pcs. Figure 9 presents the results of calculations of the generation of heat and electrical energy during the year (Perovo, Crimea).

Figure 9. s. Perovo, Crimea. Annual heat energy generation by the system based on flat and concentrator (without and with louvered heliostat) modules. Installation angle 85°

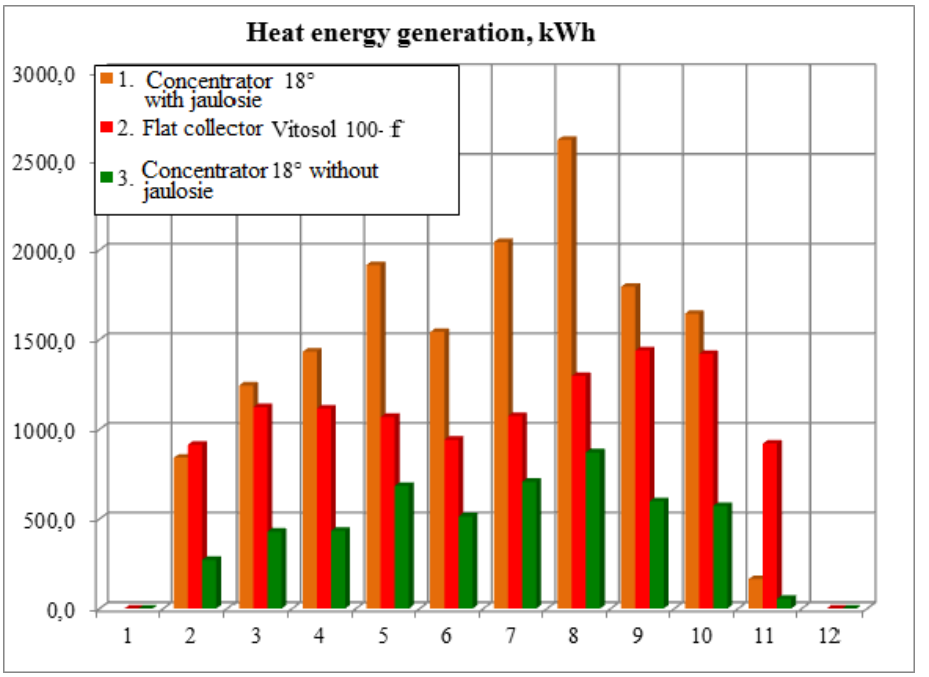

As can be seen from Figure 9, the annual generation of heat energy by the POWERTHERM flat-panel PVT-modules system will be 11,9 MWh/year, a system with PVT-concentrating modules with louvered heliostats – 15,5 MWh/year above), concentrator PVT-modules without louvered heliostats – 5,7 MW/year (2,7 times lower than those of modules with louvered heliostats); annual electricity generation by flat modules will be 2,1 MW/year, concentrator PVT-modules with louvered heliostats – 2,98 MW/year (1,5 times higher), PVT-modules without louvered heliostats – 1,1 MWh/year (2,8 times lower than for modules with louvered heliostats). Thus, according to preliminary estimates, thermal and cogeneration concentrating modules will

have the greatest investment attractiveness, while in cogeneration modules, the generation of thermal energy will be predominant, and power generation will be considered as an additional source of income.

Estimation of Economic Efficiency of Solar Concentrating Modules with Louvered Heliostats With Various Types of Receivers

It will make an economic assessment of the efficiency of solar concentrating modules with louvered heliostats on the basis of indicators of the comparative effectiveness of investments: NPV, PBP, LCOE, IRR (internal rate of return). For the options considered in clause 5.3.1, it will calculate the above indicators of economic efficiency for the three main options of solar modules with louvered heliostats taking into account auxiliary equipment: power generation in parallel with the network, heat generation, cogeneration. The Goodwe-GW1000 (Network inverter GoodWe GW1000-NS, 2017) power inverter is selected for the network PES, and the S-Tank AT battery (Heat accumulators S-Tank, 2017) is selected for thermal modules with louvered heliostats. The results of the calculations are presented in tables 2-4 and in the figures 11-13

As can be seen from Tables 2-4, thermal and PVT modules with louvered heliostats have a greater investment attractiveness — the investment return index (PI) for these projects is greater than one. At the same time, there is a noticeable decrease in the cost of electricity produced when using non-tracking concentrating modules with a louvered heliostat compared with 40-60% non-blind concentrating modules, and 50% of thermal energy.

Figures 11-13 show the NPV plots for the designed version over the entire lifetime of the project.

CONCLUSION

According to the CIPS of the UES of Russia for 2017–2023, the share of facilities based on renewable energy in the power balance of the UES of Russia will increase from 0,04% in 2016 to 0,9% by 2023, while the commissioning of new generating capacities (with a high probability of realization) The base of renewable energy sources in the UES of Russia in the period of 2017–2023 is provided for in the amount of 1,875 MW. The main share of the input generating capacity based on renewable energy is accounted for by the IES of the South (48.46%).

Figure 10. s. Perovo, Crimea. Annual production of heat (a) and electric (b) energy systems based on flat and concentrating modules (with and without louvered heliostats) modules. Installation angle 85 °

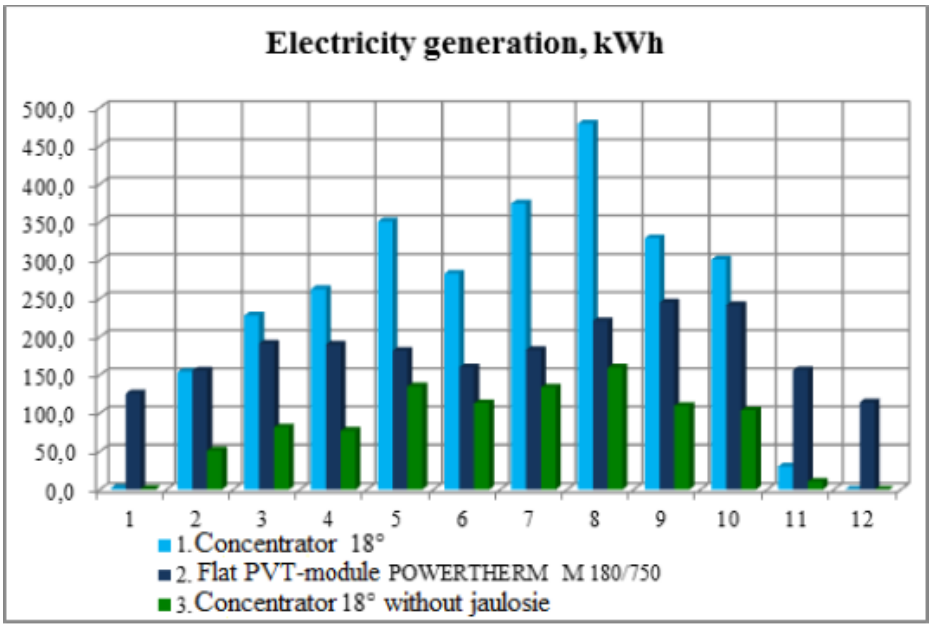

a)

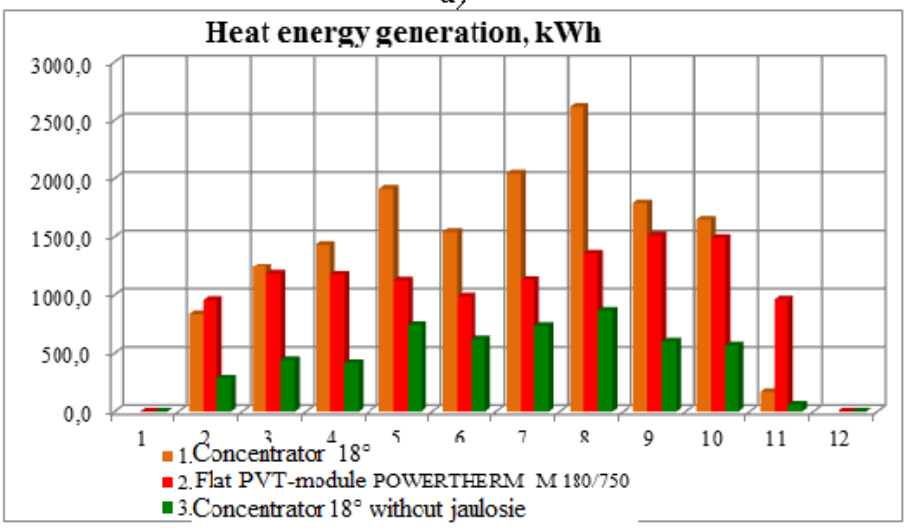

b)

Table 2. s. Perovo, Crimea. Technical and economic indicators of flat and concentrator photovoltaic modules. Discount rate 10%.

Indicator	Flat	Without jalousie (18°)	With jalousie (18°)
Photovoltaic modules			
Installed electric power, kW	10		
Capital investments (K), rub.:	419 200	390 085	490 300
- modules;	287 200	258 085	358 300
- inverters.	132 000	132 000	132 000
Net present value (NPV), rub.	3 047 355	798 943	2 389 950
Payback period (PBP), years	5	11	6
Total present value of energy ($LCOE_{el}$), rub./ kWh	7,07	12,21	6,49
Investment Return Index (PI)	1,18	1,03	1,06
Internal Rate of Return (IRR), %	22,3	11,3	18,9

Table 3. s. Perovo, Crimea. Technical and economic indicators of flat and concentrator thermal modules. Discount rate 10%.

Indicator	Flat	Without jalousie (18°)	With jalousie (18°)
Thermal modules			
Installed thermal power, kW	10		
Capital investments (K), rub.:	491 258	324 018	395 000
- modules;	385 000	217 760	288 742
- pack battery.	106 258	106 258	106 258
Net present value (NPV), rub.	382 803	572 131	962 790
Payback period (PBP), years	9	12	8
Total present value of energy ($LCOE_{el}$), rub./ kWh	2,21	2,66	2,06
Investment Return Index (PI)	1,05	1,06	2,4
Internal Rate of Return (IRR), %	9,9	10,5	14,7

The calculations confirm the high efficiency of using louvered heliostats. The maximum annual energy production by non-tracking solar concentrating modules is achieved with a vertical orientation of the concentrator, which is very important when placing solar modules on the southern facades of buildings. The annual amounts of insolation at the receiver for concentrators with a louvered heliostat with an angular aperture of 26 ° and 18 °, respectively, are on average 2 and 3.4 times higher than the total insolation on a flat surface and 1,6 and 2,2 times higher than insolation by blind surface receiving

concentrating modules with similar angular aperture values. The cost of electricity produced when using non-glare concentrating modules with louvre is reduced by 40–60% compared to concentrating modules without louver, and thermal energy by 50%.

Table 4. s. Perovo, Crimea. Technical and economic indicators of flat and concentrator PVT-modules. Discount rate 10%.

Indicator		Flat	Without jalousie (18°)	With jalousie (18°)
PVT- modules				
Installed electric power, kW		2		
Installed thermal power, kW		10		
Capital investments (K), rub.:		693 258	494 258	562 565
- modules;		455 000	256 000	324 307
- pack battery;		106 258	106 258	106 258
- inverters.		132 000	132 000	132 000
Net present value (NPV), rub.		800 657	464 176	1 262 021
Payback period (PBP), years		11	10	7
Total present value of energy ($LCOE_e$), rub./ kWh	thermal power	4,27	4,0	2,89
	electric power	10,19	12,83	7,15
Investment Return Index (PI)		1,07	1,2	3,1
Internal Rate of Return (IRR), %		9,3	8,1	22,3

Figure 11. s. Perovo, Crimea. NPV change in power generation by a system based on concentrating modules (with louvered heliostats) modules

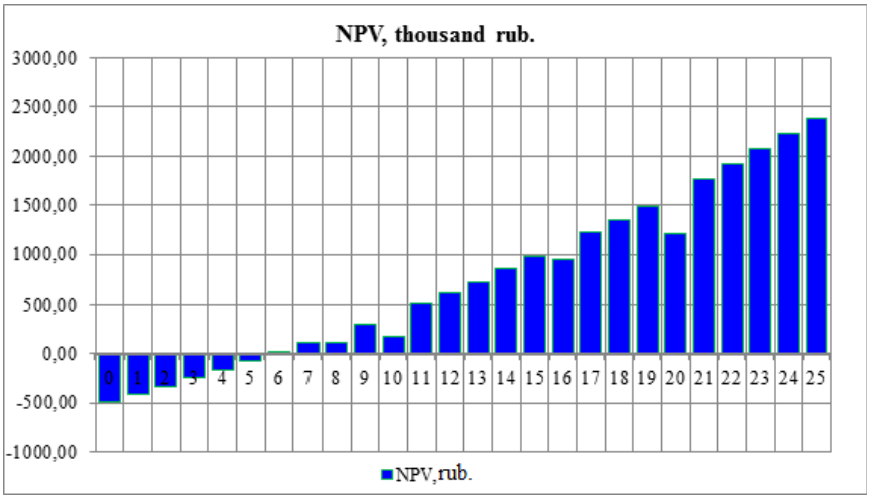

Figure 12. s. Perovo, Crimea. NPV change in the production of heat energy by a system based on concentrator (with louvered heliostats) modules

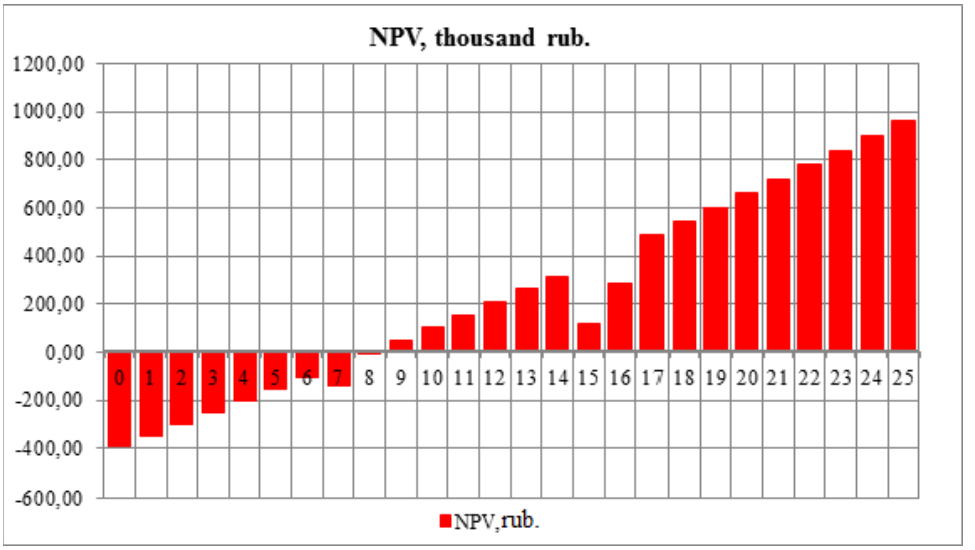

Figure 13. s. Perovo, Crimea. NPV change during cogeneration by a system based on concentrator (with louvered heliostats) modules

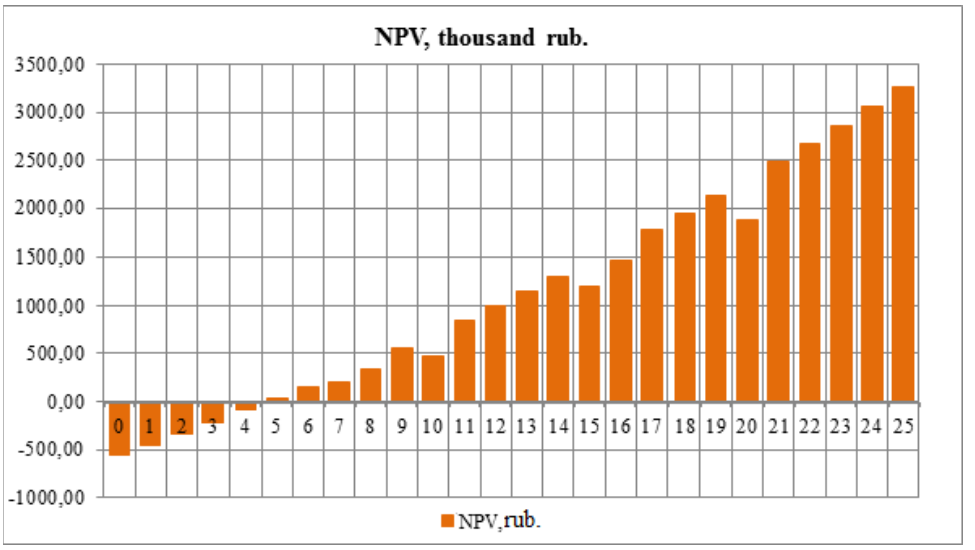

REFERENCES

Diaf, S., Diaf, D., Belhamel, M., Haddadi, M., & Louche, A. (2007). A methodology for optimal sizing of autonomous hybrid PV/wind system. *Energy Policy*, *35*(11), 5708–5718. doi:10.1016/j.enpol.2007.06.020

Electricity tariffs for the city of Sevastopol from January 1, 2018. (2017). Retrieved from https://tarif-24.ru/russia/electro/2018/676-tarify-na-elektroenergiyu-dlya-goroda-sevastopolya-s-1-iyulya-2017-goda-2.html

Electronic resource. (2017). Retrieved from http://m-batyr.ru/uroven_inflyacii_v_2017_godu__oficialnye_dannye_rosstata_na_segodnya

Executive Summary - Projected Costs of Generating Electricity – 2015 Edition. (2017). Retrieved from https://www.iea.org/textbase/npsum/eleccost2015sum.pdf

Export PV 340 W panel. (2017). Retrieved from https://russian.alibaba.com/product-detail/export-pv-panel-340w-high-quality-mono-solar-module-price-for-home-use-60561959357.html?spm=a2700.8699010.29.1.5a585cc4V5O2IX

Flat Hybrid Solar Collector POWERTHERM M 180/750. (2017). Retrieved from http://shop-oooaist74.ru/solnechnye-batarei/52-ploskij-gibridnyj-solnechnyj-kollektor-powervolt-w-200500.html

Fomina, V.N. (2005). Electric Power Economics: Textbook. *IUE GUU, VIPKenergo, IPK-state service*, 392.

Heat accumulators S-Tank. (2017). Retrieved from http://www.bigboilers.ru/shop/s-tank-teploakkumulyatory-1000/

Internal piping and sewerage buildings. SP 30.13330 «SNiP 2.04.01-85» with changes as of February 10, 2017: Order of the Ministry of Construction and Municipal and Public Utilities of the Russian Federation dated December 16. (2016) 951.

Network inverter GoodWe GW1000-NS. (2017). Retrieved from https://www.sosvetom.ru/cat/setevoy-invertor-goodwe-gw1000-ns/

Petrov, V. M. (2015). *Research of autonomous power supply system based on facade-integrated solar photovoltaic modules* (Doctoral dissertation).

Scientific and applied reference book on the climate of the USSR. Issue 08. Moscow and Moscow region. (1990). *Hydrometeoizdat*, 256.

Solar collector Viessmann Vitosol 100-F. (2017). Retrieved from https://viessmann-rus.ru/product/solar/vitosol_100f/

Surface meteorology and Solar Energy. (2017). Retrieved from https://eosweb.larc.nasa.gov/sse/

Tariffs from January 1, 2018 in the Republic of Crimea: for hot, cold water and drainage. (2017). Retrieved from http://proschetchiki.ru/tarify-na-vodu-2018-pervoe-polugodie/tarify-na-vodu-i-vodootvedenie-v-respublike-krym-s-1-yanvarya-2018-goda.html

The real inflation in Russia in 2017 is industrial development. (2017). Retrieved from https://promdevelop.ru/realnaya-inflyatsiya-v-rossii-v-2017-godu/

Section 2

Chapter 6
Advantages and Basic Areas of Application of Solar Concentrating Modules With Louvered Heliostats

ABSTRACT

In connection with the large-scale development of high-rise building projects recently in Russia and abroad and their significant energy consumption, one of the main principles in designing is the use of effective energy-saving technologies. Also, important aspects are reducing energy consumption and neutralizing the environmental impact of tall buildings. The most promising areas in the field of integration of solar modules (planar and concentrating) in the construction of buildings are development of BIPV technologies (roofing, film, facade materials), the integration of solar energy concentrators that do not require biaxial tracking (medium and low concentrations) on the facades and roofs of buildings (parabolic concentrators, lenses, and Fresnel mirrors), integration of highly concentrated modules on the roofs of buildings.

INTRODUCTION

Currently, the widespread introduction and popularization of high-rise buildings and complexes, increasing their concentration and importance in various countries of the world. In connection with the large-scale development

DOI: 10.4018/978-1-7998-4276-7.ch006

of high-rise building projects recently in Russia and abroad and their significant energy consumption, one of the main principles in the design is the use of energy-efficient technologies. Also important aspects are reducing energy consumption and neutralizing the environmental impact of the construction and operation of tall buildings.

In this regard, facade-integrated solar power plants with concentrators for buildings that meet environmental friendliness and reduce the need for centralized energy supply are becoming increasingly attractive.

ROOFING SOLAR PANEL AS AN ELEMENT OF SOLAR POWER PLANTS WITH CONCENTRATORS FOR BUILDINGS

Solar roofing is becoming increasingly popular, especially in the southern regions. The purpose of (Strebkov, Kirsanov, Irodionov, et al., 2015) is to create a roofing solar panel with high optical efficiency and low consumption of semiconductor material and low cost.

In the roofing solar panel (Strebkov, Kirsanov, Irodionov et al., 2015) mounted on an inclined roof of a building or structure, the normal to the roof surface is in the meridional plane containing the body with an internal cavity with a protective coating on the working surface, onto which the solar radiation with an angle of entry of rays β_0, and receivers from commutated solar cells, in the cavity of the housing 1, under the protective coating, a composite concentrator is installed, made in the form of a deflecting optical system transparent to radiation from a variety of prisms with sharp key Ψ between the entrance and exit surfaces of the rays and several semi-parabolic cylindrical reflectors with a parametric angle δ having the surfaces of the entry and exit of rays, the focal regions of all semi-parabolic cylindrical reflectors are shifted to the lower or upper side of the roofing solar panel, and the radiation detectors from the connected solar cells are installed in parallel focal axis and perpendicular to the plane of the roofing solar panel between the focal axis and the mirror coating of each half a parabola-cylindrical specular reflector, a plane of the entrance surface of the rays of the deflecting optical system and a plane of the entrance surface of the rays of the semi-parabolic cylindrical reflector are parallel to the plane of the protective coating, and the angle of entry of rays β_0, an acute angle Ψ and the refractive index n of the material

of the deflecting optical system are associated with the parametric angle δ of the semi-parabolic cylindrical mirror reflector as follows:

$$\beta_0 = arcsin\left\{\left\{\left\{sin\left\{\left\{arcsin\left\{sin\left[90^\circ - 2\delta + \psi\right]\frac{1}{n}\right\} - \psi\right\}\right\} n\right\}\right\}\right\}. \qquad (6.1)$$

The housing of the roofing solar panel can be made of impact-resistant plastic, ceramics, a mixture of sand and plastic. The internal cavity of the housing can be molded to accommodate a protective coating of semi-parabolic cylindrical reflectors, a deflecting optical system and receivers from commutated solar cells.

The protective coating of the roofing solar panel can be made in the form of an optical deflecting system consisting of semi-parabolic cylindrical reflectors made of flat glass mirror faces, the planes of which are parallel to the focal axis, and the width of the glass mirror faces in the meridional plane is comparable to or greater than the width of the receiver from the switched solar cells.

Mirror reflectors of the optical deflecting system can be made of polished aluminum sheet alloy.

In the roofing solar panel, each space between the additional protective coatings and the housing, in which the receivers of the switched solar cells are placed, is filled with a transparent silicone gel. Inside the housing there are panels for cable connection of receivers from commutated solar cells to a junction box, which is installed in the cavity of the housing between the semi-parabolic cylindrical reflectors on the back of the roofing solar panel and is equipped with a conductive cable for switching with other roofing solar panels. On the reverse side of the outside of the housing there are channels for laying a conductive cable to the adjacent solar roof panels. In the roofing solar panel, receivers from commutated solar cells and the focal axes of semi-parabolic cylindrical reflectors can be shifted to the upper part of the housing, and the angle of inclination of the roofing solar panel to the horizontal surface when installed on the roof in this case will be φ-23,5°-β_0, where φ is the width of the terrain. If the receivers from the switched solar cells and the focal axes of the semi-parabolic cylindrical mirror reflectors are shifted to the lower part of the housing, then the angle of inclination of the roofing solar panel to the horizontal surface when installed on the roof is $\varphi + 23.5° + \beta_0$, where φ is the width of the terrain.

Figure 1 shows a general view of the roofing solar panel from the outside (a) and the reverse side (b). Figure 2 shows the cross section of the roofing solar panel in the meridional plane.

The roofing solar panel has a housing 1, in which cavities are sealed on the reverse side to accommodate a protective coating 2 of a composite concentrator, consisting of an optical deflecting system 3 and two semi-parabolic cylindrical reflectors 4, 5, in which the focal axes 6 and 7 are shifted to the upper part 8 housing 1 and receivers 9 and 10 of commutated solar cells 11. In the cavity of housing 1 in front of receivers 9 and 10, grooves 12 and 13 are made, in which protective coatings 14 and 15 are made of glass or transparent plastic and receivers 9 and 10. The planes of the protective coating 14 and 15 of the receivers 9 and 10 are perpendicular to the plane of the protective coating 2 of the housing 1 of the roofing solar panel. The space between the protective coating 14, 15 and the part 18, 19 of the housing 1, in which the receivers 9 and 10 are installed, is filled with a transparent silicone gel 20. The side walls 21 and 22 of the internal forming cavities 23 of the housing 1 are provided with mirror coatings 24 and 25. Inside the housing 1 channels 26 and 27 are made for connecting receivers 9, 10 with cable 28 to the junction box 29. The junction box 29 is installed on the back 30 of the housing 1 and has a conductive cable 31 for switching with other solar roof panels. Outside of the housing 1, on the reverse side 30, channels 32 are made for laying the cable 31. The plane of the surface of the entrance of the rays 33 of the optical deflecting system 3 and the plane of the surface of the entrance of the rays 34 of the semi-parabolic cylindrical mirror reflectors 4, 5 are parallel to the plane of the protective coating 2.

In Figure 3, the optical deflection system 3 is made up of a plurality of prisms 35 oriented in the same direction with an acute angle Ψ between the inlet surface 33 and the ray exit surface 36.

Figure 4 shows the path of the rays in a composite concentrator consisting of a deflecting optical system 3 and a semi-parabolic cylindrical reflector 4, where β_0 is the angle of entry of the rays on the surface of the entrance 34 into the optical deflecting system 3, β_1 is the angle of refraction of the rays in the surface of the entrance 3 inside the optical deflecting systems 3, β_2 is the angle between the beam and the normal to the exit surface of 36 rays inside the optical deflecting system 3, β_3 is the angle of the rays at the exit surface 36 outside the deflecting optical system 3, β_4 is the angle of entry of the rays the entrance surface 34 of the semi-parabolic cylinder reflector 4.

Figure 1. General view of the roofing solar panel from the outside (a) and the reverse side (b) (Strebkov, Kirsanov, Irodionov et al., 2015)

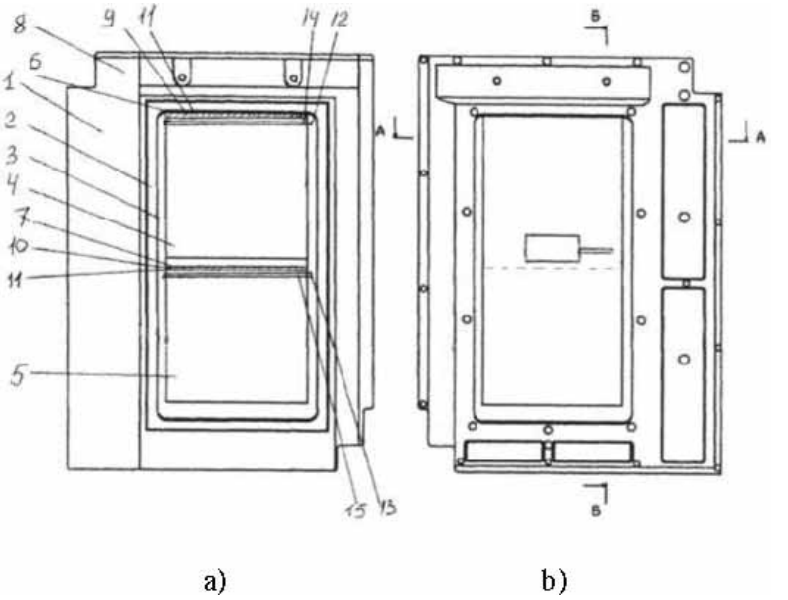

Figure 2. Cross section of roofing solar panel in the meridional plane (Strebkov, Kirsanov, Irodionov et al., 2015)

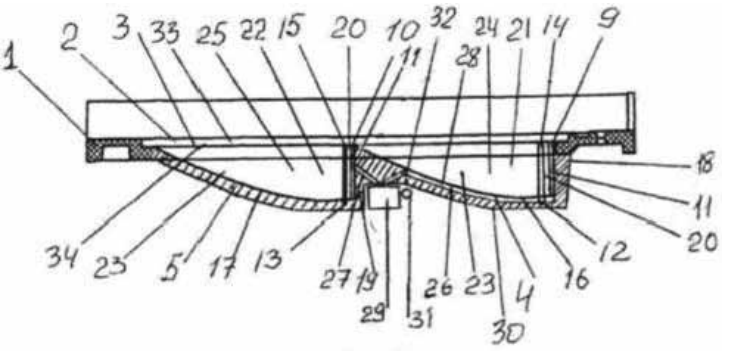

The angles β_0, β_1, β_2, β_3 and β_4 are the angles between the directions of the rays and the normal to the corresponding surface. Since the input surfaces of the rays 33 and 34 are parallel, the angle β_0 responsible for cosine losses is equal to the angle β_4 between the direction of the rays of the entrance to the semi-parabolic cylinder reflector 4 and the input surface 34 of the semi-parabolic cylinder reflector 4.

Figure 3. Roof Solar Panel Optical Deflection System (Strebkov, Kirsanov, Irodionov et al., 2015)

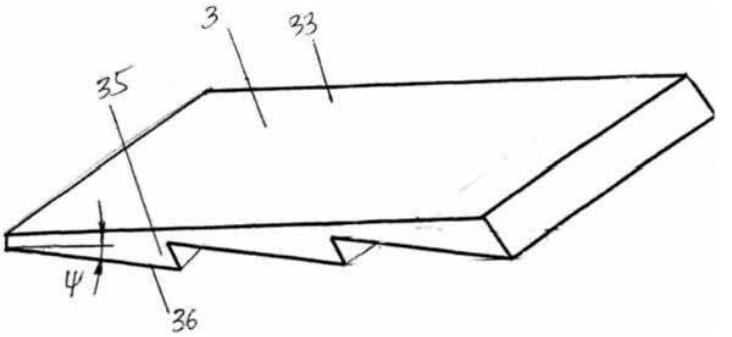

Figure 4. Beam path in a composite concentrator of a roofing solar panel (Strebkov, Kirsanov, Irodionov et al., 2015)

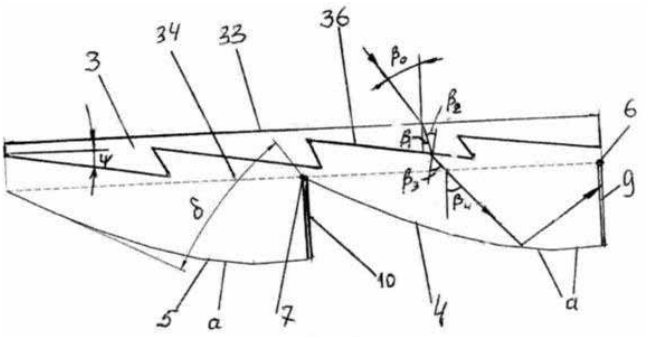

In Figure 5a, the roofing solar panels are installed on the southern slope 37 of the roof 38 of building 39. The receivers 9 and 10 and the focal axes 6 and 7 of the semi-para-cylindrical mirror reflectors 4 and 5 are shifted to the upper part 8 of building 1, and the angle of inclination of the roofing solar panel to the horizontal plane 40 when installed on the roof 38 is $\theta = \varphi - 23.5^{\circ} - \beta_0$, where φ is the width of the terrain. In this case, the normal 41 to the surface of the protective coating 2 in the meridional plane is directed to the position of the Sun 42 at noon on June 22 on the day of the summer solstice with a deviation from it upward from the horizontal plane 40 by the angle of entry of rays β_0. With this installation, the roofing solar panel receives the maximum amount of solar energy in the summer months. With a decrease in the height of the position of the Sun, the amount of incoming solar energy will decrease in proportion to $\cos \beta_0$.

Figure 5. Installation of a roofing solar panel on the roof of the building with the orientation of the panel to the sun on June 22 on the summer solstice (a), installation of the roofing solar panel on the roof of the building with the orientation of the panel on the sun on December 22 (b) (Strebkov, Kirsanov, Irodionov et al., 2015)

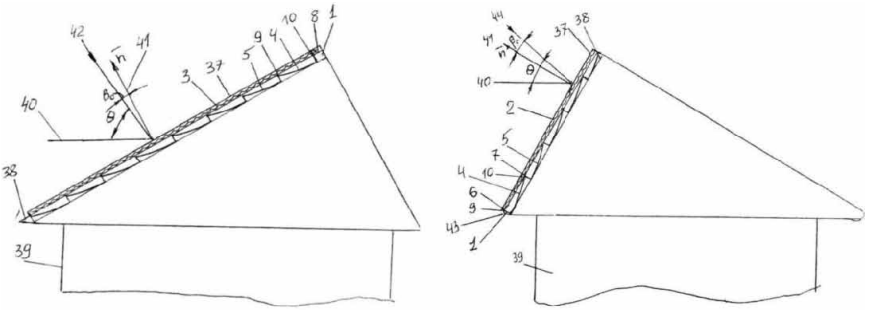

a) b)

At 5b, roofing solar panels are installed on the southern slope 37 of the roof 38 of building 39 in such a way as to use the maximum amount of incoming solar energy in the winter. The receivers 9 and 10, the focal axes 6 and 7 of the semi-para-cylindrical mirror reflectors 4 and 5 are shifted to the lower part 43 of the housing 1, and the angle of inclination of the roofing solar panel to the horizontal plane 40 when installed on the roof 38 is $\theta = \varphi + 23.5^\circ + \beta_0$. In this case, the normal 41 to the surface of the protective coating 2 in the meridional plane is directed to the position of the Sun 44 at noon on December 22 with a deviation from it down to the horizontal plane at the angle of entry of rays β_0.

Solar radiation through the protective coating 2 enters at an angle β_0 to the input surface of the rays 33 of the deflecting optical system 3 from a set of prisms 35 with an acute angle Ψ with a refractive index n, enters the prism 35 at an angle β_1, leaves the prism 35 at an angle β_3, and arrives at the input surface 34 of the semi-para-cylindrical mirror reflector 4 at an angle β_4, is reflected from the semi-para-cylindrical mirror reflector 4 and arrives at the receiver 9 under the condition $\beta_4 \geq 90^\circ - 2\delta$.

As a result of using a roofing solar panel, the efficiency of using solar energy is increased and the cost of generating electric energy and heat is reduced.

If the deflecting optical system 3 consists of a set of prisms 35 with an acute angle $\Psi = 24^\circ$, the angle of entry of the rays $\beta_0 = 17.8^\circ$, the angle $\beta_4 = 37.8^\circ$, the aperture angle δ of the semi-parabolic cylindrical reflector 4 from

polished aluminum $\delta = 26{,}1°$. The receivers 9, 10 have dimensions of 42 × 312 mm, consist of two silicon solar cells 11 of size 42 × 156 mm, connected in parallel. Between each other, the receivers 9 and 10 are connected in series. The geometric concentration coefficient $k = 4.92$, cosine losses 4.8%, optical efficiency 80%, receiver efficiency 9 and 10 15%. The active area of the roofing solar panel for using solar energy is 0.1 m^2. Total efficiency taking into account solar losses of 10%. Peak electric power 10 W at an illumination of 1 kW/m^2 and a temperature of 25°. Receivers 9 and 10 can be made with heat removal devices for generating electricity and hot water or hot air.

With the cost of semi-parabolic cylindrical reflectors 4, 5 30 \$/m^2, a concentration of 4.92, an optical efficiency of 0.8 and an electrical efficiency of 15%, the cost of a roofing solar panel will be \$ 12, or \$ 1/W, at an existing cost of \$ 3 / W, those. it will decrease by 2.5 times, while the costs of the composite concentrator and receiver 9 and 10 will be approximately equal and amount to 50% of the cost of the roofing solar panel.

SOLAR HOUSE

The objective of the work (Strebkov, Tveryanovich, Irodionov et al., 2007) is to increase the efficiency of using solar energy and reduce the cost of electricity and heat, as well as the creation of efficient solar technology built into the facades and roofs of buildings to provide them with electricity and heat.

In a solar house (Strebkov, Tveryanovich, Irodionov et al., 2007), which contains walling and a roof, two solar modules with concentrators are installed on the roof, consisting of two symmetrical conjugated semi-parabolic cylindrical reflectors with an aperture angle of 24-72°, the optical axes of which are directed along the north-south axis and are oriented southward at an angle (90-ϕ)° to the horizon, and the branches of the adjacent semi-parabolic cylindrical reflectors have one common vertical tangent plane of symmetry, the branches of each reflector are deployed relative to the focal points hydrochloric axis so that the angle between the focal planes of each of the branches is equal to 24-70°, and a solar radiation detectors installed in each reflector between the focal planes of their branches, where φ - latitude areas.

In a solar house, mirror reflectors can be made in the form of mirror facets of tempered glass with a facet width a equal to a = (0.4-1.2) OF, where OF is the focal length of the concentrator.

Figure 6 shows a general view of the solar house; Figure 7 shows a side view of the solar house for Moscow.

Figure 6. General view of a solar house (Strebkov, Tveryanovich, Irodionov et al., 2007)

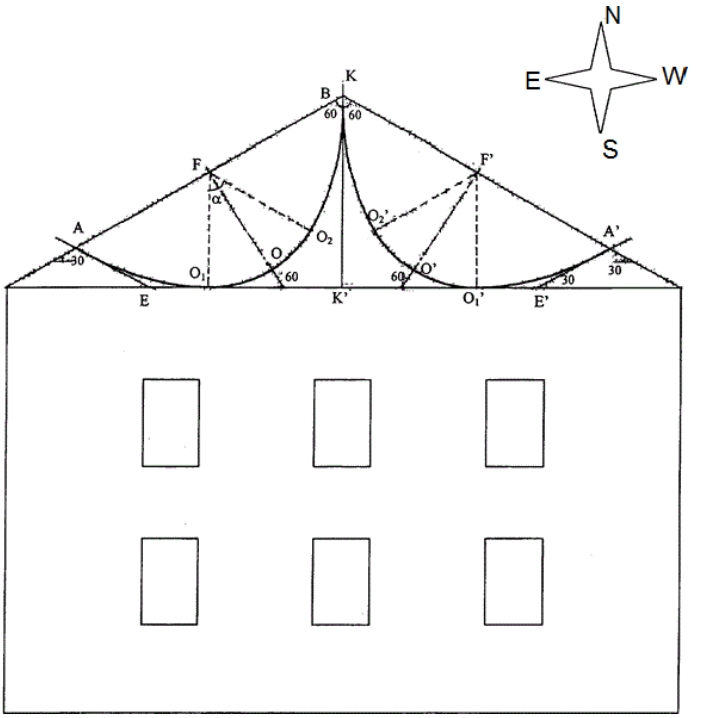

The solar house contains two solar modules with concentrators installed on the roof. The concentrator consists of two symmetric conjugated semi-parabolic cylindrical reflectors with an aperture angle of 24-72 °, the optical axes of which are directed along the north-south axis and oriented southward at an angle of (90-ϕ) ° to the horizon, where ϕ is the latitude of the area, with branches AO and OB, as well as O'B and O'A '. The branches of the adjacent semi-parabolic cylindrical reflectors have one common vertical tangent plane of symmetry KK', and the branches of each reflector are rotated relative to the focal axis so that the angle between the focal planes of each of the branches is 24-70°. Solar radiation receivers are installed in each reflector between the focal planes of their branches. Mirror reflectors can be made in the form of mirror facets made of tempered glass with a facet width "a" equal to (0.4-1.2) OF, where OF is the focal length of the concentrator.

The roof of the house is made in the form of a transparent protective coating. As the receiver, solar photovoltaic modules are used, as well as a solar

collector to produce hot water and warm air. This solar house is applicable for territories with a latitude of ± 45°.

At noon, when the sun is on the KK' line, its rays are reflected from the branches of both semi-parabolic cylindrical reflectors. Thus, all the radiation falling on the roof of the solar house is collected at the receivers of the concentrators FO and F'O'.

At sunrise, the FO receiver is illuminated by direct sunlight. When the sun rises 30° above the horizon, the rays reflected from part FAO_1 of the reflector are collected at point O_1, and the rays reflected from part FBO_1 are collected at point F. When the sun rises to 60°, the sun's rays are parallel to OF and collected on the receiver in the OF / 2 region, while the ABO reflector and part of VA'O' of the other reflector are working. Within the azimuthal angle of the sun from 60° to 120°, three of the four reflector parts work. At an angle of 90°, all four parts of the reflector work briefly. At sunset, everything happens symmetrically with the semi-parabolic-cylindrical reflector BO'A' similar to the operation of the semi-para-cylindrical reflector AOW at sunrise. A solar house uses 40-50% more solar energy than solar houses with solar concentrators located only on the southern facade or southern slope of the roof of the house.

Figure 7. Side view of a solar house for Moscow (Strebkov, Tveryanovich, Irodionov et al., 2007)

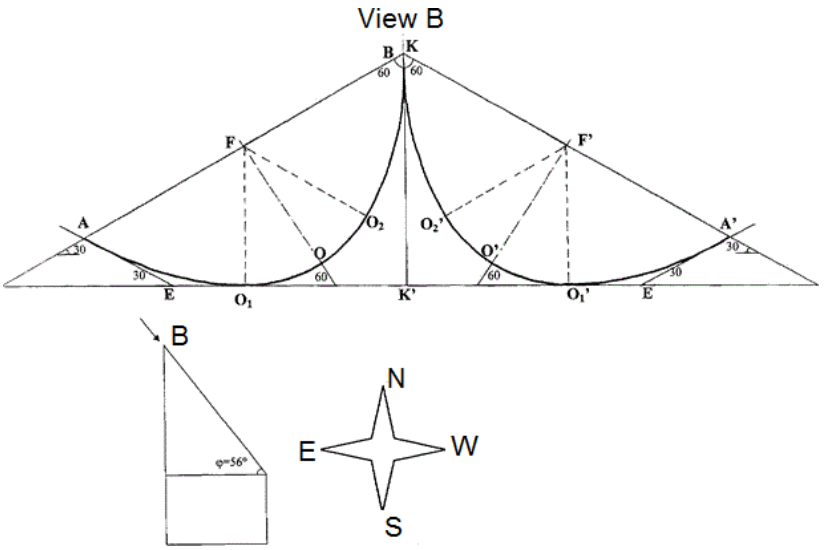

The work (Strebkov, Tveryanovich, Irodionov et al., 2008) presents options for the construction of a solar house. In a solar house containing wall cladding and a roof, solar modules are installed on the roof with concentrators consisting of n branches ($n^3 2$) of semi-parabolic cylindrical reflectors with aperture α and an angle between the focal planes of semi-parabolic cylindrical reflectors α, each semi-parabolic cylindrical reflector has an adjacent a semi-parabolic-cylindrical reflector has a common focal axis, a common tangent plane or a common line of conjugation of the branches of a semi-parabolic-cylindrical reflectors, etc. and the tangent plane to the branch of one of the above adjacent semi-parabolic-cylindrical reflectors in the common interface line coincides with the midsection plane of the adjacent semi-parabolic-cylindrical reflector, and solar radiation receivers are installed in each concentrator between the focal planes of the branches of the mirror reflectors.

In a solar house containing wall and roof enclosing structures, solar modules with concentrators consisting of n branches ($n^3 2$) of semi-parabolic-cylindrical reflectors with aperture α and an angle between the focal planes of semi-parabolic cylindrical reflectors α, each, are vertically installed along the walls the semi-parabolic-cylindrical reflector has a common focal axis with one adjacent semi-parabolic-cylindrical reflector, and with the other nearby semi-parabolic-cylindrical reflector General tangent plane, solar radiation detectors are installed in each concentrator between the focal planes of the branches of the mirror reflectors, the roof of the house in the plan forms a regular polygon, the axis of symmetry of the reflectors is vertical, the midsection planes form the walls of the house.

In a solar house containing wall and roof enclosing structures, solar modules with concentrators consisting of n branches ($n^3 2$) of semi-parabolic cylindrical reflectors with aperture α and an angle between the focal planes of semi-parabolic cylindrical reflectors α, each semi-parabolic cylindrical reflector are vertically installed along the walls has a common focal axis with one adjacent semi-parabolic-cylindrical reflector, and with another adjacent semi-parabolic-cylindrical reflector the tangent plane, solar radiation detectors are installed in each concentrator between the focal planes of the branches of the mirror reflectors, the roof of the house in the plan forms a truncated regular polygon, the axis of symmetry of the reflectors is parallel to the world axis and tilted to the horizon at an angle to the latitude of the terrain, mid ship planes form the walls of the house.

Figure 8 shows a general view of a solar house with rooftop solar modules with concentrators. Each semi-parabolic-cylindrical reflector 7 has a common focal axis 3, a common tangent plane 4 or a common interface line between

the branches 5 of the semi-para-cylindrical reflectors 7 and 2, and a tangent plane 4 to the branch of one of the aforementioned adjacent semi-parabolic-cylindrical reflectors 7 or 2 in a common line with the adjacent semi-parabolic-cylindrical reflector 2 the conjugation coincides with the midsection plane 6 of the adjacent semi-parabolic-cylindrical reflector 2. This option is applicable for territories with a latitude of $\pm$ 45°.

At noon, when the sun is on the line KK ‘, the rays reflected from the semi-parabolic-cylindrical reflector FAO_1 are collected at point F, and the rays from the semi-parabolic-cylindrical reflector FBO_2 are collected at point O. Two semi-parabolic-cylindrical reflectors on the right side from KK’ work in the same way.

Figure 8. General view of a solar house with roof mounted solar modules with concentrators (Strebkov, Tveryanovich, Irodionov et al., 2008)

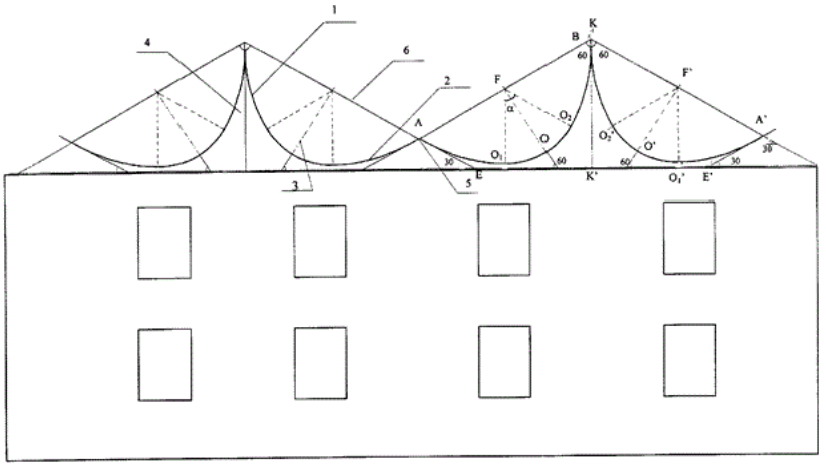

Thus, at noon all the radiation falling on the roof of the solar house is collected at the receivers of the concentrators FO and F’O’. At sunrise, the FO receiver is illuminated by direct sunlight. When the sun rises to a height of 30° above the horizon, the rays reflected from the semi-parabolic reflector FAO_1 are collected at point O_1, and the rays reflected from FBO_2 are collected at point F. When the sun rises to a height of 60°, the sun’s rays are parallel to OF and collected at the receiver in OF / 2, while the ABO concentrator and the upper half of the BA’O’ concentrator are working. Within the azimuthal angle of the sun from 60° to 120°, 3 out of four semi-parabolic reflectors

work. At an angle of 90 °, all 4 semi-parabolic reflectors work briefly. At sunset, everything happens symmetrically with a semi-parabolic reflector VO'A' similar to the work of semi-parabolic reflectors AOW at sunrise. The considered solar house uses 40-50% more solar energy than solar houses with solar installations located only on the southern facade or southern slope of the roof of the building.

Figure 9 shows a general view of a solar house with installed solar modules with concentrators. The roof of the house in plan forms a regular polygon, the axis of symmetry of all reflectors O' is vertical, and the planes of the midsection 6 form the walls of the house. The principle of operation of these solar modules is as follows. When the sun rises to an angle of 30°, the solar module is located on the east side of the house. Further, the work includes modules installed on the north or south side of the house, depending on the time of year. When the sun sets, the radiation hits the solar module installed on the west side of the house. This option is applicable for territories with a latitude of more than 60°.

Figure 9. General view of a solar house with roof mounted solar modules with concentrators (Strebkov, Tveryanovich, Irodionov et al., 2008)

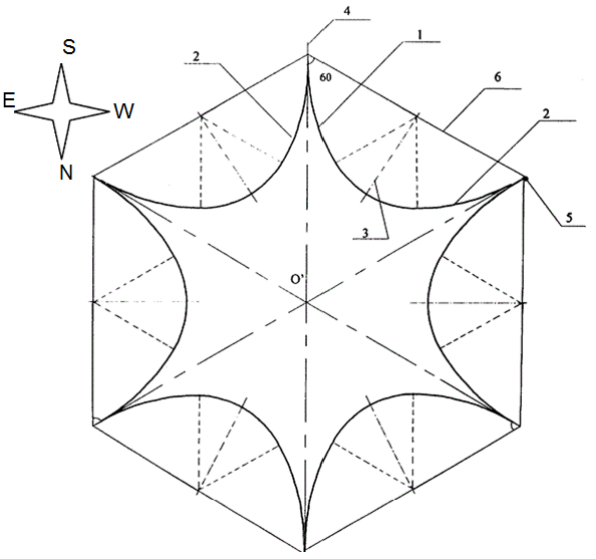

Figure 10 shows a general view of a solar house with installed solar modules with concentrators. The roof of the house in plan forms a truncated regular polygon, the axis of symmetry of all reflectors O 'is parallel to the axis of the world and tilted to the horizon at an angle ϕ equal to the latitude of the terrain, and the planes of the midsection 6 form the walls of the house. The side view shows the wall of the house, oriented east or west. The angle of inclination of the southern wall is equal to the latitude ϕ. The principle of operation of these solar modules is as follows. When the sun rises to an angle of 30 °, the solar module is located on the east side of the house. Next, the modules installed on the south side of the house are included in the work. When the sun sets, the radiation hits the solar module installed on the west side of the house. This option is applicable for territories with a latitude of 30 to 60°.

Figure 10. General view of a solar house with roof mounted solar modules with concentrators (Strebkov, Tveryanovich, Irodionov et al., 2008)

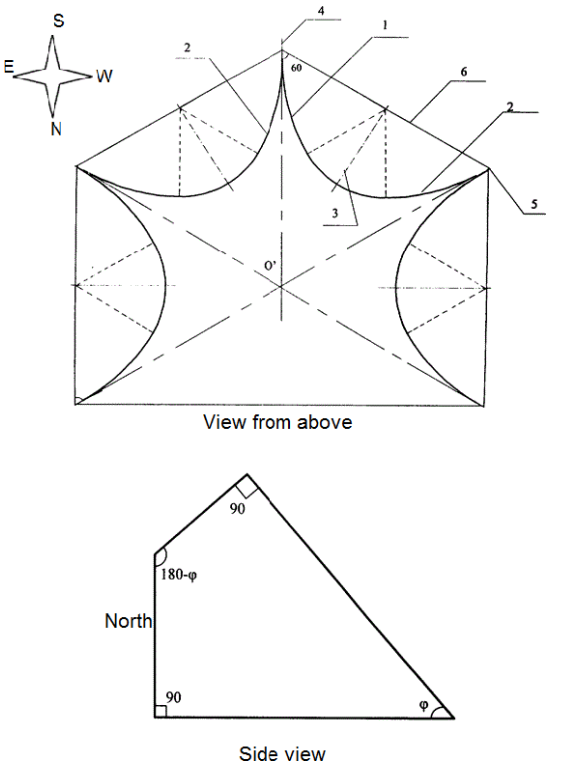

HOLOGRAPHIC PVT CONCENTRATING SYSTEM FOR BUILDING INTEGRATION APPLICATIONS

In (Marín-Sáez, Chemisana, Moreno et al., 2016) a building integrated concentrating PVT system was developed for applying a solar shading system to the blinds. In the developed system the concentrator has the advantage of tracking the shading of blinds at a solar height and has increased optical efficiency. The consider building is size to be 5.8 m height, starting the blinds at the ground floor window level, total amount of blinds is 12 (blinds' size is 9 m long by 0.4 m wide and by 0.065 m high). Both elements – holographic optical element (HOE) and PVT module are assembled in a single unit, forming a modular system with two parallel layers.

The building integrated concentrating PVT system of two holographic lenses focusing the incident radiation on the PVT module. Both holographic lenses are attached to one glass substrate covering the space between them.

The length of the PVT receiver is shorter than the length of the holographic lens to avoid vignetting effects.

As a solar concentrator HOE a cylindrical holographic lens is chosen. The lens is produced by the action of a plane wave and a cylindrical wave on a photosensitive medium, which varies the refractive index of the material. When illuminating a volume hologram, the transmitted wave and the diffracted waves are found at its output. With the adequate incident conditions the efficiency of the diffracted ray is maximal, it can reach 100% for a selected wavelength. When a holographic cylindrical lens is illuminated by a plane wave, the resulting diffracted wave is cylindrical.

The wavelength for which the HOE will be most efficient is set at 800 nm. It is a compromise between the incident solar spectrum with maximal intensity at wavelengths around 500–800 nm and the photovoltaic cell sensitivity around 700–1000 nm for mono-Si cells. The PVT module is located 5 cm from the HOE to collect more energy from the desired wavelength range, as rays with different wavelengths are directed in different directions.

When the incidence direction varies in the plane formed by the two recording rays holograms have higher angular selectivity and lower angular selectivity in the perpendicular plane. The cylindrical lens offers the possibility of overwhelming tracking in one direction. Tracking is only required along the direction with higher angular selectivity.

Two HOEs are placed separated in the same plane, so that the spatial distributions of the diffracted beams are symmetrical. A glass plate located

in this plane covers the space between the two HOEs and have the same refractive index as the photopolymer. Angles of incidence larger when vignetting would occur for the optimal bandwidth, result in total internal reflection and prevent the former effect.

The good performance of developed system is obtained due to the holographic optical element effect which concentrates on the cell only the bandwidth for which it is more sensitive and does not concentrated the infrared avoiding overheating. The temperature of the cells is controlled by the active cooling system in the PVT module.

The proposed system cover more than 15% of the space heating demand at both locations.

DIELECTRIC PVT CONCENTRATOR FOR BUILDING-FACADE INTEGRATION

The system in (Riverola, Moreno, Chemisana, 2018) designed is composed by a cylindrical case and an inner cavity filled with the circulating dielectric liquid in which the solar cells are immersed. The module tracks the change in the angle of solar altitude through rotation, is driven by one engine. The system has optical power only perpendicular to the cylinder axis. The solar movement along the azimuthal direction remains untracked taking benefit from the linear concentration, the cylinder axis lies along the east–west direction. The modules are designed to be placed south-oriented (Northern Hemisphere) as an array and can produce energy to cope with building needs. To control the vertical distance between the modules, secondary movement is provided so that there is no shadowing between them. This movement also allows to control the interior lighting of the building. The vertical distance between individual concentrators is minimum which avoids shading between modules and prevents from direct irradiance to enter inside the building.

The cylindrical tube has an outer diameter of 60 millimeters and is made of borosilicate glass. Borosilicate glass is used for exactitude lenses due to its good optical, thermal, mechanical properties and its resistance to environmental damages. Acrylics can suffer degradation exposed to some dielectrics as alcohols. To immerse the cell have been selected deionized water and isopropyl alcohol. Deionized water and isopropyl alcohol have a great heat extraction capacity and weak absorption at frequencies in which solar cells are able to generate electricity energy. These two and other dielectric

liquids are suitable candidates for PVT applications. Both dielectric liquids present high electrical insulation characteristics. The dielectric properties of both liquids vary slightly with temperature, these variations do not affect PV cell performance.

Low-medium concentration systems try to use standard PV modules and low-accuracy trackers resulting in geometric concentrations ranging from 10x to 20x. The cell has been positioned atop of a tube with a radius of 28 millimeters which serves to confine the dielectric liquid.

Incident rays is to face the concentrator perpendicularly taking into account the natural sun beam aperture (semiangle of 4.65 mrad).

The angle of incidence over the cell influences the absorptivity and therefore high angles of incidence are not desired. The deficiency of irradiance uniformity over the cell reduces the fill factor, the efficiency and the open circuit voltage.

By means of a diode laser ($\lambda = 640.1$ nm), the optical designs have been validated by comparing the widths of the simulated concentration profiles at the same wavelength with the experimental widths measured.

The optical efficiency for deionized water is 73.5% and for isopropyl alcohol 76.5%. The difference with the theoretical results is attributed to manufacturing inaccuracies. In addition, the Fill Factor remains almost constant for isopropyl alcohol being 70.1% and for deionized water is somewhat reduced but still close to the bare PV (67.5%). The refractive system in (Riverola, Moreno, Chemisana, 2018) proposed shows potential to be cost-effective due to the use of standard silicon solar cells and low-accuracy trackers to partially cover electricity and heat energy demands of buildings.

BUILDING INTEGRATION OF CONCENTRATING SOLAR SYSTEMS FOR COOLING APPLICATIONS

In the frame of (Chemisana, López-Villada, Coronas et al., 2013) a comparison between two cooling solar systems (SCCS) for a specific three-floor building, with and without solar concentration, is performed. It is assumed that the solar concentrating cooling system is installed in an office building located in Barcelona (Spain).

In (Chemisana, López-Villada, Coronas et al., 2013) the main characteristics of a SCCS system have been described. One of its major advantages in comparison to conventional solar cooling systems is integration suitability

of the solar collectors, in the present case on a building façade. Another important advantage is that it can operate at higher temperatures, allowing the use of higher efficiency double-effect absorption chillers.

The reflectors are integrated in such a way that they are operating as vertical lattices for the illumination control. Therefore, the concentrator can be considered involve in the building structure.

As reflectors can fulfill a building function the cost of the concentrator could be split and then the part corresponding to the concentrating system itself would be diminished.

SOLAR CONCENTRATING MODULES FOR SMART SOLAR BUILDINGS

Currently, the potential to increase the efficiency of energy supply to consumers can be realized through the development of complementary to the existing centralized energy system of distributed energy, in the formation of which renewable energy sources play an important role, in particular, smart solar buildings with solar energy concentrators.

One of the most important tasks of solar technology is the creation of efficient and economical concentrators of solar energy, as well as increasing their concentrating ability. Since the integrability of traditional concentrating modules in the roofs and facades of buildings is significantly complicated and requires the creation of highly accurate automated tracking systems for the Sun, non-tracking solar concentrator modules are of great interest for integration - a relatively large angular aperture allows them to work without tracking. Currently, there is the possibility of creating solar tile designs based on stationary cylindrical parabolic concentrators and a silicon solar cell of planar or multi-junction type.

Due to the fact that the solar radiation concentrator is the most capital-intensive to manufacture and the most expensive element of solar modules during operation, there is a need to optimize the optical, concentrating and design parameters of concentrators.

The purpose of this section is to increase the efficiency of the use of solar energy in the solar concentrator module and reduce the cost of generating electricity and heat. To achieve this goal, the following tasks are solved: increasing the optical efficiency of the solar concentrator module by reducing cosine losses, increasing the concentration coefficient of solar radiation and

increasing the duration of the module in a stationary state without tracking the sun.

A solar concentrator module (Strebkov, Kirsanov, Irodionov et al., 2015) was developed containing a protective coating on the working surface, a semi-parabolic cylindrical reflector with a parametric angle δ and an input and output surface of the rays, and a radiation receiver in the form of a strip. In developing the solar concentrator module, analytical methods of mathematical modeling were used. The mathematical model of the solar concentrator module is implemented in the OptiCad computer program. In the developed solar module, the focal region of the semi-para-cylindrical mirror reflector is shifted to one of the sides of the protective coating and coincides with the edge of the strip of the radiation receiver. The protective coating is made in the form of a deflecting optical system transparent to radiation from a set of prisms with an acute angle Ψ between the surfaces of the entrance and exit of the rays. A solar radiation detector is mounted in the focal plane between the focal axis and the apex of the semi-parabolic cylindrical reflector. The surface of the entrance of the rays of the deflecting optical system is parallel to the surface of the entrance of the rays of the semi-parabolic cylindrical reflector. In this case, the ray entry angle β_0, the acute angle Ψ, and the refractive index *n* of the material of the deflecting optical system are related by the following relation with the parametric angle δ of the semi-para-cylindrical mirror reflector:

$$\beta_0 = \arcsin\left\{\left\{\left\{\sin\left\{\left\{\arcsin\left\{\sin\left[90^\circ - 2\delta + \Psi\right]\frac{1}{n}\right\} - \Psi\right\}\right\}n\right\}\right\}\right\}, \qquad (6.2)$$

where: β_0 – the angle of entry of the rays; δ – the parametric angle of the semi-parabolic-cylindrical mirror reflector; Ψ – he angle between the surfaces of the entrance and exit of the rays.

Figure 11 shows the path of the rays and the general view of the solar concentrator module. The solar concentrator module in Figure 11 contains a semi-parabolic-cylindrical mirror reflector 1 with a parametric angle δ with an input surface of rays 2 whose width is D. The receiver 3 is mounted in the focal plane OF between the focal axis F and the vertex O of the semi-parabolic-cylindrical mirror reflector 1 in the form of a strip of width d = OF. The surface of the entrance 5 of the optical deflecting system 4 is parallel to the surface of the entrance 2 of the rays of the mirror reflector 1.

On the surface of the entrance of the rays 2 a protective coating is installed in the form of a transparent deflecting optical system 4 with the surface of the entrance 5 and the exit of the rays 6 from the set of prisms 7 with an acute angle Ψ and a refractive index n Figure 6.11 shows the path of rays in the solar concentrator module and indicates: β_0 is the angle of entry of rays on the input surface 5 of the deflecting optical system 4, β_1 is the angle of refraction of rays in the surface of the input 5 inside the deflecting optical system 4, β_2 is the angle between the beam normal to the surface 6 rays exit inside the deflecting optical system 4, β_3 is the angle of the rays on the exit surface 5 outside the deflecting optical system 4, β_4 is the angle of the rays at the entrance surface 2 of the semi-parabolic cylindrical reflector 1. Angles β_0, β_1, β_2, β_3, and β_4 are the angles between the directions of the rays and the normal to the respective surface. The surface of the entrance of 2 rays is parallel to the surface of the entrance of 5 rays, therefore, the angle β_0 responsible for cosine losses is equal to the angle between the direction of the rays of the entrance to the solar module with the concentrator and the surface of the entrance 2 of the semi-parabolic cylindrical reflector 1.

Figure 11. Ray path and a general view of the solar concentrating module

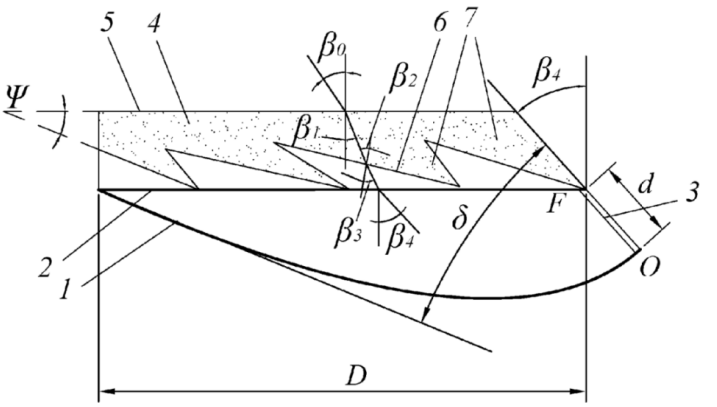

The angle β_0 is determined by (6.2). The angles β_0, β_1, β_2, β_3 and β_4 are related by the following relations:

$$\beta 0 = \arcsin[(\sin\beta 1)\cdot n], \tag{6.3}$$

$$\beta_1 = \beta_2 - \psi, \tag{6.4}$$

$$\beta_2 = \arcsin\left[\left(\sin\beta_3\right)\cdot\frac{1}{n}\right], \tag{6.5}$$

$$\beta_3 = \beta_4 + \psi, \tag{6.6}$$

$$\beta_4 = 90° - 2\delta, \tag{6.7}$$

where β1 – the angle of refraction of the rays in the entrance surface inside the deflecting optical system; β2 – the angle between the beam normal to the surface of the exit of the rays inside the deflecting optical system; β3 – the angle of the exit of the rays on the exit surface outside the deflecting optical system; β4 – the angle of entry of the rays at the entrance surface of the semi-parabolic cylindrical reflector.

Figure 6.12 shows a solar concentrator module in which the input surface of the rays of the optical deflecting system is inclined to the input surface of the rays of the semi-parabolic cylindrical mirror reflector at an angle Ψ. In Fig. 6.12, the deflecting optical system 8 is made in the form of a single prism 9, the input surface 10 of which is inclined to the input surface of the rays 2 of the semi-parabolic cylindrical reflector 1 at an angle Ψ, and the output surface 11 of the rays of the deflecting optical system 8 is parallel to the input surface 2 of the rays of the reflector 1. The angle of entry of the rays $\beta_0^{'}$, responsible for cosine losses, is the angle between the direction β0 of the rays on the surface of the entrance 10 of the rays of the deflecting optical system 8 and the normal to the surface of the entrance 2 half mirror reflector 1.

Angles β0, β'0 are determined:

$$\beta_0^{'} = \beta_0 + \Psi, \tag{6.8}$$

$$\beta_0 = \arcsin\left\{\left\{\sin\left\{\left\{\arcsin\left\{\sin\left[90^{\circ} - 2\delta\right]\frac{1}{n}\right\} - \Psi\right\}\right\}n\right\}\right\} + \Psi, \tag{6.9}$$

where β'_0 – the angle between the direction β_0 of the rays on the input surface of the rays of the deflecting optical system and the normal to the input surface of the semi-parabolic cylinder reflector.

The concentrator can be made of two symmetric mirror semi-parabolic cylindrical reflectors with a common two-sided receiver in the plane of symmetry, while the protective coating is made of two deflecting beams of counter-optical systems.

Figure 12. Ray path and a general view of the solar concentrating module with inclined entry surface

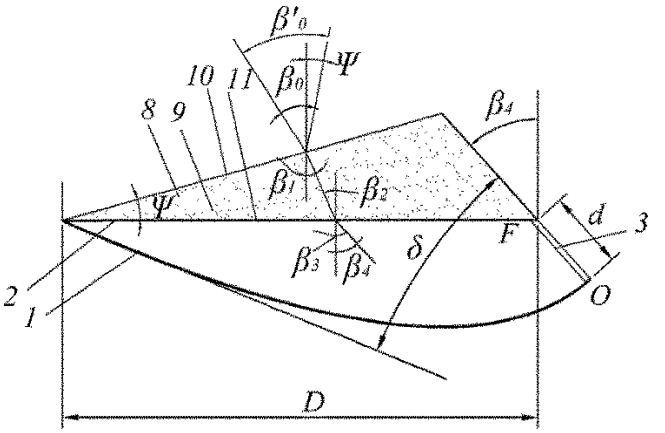

Figure 13 shows a solar concentrator module containing two deflecting optical systems 12 and 13 and two semi-parabolic cylindrical reflectors 14 and 15, in which the input surface 16 of the deflecting optical system 12 is parallel to the input surface 17 of the semi-parabolic cylindrical reflector 14. The input surface 18 of the deflecting optical system 13 is parallel to the input surface 19 of the semi-parabolic-cylindrical mirror reflector 15. The solar concentrator module in Figure 6.13 has a common focal axis F and bilateral common receiver 20 mounted in the plane of symmetry 21 of the solar module through the common focal axis F.

In this case, the angle between the input surfaces of two deflecting optical systems Θ is:

$$\Theta = 180 - 2\beta 0, \tag{6.10}$$

Figure 13. General view of the solar concentrating module with two deflecting optical systems and two-way receiver

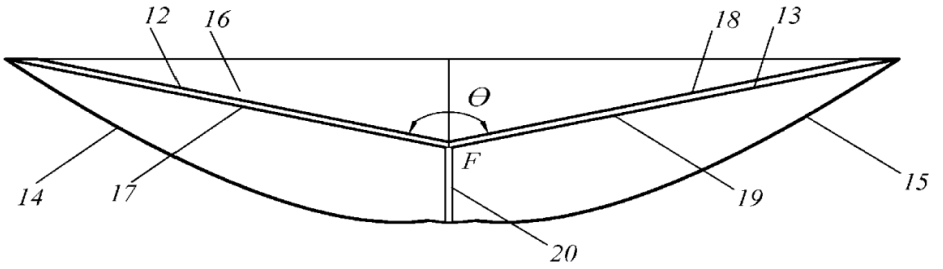

where Θ – the angle between the input surfaces of two deflecting optical systems.

The concentration coefficient of a solar module with a concentrator, taking into account cosine losses for solar concentrator modules in Figures 11-13, is:

$$k_1 = \frac{D \cdot \cos\beta_0}{d} = \frac{2\cos\beta_0}{1-\cos(2\delta)}, \tag{6.11}$$

$$k_2 = \frac{D \cdot \cos\beta_0}{d} = \frac{2\cos\beta_0^{'}}{1-\cos(2\delta)}, \tag{6.12}$$

$$k_3 = \frac{4\cos\beta_0}{1-\cos(2\delta)} = 2k_1, \tag{6.13}$$

where k_1, k_2, k_3 – concentration coefficients taking into account cosine losses for solar concentrator modules in figures 6.11-6.13, respectively; D – the width of the surface of the entrance of the rays; d – the width of the solar radiation receiver.

The solar concentrator modules shown in figures 6.11-6.12 can operate in a stationary mode without tracking the sun, while concentrating both direct and scattered solar radiation within the aperture angle δ. The solar concentrator module in Figure 6.13 also concentrates direct and scattered solar radiation, but requires tracking the sun, since the deflecting optical systems and semi-parabolic cylindrical reflectors are installed counterclockwise to collect the rays on a common two-way solar radiation receiver. In this case,

the concentration coefficient of solar radiation doubles in comparison with the solar concentrator module in Figure 6.11.

Consider the principle of operation of the solar concentrator module on the example of Figure 6.11. Solar radiation enters at an angle β0 on the surface 1 of the input of rays 5 of the deflecting optical system 4, consisting of a set of prisms 7 with an acute angle Ψ and with a refractive index n. Next, the solar radiation enters the prism at an angle β1, leaves the prism at an angle β3, and enters the input surface 2 of the semi-para-cylindrical mirror reflector 1 at an angle β4 and is reflected from the semi-para-cylindrical mirror reflector 1 to the receiver 3 under the condition $\beta_4 {}^3 90°\text{-}2\delta$.

Cosine losses due to deviation of the solar radiation flux from the normal to the input surface of the rays 2 of the semi-parabolic cylinder reflector are calculated:

$$P = 1 - \cos\beta 0, \tag{6.14}$$

where P – cosine losses.

The proposed design of the solar concentrator module allows reducing cosine losses compared to the solar module without a concentrator from 21% ($\Psi = 0$) to 7% at $\Psi = 20°$ and up to 1.4% at $\Psi = 32°$.

The effective aperture angle of the solar module with the concentrator increases from δ to the value $\frac{90^\circ - \beta_0}{2}$. For $\Psi = 24\ ° \beta_0 = 17.8°$, the effective aperture angle of the solar module with the concentrator increases from $\delta =$ 26.1 to $\frac{90^\circ - 1\beta_0}{2} = 36^\circ$, which for a change in solar declination of 7.83° per month corresponds to an increase in the duration of stationary operation by $\frac{26,1^\circ}{7,83^\circ} \cdot 2 = 6,7$ months to $\frac{36^\circ}{7,83^\circ} \cdot 2 = 9,2$ months.

The arrangement of prism reflectors according to Figure 6.11 is preferable, since at the same angle Ψ it increases the angular aperture of the solar module with the concentrator by a larger amount compared to the solar concentrator module in Figure 6.12 with significantly smaller cosine losses.

The developed solar concentrator module for smart solar buildings can be performed as follows. The deflecting optical system 4 is made of a set of prisms with an acute angle $\Psi = 24°$, D = 0.550 m, length 4.25 m. The angle of entry of the rays $\beta_0 = 17.8°$, angle $\beta_4 = 37.8°$, the aperture angle of the semi-parabolic cylindrical reflector 1 $\delta = 26.1°$. Mirror reflector 1 is made of

glass bezels. The solar radiation receiver 3 has dimensions 125 × 1250 mm, consists of 36 silicon solar cells with a size of 125 × 31.25 mm, connected in series. The geometric concentration coefficient is k = 4.92, the cosine loss is 4.8%, the optical efficiency is 80%, the efficiency of the receiver is 15%, and the total efficiency of the module is 11.946%. The area of the module is 0.6875 m^2. The peak electrical power of the module is 82.13 W with an illumination of 1 kW/m^2 and a temperature of 25°C.

The main requirements for solar concentrator modules with a silicon photo-electric receiver: a concentration coefficient of not more than 4-5 from the conditions for the natural cooling of the modules and the use of scattered radiation within the aperture angle of the concentrator. The solar concentrator modules shown in figures 6.11-6.12 can be used in a stationary version for roofs and facades of houses and in figure 6.13 with tracking systems for installation on the ground.

The developed solar concentrator module has small cosine losses, long life and low cost. The receiver of solar radiation can be made with a heat removal device for generating electricity and hot water.

With an efficiency of 20%, the cost of flat modules is $ 0.3/W, $ 60/m^2 in China (Kreutzmanna, 2018).

At a cost of specular reflectors of $ 15/m^2, a concentration of 4 times, an optical efficiency of 0.9 and an electrical efficiency of 18%, the cost of a solar module with a concentrator will be 0.183 $/W, 32.97 $/$m^2$, i.e. will decrease by 1.64 times compared with a solar module without a concentrator, while the costs of the concentrator and receiver will be approximately equal and amount to 50% of the cost of the module.

ENSURING ENVIRONMENTAL PERFORMANCE OF ENERGY PRODUCTION

Mankind is not in danger of an energy crisis associated with the depletion of oil, gas, coal, if it learns the technology of using renewable energy. In this case, the problems of environmental pollution by emissions from power plants and transport, the provision of quality food, education, medical care, and the increase in the duration and quality of life will also be solved. Solar power stations (SPS) create new jobs, improve the quality of life and increase the energy security and independence of SPS owners through fuel-free and distributed energy production.

Technological processes are being developed for the production of SPS components, in which environmentally unacceptable chemical etching and processing processes are replaced by vacuum, plasma-chemical, electron-beam and laser processes. Serious attention is paid to the disposal of industrial waste, as well as the recycling of SPS components after the end of their life.

When using SPS, natural landscapes and habitats are organically combined with energy installations. SPS form spatial and architectural compositions, which are solar facades or solar roofs of buildings, farms, shopping centers, warehouses, and indoor parking lots.

In connection with the development of integrated energy systems in Europe, North and South America and proposals for the creation of a global solar energy system, tasks have arisen to create devices for transmitting terawatt transcontinental flows of electric energy. The third method may enter into competition between AC and DC transmission systems: the resonant waveguide method of transmitting electric energy at an increased frequency, first proposed by N. Tesla in 1897.

N. Tesla considered his resonant single-conductor system for transmitting electrical energy as an alternative to the direct current power transmission system proposed by T. Edison. The competition between direct and alternating electric power transmission systems continues to the present, however, all this takes place within the framework of classic two-three-wire closed power lines. Single-conductor resonant systems open up possibilities for creating ultra-long cable power lines and, in the future, replacing existing overhead lines with single-conductor cable lines. This will solve one of the most important energy problems - increasing the reliability of power supply.

Until the 17th century, solar energy and wood burning energy, in which solar energy is accumulated due to photosynthesis, were the only sources of energy for humans. And now 20% of global energy production is based on burning wood, river energy and wind energy, which are based on solar energy. New energy technologies, new principles of renewable energy conversion, new technologies of solar silicon, production of solar cells, sealing of solar modules, the use of stationary solar concentrators and new methods of transferring electric energy to the global solar energy system will provide by the end of the century 80–90% of the world's solar energy energy production. Thus, the 21st century before our eyes becomes the century of solar energy.

In Russia there are over 2 million kilometers of networks, more than half of which have developed their normative term. The history of science shows that very rarely global inventions appear that significantly change our ideas about the world around us and the possibilities of human development. An

example is the discovery of electricity, the emergence of nuclear and solar energy, aviation and rocket technology, computers and telecommunication technologies.

N. Tesla suggested using the Earth as a single-conductor line for power supply of land, sea and air electric vehicles.

The project envisaged the creation of a network of power plants with energy transfer systems to anywhere in the world on the surface of land, oceans and in the atmosphere, using the earth as a single-conductor line. At the same time, oceans and cities were supposed to be illuminated at night due to ionization of the atmosphere. Testing of experimental systems in Colorado Springs and near New York revealed environmental problems during the operation of the system: sparks from taps with water and from horses' hooves, glow of people's hands and hair, accident at a power plant, etc.

However, in our time, we are witnesses and participants in the creation of new technologies that change the world, make it better, cleaner and safer. First of all, these are the energy systems that N. Tesla proposed a hundred years ago. N. Tesla created alternating current electrical engineering, but he did not manage to develop his main project "Global Earth Power Supply System".

Tesla's energy systems are based on the use of reactive currents in single-wire open lines.

N. Tesla left thousands of pages of books with the results of experiments, articles and patents. VIESH scientists received 50 patents for new technologies that develop N. Tesla's energy systems.

At the beginning of the 19th century there were no diodes and transistors, and N. Tesla used the shock excitation method with a spark gap with a transmission efficiency of 96% to pump the resonant circuit and Tesla transformer. Currently, frequency inverters using IGBT silicon transistors with an efficiency of 97% and a mass of 30 kg are used. ReFuSol developed and put on sale a 20 kW inverter based on silicon carbide transistors with an efficiency of 98%.

Unlike DC power lines with converter substations on the high side of transformers, N. Tesla's technology uses frequency converters and inverters on the low side of transformers, which reduces their cost to the level of 100-200 US dollars per 1 kW.

N. Tesla left us the following technologies for development:

1. Single-wire resonant power supply technologies for stationary consumers.
2. Technologies for wireless power supply of electric land and sea transport.

3. Technologies for directional wireless transmission of electrical energy through conducting channels in the atmosphere and outer space.

The use of isolated single-conductor cable lines instead of Earth will help to avoid environmental problems associated with the implementation of N. Tesla's project to create a global power supply system. N. Tesla published two patents for cable single-wire lines that can be used for the project of a unified energy system of Russia from Chukotka to Kaliningrad. The first patent proposes the use of cables with special shields that reduce the energy loss to radiation to almost zero. The diameter of the current-carrying core of the cable is 1–5 mm, which ensures a small electric capacity of the cable. In the second patent, N. Tesla proposed laying waveguide single-conductor cable lines in the permafrost zone to increase the insulation strength, and to create an permafrost zone around the cable, use an electrically insulated metal pipe as a conductor, through which a gaseous or liquid refrigerant with a low temperature is pumped.

Single-conductor cable lines, for which N. Tesla's patents are available, will replace overhead power lines, which will significantly increase the reliability of power supply, reduce electrical injuries and free up significant areas in the fields, in cities and forests of Russia. Energy systems of N. Tesla in the future can be used to create a global solar energy system.

CONCLUSION

In connection with the large-scale development of high-rise building projects recently in Russia and abroad and their significant energy consumption, one of the main principles in designing is the use of effective energy-saving technologies. Also important aspects are reducing energy consumption and neutralizing the environmental impact of tall buildings.

The basic requirements for solar power plants with concentrators integrated into buildings are identified. The designs of a solar house containing solar concentrator modules have been developed. The result of the development of solar house designs is an increase in the efficiency of using solar energy and a reduction in the cost of electricity and heat, as well as the creation of efficient solar systems built into the facades and roofs of buildings to provide them with electricity and heat. The design of a roofing solar panel with high optical efficiency and low consumption of semiconductor material and low cost has been developed and patented. As a result of using a roofing solar panel,

the efficiency of using solar energy is increased and the cost of generating electric energy and heat is reduced. With the cost of semi-parabolic cylindrical reflectors 4, 5 30 $/m^2$, a concentration of 4.92, an optical efficiency of 0.8 and an electrical efficiency of 15%, the cost of a roofing solar panel will be $ 12, or $ 1/W, at an existing cost of $ 3 / W, those it will decrease by 2.5 times, while the costs of the composite concentrator and receiver will be approximately equal and amount to 50% of the cost of the roofing solar panel.

The integrated concentrated PVT system of the building, designed for applying a solar-grid shading system to the blinds, is considered. In this way, the concentrator takes advantage of tracking the shading of the blinds at a sunny height and thus increases the optical efficiency. The optical efficiency for DIW is 73.5% and for IPA 76.5%.

The most promising areas in the field of integration of solar modules (planar and concentrating) in the construction of buildings are: development of BIPV technologies (roofing, film, facade materials); the integration of solar energy concentrators that do not require biaxial tracking (medium and low concentrations) on the facades and roofs of buildings (parabolic concentrators, lenses and Fresnel mirrors); integration of highly concentrated modules on the roofs of buildings.

REFERENCES

Chemisana, D., López-Villada, J., Coronas, A., Rosell, J. I., & Lodi, C. (2013). Building integration of concentrating systems for solar cooling applications. *Applied Thermal Engineering*, *50*(2), 1472–1479. doi:10.1016/j.applthermaleng.2011.12.005

Kreutzmanna, A. (2018). Healthy selfconfidence. *Photon International*, 40-41.

Marín-Sáez, J., Chemisana, D., Moreno, A., Riverola, A., Collados, J. A., & Collados, M. V. (2016). Energy Simulation of a Holographic PVT Concentrating System for Building *Integration Applications. –. Energies*, *9*(577), 2–19. doi:10.3390/en9080577

Riverola, A., Moreno, A., & Chemisana, D. (2018). Performance of a dielectric PVT concentrator for building-façade integration. *OPTICS EXPRESS A892*, 26,18.

Strebkov, D.S., Kirsanov, A.I., Irodionov, A.E., Panchenko, V.A., & Mayorov, V.A. (2015). *Roofing solar panel.* Patent for invention No. 2557272 of the Russian Federation, IPC E04D 13/18. No. 2014123409/03; publ. 07/20/2015.

Strebkov, D.S., Tveryanovich, E.V., Irodionov, A.E., & Polushin, S.A. (2007). *Solar house.* Patent for invention No. 2303753 of the Russian Federation, IPC F24J 2/42, F24J 2/14. No. 2006117115/06; publ. 07/27/2007.

Strebkov, D.S., Kirsanov, A.I., Irodionov, A.E., & Panchenko, V.A. (2015). *Solar module with a concentrator (options).* Patent of the Russian Federation. 2572167, 12/27/2015.

Strebkov, D.S., Tveryanovich, E.V., Irodionov, A.E., & Polushin, S.A. (2008). *Solar house (options).* Patent for invention No. 2338129 of the Russian Federation, IPC F24J 2/14. No. 2007110540/06; publ. 11/10/2008.

Chapter 7
Evaluation of the Use of Artificial Neural Networks in Solar Energy

ABSTRACT

Artificial neural network (ANN) is initially used to forecast the solar insolation level and followed by the particle swarm optimisation (PSO) to optimise the power generation of the PV system based on the solar insolation level, cell temperature, efficiency of PV panel, and output voltage requirements. Genetic algorithm is a general-purpose optimization algorithm that is distinguished from conventional optimization techniques by the use of concepts of population genetics to guide the optimization search. Tabu search algorithm is a conceptually simple and an elegant iterative technique for finding good solutions to optimization problems. Simulated annealing algorithms appeared as a promising heuristic algorithm for handling the combinatorial optimization problems. Fuzzy logic algorithms set theory can be considered as a generation of the classical set theory. The artificial neural network (ANN)-based solar insolation forecast has shown satisfactory results with minimal error, and the generated PV power can be optimised significantly with the aids of the PSO algorithm.

DOI: 10.4018/978-1-7998-4276-7.ch007

INTRODUCTION

Artificial neural networks are mathematical models, as well as software or hardware implementations, built on the principle of organization and functioning of biological neural networks - networks of nerve cells of a living organism.

THE PRINCIPLE OF OPERATION OF AN ARTIFICIAL NEURAL NETWORK

In 1957, the American physiologist F. Rosenblatt made an attempt to technically implement a physiological model of perception, based on the assumption that perception is carried out by a network of neurons. According to the common and simplest model of a neuron (the McCallock-Pits model), a neuron is a nerve cell that has several inputs - dendrites and one output - an axon. The inputs are either exciting or inhibitory. A neuron is excited and sends pulses in the event that the number of signals arriving at the exciting inputs exceeds the number of signals arriving at the inhibitory inputs of the neuron. The perception model consists of a receptor layer S, a layer of transforming neurons A and a layer of reacting neurons R (Kamenev, Korolev, Sokotuschenko, 2012; Vapnik, Chervonenkis, 1974).

Currently, mathematical models of neural networks are widely used. Graphically, such models are depicted in the form of the graph shown in Figure 1, which depicts a simple multilayer direct distribution neural network.

The circles in Figure 1 indicate the conditional inputs of neurons that simply distribute the input values across all neurons in the network. In the mathematical model of a neuron, all incoming arrows have weights, and a nonlinear function of the average sum of these weights with some additional arithmetic operations is calculated at the output.

To use a direct distribution neural network when solving a specific problem, it must first be "trained". To do this, any data is supplied to the input of the neural network, and the resulting values are taken at the output, which are compared with those values that should be there. If the output values of the neural network differ from the required values, then the weights of the neural network are optimized by any of the mathematical algorithms until these

Figure 1. Graphical representation of a mathematical model of a direct distribution neural network

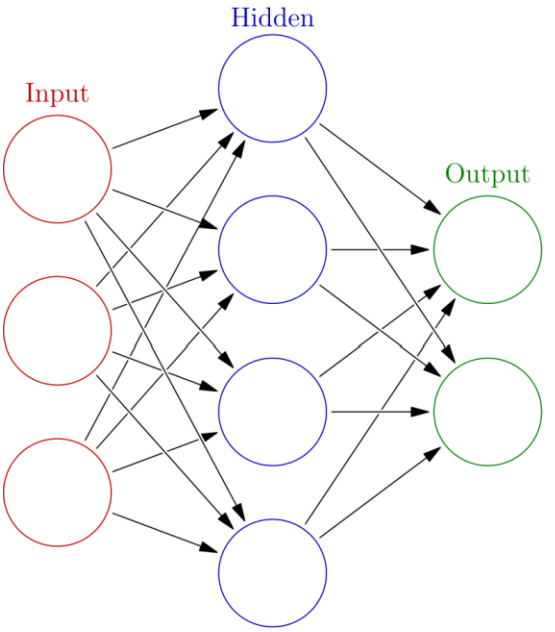

values correspond to them with a given accuracy. A sequence of situations indicating which class they belong to is called a learning sequence.

The task is to build a program that, using the training sequence, would develop a rule that allows us to classify newly presented "unfamiliar" situations (generally speaking, different from those in the training sequence) in much the same way as a teacher. After this, the neural network can be considered trained.

Like the human brain, the neural network is capable of solving a large number of diverse tasks. Figure 2 presents typical tasks that can be solved using artificial neural networks.

A wide range of tasks speaks about the great possibilities of using artificial neural networks. Due to this, their applications are very diverse. In almost

Figure 2. Typical tasks solved using artificial neural networks

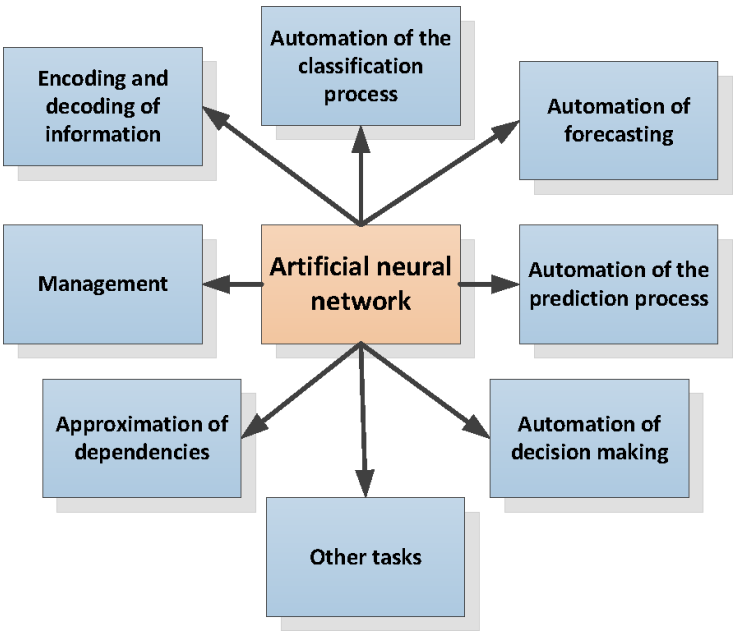

Figure 3. Scopes of artificial neural networks

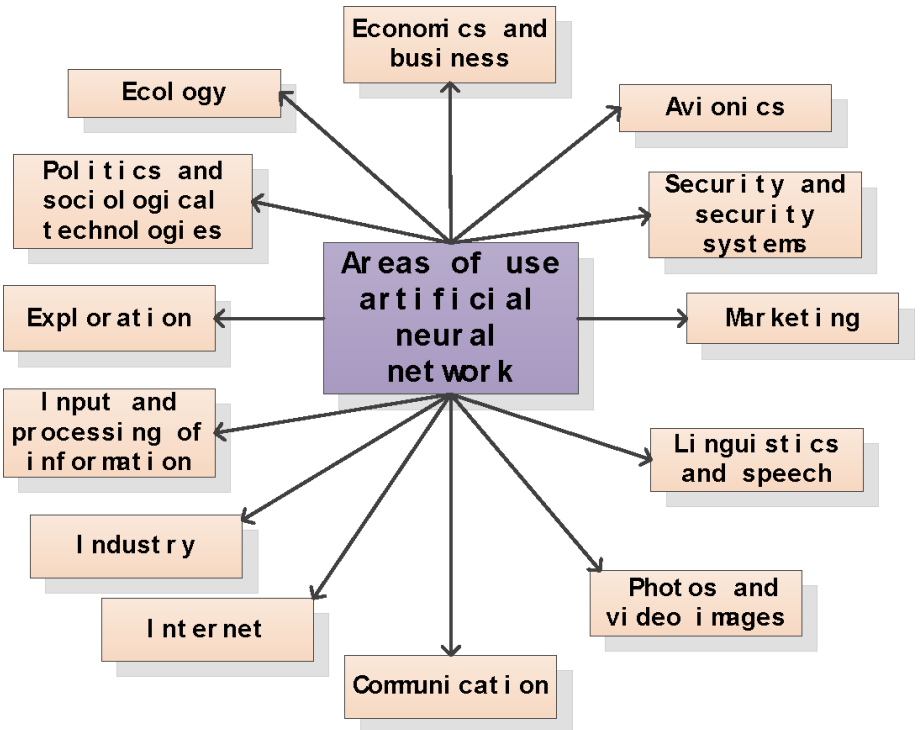

every subject area, upon closer examination, one can find problem statements for artificial neural networks (Figure 3).

ARTIFICIAL NEURAL NETWORK ARCHITECTURE

The structure of neural networks is closely related to the training algorithms used. Three main classes of neural network architectures can be distinguished: single-layer direct distribution networks, multilayer direct distribution networks, recurrent networks.

Single-Layer Direct Distribution Neural Networks

In the simplest case, in the neural network there is an input layer of source

Figure 4. Single layer artificial neural network direct distribution

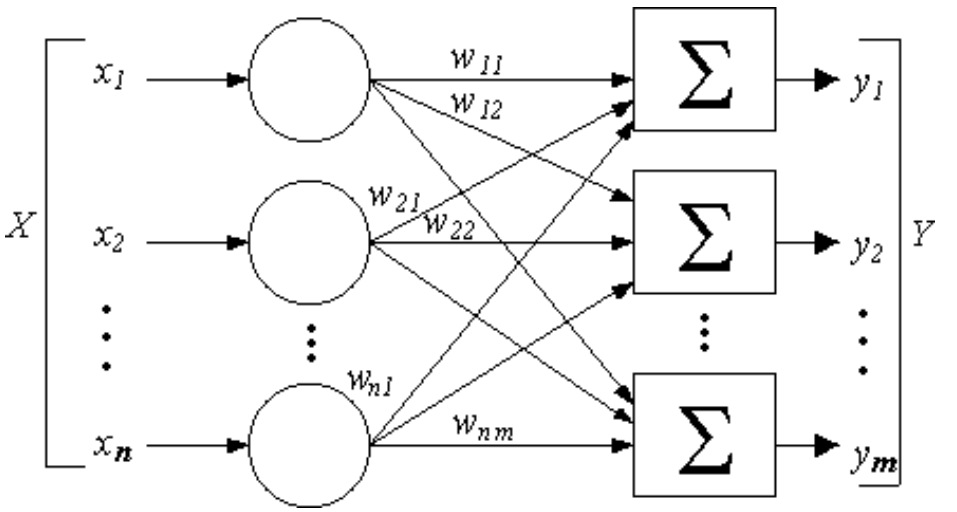

nodes, information from which is transmitted to the output layer of neurons (computational nodes), but not vice versa. Such a neural network is called a single layer direct distribution network. In this case, the only layer is the layer of computational elements (neurons) (Haikin, 2006).

Figure 5. Multilayer artificial neural network direct distribution

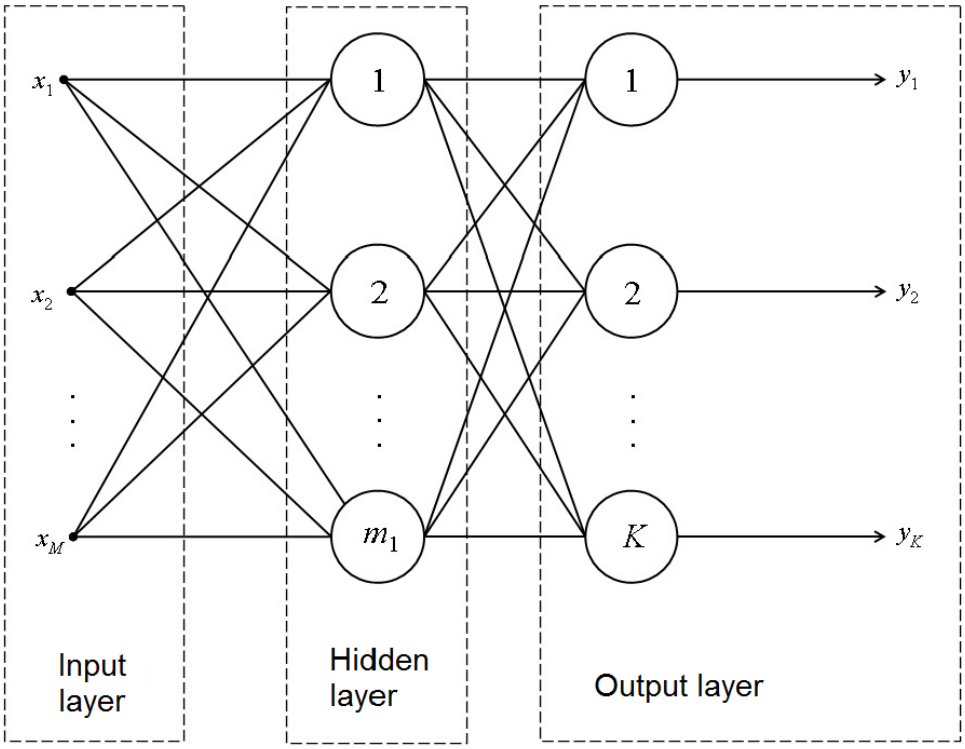

Multilayer Direct Distribution Neural Networks

This class of artificial neural networks is distinguished by the presence of one or more hidden layers, the nodes of which are called hidden neurons. Hidden layers act as intermediaries between the external input signal and the output of the neural network (Figure 5)

The source nodes of the input layer of the network form the corresponding elements of the activation pattern (input vector), which make up the input signal to the neurons (computational elements) of the second layer (Haikin, 2006).

Recurrent Neural Networks

Recurrent neural networks differ from direct distribution networks in the presence of feedback. A recurrent network can consist of a single layer of neurons, each of which directs its input signal to the inputs of all other

neurons in the layer. In this architecture, there is no feedback from neurons to themselves. The presence of feedbacks in recurrent networks affects the learning ability of such networks and their performance (Haikin, 2006).

Neural Network Training

Many pairs of input-output signals, each of which consists of an input signal and the corresponding desired output signal, are called training data or training sample. An example would be the digit recognition problem (Haikin, 2006). Here, the input signal in the form of an image is a matrix consisting of black and white dots. Each image represents one of ten handwritten numbers on a white background. The desired network response is a specific digit, the image of which is supplied as an input signal. Typically, a training sample consists of a large number of handwritten numbers. The algorithm here is as follows:

- the corresponding neural network architecture is selected in which the size of the input layer corresponds to the number of pixels in the figure, and the output layer contains ten neurons corresponding to the numbers;
- the weighting coefficients of the network are set up on the basis of the training set - training the neural network;
- the effectiveness of training is checked on a variety of examples other than those used in training, the recognition results are compared with real numbers - the process of generalization.

The basic rules for presenting data in a neural network are presented in (Anderson, Rosenfeld et al., 1988). The following rules can be distinguished here:

1. Similar input signals from similar classes should form a single representation in an artificial neural network - they should be classified as belonging to the same category, and the degree of similarity is determined based on the Euclidean distance.
2. Elements assigned to different classes should have as excellent representations on the network as possible.
3. If some property is more important, then for its representation in the network it is necessary to use a large number of neurons.

4. A priori information and invariants should be embedded in the structure of the neural network, which simplifies the network architecture and the process of its training.

THE USE OF ARTIFICIAL NEURAL NETWORKS TO EVALUATE THE EFFECTIVENESS OF BIPV SYSTEMS

The One Million Solar Roofs programs are implemented in Europe, the USA and Japan (Strebkov, 2019). The programs include state subsidies for installing solar modules on roofs of buildings with a total electric power of up to 3.5 kW per family and connecting to the electric network through an inverter and electric meter. The benefits of the program are as follows:

1. Combining the functions of the solar module and the roof of the building reduces their total cost.
2. Solar modules do not occupy an area on the earth and do not require payment for the earth.
3. The owners of the solar roof sell expensive electricity during peak hours on the grid, and buy cheap off-peak electricity from the grid.

The VIESH has developed a solar roofing panel (solar shingles) (Figure 6), which combines the functions of a roof and a solar module.

Unlike foreign samples, built-in stationary solar concentrators are used in the solar shingles, which made it possible to reduce the area of silicon solar cells by 4 times and receive electric energy and hot water from the solar roof. The solar tile has a protective anti-vandal coating of tempered glass and a cable for connecting to the adjacent solar tile (Figure 7).

Operating voltage 1–1.2 V, peak electric power 5–7 W, depending on the efficiency of solar cells. On 1 m^2 of the roof there are 14 solar roof tiles with a peak electric power of 70-100 watts. Solar tiles with a peak power of 3.5 kW occupy 30–40% of the roof area.

The price of one solar tile is $ 12 compared with the price of Chinese solar tiles in China, $ 14, and in Russia, taking into account transportation and customs duties, $ 20–24. In conditions of mass production, the cost of the "solar roof" will be $ 1,000. US / 1 kW.

The price of one solar tile is $ 12 compared with the price of Chinese solar tiles in China, $ 14, and in Russia, taking into account transportation

Figure 6. VIESH roofing solar panel (contains built-in stationary mirror concentrators with a concentration of 4x and solar cells made of silicon)

Figure 7. "Solar House" in Anapa with a living area of 150 m² with a roof of a solar tile with an electric power of 2 kW

and customs duties, $ 20–24. In conditions of mass production, the cost of the "solar roof" will be $ 1,000. US / 1 kW.

Unlike central power plants using fossil fuels, distributed energy has zero capital costs and zero losses in the transmission of electrical energy.

A significant contribution to the price of electricity from SPP is made by land fees, therefore, the most economical solution, excluding land fees, is the use of solar energy in the One Million Solar Roofs programs in the form of a solar roofing panel (solar roof tile).

Figure 8. The results of calculating the annual productivity of the solar roof of buildings located in the vicinity of Anapa

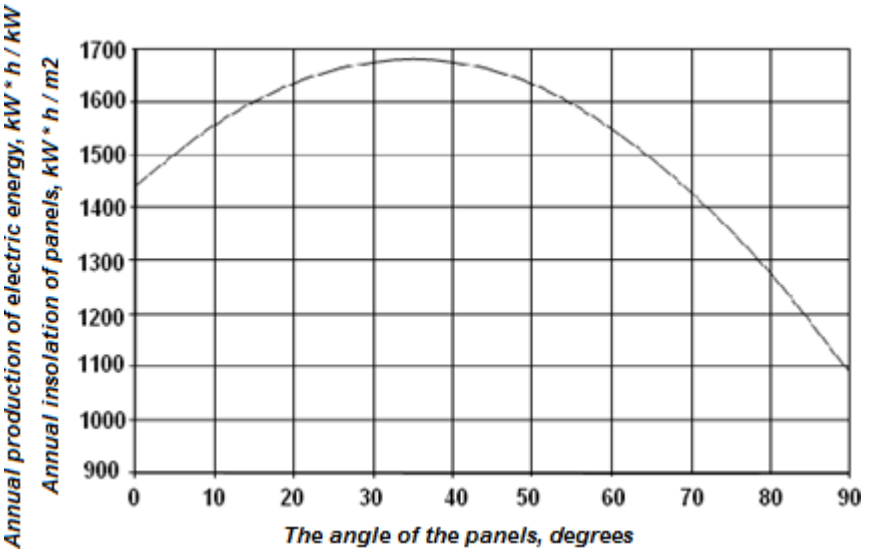

Figure 9. Estimated annual total solar radiation on the surface of stationary panels located in the vicinity of Luxor (Egypt)

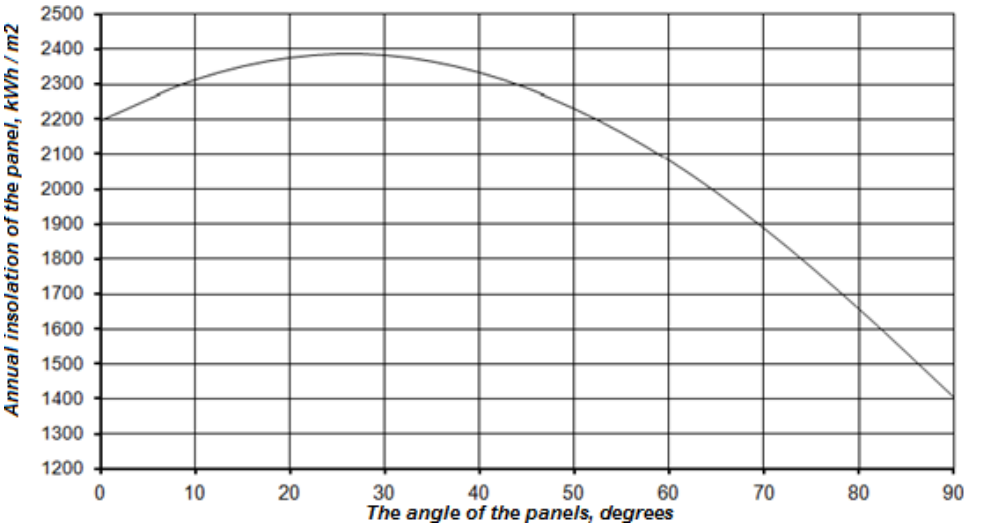

Computer simulations have shown that the annual output of electrical energy for double-sided vertical modules is 1.5–1.67 times higher than for standard south-oriented modules (Figure 9).

The program "One Million Solar Roofs in Russia" with a peak electric power of one solar roof of 3.5 kW gives an annual savings of peak electricity of 5.887 billion kWh in the southern regions of Russia or 3.5 billion kWh in the middle zone of Russia. Due to cogeneration, savings in electricity costs for hot water supply will amount to 17.774 billion kWh per year in the southern regions of Russia and 7 billion kWh per year in the middle zone of Russia. The total installed peak power of solar roofs under the program will be 3.5 GW, or about 3% of the installed capacity of power plants in the Russian energy system. Previously it was believed that the power system remains stable and performs the functions of accumulating SPP energy if the installed capacity of the SPP does not exceed 15% of the capacity of power plants in the power system. In connection with the development of smart grids, the share of distributed solar generation can be increased. For example, in Germany in July 2015, the share of electricity generated by power plants using renewable energy sources was 78%.

The One Million Solar Roofs in Russia program will not require government subsidies. The only thing that can be done is to allow the supply of electricity from the solar roof to the network at the price at which the owner of the house buys electric energy from the network. Abroad, this is done using two electric meters: one fixes the value of the purchased, and the second - the cost of electricity sold. If the cost of purchased and sold electricity is equal for a month or a year, the owner of the solar house and the network company pay nothing to each other.

The program "One billion solar roofs" for planet Earth with a total installed capacity of 3.5 TW will provide all countries of the world with clean and cheap electric energy.

In article (Aristizábal, 2017) describes a 6 kW BIPV system installed at Universidad de Bogotá Jorge Tadeo Lozano in Bogotá, Colombia and a mathematical model is prposed through the implementation of an artificial neural network to estimate the output power of the photovoltaic system.

The grid–connected BIPV system in (Aristizábal, 2017) installed at the Universidad de Bogotá Jorge Tadeo Lozano includes a PV-array of 24 modules of poly-crystalline silicon (Trina Solar TSM-PA05.08), each one of 250 Wp and an inverter Sunny Boy 5000-US model of 5000 W. Taking into account that the DC input of the SB 5000-US inverter varies between 175 V and 480 V and the voltage at maximum power point (VMPP) of the

module is 38V, the PV array was built interconnecting 2 branches in parallel of 12 modules in series each one. Under these conditions the nominal power of the PV array is 6000 Wp.

The PV system is fully monitored to evaluate and analyze the performance and the power quality of the BIPV system.

Figure 10 shows a sketch of the whole system, including the monitoring system. The monitoring system was developed using Virtual Instrumentation and it includes a unit for measuring the power quality parameters because the power quality standards set by the utility companies for decentralized power

Figure 10. Overview of the grid-connected BIPV system and the devices of the monitoring system (Aristizábal, 2017)

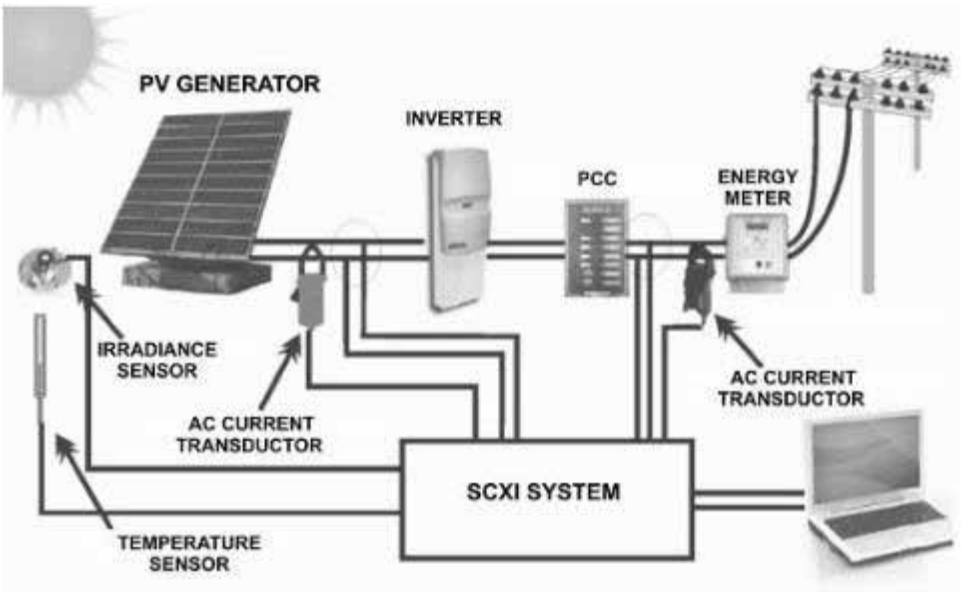

plants must be fulfilled in order to prevent overstressing the equipment in the distribution grid. Independent power producers, who want to sell electricity to utility companies, must accomplish these standards.

This monitoring system creates the necessary database for use in the proposed artificial neural network. Saved variables are: solar radiation, ambient temperature, DC current and voltage, and AC voltage and current.

The monitoring system saves 1 data per minute of each variable; between 5 am and 7 pm. Files are saved in .xls format on a daily basis. Solar zenith

angle and solar azimuth angle are derived from time of day and day of year by using the solar position algorithm developed by NREL. The 12-month (2016) monitoring data are used to train our model and perform performance testing.

The neural network in (Aristizábal, 2017) can be used to fit any kind of finite input to output mapping problem with enough neurons in the hidden layer. The input layer accepts inputs of an M-dimensional vector, X; the hidden layer, H, is composed of N neurons; and the output layer, Y, has Q outputs. This model is used to estimate PV power output from environmental information. Before training the network, the input and output data sets are normalized to (1,1) according to the following expression. The Levenberg-Marquardt (LM) algorithm, a widely used back- propagation algorithm for supervised learning, is employed to update the network weights and biases in the following way.

The model was developed in Matlab and the program creates an .xls file with the results. The meteorological information to train the neural network corresponds to a year of data of solar radiation and ambient temperature acquired by the system of monitoring during 2016. Using the described neural network, it is possible to model the behavior of the dc-ac power or any other variable of the BIPV system. The model data are then validated with the data measured by the monitoring system. After performing the respective tests, it was found that with 12 neurons it is enough to estimate the power using four inputs: solar radiation, ambient temperature, azimuth angle and zenith angle. The neural network was trained using the group of measured data of the whole year 2016: one data per minute for 365 days (between 5 am and 7 pm; daily). The day analyzed was characterized by high cloudiness and rain that did not allow the inverter to reach a value close to its nominal power of 5000 W. The maximum power generated by the inverter was 3600W. The ac power estimated by the neural network has an approximation of 98% in comparison to the ac power measured by the monitoring system. In this case, the BIPVS system starts its dc power production at 6:22 am and ends at 6 pm. It is possible to observe a period of cloudiness and rain between 9:30 am and 11:50 am. The greater power reaches the 4600 W. The correlation between the estimated power and meaured power was 97.6%. Finally, the artificial neural network is evaluated by estimating the dc power and ac power produced by the BIPV system.

The artificial neural network presented in (Aristizábal, 2017), is a useful tool that could be applied to predict the power generated by BIPV systems. The correlation coefficient of 98% allows to guarantee the accuracy in the estimation of the power of the system. A total of 12 neurons were sufficient to

estimate the power with a good degree of accuracy. It was found that a larger number of neurons did not provide a significant improvement in accuracy. The amount of data to train the artificial neural network is a key point to achieve a good degree of accuracy in power estimation. Thanks to the reliability of the artificial neural network and the availability of the data, it is possible to apply the same study to any BIPV system variable: energy, photo-generated current and dc-ac voltage.

PROSPECTS FOR THE DEVELOPMENT OF SOLAR ENERGY

The role of solar energy in the energy of the future is determined by the possibilities of industrial use of new physical principles, technologies, materials and designs of solar cells, modules and power plants developed in Russia.

In order to compete with fuel energy, solar energy must meet the following criteria:

- The efficiency of solar power plants should be at least 25%;
- the life of a solar power plant should be 50 years;
- the cost of the installed kilowatt of peak power of a solar power plant should not exceed $ 1,000;
- the production volume of solar modules should be 100 GW per year;
- the production of semiconductor material for SPP should exceed 1 million tons per year at a price of not more than 25 US dollars / kg.
- round-the-clock production of electric energy by the solar energy system;
- Materials and technologies for the production of solar cells and modules should be environmentally friendly and safe.

Improving the Efficiency of Solar Energy Conversion

The maximum achieved in the laboratory efficiency of solar cells (SC) based on cascade heterostructures is 44%, for silicon SC 24%. Almost all plants in Russia and abroad produce solar cells with an efficiency of 16–22%.

VIESH created new designs and technologies for the production of matrix silicon solar cells from silicon, which allow producing solar cells with an efficiency of 25% when working with solar radiation concentrators.

In Russia and abroad, a new generation of solar cells is being developed with an ultimate efficiency of up to 93%, using new physical principles, materials and structures. The main efforts are aimed at a more complete use of the entire spectrum of solar radiation and the total energy of photons according to the principle: each photon must be absorbed in a graded-gap or cascade semiconductor with a forbidden band whose width corresponds to the energy of this photon. This will reduce losses in solar cells by 47%. For this, the following are being developed:

- cascading solar cells from semiconductors with different bandgaps;
- solar cells with a variable band gap;
- solar cells with impurity energy levels in the forbidden zone.

Other approaches to increasing the efficiency of solar cells are associated with the use of concentrated solar radiation, the creation of nanocrystalline solar cells and solar cells based on perovskites.

In the next five years, new technologies and materials will increase the efficiency of solar cells based on cascade heterostructures in the laboratory up to 45%, in production up to 30%, the efficiency of silicon solar cells in the laboratory up to 30%, and in industry up to 25%.

Increase in Service Life of SPP to 50 Years

To increase the life of the modules, it is necessary to exclude from the module design polymer materials ethylene vinyl acetate and tedlar, which limit the life of the modules to 20–25 years. In the new design of the solar module developed at VIESH, the solar cells are placed in a double-glazed window of two sheets of glass, connected at the ends by soldering or welding.

Sealing technology guarantees a module's service life of 40–50 years. To reduce the temperature of the solar cells and optical losses, the internal cavity of the module is filled with an organosilicon polymer.

Decrease in Cost of Solar Power Plants

The main ways to reduce the cost of SPP: increasing efficiency up to 25%, increasing the capacity of production lines to 1 GW per year or more, reducing the consumption of silicon and its cost by more than 2 times.

New technologies play a decisive role in reducing the cost of solar power plants. Of the innovations of recent years, it is noted the most significant in

terms of their impact on the economy of solar energy. Creation of double-sided solar modules with an efficiency of 22% from the working surface and 19.2% from the back surface of the German company Almaden Europe Gmbh and the organization of gigawatt production of double-sided solar modules in China. For the first time, bilateral solar cells were developed in the USSR and were widely used on low-orbit satellites in the seventies of the last century to increase electric power due to the use of solar radiation reflected from the Earth by the back surface.

The use of vertical double-sided modules in solar power plants with the orientation of the working and back surfaces to the east and west allows 95% of the Earth's area to be freed for agricultural production.

New technologies for sealing solar modules using polysiloxane sealants can double the service life to 40-50 years, reduce depreciation costs in the cost of electric energy and double the income from the sale of electricity. Creating high-voltage silicon solar modules with a voltage of 1000 V instead of 12-24 V reduces switching losses and increases the reliability of large-capacity solar power plants. New optical-concentrating systems based on linear louvre heliostats and stationary concentrators with zero blocking loss, shading and transmission of solar radiation have increased the angular aperture and operating time without tracking the sun of non-tracking concentrator solar modules. Based on this concept, a technology has been developed for the production of solar tiles with built-in stationary concentrators with four-fold saving of silicon area in the module. The new support structure for solar power plants saves 60% of materials, labor and logistics.

The fastest way to reduce costs and achieve gigawatt levels of SPP production is to use solar radiation concentrators. The cost of 1 m^2 of the glass mirror concentrator is 10 times less than the cost of 1 m^2 of the solar module. In VIESH, stationary concentrators with a concentration coefficient of 3.5-10 with an angular aperture of 120-180 ° have been developed, which make it possible to concentrate the direct and scattered component of solar radiation within the aperture angle. The use of low cost solar polysilicon and stationary concentrators allows us to organize the production of concentrator solar modules at a cost of $ 1,000 / kW, which is comparable to the cost of a coal-fired power plant.

Solar Silicon Production

In the price structure of a solar cell, the cost of silicon and other materials is 76%.

Methods to reduce silicon consumption include increasing the volume and size of grown crystalline silicon ingots and reducing the thickness of solar cells. In 2010, the mass of silicon ingot obtained by directional crystallization reached 1000 kg, and the volume was 0.4 m3. The thickness of solar cells decreased from 400 microns in 2000 to 200 microns in 2008, to 108 microns in 2010.

With the current volume of SPP production of 50 GW / year, silicon solar modules make up more than 85% of the production volume. According to our forecasts, solar silicon will continue to dominate the photovoltaic industry, based on the principle: the structure of resource consumption in the long term seeks the structure of their available reserves on Earth. The Earth's crust consists of 29.5% of silicon, which ranks second in reserves after oxygen.

With a production volume of 100 GW per year and a solar silicon consumption of 10,000 tons / GW, global silicon consumption will be 1 million tons per year. In addition to the chlorine-free chemical technology for producing silicon, electrophysical methods are being developed for the recovery of solar silicon from highly pure quartzites using plasmatrons. New technologies are being developed for producing silicon in the form of thin sheets, ribbons, films with laser cutting and automation of the manufacturing process of solar cells.

Global Solar Power System

The average number of hours of using installed capacity per year is 5200 hours for thermal power plants, 1000-4800 hours for hydroelectric power stations, 2000-3000 hours for wind power plants, and 1000-2500 hours for solar power plants.

A stationary solar power plant with an efficiency of 25%, with a peak power of 1 kW produces 1000 kWh per year in central Russia and Germany, and up to 1800 kWh per year in the Sahara desert. When tracking the position of the Sun, electricity production under the same conditions will increase in Russia up to 1300 kWh / kW per year, in the Sahara - up to 2500 kWh / kW per year. The dependence of the generated SPP energy on the time of day and weather conditions is the Achilles heel of the SPP in competition with

fossil fuel power plants. A promising method of accumulating solar energy is the production of hydrocarbon fuel and hydrogen using SPP, followed by the accumulation of gaseous fuel in underground storages and use in existing thermal gas turbine power plants at night and winter.

Seasonal natural gas storage is widely used in Europe and other regions of the world. It is assumed that the efficiency of the technological cycle for the production of hydrocarbon fuels and hydrogen can be increased from 56% at present to 85% in the near future.

Another direction in the development of solar energy is the global solar energy system proposed and patented in Russia in 2004, discussed in Section 7.5. The VIESH computer-aided simulation of the parameters of the global solar energy system, consisting of three solar power plants installed in Australia, Africa and Latin America, connected by a low-voltage power line. In the simulation, data on solar radiation for the entire observation period were used. The efficiency of SPP was taken equal to 25%, the electric power of each SPP was 2.5 GW, the size was 200-200 km2.

The global solar energy system generates electric energy around the clock and evenly throughout the year in the amount of 20,000 TWh / year, equal to the current global consumption of electric energy. This will make it possible to transfer all coal, gas and nuclear plants to the category of reserve power plants.

Base solar power plants of modular type will annually increase their capacity by 100-300 GW. The launch of the global solar energy system is forecasted in 2050, reaching full capacity in 2090. As a result of the project, the share of solar energy in global energy consumption will be 75–90%, and greenhouse gas emissions will be reduced by 10 times.

TECHNICAL AND ECONOMIC PARAMETERS OF SOLAR POWER PLANTS

In the price structure of a solar cell, the cost of silicon and other materials is more than 80%. Methods to reduce silicon consumption include increasing the volume and size of grown crystalline silicon ingots and reducing the thickness of solar cells. In 2010, the mass of silicon ingot obtained by directional crystallization reached 1000 kg, and the volume was 0.4 m3. The thickness of solar cells decreased from 400 microns in 2000 to 200 microns in 2008, to 180 microns in 2014.

New technologies are being developed for producing silicon in the form of thin sheets, ribbons, films with laser cutting and automation of the manufacturing process of SCs (Strebkov, 2019).

The German company Nex Wafe uses the process of epitaxial growth of thin silicon wafers on single-crystal substrates 156-156 mm in size, followed by multiple separation (up to 30 times) of wafers and substrates developed at the Fraunhofer ISE Institute of Solar Energy Systems. The growth rate is at a temperature of 1000 ° C 3 μm / min., The maximum thickness of the plates is 170 μm. The substrate is etched in potassium hydroxide, acquires surface structures, which allows you to separate the epitaxial layers from the substrate. The cost of silicon wafers 156x156x0.035 mm will decrease from $ 1.2 to $ 0.11 (from $ 0.24 / W to $ 0.022 / W), i.e. more than 10 times. Reducing the cost of solar cells will be achieved by eliminating from the production cycle the processes of growing silicon single crystals and diamond cutting crystals, as well as reducing the consumption of silicon. The number of wafers with 1 kg of silicon will increase 15 times, the wafer quality will increase due to a decrease in carbon and oxygen and an increase in lifetime up to 1 ms. The company expects to produce 50 million wafers per year in 2018, which will be enough for annual production at a lower price of 250 MW / year of solar cells.

The cost of a solar cell based on three-stage heterostructures of AIIIB5 compounds measuring 27–27 mm with an efficiency of 30% in the Western market is $ 190, or $ 26.1 / cm^2. The cost of a silicon solar cell with a size of 156-156 mm with a peak power of 5 W and an efficiency of 18% is at a price of $ 0.3 / W $ 1.5 for one solar cell, or $ 0.006 / cm2, which is less than the cost of solar cells based on cascade heterostructures 4350 times. The difference in the cost of one watt of peak power will be less by an amount of efficiency ratios of 1.67 and will be 2605 times. The main reason for such a difference in price is the shortage and high cost of gallium, in the complex manufacturing technology of cascade heterostructures based on gallium arsenide. Therefore, cascade heterostructures are used for the manufacture of radiation-resistant high-efficiency solar space batteries, and a concentration of 500-1000 is needed in terrestrial conditions.

Scientists at Samara University (combined SSAU and SamSU) have developed the basics of the technology of new silicon SC, the efficiency of which, according to laboratory studies, can reach 30% and higher. It is these parameters that have the most effective nanoheterostructural SCs based on III – V compounds today. However, their production uses a much more complex, expensive and dangerous technology associated with toxic compounds of

arsenic and phosphorus and expensive sources of raw materials (gallium, indium, germanium). In addition, according to the US Geological Survey, 9/10 sources of germanium on Earth are located outside of Russia - in the USA and China.

It is important that nanoheterostructured SCs based on III – V compounds are heavier than silicon ones — their specific gravity is up to 1.9 kg / m^2 versus 1.7 kg / m^2 for silicon, which is essential for space applications.

The basis of an effective silicon SC created by scientists at Samara University is a multilayer structure containing layers with silicon nanocrystals and silicon carbide, as well as special coatings with rare-earth ions. Each layer "works" on its own part of the solar spectrum, increasing the share of absorbed energy in this part, so that on the whole a tangible increase in conversion efficiency is obtained. The manufacturing technology of such a structure is based on a well-established technology for the production of silicon devices, the materials used (silicon, carbon, silicon carbide) are low toxic, the sources of raw materials for their production are almost unlimited.

In the spring of 2016, prototypes of solar cells developed by scientists at Samara University went for space tests aboard the Aist-2 spacecraft, which, as part of the first launch campaign, will start from the new Russian space center Vostochny.

The current price of a 100 kW inverter in China is $ 7,000, and a uniaxial tracking system is $ 150 / kW. With a home battery price of $ 3,000, all houses in the world will be able to switch to autonomous solar power supply with an electricity price of less than $ 0.10 / kWh, while existing electricity networks will be saved to supply surplus solar electricity to the power system and as understudy with prolonged inclement weather.

Despite the fact that the cost of the installed capacity of solar power plants is equal to the cost of coal-fired power plants, the cost of electric energy generated by solar power plants exceeds the cost of electric energy from traditional energy sources. The main reason is the low installed capacity utilization factor (KIUM) of solar power plants from 0.114 in Germany to 0.17 in Anapa (Russia) and 0.25 in equatorial countries. The average number of hours of using installed capacity per year is 5200 h for thermal power plants, 1000 ... 4800 h for hydropower plants, 2000 ... 3000 h for wind farms, 1000 ... 2500 h for solar power plants. Stationary solar power plant with Efficiency of 25%, with a peak power of 1 kW, produces 1000 kWh per year in central Russia and Germany, and up to 1800 kWh per year in the Sahara desert.

When tracking the position of the Sun, electricity production under the same conditions will increase in Russia up to 1300 kWh / kW per year, in

the Sahara - up to 2500 kWh / kW per year. To make up for the low KIUM, it is necessary to further reduce the cost of solar cells and modules and the use of solar concentrators.

The main requirements for solar concentrators for planar solar modules made of silicon: a concentration coefficient of not more than 4–5 from the conditions for the natural cooling of the modules and the use of scattered radiation within the aperture angle of the concentrator. In VIESH, stationary concentrators with a concentration coefficient of 3.5 ... 10 with an angular aperture of 120 ... 180 ° have been developed, which make it possible to concentrate the direct and scattered component of solar radiation within the aperture angle. The use of low-cost solar polysilicon and stationary concentrators makes it possible to organize the production of solar power plants with a cost of $ 1,000 USD / kW, which is comparable to the cost of a coal-fired power plant. Such concentrators were created in Russia in a stationary version for roofs and facades of houses and with tracking systems for installation on the ground. If the cost of mirror reflectors is $ 20 / m^2, concentration 4, optical efficiency of 0.85 and electrical efficiency of 20%, the cost of a solar module with a hub will be $ 0.21 / W, i.e. will decrease by 2 times, while the costs of the concentrator and receiver will be approximately equal and amount to 50% of the module cost.

For high-voltage solar modules (HFMs) made of silicon, the optimal concentration is 50-60 from the condition of reducing the temperature coefficient of efficiency by 2 times compared to HFMs made of silicon without concentrators. In this case, the cost of the solar concentrator module will be determined not by the cost of the photodetector based on the HSR, but by the cost of the concentrator, cooling system and tracking the Sun.

INFLUENCE OF SERVICE LIFE ON THE TECHNICAL AND ECONOMIC INDICATORS OF SOLAR POWER PLANTS

The life of the SPP is determined mainly by the durability of the solar modules, which depends on the technology and materials used to seal the solar modules. Sealing standard modules by laminating an ethylene vinyl acetate (EVA) film provides an SPP service life of 25 years in cold climates and 20 years in tropical climates. Sealing the modules with polysiloxane gel extends the service life of the SPP to 40-50 years.

It is calculated the electricity production for SPP with a standard extended service life from 20 to 40 years. In the southern regions of Russia and Europe, the production of electric energy is 1,500 kWh / kW for SPPs installed stationary at an angle equal to the latitude of the terrain, and 2,000 kWh / kW for SPPs tracking the Sun.

For SPPs installed in the equatorial zone, as well as for SPPs with two-sided modules and tracking the Sun, power generation will be 1.5-2 times higher. The cost of electricity from a solar power station in the Belgorod Region, Russia, is 9 rubles / kWh.

Table 8.7 compares the economic performance of SPPs manufactured using VIESHA technology with silicone gel sealing of solar modules and standard SPPs with sealing of solar modules with an ethylene vinyl acetate (EVA) film at an SPP output of 1500 kWh / kW year.

The economic effect of using SPP with a service life of 40 years is to increase electricity production by increasing the service life by 20 years by 30 MWh / kW. Given the average cost of installed SPP power in the world in 2013, $ 2600 / kW (93,600 rubles / kW at a rate of 36 rubles / dollar), the cost of the SPP energy produced with a peak power of 1 kW for a service life of 40 years at a price of $ 0.25. / kWh (9 rubles / kWh) will be 540,000 rubles. and will exceed initial costs by 5.77 times. With an estimated production volume of SPP 50 GW in 2014, an increase in electricity production due to an increase in the service life by 20 years will be 1,500 TWh worth $ 375 billion. At the same time, the market volume of SPP 50 GW at a price of $ 2,600 / kW will be: 50 GW· $ 2.6 / W = $ 130 billion. The total volume of electricity sales for 40 years is 3,000 TWh at a price of $ 0.25 / kWh for $ 750 billion. With the price of grid electricity for consumers in Russia 4.5 rubles / kWh, the

Table 1. Comparison of SPP economic indicators with various types of modules (Strebkov, 2019)

Indicators	Standard sealed modules EVA	VIESH modules with silicone gel sealing
The service life of the modules, years	20	40
Electricity production for the service life, kW · h / kW	30 000	60 000
Revenue from the sale of electricity over the life of 1 kW modules at a price of 9 rubles / kW·h	270 000	540 000
Revenue from the sale of electricity over the life of modules with a total capacity of 50 GW: - at the price of electricity from SPP 0.25 dollars / kW·h - at a price of 4.5 rubles per kWh for consumers of grid electricity in Russia	375 billion dollars 6,75 trillion rubles	750 billion dollars 13,5 trillion rubles

total sales of 3,000 TWh x h of electricity over 40 years will amount to 13.5 trillion rubles, and income from an increase in the service life of SPP for 20 years will amount to 6.75 trillion rubles. Table 1 presents a comparison of the economic performance of SPP with modules of various types.

The energy payback period of SPP is significantly less than the service life. The energy payback period of SPP is defined as the number of years during which SPP produce the amount of energy that was spent on their production.

In a study carried out in 2011, for photovoltaic installations located on the roofs of houses in Southern Europe, where the solar radiation is 1700 kWh / m^2 per year, built in 2005-2006, the payback period was: for installations and from single-crystal silicon with an efficiency of 14% - 2.2 years, for polycrystalline silicon with an efficiency of 13.2% - 2.0 years, for thin-film modules of amorphous silicon with an efficiency of 12.0% - 1.7 years, for modules of cadmium telluride with an efficiency of 10.9% - 0.75 years.

The return time of energy spent on solar energy systems in northern Europe is 2.5 years, while solar systems located in the south return energy spent in 1.5 years.

Solar power plants with modules based on polycrystalline silicon, installed in Sicily, in one year returned the spent energy. Provided that the indicated power plants are operational for 20 years, this type of solar power systems can produce twenty times more energy than is spent on their creation. In southern Europe, the time taken to recover the energy spent on building solar power plants is less than one year. Thus, it can be stated that solar energy has high energy efficiency, because it quickly "returns" the energy spent on their production. New chlorine-free silicon production technologies will reduce the SPP energy payback period of less than 1 year.

THE USE OF ARTIFICIAL NEURAL NETWORKS IN SOLAR ENERGY

In work (Soumya, Chinmaya, Ali, et al., 2012) has been proposed an integrated scheme for optimal power tracking. With the aid of this method, the PV system is able to perform and to enhance the production of the electrical energy at an optimal solution under various operating conditions. As a result, a precise estimation of the PV power generation is known through the optimisation technique as it is to curb the conversion efficiency of the PV system. Likewise, it gives opportunity for any designer to deploy a stationary mounted rooftop

PV system to fully harvest the solar energy at any potential location. Due to the offline optimization technique, this method has its limitation. In contrast to the online optimisation technique, this method requires to store the collected data in a database which is normally done manually. Although this method has its setback, yet it can be modified in the future for online application purposes. The proposed method can become a useful tool in any possible applications regarding to economic power dispatch. The integrated scheme of optimal power tracking can be included into a control system as it can optimally dispatch power to the random loads based on the estimated power generated. Thus, this improves the power dispatch of the PV generator in order to avoid any electrical breakdown as the load fluctuates.

Various Artificial Intelligence techniques are used. They are as follows (Soumya, Chinmaya, Ali, et al., 2012):

- **Genetic Algorithm (GA):** GA is a global search technique based on mechanics of natural Selection and genetics. It is a general purpose optimization algorithm that is distinguished from conventional optimization techniques by the use of concepts of population genetics to guide the optimization search. Instead of point to point search, GA searches from population to population. The advantages of GA over traditional techniques is that it needs only rough information of the objective function and places no restriction such as differentiability and convexity on the objective function, the method works with a set of solutions from one generation to next, and not a single solution, thus making it less likely to converge on local minima, and the solutions developed are randomly based on the probability rate of the genetic operators such as mutation and crossover; the initial solutions thus would not dictate the search direction of GA.A major disadvantage of GA method is that it requires tremendously high time.
- **Tabu Search Algorithms:** Tabu search (TS) algorithm was originally proposed as an optimization tool by Glover in 1977. It is a conceptually simple and an elegant iterative technique for finding good solutions to optimization problems. In general terms, TS is characterized by its ability to escape local optima by using a short term memory of recent solutions called the tabu list. Moreover, tabu search permits back tracking to previous solutions by using the aspiration criterion. Reference, a tabu search algorithm has been addressed for robust tuning of power system stabilizers in multi-machine power systems, operating at different loading conditions.

- **Simulated Annealing Algorithms:** In the last few years, Simulated Annealing (SA) algorithm appeared as a promising heuristic algorithm for handling the combinatorial optimization problems. It has been theoretically proved that the SA algorithm converges to the optimum solution. The SA algorithm is robust i.e. the final solution quality does not strongly depend on the choice of the initial solution. Therefore, the algorithm can be used to improve the solution of other methods. Another strong feature of SA algorithm is that a complicated mathematical model is not needed and the constraints can be easily incorporated unlike the gradient descent technique, SA is a derivative free optimization algorithm and no sensitivity analysis is required to evaluate the objective function. This feature simplifies the constraints imposed on the objective function considered.
- **Particle Swarm Optimization (PSO) Algorithms**: Recently, Particle Swarm Optimization (PSO) algorithm appeared as a promising algorithm for handling the optimization problems. PSO shares many similarities with GA optimization technique, like initialization of population of random solutions and search for the optimal by updating generations. However, unlike GA, PSO has no evolution operators such as crossover and mutation. One of the most promising advantages of PSO over GA is its algorithmic simplicity as it uses a few parameters and easy to implement. In PSO, the potential solutions, called particle, fly through the problem space by following the current optimum particles.
- **Fuzzy Logic (FL) Algorithms**: Fuzzy logic was developed by Zadeh in 1964 to address uncertainty and imprecision which widely exist in the engineering problems and it was first introduced in 1979 for solving power system problems. Fuzzy set theory can be considered as a generation of the classical set theory. In classical set theory an element of the universe either belongs to or does not belong to the set. Thus the degree of associations of an element is crisp. In a fuzzy set theory the association of an element can be continuously varying. Mathematically, a fuzzy set is a mapping (known as membership function) from the universe of discourse to the closed interval. The membership function is usually designed by taking into consideration the requirement and constraints of the problem. Fuzzy logic implements human experiences and preferences via membership functions and fuzzy rules.

ANN has been widely used in many applications especially and forecasting due to its well known fees-forward structure. The MLP structure presented in this research comprises of an input, output and a hidden layers. This structure imitates the basic function of the human brain as it receives inputs, combine them and produce final output result. The input data are divided into training, validation and test sets. The input and output data are normalised in the range between -1 and 1. The MLP structure presented in this research comprises of an input, output and a hidden layers. This structure imitates the basic function of the human brain as it receives inputs, combine them and produce final output result.

MLP network has various connection styles and learning algorithms as it is adapted to its structure and convergence time. Without supervised learning algorithm, the weights are not adjusted to the target data as the desired output is unachievable.

The best MLP structure depends on the best activation function and number of neurons in the hidden layer. Trial and error method determine the results of a suitable number of neuron in each model.

In work (Yu, Yau, Li, 2014) the chaotic extension neural network diagnosis is integrated with error backpropagation neural network. It can remedy the defect of large decrease in diagnostic rate when the irradiance and temperature have changed in the original literature effectively. The defect in the original literature is remedied, and the high diagnostic rate in the original literature is maintained. In comparison to the original neural network diagnosis, the addition of extension theory reduces the time of repeated training. In addition, as the chaos synchronization theory is used, when the diagnosis is difficult due to undervoltage caused by the environment, the signal can be amplified by using the advantages of chaos theory for diagnosis.

The chaos synchronization theory designs a slave system to synchronize a master system. The chaos synchronization system consists of two subsystems, a master system and a slave system, representing the relation between master and servant. This paper uses Lorenz chaos synchronization system, which is highly sensitive to parametric variation, to capture the voltage signal of photovoltaic system and extract the kinematic trajectory of dynamic error. The center of this kinematic trajectory is used as the eigenvalue of fault. The extension theory solves contradiction problem quantitatively and qualitatively to change it into compatibility problem. The difference between extension theory and fuzzy theory is that the range of fuzzy set is (0, 1), whereas the extension is a real number extended from (0, 1) to $(-\infty, \infty)$. The extension theory is characterized by a small amount of calculation and simplicity, and

it has high accuracy rate in evaluating multiple parameters and complex construction. This paper uses this feature to judge the eigenvalue captured by Lorenz chaos synchronization system to identify the fault category of photovoltaic system.

In the extension theory, the matter-element is the basic element describing things. The general matter-element model is the mathematical model applied to extension.

First, the measured irradiance, temperature, and VM_{PPT} are recorded, and the recorded irradiance and temperature are imported into the BP neural network system to obtain the extension classical domain range of chaos center eigenvalue at current irradiance and temperature, and then the recorded voltage is imported into the chaos synchronization system to obtain a kinematic trajectory of chaotic dynamic system. The center point of kinematic trajectory is taken as the basis of diagnosis. Finally, the fault category of photovoltaic system can be identified as long as the obtained signal is imported into the diagnostic system of chaotic extension neural network.

CONCLUSION

Solar energy and BIPV- systems is rapidly gaining notoriety as an important means of expanding renewable energy resources. The VIESH has developed a solar roofing panel (solar shingles), which combines the functions of a roof and a solar module.

Unlike foreign samples, built-in stationary solar concentrators are used in the solar shingles, which made it possible to reduce the area of silicon solar cells by 4 times and receive electric energy and hot water from the solar roof. The solar tile has a protective anti-vandal coating of tempered glass and a cable for connecting to the adjacent solar tile.

The life of the SPP is determined mainly by the durability of the solar modules, which depends on the technology and materials used to seal the solar modules. Sealing standard modules by laminating an ethylene vinyl acetate (EVA) film provides an SPP service life of 25 years in cold climates and 20 years in tropical climates. Sealing the modules with polysiloxane gel extends the service life of the SPP to 40-50 years.

More energy is produced by tracking the solar panel to remain aligned to the sun at a right angle to the rays of light. Now-a-days various artificial techniques are introduced into photovoltaic (PV) system for utilisation of renewable energy. It is essential to track the generated power of the PV system

and utilise the collected solar energy optimally. Artificial Neural Network (ANN) is initially used to forecast the solar insolation level and followed by the Particle Swarm Optimisation to optimise the power generation of the PV system based on the solar insolation level, cell temperature, efficiency of PV panel and output voltage requirements.

Genetic Algorithm is a general purpose optimization algorithm that is distinguished from conventional optimization techniques by the use of concepts of population genetics to guide the optimization search. Tabu Search Algorithms is a conceptually simple and an elegant iterative technique for finding good solutions to optimization problems. Simulated Annealing Algorithms appeared as a promising heuristic algorithm for handling the combinatorial optimization problems. Fuzzy logic Algorithms set theory can be considered as a generation of the classical set theory.

The ANN based solar insolation forecast has shown satisfactory results with minimal error and the generated PV power can be optimised significantly with the aids of the PSO algorithm.

REFERENCES

Anderson, J. A., & Rosenfeld, E. (Eds.). (1988). *Neurocomputing: Foundations of Research*. MIT Press.

Aristizábal, A. J. (2017). Artificial Neural Network Applied to Estimate the Power Output of BIPV Systems. *IOSR Journal of Computer Engineering, 19, 1*, 73-78.

Haikin, S. (2006). *Neural networks: full course* (2nd ed.). Williams Publishing House.

Kamenev, A. S., Korolev, S. Yu., & Sokotuschenko, V. N. (2012). Neuromodeling as a tool of intellectualization of energy-information networks. IC Energy.

Soumya, R. N., Chinmaya, R. P., Ali, S. M., & Sabat, R. R. (2012). Application of solar energy using artificial neural network and particle swarm optimization. *International Journal of Advances in Engineering and Technology*, *4*(1), 550–560.

Strebkov, D.S. (2019). Fundamentals of Solar Energy / ed. Doctor of Technical Sciences Bezrukikh P.P. *SAM Polygraphist*, 326.

Strebkov, D. S., Bobovnikov, N. Yu., Irodionov, A. E., Kirsanov, A. I., Panchenko, V. A., & Filippchenkova, N. S. (2016). The program «One Million Solar Roofs» in Russia. *Bulletin of the All-Russian (All-Union) Research Institute of Electrification of Agriculture*, *3*(24), 84–87.

Vapnik, N. V., & Chervonenkis, A. Ya. (1974). Theory of pattern recognition (statistical problems of learning). Nauka, 415.

Yu, K. N., Yau, H. T., & Li, J. Y. (2014). Chaotic Extension Neural Network-Based Fault Diagnosis Method for Solar Photovoltaic Systems. *Mathematical Problems in Engineering*, *280520*, 1–9.

Chapter 8
Opportunities and Prospects for the Implementation of Artificial Intelligence Systems in Solar Energy

ABSTRACT

In connection with the large-scale development of high-rise building projects recently in Russia and abroad and their significant energy consumption, one of the main principles in designing is the use of effective energy-saving technologies. Also important aspects are reducing energy consumption and neutralizing the environmental impact of tall buildings. The most promising areas in the field of integration of solar modules (planar and concentrating) in the construction of buildings are development of BIPV technologies (roofing, film, facade materials), the integration of solar energy concentrators that do not require biaxial tracking (medium and low concentrations) on the facades and roofs of buildings (parabolic concentrators, lenses, and Fresnel mirrors), integration of highly concentrated modules on the roofs of buildings.

INTRODUCTION

The creation of artificial intelligence technologies is the most important strategic project of the 21st century, the cherished dream of science fiction writers, and now it is more than ever close to implementation. New technologies

DOI: 10.4018/978-1-7998-4276-7.ch008

appear almost daily, and the machines around us are becoming more intelligent, changing the world around.

Artificial intelligence (AI) is a field of science and engineering that is engaged in the creation of machines and computer programs with intelligence. It is related to the task of using computers to understand human intelligence. Moreover, artificial intelligence should not be limited only to biologically observable methods. Two main goals of the development of AI technologies can be distinguished – this is the automation of human activity, especially those of its types that have traditionally been considered intellectual, and the creation of computer models that mimic the processes by which people solve certain intellectual problems in order to explain the essence of these processes.

Examples of the use of artificial intelligence algorithms in renewable energy are enough today. The dependence of renewable energy production on weather conditions has significantly increased the need for accurate forecasting. So, for example, IBM, together with the US Department of Energy (US Department of Energy), implements the SunShot initiative, in which a self-learning program can reliably predict the generation of renewable sources (solar, wind and hydro). The algorithm uses a large amount of historical data along with real-time weather monitoring information.

In this regard, the introduction of artificial intelligence technologies in solar energy is of great scientific interest and is an urgent scientific and technical task.

NETWORK SOLAR POWER STATIONS

In modern solar energy, two main target areas of conversion and use of solar energy can be distinguished: the creation of solar power stations (SPS) designed to produce heat and / or electricity; solar energy technology complexes (SETC) producing chemical raw materials, synthetic materials and energy carriers (hydrogen, methane, ammonia, etc.) (Strebkov, 2019). SETCs also include solar furnaces, which have been experimentally introduced in many countries of the world. However, the experience in creating SETC is still not so great, while there is considerable international experience in the design, construction and operation of power plants with power from 1 kW to 100 MW. The presence of a variety of technical solutions and a wide range of functional types of SPS makes it necessary to scientifically systematize the experience gained in the design and construction of SPS. The well-known classifications of SPS and solar collectors of SPS do not fully reflect the

specifics of the functional structure of SPS as "pure" energy objects of terrestrial solar energy.

SPS represents a new class of energy and architectural and construction objects, consisting of interconnected solar systems and devices (solar collector of the station), various equipment and apparatus, as well as necessary buildings and structures intended for the production of heat and / or electricity through the use and conversion of radiant energy of the sun. The main structural element of the SPS is the solar collector (SC) of the station, which provides absorption, re-radiation (re-reflection) and energy transfer of solar radiation to the receiver-converter, as well as heat and / or electricity, in some cases, and storage. In addition to the above functions of the SC, the SPS carries out management and control, machine (thermodynamic) conversion, accumulation and distribution, maintenance and operation of equipment, etc.

Solar power plants (SPP) are assembled by serial and parallel switching of solar modules (Vissarionov, 2008). Figure 8.1 presents an option for placing an average sized SPS connected to an electrical network.

Figure 1. The scheme of a network solar power station (SPS) with the placement of solar modules on the roof of buildings and on the ground

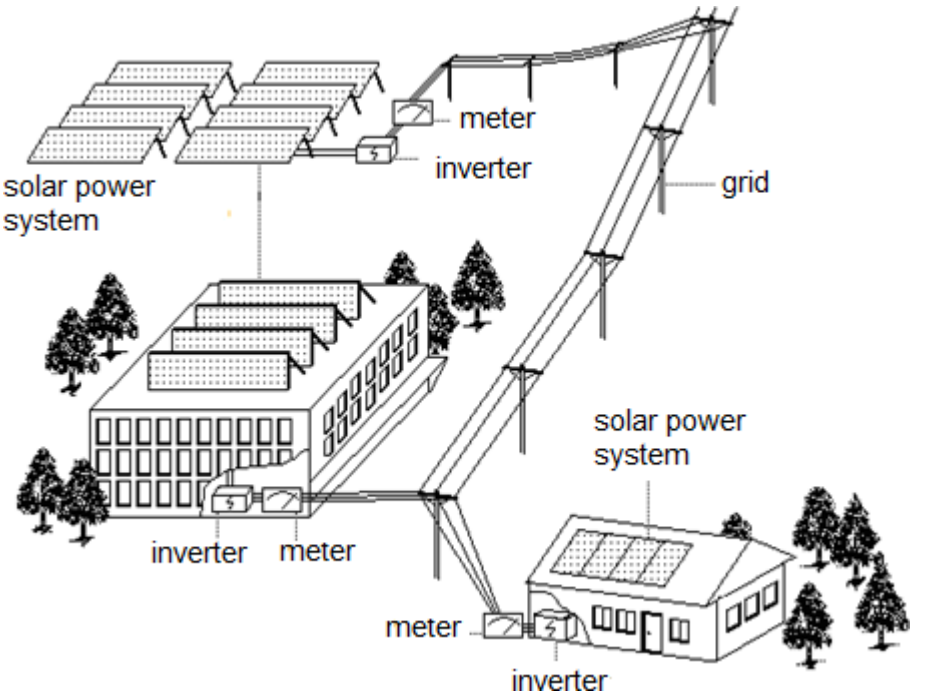

The main schemes of network SPS (Polek, Libra, Strebkov et al., 2013):

- SPS scheme in which each solar module has its own single-phase inverter, synchronized with the frequency of the power system;
- SPS scheme with single-phase sectional inverters;
- a circuit where in each section the modules are connected in series and in parallel and SPS with one central three-phase inverter.

The total installed capacity of the four network SPS in Crimea is 227.5 MW. In 2012, these solar power plants generated 303 million kWh of electricity, which is 38% of electricity production in Crimea and 5% of consumption. In recent years, the number of SPS using solar concentrators has been increasing (Strebkov, Pendzhiev, Mammadsakhatov et al., 2012).

In Germany in 2009, a photoelectric SPS with concentrators based on concentric Fresnel lenses from Concentrix Solar GmbH (Freiburg, Germany) was developed.

Sol Focus (USA) together with the Greek companies Samaras Group and Concept signed an agreement to increase the capacity of photovoltaic solar power plants with concentrators from 1.6 MW to 10 MW. Sol Focus has headquarters in Mountain View (California), a plant in Meza (Arizona) and a European representative office in Madrid (Spain).

Sol Focus produces 30 W square paraboloid modules with an efficiency of 26% at a concentration of 500%. Module sizes are 35–35 cm. Sol Focus receives photodetectors from Emcore Corp (USA), manufactures T1000 cell modules with a 50 W acrylic Fresnel lens with an efficiency of 26, 8% at a concentration of 450. The dimensions of the module are 43–43 cm. The dimensions of the cascade hetero-photodetector are 12.58–12.58 mm. Efficiency of industrial receiver 35%. Emcore Corp together with the University of Delaware (USA) received 42.8% at 20-fold concentration and 39% at 1000-fold concentration on laboratory samples. She built 3 lines for the production of photodetectors in the United States and one line in China with a total capacity of 150 MW/year. Delivers photodetectors to Concentrix GmbH, SolFocus, Isofoton, has received orders for deliveries to Canada, South Korea and Australia.

In 2013, in the United States, the total capacity of SPS with concentrators reached 918 MW.

AUTONOMOUS SOLAR POWER PLANTS

The development of photovoltaic energy is based on the following factors specific to solar power plants: the possibility of autonomous production of electricity in almost any geographical area, high reliability, long service life in all climatic zones without noticeable degradation of output parameters, independence of conversion efficiency from the generated power, and autonomy of operation in for a long period of time, ecological purity of the energy source (Strebkov, 2019; Polek, Libra, Strebkov et al., 2013).

At present, it is economically justified to use SPS to power autonomous consumers working in automatic mode in areas remote from the centralized power supply network.

For the power supply of such consumers, diesel power plants and gas units, replaceable batteries and galvanic cells are used. In 1970–1990, prototype SPS based on photovoltaic modules in gas-filled glass protective shells were developed and passed operational research and life tests at NPO Kvant and VIESH. More than 100 SPS power units with a capacity of 5 to 500 W were operated on lighthouses and navigation signs of the Barents Sea, the Rybinsk Reservoir, Lake Baikal, Lake Ladoga, the Black and Aral Seas, on the VHF radio relay link of the Central Asia - Center gas pipeline, on water-lifting complexes and power supply systems “solar” houses. SPS parameters: Efficiency 7–8%, predicted service life - 30 years. As shown by 10 years of operating experience, the replacement of traditional sources of electricity with autonomous SPS significantly reduces the labor costs for maintenance, saves electricity and fuel.

Of particular interest are solar energy systems in buildings. On the roof of a single-family house with an area of 100 m^2, depending on the time of year and the latitude of the terrain, mid-latitudes receive 200-700 kWh of solar energy per day. In the coldest winter months, the energy consumption for heating well-insulated houses is 60–200 kWh per day, and the daily electricity consumption is about 20 kWh. Thus, a solar power station with an electrical efficiency of 10–15% and a thermal efficiency of 30–50%, located on the roof of the building, having an accumulation system or a backup in the form of an energy system in case of inclement weather, would provide all the energy needs of a solar house.

For solar houses, the generation of thermal energy should be 1.5–3 times higher than the generation of electricity. Since the cost of electric energy is

more expensive than heat, the increase in the cost of combined SPS compared to a SPS that produces only electricity will not exceed 30%.

On June 4, 2009, Greece launched a state subsidy program for owners of photovoltaic solar power plants with a capacity of up to 10 kW installed on roofs of houses. Over the course of 25 years, according to the simplified procedure, SPS owners will receive 78 € / kW·h (55 Eurocent / kW·h) for the electricity supplied to the network. SPS owners are exempted for 25 years from all taxes associated with the purchase of SPS and the sale of electricity, including value added tax. SPS with a capacity of 10 kW produces 14,000 kWh of electricity per year in Greece

When analyzing the technical and economic indicators of the cost of SPS, the dependence of the cost of electricity on efficiency should be taken into account. If the costs of the accumulation subsystems and the inverter per unit area of solar cells are proportional to the efficiency, then the costs of sealing, installation and foundations are independent or inversely proportional to the efficiency. Hence, the inefficiency of SPS with low efficiency is clear. According to generally accepted estimates, SPS specialists with an efficiency of less than 10% are economically unacceptable.

Autonomous SPS of small capacity (Figure 2) have energy storage systems, a battery charge controller (AB) and a single-phase inverter.

The charge controller measures the voltage of the battery and disconnects the load when the battery is discharged and turns off the SPS when the battery is fully charged. Diode D1 prevents battery discharge. It is assumed that the power system can serve as a storage of energy if the capacity of the SPS does not exceed 15% of the power of the power system.

Figure 2. Autonomous solar power station (SPS)
**1 – solar modules; 2 – charge controller; 3– blocking diode; 4 – controlled switches; 5 – accumulator battery; 6 – inverter.*

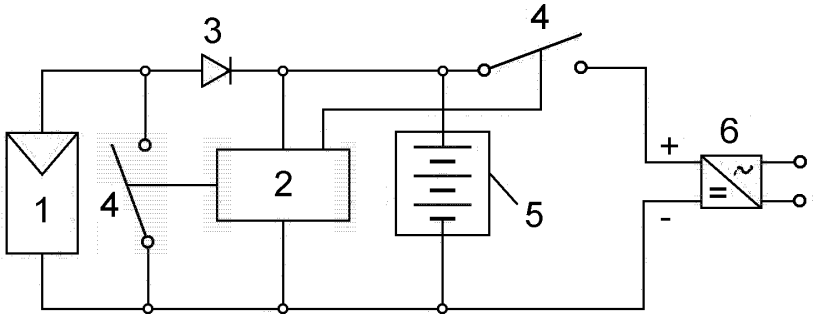

POWER CHARACTERISTICS OF SOLAR POWER PLANTS

Solar energy entering the surface of the SPS for a certain period of time is usually measured in joules or kilowatt hours.

1 kWh/m^2 = 3.6 MJ/m^2 = 860 cal/m^2 = 1 peak sun-hour.

The term "X peak sun-hours" means the number of hours X of solar radiation with a peak illumination of 1000 W/m^2, equivalent in energy to the actual supply of solar energy per 1 m2 of surface of the SPS for a certain period of time.

For example, the energy illuminance (total solar radiation) of a solar module of 5 kWh/m^2 for 12 hours is 5 peak sun-hours and is equivalent to the solar energy received by the SPS for 5 hours at a peak illumination of 1 kW/m^2.

Measurements and calculations show that the maximum amount of solar energy enters the SPS during the year if the slope of the SPS plane to the horizon to the south is approximately equal to the latitude of the terrain minus 10 °. The maximum illumination in the winter months and more uniform illumination of the SPS during the year is achieved if its plane is oriented to the south and tilted at an angle to the horizon, approximately equal to the latitude plus 15. The maximum solar energy in the plane of the SPS in the summer months corresponds to the inclination of the SPS to the horizon in southward at an angle equal to the latitude of the area minus 15 °.

The maximum energy illumination has a SPS, constantly oriented to the Sun.

Since solar energy is measured by weather stations on a horizontal surface, there are formulas, nomograms, and computer programs for converting the energy illuminance of a horizontal surface to solar energy supplied to an arbitrarily oriented fixed or sun-tracking surface of an SPS. Head of the Laboratory of Solar Power Plants VIESH Ph.D. A.E. Irodionov developed a computer program for calculating the energy illumination of SPS arbitrary orientation anywhere in the region of the Earth.

Annual amount of electrical energy generated by a solar power plant:

$$E_{el} = \frac{P_{peak}}{P_{s.peak}} \frac{\eta}{\eta_{st}} E_{sol.}, \tag{8.1}$$

where P_{peak} – peak power of a solar power station;

$P_{s.peak}$ – peak solar radiation power under standard conditions;
η – equivalent annual average solar energy conversion efficiency;
η_{st} – Efficiency of the reference photovoltaic module;
E_{sol} – average annual total energy illuminance in the plane of the solar module.

Assuming that the number of peak sun-hours $T_{s.peak} = \frac{E_{sol.}}{P_{s.peak}}$ and $\frac{\eta}{\eta_{st}} = k_p$:

$$E_{el} = k_p \cdot T_{s.peak} \cdot P_{peak}. \quad (8.2)$$

For a solar power plant connected to the power system k_p values are taken in the range (0.7 – 0.9), for an autonomous power plant k_p = 0.5 – 0.7.

The maximum values of k_p correspond to the operation of a solar power plant in conditions of average annual negative temperatures (for example, in mountainous areas) and high values of energy illumination E_{sol}..

REGIONAL SOLAR POWER SYSTEMS

The development of world energy for the next period will be determined by the need to solve a number of problems related to climate change and global warming, energy shortages that are distributed extremely unevenly and are depleted, constant instability in the world, largely due to the above factors, as well as the problem of maintaining the energy security of each country and global security in general (Strebkov, 2019).

These problems will significantly affect the direction of global energy development and the formation of a future energy strategy, which currently has two main trends:

1) the formation of a global energy system;
2) development of distributed energy production.

It is simply hard to imagine the solution to these global problems without the widespread use of renewable energy sources, which will gradually occupy leading positions in the global energy balance.

It can be assumed that the global energy system will be formed to a large extent due to the creation and subsequent integration of large solar power plants, and for the development of distributed energy production for energy supply to local consumers, the whole spectrum of renewable energy sources

and, first of all, solar energy will be widely used. Significant impact on future energy policy will be provided by such factors as the transition from energy based on fossil fuels to non-fuel energy using renewable energy sources, the replacement of petroleum products and natural gas with liquid and gaseous biofuels, and fossil solid fuel with the use of energy plantations of biomass, replacement overhead power lines to underground and submarine cable lines, the use of new technologies for transferring significant amounts of electricity to significant distances ence to combine large electric stations (preferably solar) in large regional power grid with the subsequent creation of the global grid.

Currently, the concept of creating a global energy supply system of the Earth continues to be formed by consistently enlarging existing and creating new regional energy systems with their subsequent integration into a single global energy system. The idea of combining regional energy systems into the Unified Energy System of the Earth was proposed back in 1975. This idea is actively developed and promoted by the GENI Global Energy Network Institute (GLOBAL ENERGY NETWORK INSTITUTE), registered in California (USA). GENI President Peter Meissen, during his participation in the International Solar Congress in Moscow in 1997, made a report on this issue at VIESH.

The creation of a number of transcontinental systems is planned in the future, combining transport and energy flows and combining waveguide cable lines, transmission lines, railways and highways.

First of all, it is a latitudinal transport and energy highway from West to East: Lisbon - Vladivostok, as well as the meridional highway from South to North: Australia, Indonesia, Thailand, Vietnam - China - Bering Strait - Alaska - Canada - America. The second meridional (energy) flow can go along the Great Silk Road: India - Afghanistan - Kyrgyzstan - Tajikistan - Uzbekistan - Turkmenistan - Kazakhstan, North of Western Siberia. The indicated meridional energy and transport flows intersect in Eastern and Western Siberia with a latitudinal energy and transport trunk, forming a great cross between Europe and Asia.

The third meridional transport and energy line will connect Cape Town with Oslo via East Africa, Arab countries, Turkey, the Black Sea, Eastern Europe and Scandinavia. The fourth meridional energy line will connect the countries of West Africa, the Mediterranean, Western Europe, England and Ireland. The meridional energy line will also connect the countries of South and North America.

The latitudinal energy line in the equatorial zone from 0° to 30° north latitude will connect the countries of Asia, Africa and Latin America.

The equatorial energy line, as well as the latitudinal energy line Lisbon - Vladivostok, will be closed through the Pacific and Atlantic Ocean, North and Central America. A network of meridional and latitudinal energy lines form the United Energy System of the Earth.

The foregoing assumptions, at first glance, border on fantasy. However, in reality, sufficient groundwork has already been created today for a more careful consideration of the above large-scale projects. An energy system is being developed in 10 South American countries and Arab states, the issue of creating the Baltic and Black Sea energy rings, and the Siberia-China power transmission line are being considered. The combined energy systems of Russia, the countries of the Central Asian region, as well as the USA and Canada, Scandinavian and European countries have been created.

The task of creating a global energy system as a whole can be divided into two two-fold tasks: the formation of generating centers of high power and the development with subsequent practical implementation of technologies for efficient transmission of electricity over long distances to ensure energy flows in the global system. The potential of solar energy to solve the first of these problems is difficult to overestimate.

Currently, an increasing number of countries prefer solar energy, and solar power plants, originally actively created in the United States, have become widespread in Europe. Solar power plants are increasingly being built in the People's Republic of China, including those combined with high-power wind turbines.

At the same time, it is impossible to use solar power plants as the main component of the regional energy system, since smoothing periodic and stochastic processes that affect the output power of solar cells requires very powerful buffer energy storage devices with high maneuverability, the creation of which in modern conditions is not yet feasible for economic considerations. It is generally accepted that the installed capacity of solar power plants in the peak mode of operation of the power system should not exceed 10 - 15% of the total installed capacity of power plants in the regional power system. Under such conditions, fluctuations in the power of solar power plants do not significantly affect the quality of power supply.

The creation of an interregional, and subsequently global solar energy system will minimize or even completely eliminate the daily and seasonal unevenness of electricity generation and ensure round-the-clock reliable, environmentally friendly power supply to consumers.

At the same time, the greenhouse effect will be reduced and the negative impact of fuel power plants on the environment will be reduced.

A serious obstacle to the development of this direction of global energy can be considered the problem of organizing overflows of large amounts of electricity, which will inevitably need to be realized due to the uneven consumption of electric energy and its generation in different zones of the global or regional energy system. However, serious shifts are outlined in solving this problem. Work on the creation of effective technologies for the transfer of large amounts of electricity over long distances is developing quite widely. They are carried out by the Siberian Energy Institute, St. Petersburg State Technical University, VEI, as well as ABB, Siemens and other companies.

Serious work in this direction is also being carried out at VIESH. Resonance technologies, being fully implemented in practice, will allow the transmission of electricity flows with a power of several TW at distances of tens of thousands of kilometers.

The distribution of potential RES resources on the Earth's surface is uneven. Moreover, often territories with high potential for renewable energy sources are less populated, are not used for economic activities and, therefore, in the existing realities are of little use for practical use (desert and semi-desert territories, tundra, prairies, etc.).

The ability to provide efficient and without significant losses overflow of large amounts of electricity over long distances virtually removes this limitation.

A number of countries (mainly developing) in comparison with the countries of Europe and North America have a significantly higher potential for solar energy. Already in the foreseeable future, they will be able to use the seasonal change in solar energy and in the winter months sell electricity received from solar power plants to the Nordic countries, where solar energy is available in relatively sufficient quantities only from March to September. For this, it is necessary to organize the flow of electricity in the meridional direction. Electric energy flows in the latitudinal direction West - East make it possible to use the daily change in solar energy associated with the rotation of the Earth around its axis.

The network of solar power plants on the roofs and facades of houses, as well as in deserts, will be connected into a single energy system with a network of wind power plants (wind farms) located along the sea coast, where there is a constant transfer of air masses. An important component of the future integrated energy system will be hydroelectric power plants and power plants using biomass energy plantations.

In the general case, a solar energy system can consist not only of solar power plants, but also include power plants using other renewable energy

sources, connected to each other and to energy consumers by electric power transmission lines.

The global power system monitoring and control system can include geostationary cloud cover observation satellites and solar power plant output power prediction systems, as well as actuators for launching backup power plants with different maneuverability and power characteristics to cover the power system load schedule.

GLOBAL SOLAR ENERGY SYSTEM

The results of evaluating the parameters of the global solar energy system, which consists of three solar power plants installed in Australia, Africa and Mexico and connected by a low-voltage power line made by VIESH employees using computer simulation, are presented in Figure 3 (Strebkov, 2019).

In the simulation, data on solar radiation for the entire observation period were used. The efficiency of SPS was taken equal to 25%. The presented results show that such a system could generate electricity around the clock and evenly throughout the year. The sizes of each of the three SPPs are 200×200 km^2, and the electric power is 2.0 TW. The annual production of electric energy (24,000 TW · h) corresponds to the annual world energy consumption.

Solar power plants in the system are distributed in the latitudinal direction so that the end of illumination of the photoactive surface of one power plant coincides with the start of illumination of the panels of another station closest to the sun. By changing the distance between the stations in longitude, it is possible to achieve not only the continuity of the daily course of the average output power of the system, but also significantly increase the uniformity of electricity production.

It must be specially emphasized that the location of the stations was chosen in desert territories that are not used now and, with a high probability, will not be used in the foreseeable future.

Block-modular type solar power plants can annually increase their capacity by 100-300 GW. The beginning of the functioning of the global solar energy system can be predicted by 2050, reaching full capacity in 2090. As a result of the implementation of such a project, the share of solar energy in global electricity production will be 75–90%, and greenhouse gas emissions will be reduced by 10 times. Placing solar power plants on the power system on either side of the equator eliminates seasonal fluctuations in power generation - a

winter decline in one hemisphere is offset by a summer increase in generation in the other.

Such a system allows you to completely abandon or minimize the need for instant buffer storage.

Figure 3. Global Solar Power Generation

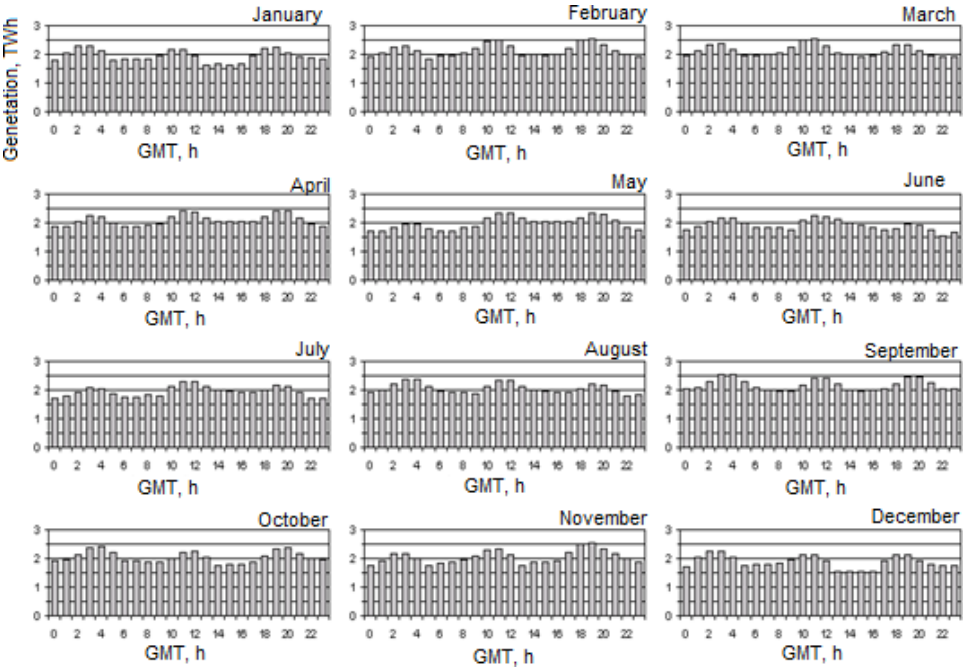

SMART SOLAR POWER SYSTEMS

The results of a new study show that in the near future, artificial intelligence will significantly automate the process of converting wind and solar energy. The effectiveness of this activity will increase in such areas as planning, decision making, robotics, monitoring and control.

The international certification and classification society DNV GL, located near Oslo, published the report "Smart Renewable Energy: Benefits, Risks and the Future of Using Artificial Intelligence in Transforming Solar and Wind Energy". It reports that the achievements and achievements in automation, monitoring, resource logistics and labor organization demonstrate many

opportunities for the use of artificial intelligence (AI) in order to increase work efficiency.

Today it is customary to talk about two approaches to the creation of artificial intelligence: semiotic (descending), aimed at building expert systems and knowledge bases that mimic high-level mental processes (reasoning, thinking, speech); biological (ascendant), aimed at building artificial intelligence (AI) systems, including distributed ones (swarm intelligence, etc.), modeling intelligence based on biological elements (Kamenev, Korolev, Sokotuschenko, 2012).

The semiotic approach can be successful at the stage of "smart" solar energy systems in a strict hierarchy, mainly for building decision support systems. Given the development of energy in the direction of mass decentralization with the emergence of a large number of subjects and objects of management in the context of globalization and intersectoral integration, something similar has already happened with information networks (the emergence and development of the Internet), a different type of intelligence will be required - a collective one, built from many partially independent intellectual agents in a constantly changing environment. Consequently, the biological approach mimicking the behavior of complex biological systems comes to the fore, the representatives of which are artificial neural networks and evolutionary algorithms. Taking into account the condition of a constantly changing environment and structure, the main task will be the task of machine learning, which gives artificial intelligence algorithms an undeniable advantage.

From the point of view of using AI, all the developments and results obtained in electric networks can be extended to other infrastructures, such as gas distribution networks, with their subsequent integration into a single energy information system.

In general, the configuration of an intelligent energy-information network can be described as a multi-agent system formed by a large number of partially independent intelligent agents built on the basis of artificial intelligence algorithms that perform the functions of risk assessment and coordination of interests.

In addition to the technological, managerial and economic aspects in the energy sector of the future, socio-psychological ones will also be extremely important, since the consumer will come first and his preferences will become decisive.

The first step towards intellectualization of the industry will be the construction of an energy-information infrastructure through the transition from

analog to digital control systems with extensive use of network technologies. That is, before smart networks appear, smart networks must be built.

The transition to work on the principle of a "smart" network based on advanced network analytics, automated control of metering devices, remote monitoring and control of equipment, management of mobile human resources and the use of modern SCADA systems working via IP will help network companies extend equipment life, determine prioritize hardware replacement, defer costly network updates and prevent network outages. In any case, the "smart" network was created in order to allow network companies to provide better quality services without a sharp increase in prices, as well as become the first step in building the infrastructure of a new energy sector.

Over time, rising consumption raises annual costs for network availability. In a situation of tight control of tariffs by regulatory authorities, when tariff increases are problematic at best, the alternative is clear: you need to comply with the growth rate or risk lowering the level of service. If this problem is not solved, then the increase in consumption can lead to major problems for the network company at peak load times. In extreme cases, you will have to disconnect clients to avoid network congestion.

The economy of the electric power industry begins to give preference to small generation of electricity connected to a common distribution network. This shift in electricity production is caused by the following trends. The problem of environmental pollution and climate change has generated interest in new technologies for generating electricity. Many governments subsidize the development of environmentally friendly methods for generating electricity, including solar, wind, fuel cells, even tidal power and Earth's thermal energy. The desire to improve efficiency leads to the use of small generation due to the use of gas generators. New technologies, such as fuel cells, will also be used in public buildings and residential buildings to generate electricity and heat water.

When generating electricity with a large number of smaller generators, from an economic point of view, it is more expedient to place the generator closer to the consumer so that less electricity is lost in the network. As a result, a myriad of small sources of electricity generation are built into networks that were originally created for large centralized power plants.

Distribution networks are designed to automatically adjust the voltage in accordance with specified or regulatory requirements within a certain allowable limit. The presence of a large number of small generators will require a change in the principles of constructing a traditional control system. Distribution networks are not designed to work with the complex tasks of

managing energy flows that will appear with the transition to distributed generation, for example, with unexpected reverse flows - when the generators are turned off increased use of distributed generation will increasingly require the use of metering devices and commercial agreements to support the import and export of electricity.

Managing the transition to a smart network can be a difficult task in itself, but the potential benefits are worth it. In addition to the benefits brought by individual technologies of the smart network, its implementation can give a synergistic effect between the constituent parts. The scalability of SCADA based on the IP network, for example, can lower the cost of implementing the systems and devices that make up a smart network. Each of these systems and devices relies to some extent on communication. Using IP-based SCADA technologies, you can significantly reduce the cost of expanding your network and introducing new components.

DIAGNOSTICS OF EQUIPMENT FOR SOLAR ENERGY SYSTEMS USING ARTIFICIAL INTELLIGENCE ALGORITHMS

Neural networks make it possible to effectively determine the cause and types of damage and emergencies, work with noisy data, eliminating the need for intermediate electronic filters from interference or filtering by mathematical methods, as well as adapt to a specific type of electrical equipment.

To create diagnostic devices and hardware and software systems, it is highly desirable to use artificial neural networks, since they are a powerful means of recognizing and predicting signals, and their ability to learn makes it possible to develop adaptive systems of protection and diagnostics of electrical equipment.

An interesting application of artificial intelligence methods was reported by the German company Schleswig-Holstein Netz AG, which operates electrical networks in the federal state of Schleswig-Holstein. Here, a self-learning network is used to identify the locations of the alleged damage. As the initial data, information is used on the life of the components of the electric networks and the repairs carried out, as well as information on loads and weather conditions.

And the American company AirFusion, which uses unmanned aerial vehicles to monitor the status of high-voltage power lines and wind power

plants, uses software with artificial intelligence algorithms to process monitoring results. A neural network helps to better solve the problem of pattern recognition, for which, during the training process, thousands of images of damaged wind turbines are loaded into the program (including the consequences of lightning strikes, delamination, coating erosion, etc.).

In 2017, by order of Rosstandart, a technical committee (TC) for standardization "Cyber-physical systems" was organized. Rosstandart instructed the technical committee to create national standards in the field of artificial intelligence and "smart energy". Smart energy standards are needed to develop new technologies in this industry. This will improve the quality of service and monitoring of power grids, and optimize the costs of their operation. The Cyber-Physical Systems Technical Committee unites scientific and public organizations, technology companies, non-profit organizations of hardware and software developers.

Many technologies of artificial intelligence are already actively developing in the energy sector of Russia.

In April 2019, the Holding Roselektronika and the Avtomatika concern, which are part of the Rostec state corporation, tested an automated complex designed to monitor the status of power lines (power lines). Special software developed by Avtomatika concern for processing and analyzing data received from drones helped automate the process of detecting power line defects. The program conducts 3D-modeling of the terrain based on the geodata that it receives from the drone, and analyzes the geometry of the overhead power lines. According to the developers, on the basis of these data, the system using machine learning identifies defects of almost any nature: sagging wires, dangerous tilt of poles, damage to insulation and contacts, and also detects foreign objects in the security zone that can affect the performance of power lines.

The creation of such complexes and systems allows you to automate processes that previously required human participation. Drones can work around the clock in any weather. Unmanned technologies make it possible to improve the quality of monitoring in the power grid complex, reduce the number of errors and respond more quickly to emergency situations.

In (Rizwan, Jamil, Kothari, 2012; Talebi, Khorasani, 2013; Yousef & Mahmood, 2014) presented a study on traditional fault diagnosis technologies based on intelligent algorithms including neural network. Wu et al. used BP neural network for fault diagnosis, the diagnostic rate was very high, but a large amount of data was required for learning and training. The convergence of samples was time consuming (Wu, Lan, Sun, 2009). Syafaruddin et al.

used three layer artificial neural network for fault diagnosis and provided more accurate diagnostic result than one-layer fault diagnosis. However, this method was also time consuming (Syafaruddin, Karatepe, Hiyama, 2011).

Shimakage et al. discussed photovoltaic system fault diagnosis and used measurement and observation for diagnosis. Team of Authors recorded the power generated by the faulted photovoltaic system and compared it with the presently measured power. However, the data for comparison, were required and time was required to create the database (Shimakage, Nishioka, Yamane et al., 2011). Zhao et al. proposed a decision tree-based diagnostic method for photovoltaic cell. Thediagnostic rate of this method was as high as 99.8%, but more than 1,000 times of inter comparison were required in the course of diagnosis (Zhao, Yang, Lehman et al., 2012). Tadj et al. proposed a GISTEL (gisement solaire par teledetection: solar radiation by teledetection) model to improve the photovoltaic cell diagnosis on fuzzy logic estimated satellite image. The method was difficult to be implemented (Tadj, Benmouiza, Cheknane et al., 2014). Hsieh et al. used chaotic extension theory for diagnosis, and the accuracy rate was very high. However, due to the limitation of extension theory, the diagnostic rate decreased greatly when the temperature and irradiance changed (Hsieh, Yau, Shiu, 2014).

In (Kalogirou, Lalot, Florides et al., 2008) presented the development of an automatic solar water heater (SWH) fault diagnosis system (FDS). In this paper, the design of a solar system fault diagnostic system is presented. The system consists of a prediction module, a residual calculator and the diagnosis module. A data acquisition system measures the temperatures at four locations of the SWH system and the mean storage tank temperature. In the prediction module a number of artificial neural networks are used, trained with values obtained from a TRNSYS model of a fault-free system operated with the typical meteorological year (TMY) for Nicosia, Cyprus and Paris, France. Thus, the neural networks are able to predict the fault-free temperatures under different environmental conditions. The input data to the ANNs are the time of the year, various weather parameters and one input temperature. The residual calculator receives both the current measurement data from the data acquisition system and the fault-free predictions from the prediction module. The system can predict three types of faults; collector faults and faults in insulation of pipes connecting the collector with the storage tank. The system was validated by using input values representing various faults of the system. In all cases, the faulty operation was predicted satisfactorily. In a future research, it is planning to develop a system, which will be able to identify the exact cause of each fault. The link between the three thresholds

of the categorization and the threshold for detection will also be addressed. Due to the fact that the M10a method is based on a larger number of values, the authors believe that it is more stable than the M5c method. In fact it has been shown that the detection occurs at the same time with a tolerance of a few hours for both methods. But it has also been shown that an alarm could be fired quite early using the M10a method. Hence it can be considered that the latter is the one which can be recommended. Furthermore, if the maintenance staff wants to know the current functioning state of the system, the M10a method is more suitable. It is believed by the authors that solar FDS can increase the reliability of the solar hot water systems and thus the economic benefits resulting by their use. Its cost should not be significant especially in cases, like hotels, where a building management system, capable of measuring the required temperatures, is already available.

DISPATCHING SMART SOLAR POWER SYSTEMS

Traditional telemetry networks rely on point-to-point communications systems, connecting a central control room with fault indicators and network switches. To send or receive messages, each device needs a dedicated communication channel. Many devices are simply not interconnected. The readings of the vast majority of metering devices, for example, are read by workers manually. As a result, network management is based on limited information arriving with a time delay. Investments in equipment are based on assumptions about the age of the equipment and on manual verification, and the operator usually finds out about defects only when calls begin to arrive with complaints from consumers. Only then can technicians be sent to diagnose the problem and initiate repair work.

The smart network offers a more detailed real-time status display. It allows you to replace a point-to-point connection with a standardized packet data connection. Simple failure indicators are replaced by more sophisticated monitoring sensors, which provide detailed information on the status of the equipment and help dispatchers determine when a failure can occur. Smart networks provide not only data that helps predict and prevent malfunctions, but also the image of what is happening in real time when a malfunction occurs, which allows network operators to send technicians to the right place and with the right equipment.

Branches of the JSC “System Operator of the Unified Energy System” “United Dispatch Office of the Urals Energy System” (UDO of the

Urals), "Regional Dispatch Office of the Energy System of the Republic of Bashkortostan" (Bashkir RDU) together with the group of companies "Hevel" on September 2, 2019 put into operation a remote control system control modes of operation of the Buribaevskaya solar power station from the Bashkir RDU. The SPS remote control system was put into operation after the successful completion of its trial operation from October 2018. Buribaevskaya SPS with an installed capacity of 20 MW was the first solar power station in Russia to implement a remote control project from the dispatch center of the System Operator. The implemented project allows for the remote control of the active and reactive power of the power plant, which increases the speed of implementing control actions to bring the parameters of the electric power regime of the power system to acceptable limits while preventing the development and elimination of accidents in the power system, and also allows for operational maintenance of the solar power plants without the constant duty of operational personnel on the object.

The implementation of remote control of the SPS operating modes, along with the development of remote control of substation equipment, the introduction of a stability monitoring system and the introduction of centralized third-generation emergency control systems, is another real step towards energy digitalization. With an increase in the number and size of the power of renewable energy power plants in the UES of Russia, the importance of remote control of their operation modes will increase. Digitalization, including through the implementation of such projects, is becoming a tool to increase the efficiency of operational dispatch control. In addition to increasing the speed of implementation of control actions, remote control also has a direct economic effect for the owner, as it allows you to switch from the constant duty of operational personnel at the facility to servicing by an on-site crew.

As part of the implementation of the remote power control project of the Buribaevskaya SPS, the system operator and Hevel specialists developed a joint schedule for its implementation, tested and tested the remote control of the Buribaevskaya SPS operation modes from the Bashkir RDU, during which the team implementation algorithms were debugged remote control, eliminated identified comments. The pilot operation of the system was carried out by the dispatchers of the Bashkir RDU together with the engineering and operational personnel of the power plant in accordance with the approved program, which provides for operations to change the active and reactive power of the SPS, including the complete cessation of power output. Tests were also carried out with the Buribaevskaya SPS completely disconnected from the network and then supplying voltage to the power plant to check

the automatic inclusion of inverters in operation with the resumption of the supply of active and reactive power to the network. In addition, during the implementation of the project, teams were formalized to manage the generation of solar power plants from the dispatch center of JSC "SO UES", as a result of which the list of standard documented dispatch teams was expanded taking into account the specifics of renewable energy plants. The experience gained during the implementation of the project makes it possible to disseminate the used technical and organizational solutions for implementing remote control of the operating modes of other power plants operating on renewable energy sources.

JSC "STC UES" has developed a draft requirements for power equipment and regulation systems for solar electric power plants regarding their parallel operation with the UES of Russia.

Solar installations are new elements in the domestic energy sector, technical requirements for which in terms of their parallel operation with the power system have not yet been developed. At the same time, extensive experience in the use of wind and solar installations has been accumulated abroad. This experience served as the basis for the development of requirements for installations of this type, which were included as an integral part in the following foreign regulatory and regulatory technical documents:

- codes prepared by the association of European network operators ENTSO-E, regulating requirements for adjacency of all types of generators to the network and requirements for frequency regulation and redundancy;
- The standard of the American Institute of Electrical Engineers and Electronics Engineers IEEE 1547 regarding the requirements for connecting distributed generation to electrical systems;
- network codes of Germany, Great Britain, Ireland, Denmark, Scandinavian countries, China, Poland and other countries;
- Material from the US Federal Energy Regulatory Commission (FERC) and the North American Electricity Reliability Corporation (NERC);
- Materials of the European Association of Wind Energy "Powering Europe: wind energy and the electricity grid".

In these documents, as the main requirements for power equipment and regulation systems of power plants in terms of their parallel operation with the power system are considered:

- permissible operating conditions for voltage and frequency;
- regulation of voltage and reactive power;
- operation of the power plant during and after emergency disturbances;
- regulation of active power and frequency;
- quality of generated electricity.

These requirements vary in different documents and for different countries. In addition, requirements quickly become obsolete and re-reviewed. The approach to the development of these requirements should be used as one of the components in the formulation of domestic requirements for installations of the type in question. At the same time, it seems that for the UES of Russia a modern approach should be taken to the reliability of the operation of alternative generation, taking into account the characteristics of modern plants and the systemic aspects of their application from the very initial stages of its development.

In the European Code ENTSO-E, ranges and durations of permissible voltage deviations are standardized separately for generators adjacent to a network with a voltage of 110-300 kV (excluding the last level) and adjacent to a network with a voltage of 300-400 kV.

One of the mandatory requirements for the operation of generating plants abroad is their response to typical disturbances in the power system, accompanied by short-term voltage drops. In foreign network codes, requirements are formulated on the inadmissibility of shutting down generating installations with design types of disturbances. Such requirements are known as the ability to maintain continuity of power supply during disturbances or the ability to maintain continuity of power supply at low voltage (Fault Ride-Through (FRT) or Low Voltage Ride-Through (LVRT) capabilities, respectively). Such requirements are included in network codes, in particular, in the European Network Code, which proposes the structure of the voltage dependence at the point of contact of a wind farm versus time for a phase corresponding to the occurrence of a short circuit in the power system and the transition to an emergency mode.

The ranges of changes in the coordinates of the characteristic points of this dependence are also presented, which differ for synchronous generators and wind generators, as well as for different generation levels. The requirements for solar power plants are less common than the requirements for wind farms. However, the network codes of Germany, Italy and Spain include such requirements.

The requirements for regulating the reactive power of photovoltaic stations according to the ENTSO-E code are less developed than the requirements for wind farms. At present, the requirements for regulating the reactive power of photovoltaic stations are starting to approach the requirements adopted for wind farms. For example, in the German Grid Code, the requirements for the use of photovoltaic stations are equivalent to the requirements for the use of other renewable energy sources, in particular wind generation.

Modern generation based on renewable energy provides great opportunities to reduce the level of power output. Thus, in accordance with the German grid code, the rate of power reduction for renewable energy-based power plants should be at least 10% of the nominal power per minute. These requirements do not imply any restrictions in the frequency range of 47.5-50.2 Hz, in the range of 50.2-51.5 Hz, they suggest unloading in active power with a gradient of 40% of the original per Hz, outside of range 47,5-51.5 Hz indicates the need to turn off the station. A different approach is used in the energy system of Ireland, where wind turbines with a capacity of more than 5 MW must operate with a 5% reserve of available power in order to regulate in a certain frequency range (for example, 49.6-50.5 Hz).

The proposed JSC "STC UES" project includes the following requirements for power equipment and regulation systems for wind and solar power plants in terms of their parallel operation with the UES of Russia:

Solar power plants must operate using the full regulatory range:

1. For a long time when the frequency of the electric current changes in the range of 49.0-51 Hz, including the upper limit of the frequency range.
2. Briefly in the frequency range of the electric current (including the upper limit of the indicated frequency ranges):
    - 51.0 - 55.0 Hz - the duration set by the equipment manufacturer;
    - 49.0 - 48.0 Hz - lasting at least 5 minutes;
    - 48.0 - 47.0 Hz - lasting at least 1 minute;
    - 47.0 - 46.0 Hz - with a duration of at least 1 second;
    - 46.0 Hz - at least 1 second.

Solar power plants, regardless of the type of generating equipment used, should operate using the full control range for active and reactive power:

- for a long time with a decrease in the voltage at the point of contact of the power plant with the power system by 25% of the nominal value (0.75Unom);

- for a long time with increasing voltage at the junction of the power plant with the power system to the highest operating value (Umax);
- briefly with increasing voltage at the point of contact of the power plant with the power system in the ranges of voltage changes (including the upper limit of the indicated voltage ranges):
  1.1 Unom - 1.1 Umax lasting at least 20 minutes,
  1.1 Umax - 1.25 Umax lasting at least 20 s,
  1.25 Umax - 1.5 Umax lasting at least 1 s.

Solar power plants should provide output and consumption of reactive power with $\cos\varphi = 0.855$ at the point of contact of the power plant with the power system, when the active power of the power plant changes in the range from the nominal value to 20% of the nominal value. For the duration of a short circuit, wind and solar power plants, in order to maintain voltage at the point of contact with the power system, must ensure the delivery of the maximum possible reactive power.

Solar power plants that are part of the power system should provide the ability to reduce the volume of power output at the command of the subject of operational dispatch control by at least 20% of rated active power, at a speed of at least 10 percent per minute of rated power SPS.

SPS should provide the ability to load by active power to a value determined by current weather conditions, at the command of the subject of operational dispatch control at a speed of at least 10 percent per minute of the rated power of SPS.

At the request of the operator of operational dispatch control, electric power storage devices should be provided at the power plants, which, if necessary, allow for guaranteed frequency control when the power plant is allocated for isolated operation.

Connection and synchronization of solar power plants should be carried out under conditions of long-term acceptable levels of frequency and voltage, that is, at levels of frequency difference in the range of 49.2-50.5 Hz and voltage difference levels in the range of 0.9-1.1 of the nominal voltage.

In the conditions of transition to an isolated mode of operation, solar power plants should continue to operate, provided that the frequency and voltage levels are within acceptable ranges. Solar power plants connected to the electric network through electronic devices made on the basis of voltage converters must remain in operation. It should be possible to remotely control the active and reactive power of solar power equipment. At solar power plants, a central device must be provided that provides the ability to implement control actions

from emergency automation to reduce the output of power by at least 20% of the rated power and/or shut off generating equipment.

Owners of wind and solar power plants, upon request of the subject of operational dispatch control, must provide all the necessary information about the types, parameters and characteristics of the generating equipment and its regulatory systems with which the power plants are equipped.

JSC "Institute" Energosetproekt "offers the following proposals for the draft Technical requirements for the characteristics of power equipment and regulation systems for wind and solar power plants during their operation as part of the UES of Russia, represented by JSC" STC UES ":

1. The current requirements for energy facilities in the UES of Russia should be taken as a basis, their weakening and tightening in relation to SPS should be justified.
2. The formulation of requirements for SPS power equipment in terms of their parallel operation with the UES of Russia only on the basis of a review of the requirements existing in the power systems of other countries is insufficient.
3. Connecting SPS to the power system should not lead to a deterioration of the standardized indicators of the reliability of the power system and the quality of electricity.
4. When developing requirements, it is necessary to take into account the dependence of the produced SPS power on weather conditions, since SPS cannot fully participate in frequency regulation in the power system.

CONCLUSION

At the moment, the main directions of the application of artificial intelligence in solar energy can now be combined into three groups:

- forecasting tasks (using artificial intelligence algorithms to predict energy production and consumption, optimizing equipment operation, etc.);
- tasks of increasing energy efficiency (in terms of monitoring data on actual energy consumption);
- intellectualization tasks (processing the results of monitoring the state of energy facilities, algorithms for the functioning of a smart home, load management, etc.).

The main goal of optimizing load balancing (Economic Dispatch) is to minimize operating costs depending on demand, that is, to optimally distribute the load between existing generating sources. One of the main difficulties with ED is that, in practice, the entire operating range of generating sources is not always available for load balancing due to physical limitations.

Neural networks make it possible to effectively determine the cause and types of damage and emergencies, work with noisy data, eliminating the need for intermediate electronic filters from interference or filtering by mathematical methods, as well as adapt to a specific type of electrical equipment.

To create diagnostic devices and hardware and software systems, it is highly desirable to use artificial neural networks, since they are a powerful means of recognizing and predicting signals, and their ability to learn makes it possible to develop adaptive systems of protection and diagnostics of electrical equipment.

The "New Electric World" is a quantitative and qualitative increase in the electric and information armament of work and life. The formation of this "world" requires a fundamentally different approach - the creation of intelligent energy-information systems with the active participation of the consumer himself. The "new" infrastructure and ideology are called upon to be "intelligent" energy-information networks built as multi-agent systems based on artificial intelligence algorithms.

Thus, smart energy-information networks should become the new economic, technological, managerial and socio-psychological infrastructure and energy ideology of the 21st century.

REFERENCES

Hsieh, C.-T., Yau, H.-T., & Shiu, J. (2014). Chaos synchronization based novel real-time intelligent fault diagnosis for photovoltaic systems. *International Journal of Photoenergy*, *759819*, 9.

Kalogirou, S., Lalot, S., Florides, G., & Desmet, B. (2008). Development of a neural network-based fault diagnostic system for solar thermal applications. *Solar Energy*, *82*(2), 164–172. doi:10.1016/j.solener.2007.06.010

Kamenev, A.S., Korolev, S.Yu., & Sokotuschenko, V.N. (2012). Neuromodeling as a tool of intellectualization of energy-information networks. *IC Energy*, 124.

Polek, V., Libra, M., Strebkov, D., & Kharchenko, V. (2013). Photovoltaic conversion of solar energy. Theory and practice of using solar energy. Ed. GNU VIESH, 321.

Rizwan, M., Jamil, M., & Kothari, D. P. (2012). Generalized neural network approach for global solar energy estimation in India. *IEEE Transactions on Sustainable Energy*, *3*(3), 576–584. doi:10.1109/TSTE.2012.2193907

Shimakage, T., Nishioka, K., Yamane, H., Nagura, M., & Kudo, M. (2011). Development of fault detection systemin PV system. *Proceedings of the IEEE 33rd International Telecommunications Energy Conference (INTELEC '11)*, 1–5.

Strebkov, D.S. (2019). Fundamentals of Solar Energy. *SAM Polygraphist*, 326.

Strebkov, D. S., Pendzhiev, A. M., & Mammadsakhatov, B. D. (2012). The use of solar energy in Turkmenistan. Ed. GNU VIESH, 495.

Syafaruddin, S., Karatepe, E., & Hiyama, T. (2011). Controlling of artificial neural network for fault diagnosis of photovoltaic array. *Proceedings of the 16th International Conference on Intelligent System Applications to Power Systems (ISAP '11)*. 10.1109/ISAP.2011.6082219

Tadj, M., Benmouiza, K., Cheknane, A., & Silvestre, S. (2014). Improving the performance of PV systems by faults detection using GISTEL approach. *Energy Conversion and Management*, *80*, 298–304. doi:10.1016/j.enconman.2014.01.030

Talebi, H. A., & Khorasani, K. (2013). A neural network-based multiplicative actuator fault detection and isolation of nonlinear systems. *IEEE Transactions on Control Systems Technology*, *21*(3), 842–851. doi:10.1109/TCST.2012.2186634

Vissarionov, V.I. (2008). Solar power. Textbook. *Publishing House MPEI*, 276.

Wu, Y., Lan, Q., & Sun, Y. (2009). Application of BP neural network fault diagnosis in solar photovoltaic system. *Proceedings of the IEEE International Conference on Mechatronics and Automation (ICMA '09)*, 2581–2585.

Yousef, S., & Mahmood, A. K. (2014). Fault diagnosis in internal combustion engines using extension neural network. *IEEE Transactions on Industrial Electronics*, *61*(3), 1434–1443. doi:10.1109/TIE.2013.2261033

Zhao, Y., Yang, L., Lehman, B., de Palma, J.-F., Mosesian, J., & Lyons, R. (2012). Decision tree-based fault detection and classification in solar photovoltaic arrays. *Proceedings of the 27th Annual IEEE Applied Power Electronics Conference and Exposition (APEC '12)*, 93–99. 10.1109/APEC.2012.6165803

Conclusion

The principles of construction and operation of the main concentrating systems, including non-followable modules, are reviewed, and the work of the concentrators is analyzed. An analytical review of modern facade-integrated photovoltaic technologies was carried out, their classification was given.

When developing existing designs of non-glare parabolic cylindrical concentrators with fixed linear and angular mirror lamellae, the possibilities of increasing the duration of the concentrator operation due to rotation of the mirror lamellaee system following the solar rays and, as a result, increasing the annual productivity of solar concentrating modules were not considered.

The known methods for calculating a flat (two-dimensional) scheme for passing the sun's rays through a louvered heliostat make it impossible to assess the real effectiveness of using louvered heliostats with non-tracking solar concentrators, which makes it necessary to consider the practically important three-dimensional problem of calculating the solar radiation flux on the receiving surface of an unfollowing parabolic-cylindrical solar concentrator with louver heliostat.

A functional relationship was obtained linking the position of the Sun, the step of the mirror lamellae of the heliostat and their orientation to ensure zero blocking and shading losses in the louvered heliostat.

Based on the consideration of a three-dimensional problem, the algorithm for calculating the passage of sunlight through the mirror surface of the lamellae and parabolic cylinder allows calculating the flux of solar radiation on the receiving surface of the solar concentrator.

An algorithm for controlling lamellar heliostat mirror lamellas has been developed that significantly increases the efficiency of a solar concentrator — using a louvre heliostat with a constant lamella pitch is equivalent to increasing the angular aperture of the concentrator from 26° to 70° without reducing the concentration ratio.

Optical schemes and designs of four types of solar modules with louvered heliostats and concentrators with zero shading losses and blocking of solar radiation have been developed.

The design of a compact thermal photovoltaic solar radiation detector for a non-tracking parabolic-cylindrical solar concentrator provides the thermal efficiency of the module in the range of 0,6–0,7, the service life of at least 25 years due to the sealing of the photoelectric elements using a two-component polysiloxane gel.

The thermal calculation of the PVT receiver of the solar concentrating module showed that with a water flow rate of 11 *l/h*, the temperature of the photovoltaic cells does not exceed 60 ºC. Rated thermal power of the module is 348 W at a temperature of 53ºC.

The developed system of automatic measurement of the main parameters of a solar concentrating module with PV, PVT and heat receivers allows you to save time during information processing, to obtain data on the dynamics of the processes in the solar concentrating module with the required measurement periodicity.

During the experimental study of a concentrating module with a PVT receiver, it was found that the ratio of the thermal power of the PVT receiver to the electric one with direct insolation values of 800 ± 100 W/m^2 is in the range from 1:1 to 5:1 with a thermal efficiency of 0,6–0,7. With equal values of insolation and ambient temperature, the production of electricity by the PVT-receiver photovoltaic panel is on average 10–25% higher than that of the PV-receiver.

The developed algorithm for calculating the passage of sunlight through the mirror surface of the lamellae and the parabolic cylinder, implemented as a computer program, allows calculating the flow of solar radiation on the receiving surface of the solar concentrator with a relative error of not more than 5%, which is confirmed by experimental data.

According to the CIPS of the UES of Russia for 2017–2023, the share of facilities based on renewable energy in the power balance of the UES of Russia will increase from 0,04% in 2016 to 0,9% by 2023, while the commissioning of new generating capacities (with a high probability of realization) The base of renewable energy sources in the UES of Russia in the period of 2017–2023 is provided for in the amount of 1,875 MW. The main share of the input generating capacity based on renewable energy is accounted for by the IES of the South (48.46%).

The calculations confirm the high efficiency of using louvered heliostats. The maximum annual energy production by non-tracking solar concentrating

modules is achieved with a vertical orientation of the concentrator, which is very important when placing solar modules on the southern facades of buildings. The annual amounts of insolation at the receiver for concentrators with a louvered heliostat with an angular aperture of 26 ° and 18 °, respectively, are on average 2 and 3.4 times higher than the total insolation on a flat surface and 1,6 and 2,2 times higher than insolation by blind surface receiving concentrating modules with similar angular aperture values. The cost of electricity produced when using non-glare concentrating modules with louvre is reduced by 40–60% compared to concentrating modules without louver, and thermal energy by 50%.

The basic requirements for solar power plants with concentrators integrated into buildings are identified. The designs of a solar house containing solar concentrator modules have been developed. The result of the development of solar house designs is an increase in the efficiency of using solar energy and a reduction in the cost of electricity and heat, as well as the creation of efficient solar systems built into the facades and roofs of buildings to provide them with electricity and heat. The design of a roofing solar panel with high optical efficiency and low consumption of semiconductor material and low cost has been developed and patented. As a result of using a roofing solar panel, the efficiency of using solar energy is increased and the cost of generating electric energy and heat is reduced. With the cost of semi-parabolic cylindrical reflectors 4, 5 30 $/m^2, a concentration of 4.92, an optical efficiency of 0.8 and an electrical efficiency of 15%, the cost of a roofing solar panel will be $ 12, or $ 1/W, at an existing cost of $ 3 / W, those it will decrease by 2.5 times, while the costs of the composite hub and receiver will be approximately equal and amount to 50% of the cost of the roofing solar panel.

The integrated concentrated PVT system of the building, designed for applying a solar-grid shading system to the blinds, is considered. In this way, the concentrator takes advantage of tracking the shading of the blinds at a sunny height and thus increases the optical efficiency. The optical efficiency for DIW is 73.5% and for IPA 76.5%. The refractive system shows potential to be cost-effective due to the use of standard silicon solar cells and low-accuracy trackers to partially cover electricity and heat energy demands of buildings. As reflectors can fulfill a building function the cost of the concentrator could be split and then the part corresponding to the concentrating system itself would be diminished.

The most promising areas in the field of integration of solar modules (planar and concentrating) in the construction of buildings are: development of BIPV technologies (roofing, film, facade materials); the integration of solar

energy concentrators that do not require biaxial tracking (medium and low concentrations) on the facades and roofs of buildings (parabolic concentrators, lenses and Fresnel mirrors); integration of highly concentrated modules on the roofs of buildings.

The VIESH has developed a solar roofing panel (solar shingles), which combines the functions of a roof and a solar module.

Unlike foreign samples, built-in stationary solar concentrators are used in the solar shingles, which made it possible to reduce the area of silicon solar cells by 4 times and receive electric energy and hot water from the solar roof. The solar tile has a protective anti-vandal coating of tempered glass and a cable for connecting to the adjacent solar tile.

The life of the SPP is determined mainly by the durability of the solar modules, which depends on the technology and materials used to seal the solar modules. Sealing standard modules by laminating an ethylene vinyl acetate (EVA) film provides an SPP service life of 25 years in cold climates and 20 years in tropical climates. Sealing the modules with polysiloxane gel extends the service life of the SPP to 40-50 years.

More energy is produced by tracking the solar panel to remain aligned to the sun at a right angle to the rays of light. Now-a-days various artificial techniques are introduced into photovoltaic (PV) system for utilisation of renewable energy. It is essential to track the generated power of the PV system and utilise the collected solar energy optimally. Artificial Neural Network (ANN) is initially used to forecast the solar insolation level and followed by the Particle Swarm Optimisation to optimise the power generation of the PV system based on the solar insolation level, cell temperature, efficiency of PV panel and output voltage requirements.

Genetic Algorithm is a general purpose optimization algorithm that is distinguished from conventional optimization techniques by the use of concepts of population genetics to guide the optimization search. Tabu Search Algorithms is a conceptually simple and an elegant iterative technique for finding good solutions to optimization problems. Simulated Annealing Algorithms appeared as a promising heuristic algorithm for handling the combinatorial optimization problems. Fuzzy logic Algorithms set theory can be considered as a generation of the classical set theory.

The ANN based solar insolation forecast has shown satisfactory results with minimal error and the generated PV power can be optimised significantly with the aids of the PSO algorithm.

Related Readings

To continue IGI Global's long-standing tradition of advancing innovation through emerging research, please find below a compiled list of recommended IGI Global book chapters and journal articles in the areas of energy planning, climate change, and efficient energy. These related readings will provide additional information and guidance to further enrich your knowledge and assist you with your own research.

Adler, M. (2015). Floods Monitoring. In C. Maftei (Ed.), *Extreme Weather and Impacts of Climate Change on Water Resources in the Dobrogea Region* (pp. 312–344). IGI Global. doi:10.4018/978-1-4666-8438-6.ch011

Afzal, S. (2016). Implementation of Flooding Free Routing in Smart Grid: VCP Routing in Smart Gird. In A. Ahmad & N. Hassan (Eds.), *Smart Grid as a Solution for Renewable and Efficient Energy* (pp. 298–322). IGI Global. doi:10.4018/978-1-5225-0072-8.ch013

Ahmad, S., Ahmad, A., & Yaqub, R. (2016). Optimized Energy Consumption and Demand Side Management in Smart Grid. In A. Ahmad & N. Hassan (Eds.), *Smart Grid as a Solution for Renewable and Efficient Energy* (pp. 1–25). IGI Global. doi:10.4018/978-1-5225-0072-8.ch001

Arbaiy, N., Watada, J., & Lin, P. (2016). Fuzzy Random Regression-Based Modeling in Uncertain Environment. In P. Vasant & N. Voropai (Eds.), *Sustaining Power Resources through Energy Optimization and Engineering* (pp. 127–146). IGI Global. doi:10.4018/978-1-4666-9755-3.ch006

Arhin, A. (2016). Improving Sustainability of the Environment in a Changing Climate: Can REDD+ Rise to the Challenge? In S. Dinda (Ed.), *Handbook of Research on Climate Change Impact on Health and Environmental Sustainability* (pp. 327–346). IGI Global. doi:10.4018/978-1-4666-8814-8.ch016

Bahinipati, C. S., Patnaik, U., & Viswanathan, P. K. (2016). What Causes Economic Losses from Natural Disasters in India? In S. Dinda (Ed.), *Handbook of Research on Climate Change Impact on Health and Environmental Sustainability* (pp. 157–175). IGI Global. doi:10.4018/978-1-4666-8814-8.ch008

Banerjee, S. (2016). Social Innovation: A Theoretical Approach in Intertwining Climate Change with Social Innovation. In S. Dinda (Ed.), *Handbook of Research on Climate Change Impact on Health and Environmental Sustainability* (pp. 593–618). IGI Global. doi:10.4018/978-1-4666-8814-8.ch029

Barakabitze, A. A., Fue, K. G., Kitindi, E. J., & Sanga, C. A. (2016). Developing a Framework for Next Generation Integrated Agro Food-Advisory Systems in Developing Countries. *International Journal of Information Communication Technologies and Human Development*, *8*(4), 13–31. doi:10.4018/IJICTHD.2016100102

Basu, J. P. (2016). Coastal Poverty, Resource-Dependent Livelihood, Climate Change, and Adaptation: An Empirical Study in Indian Coastal Sunderbans. In S. Dinda (Ed.), *Handbook of Research on Climate Change Impact on Health and Environmental Sustainability* (pp. 441–454). IGI Global. doi:10.4018/978-1-4666-8814-8.ch022

Bekele, I., & Ganpat, W. (2015). Education, Extension, and Training for Climate Change. In W. Ganpat & W. Isaac (Eds.), *Impacts of Climate Change on Food Security in Small Island Developing States* (pp. 361–388). IGI Global. doi:10.4018/978-1-4666-6501-9.ch012

Bhaskar, A., Rao, G. B., & Vencatesan, J. (2017). Characterization and Management Concerns of Water Resources around Pallikaranai Marsh, South Chennai. In P. Rao & Y. Patil (Eds.), *Reconsidering the Impact of Climate Change on Global Water Supply, Use, and Management* (pp. 102–121). IGI Global. doi:10.4018/978-1-5225-1046-8.ch007

Bhatt, R. (2017). Zero Tillage for Mitigating Global Warming Consequences and Improving Livelihoods in South Asia. In W. Ganpat & W. Isaac (Eds.), *Environmental Sustainability and Climate Change Adaptation Strategies* (pp. 126–161). IGI Global. doi:10.4018/978-1-5225-1607-1.ch005

Bit, J., & Banerjee, S. (2016). Sustainable Forest Use and India's Economic Growth: A Structural Decomposition Analysis of Direct Forest Intensity. In S. Dinda (Ed.), *Handbook of Research on Climate Change Impact on Health and Environmental Sustainability* (pp. 306–326). IGI Global. doi:10.4018/978-1-4666-8814-8.ch015

Boonkerd, K. (2017). Development and Modification of Natural Rubber for Advanced Application. In T. Kobayashi (Ed.), *Applied Environmental Materials Science for Sustainability* (pp. 44–76). IGI Global. doi:10.4018/978-1-5225-1971-3.ch003

Boonmahitthisud, A. (2017). Natural Rubber and Rubber Blend Nanocomposites: Reinforcement of Natural Rubber with Polymer-Encapsulated Inorganic Nanohybrid Particles. In T. Kobayashi (Ed.), *Applied Environmental Materials Science for Sustainability* (pp. 77–105). IGI Global. doi:10.4018/978-1-5225-1971-3.ch004

Bostanci, S. H., & Albayrak, A. N. (2017). The Role of Eco-Municipalities in Climate Change for a Sustainable Future. In W. Ganpat & W. Isaac (Eds.), *Environmental Sustainability and Climate Change Adaptation Strategies* (pp. 213–231). IGI Global. doi:10.4018/978-1-5225-1607-1.ch008

Buta, C., Omer, I., & Andronic, A. (2015). Hydrological Risk Phenomena and Flood Analysis: Study Case – Taita Catchment, Romania. In C. Maftei (Ed.), *Extreme Weather and Impacts of Climate Change on Water Resources in the Dobrogea Region* (pp. 284–311). IGI Global. doi:10.4018/978-1-4666-8438-6.ch010

Carrillo, K. L., & Kobayashi, T. (2017). Natural Material Source of Bagasse Cellulose and Their Application to Hydrogel Films. In T. Kobayashi (Ed.), *Applied Environmental Materials Science for Sustainability* (pp. 19–43). IGI Global. doi:10.4018/978-1-5225-1971-3.ch002

Cazacu, G. B. (2015). Dobrogea Geology. In C. Maftei (Ed.), *Extreme Weather and Impacts of Climate Change on Water Resources in the Dobrogea Region* (pp. 73–118). IGI Global. doi:10.4018/978-1-4666-8438-6.ch004

Chai-Ittipornwong, T. (2017). Participation Framework to Sustainability: The Undercurrents in Bottled-Water Production and Consumption. In P. Rao & Y. Patil (Eds.), *Reconsidering the Impact of Climate Change on Global Water Supply, Use, and Management* (pp. 272–293). IGI Global. doi:10.4018/978-1-5225-1046-8.ch015

Chatterjee, T., & Dinda, S. (2016). Climate Change, Human Health and Some Economic Issues. In S. Dinda (Ed.), *Handbook of Research on Climate Change Impact on Health and Environmental Sustainability* (pp. 26–41). IGI Global. doi:10.4018/978-1-4666-8814-8.ch002

Chaudhary, N., & Pisolkar, Y. (2017). Issues, Concerns, and Local Stakes: Future of Water Resources in Coastal Villages of Devbag and Tarkarli, Coastal Maharashtra, India. In P. Rao & Y. Patil (Eds.), *Reconsidering the Impact of Climate Change on Global Water Supply, Use, and Management* (pp. 50–69). IGI Global. doi:10.4018/978-1-5225-1046-8.ch004

Chelcea, S., Ionita, M., & Adler, M. (2015). Identification of Dry Periods in the Dobrogea Region. In C. Maftei (Ed.), *Extreme Weather and Impacts of Climate Change on Water Resources in the Dobrogea Region* (pp. 52–72). IGI Global. doi:10.4018/978-1-4666-8438-6.ch003

Cohen, J. E., Clarke-Harris, D. O., Khan, A., & Isaac, W. P. (2015). Sustainable Management of Invasive Species for Small Island Developing States under Changing Climates. In W. Ganpat & W. Isaac (Eds.), *Impacts of Climate Change on Food Security in Small Island Developing States* (pp. 312–360). IGI Global. doi:10.4018/978-1-4666-6501-9.ch011

Das, S. (2016). Health Impact of Water-Related Diseases in Developing Countries on Account of Climate Change – A Systematic Review: A Study in Regard to South Asian Countries. In S. Dinda (Ed.), *Handbook of Research on Climate Change Impact on Health and Environmental Sustainability* (pp. 42–60). IGI Global. doi:10.4018/978-1-4666-8814-8.ch003

David, I., Beilicci, E., & Beilicci, R. (2015). Basics for Hydraulic Modelling of Flood Runoff Using Advanced Hydroinformatic Tools. In C. Maftei (Ed.), *Extreme Weather and Impacts of Climate Change on Water Resources in the Dobrogea Region* (pp. 205–239). IGI Global. doi:10.4018/978-1-4666-8438-6.ch008

Deenapanray, P. N., & Ramma, I. (2015). Adaptations to Climate Change and Climate Variability in the Agriculture Sector in Mauritius: Lessons from a Technical Needs Assessment. In W. Ganpat & W. Isaac (Eds.), *Impacts of Climate Change on Food Security in Small Island Developing States* (pp. 130–165). IGI Global. doi:10.4018/978-1-4666-6501-9.ch005

Dinda, S. (2016). Adaptation to Climate Change for Sustainable Development: A Survey. In S. Dinda (Ed.), *Handbook of Research on Climate Change Impact on Health and Environmental Sustainability* (pp. 363–391). IGI Global. doi:10.4018/978-1-4666-8814-8.ch018

Dinda, S. (2016). Climate Change, Trade Competitiveness, and Opportunity for Climate Friendly Goods in SAARC and Asia Pacific Regions. In S. Dinda (Ed.), *Handbook of Research on Climate Change Impact on Health and Environmental Sustainability* (pp. 515–536). IGI Global. doi:10.4018/978-1-4666-8814-8.ch026

Dongol, D., Bollin, E., & Feldmann, T. (2016). Battery Management Based on Predictive Control and Demand-Side Management: Smart Integration of Renewable Energy Sources. In A. Ahmad & N. Hassan (Eds.), *Smart Grid as a Solution for Renewable and Efficient Energy* (pp. 149–180). IGI Global. doi:10.4018/978-1-5225-0072-8.ch007

Drăguşin, D. (2015). Drought Effects on Groundwater in Dobrogea Plateau. In C. Maftei (Ed.), *Extreme Weather and Impacts of Climate Change on Water Resources in the Dobrogea Region* (pp. 119–144). IGI Global. doi:10.4018/978-1-4666-8438-6.ch005

Elsayed, A. M., Dakkama, H. J., Mahmoud, S., Al-Dadah, R., & Kaialy, W. (2017). Sustainable Cooling Research Using Activated Carbon Adsorbents and Their Environmental Impact. In T. Kobayashi (Ed.), *Applied Environmental Materials Science for Sustainability* (pp. 186–221). IGI Global. doi:10.4018/978-1-5225-1971-3.ch009

Emmanuel, M., Muasa, L., Chen, C., Mutisya, F., & Avtar, R. (2016). Impact of Rapid Urbanization and Climate Change on Agricultural Productivity in Africa: Climate Change Policies in the Agricultural Sector. In S. Dinda (Ed.), *Handbook of Research on Climate Change Impact on Health and Environmental Sustainability* (pp. 416–426). IGI Global. doi:10.4018/978-1-4666-8814-8.ch020

Emran, A., Rob, M. A., & Kabir, M. H. (2017). Coastline Change and Erosion-Accretion Evolution of the Sandwip Island, Bangladesh. *International Journal of Applied Geospatial Research*, *8*(2), 33–44. doi:10.4018/IJAGR.2017040103

Eudoxie, G., & Roopnarine, R. (2017). Climate Change Adaptation and Disaster Risk Management in the Caribbean. In W. Ganpat & W. Isaac (Eds.), *Environmental Sustainability and Climate Change Adaptation Strategies* (pp. 97–125). IGI Global. doi:10.4018/978-1-5225-1607-1.ch004

Eudoxie, G. D., & Wuddivira, M. (2015). Soil, Water, and Agricultural Adaptations. In W. Ganpat & W. Isaac (Eds.), *Impacts of Climate Change on Food Security in Small Island Developing States* (pp. 255–279). IGI Global. doi:10.4018/978-1-4666-6501-9.ch009

Fernández, F. J., Jiménez, A. D., Manzano, F. S., & Márquez, J. M. (2017). An Energy Management Strategy and Fuel Cell Configuration Proposal for a Hybrid Renewable System with Hydrogen Backup. *International Journal of Energy Optimization and Engineering*, *6*(1), 1–22. doi:10.4018/IJEOE.2017010101

Fernando, Y., & Wah, W. X. (2016). Moving forward a Parsimonious Model of Eco-Innovation: Results from a Content Analysis. In S. Dinda (Ed.), *Handbook of Research on Climate Change Impact on Health and Environmental Sustainability* (pp. 619–631). IGI Global. doi:10.4018/978-1-4666-8814-8.ch030

Garrick, T. A., & Liburd, O. E. (2017). Impact of Climate Change on a Key Agricultural Pest: Thrips. In W. Ganpat & W. Isaac (Eds.), *Environmental Sustainability and Climate Change Adaptation Strategies* (pp. 232–254). IGI Global. doi:10.4018/978-1-5225-1607-1.ch009

Goundar, S., & Appana, S. (2017). Mainstreaming Development Policies for Climate Change in Fiji: A Policy Gap Analysis and the Role of ICTs. In W. Ganpat & W. Isaac (Eds.), *Environmental Sustainability and Climate Change Adaptation Strategies* (pp. 1–31). IGI Global. doi:10.4018/978-1-5225-1607-1.ch001

Gupta, A. C. (2016). Bioeconomic Fishery Management: Changing Paradigms towards Eco-System Based Management. In S. Dinda (Ed.), *Handbook of Research on Climate Change Impact on Health and Environmental Sustainability* (pp. 261–281). IGI Global. doi:10.4018/978-1-4666-8814-8.ch013

Hiremath, R., Kumar, B., Bansode, S. S., Nulkar, G., Patil, S. S., & Murali, J. (2017). Industrial Wastewater Management in the Context of Climate Change Adaptation in Selected Cities of India: A Business Approach. In P. Rao & Y. Patil (Eds.), *Reconsidering the Impact of Climate Change on Global Water Supply, Use, and Management* (pp. 294–313). IGI Global. doi:10.4018/978-1-5225-1046-8.ch016

Huyen, P. T. (2017). Clay Minerals Converted to Porous Materials and Their Application: Challenge and Perspective. In T. Kobayashi (Ed.), *Applied Environmental Materials Science for Sustainability* (pp. 141–164). IGI Global. doi:10.4018/978-1-5225-1971-3.ch007

Iese, V., Maeke, J., Holland, E., Wairiu, M., & Naidu, S. (2015). Farming Adaptations to the Impacts of Climate Change and Extreme Events in Pacific Island Countries: Case Study of Bellona Atoll, Solomon Islands. In W. Ganpat & W. Isaac (Eds.), *Impacts of Climate Change on Food Security in Small Island Developing States* (pp. 166–194). IGI Global. doi:10.4018/978-1-4666-6501-9.ch006

Ikematsu, S., Tada, I., & Nagasaki, Y. (2017). Analysis of Lipids Produced by Microalgae Isolated from the Area around Okinawa, Japan. In T. Kobayashi (Ed.), *Applied Environmental Materials Science for Sustainability* (pp. 222–233). IGI Global. doi:10.4018/978-1-5225-1971-3.ch010

Inogwabini, B. (2017). Congo Basin's Shrinking Watersheds: Potential Consequences on Local Communities. In P. Rao & Y. Patil (Eds.), *Reconsidering the Impact of Climate Change on Global Water Supply, Use, and Management* (pp. 211–226). IGI Global. doi:10.4018/978-1-5225-1046-8.ch012

Ionita, M., & Chelcea, S. (2015). Spatio-Temporal Variability of Seasonal Drought over the Dobrogea Region. In C. Maftei (Ed.), *Extreme Weather and Impacts of Climate Change on Water Resources in the Dobrogea Region* (pp. 17–51). IGI Global. doi:10.4018/978-1-4666-8438-6.ch002

Issakhov, A. (2016). Mathematical Modelling of the Thermal Process in the Aquatic Environment with Considering the Hydrometeorological Condition at the Reservoir-Cooler by Using Parallel Technologies. In P. Vasant & N. Voropai (Eds.), *Sustaining Power Resources through Energy Optimization and Engineering* (pp. 227–243). IGI Global. doi:10.4018/978-1-4666-9755-3.ch010

Javid, T. (2016). Geographic Information System for the Smart Grid. In A. Ahmad & N. Hassan (Eds.), *Smart Grid as a Solution for Renewable and Efficient Energy* (pp. 344–362). IGI Global. doi:10.4018/978-1-5225-0072-8.ch015

Juma, D. W., Reuben, M., Wang, H., & Li, F. (2017). Adaptive Coevolution: Realigning the Water Governance Regime to the Changing Climate. In P. Rao & Y. Patil (Eds.), *Reconsidering the Impact of Climate Change on Global Water Supply, Use, and Management* (pp. 314–325). IGI Global. doi:10.4018/978-1-5225-1046-8.ch017

Kais, S. M. (2017). Climate Change: Vulnerability and Resilience in Commercial Shrimp Aquaculture in Bangladesh. In W. Ganpat & W. Isaac (Eds.), *Environmental Sustainability and Climate Change Adaptation Strategies* (pp. 162–187). IGI Global. doi:10.4018/978-1-5225-1607-1.ch006

Kamboj, V. K., & Bath, S. K. (2016). Scope of Biogeography-Based Optimization for Economic Load Dispatch and Multi-Objective Unit Commitment Problem. In P. Vasant & N. Voropai (Eds.), *Sustaining Power Resources through Energy Optimization and Engineering* (pp. 360–389). IGI Global. doi:10.4018/978-1-4666-9755-3.ch015

Karmaoui, A. (2016). Environmental Vulnerability to Climate Change in Mediterranean Basin: Socio-Ecological Interactions between North and South. In S. Dinda (Ed.), *Handbook of Research on Climate Change Impact on Health and Environmental Sustainability* (pp. 105–138). IGI Global. doi:10.4018/978-1-4666-8814-8.ch006

Khai, H. V. (2016). Assessing Urban Residents' Willingness to Pay for Preserving the Biodiversity of Swamp Forest. In S. Dinda (Ed.), *Handbook of Research on Climate Change Impact on Health and Environmental Sustainability* (pp. 283–305). IGI Global. doi:10.4018/978-1-4666-8814-8.ch014

Khalid, S. (2016). Application of Adaptive Tabu Search Algorithm in Hybrid Power Filter and Shunt Active Power Filters: Application of ATS Algorithm in HPF and APF. In P. Vasant & N. Voropai (Eds.), *Sustaining Power Resources through Energy Optimization and Engineering* (pp. 276–308). IGI Global. doi:10.4018/978-1-4666-9755-3.ch012

Khan, S. S. (2016). Modeling and Operating Strategies of Micro-Grids for Renewable Energy Communities. In A. Ahmad & N. Hassan (Eds.), *Smart Grid as a Solution for Renewable and Efficient Energy* (pp. 97–122). IGI Global. doi:10.4018/978-1-5225-0072-8.ch005

Khanna, B. K. (2017). Indian National Strategy for Climate Change Adaptation and Mitigation. In W. Ganpat & W. Isaac (Eds.), *Environmental Sustainability and Climate Change Adaptation Strategies* (pp. 32–63). IGI Global. doi:10.4018/978-1-5225-1607-1.ch002

Khanna, B. K. (2017). Vulnerability of the Lakshadweep Coral Islands in India and Strategies for Mitigating Climate Change Impacts. In W. Ganpat & W. Isaac (Eds.), *Environmental Sustainability and Climate Change Adaptation Strategies* (pp. 64–96). IGI Global. doi:10.4018/978-1-5225-1607-1.ch003

Kobayashi, T. (2017). Introduction of Environmental Materials. In T. Kobayashi (Ed.), *Applied Environmental Materials Science for Sustainability* (pp. 1–18). IGI Global. doi:10.4018/978-1-5225-1971-3.ch001

Kumar, C. P. (2016). Impact of Climate Change on Groundwater Resources. In S. Dinda (Ed.), *Handbook of Research on Climate Change Impact on Health and Environmental Sustainability* (pp. 196–221). IGI Global. doi:10.4018/978-1-4666-8814-8.ch010

Kumar, K. V., Kumar, S. S., Selvakumar, A. I., & Kumar, R. S. (2016). Recent Techniques to Identify the Stator Fault Diagnosis in Three Phase Induction Motor. In P. Vasant & N. Voropai (Eds.), *Sustaining Power Resources through Energy Optimization and Engineering* (pp. 309–325). IGI Global. doi:10.4018/978-1-4666-9755-3.ch013

Kumar, M. (2016). Environmental Sustainability in the Fashion Supply Chain in India. *International Journal of Social Ecology and Sustainable Development*, *7*(3), 1–33. doi:10.4018/IJSESD.2016070101

Kumar, M. (2017). Economic Evaluation of Solar Cooling Schemes. *International Journal of Energy Optimization and Engineering*, *6*(1), 23–48. doi:10.4018/IJEOE.2017010102

Kumar, R., Rao, P., & Areendran, G. (2017). Understanding Glacial Retreat in the Indian Himalaya: Historical Trends and Field Studies from a Large Glacier. In P. Rao & Y. Patil (Eds.), *Reconsidering the Impact of Climate Change on Global Water Supply, Use, and Management* (pp. 33–49). IGI Global. doi:10.4018/978-1-5225-1046-8.ch003

Kumari, S., & Patil, Y. (2017). Achieving Climate Smart Agriculture with a Sustainable Use of Water: A Conceptual Framework for Sustaining the Use of Water for Agriculture in the Era of Climate Change. In P. Rao & Y. Patil (Eds.), *Reconsidering the Impact of Climate Change on Global Water Supply, Use, and Management* (pp. 122–143). IGI Global. doi:10.4018/978-1-5225-1046-8.ch008

Kumari, S., Patil, Y., & Rao, P. (2017). An Approach to Sustainable Watershed Management: Case Studies on Enhancing Sustainability with Challenges of Water in Western Maharashtra. In P. Rao & Y. Patil (Eds.), *Reconsidering the Impact of Climate Change on Global Water Supply, Use, and Management* (pp. 252–271). IGI Global. doi:10.4018/978-1-5225-1046-8.ch014

Lallo, C. H., Smalling, S., Facey, A., & Hughes, M. (2017). The Impact of Climate Change on Small Ruminant Performance in Caribbean Communities. In W. Ganpat & W. Isaac (Eds.), *Environmental Sustainability and Climate Change Adaptation Strategies* (pp. 296–321). IGI Global. doi:10.4018/978-1-5225-1607-1.ch011

Lawrence, J., Simpson, L., & Piggott, A. (2015). Protected Agriculture: A Climate Change Adaptation for Food and Nutrition Security. In W. Ganpat & W. Isaac (Eds.), *Impacts of Climate Change on Food Security in Small Island Developing States* (pp. 196–220). IGI Global. doi:10.4018/978-1-4666-6501-9.ch007

Li, K., & Kobayashi, T. (2017). Ionic Liquids and Poly (Ionic Liquid)s Used as Green Solvent and Ultrasound Responded Materials. In T. Kobayashi (Ed.), *Applied Environmental Materials Science for Sustainability* (pp. 327–346). IGI Global. doi:10.4018/978-1-5225-1971-3.ch015

Liapakis, A., Costopoulou, C., Tsiligiridis, T., & Sideridis, A. (2017). Studying Corporate Social Responsibility Activities in the Agri-Food Sector: The Greek Case. *International Journal of Agricultural and Environmental Information Systems*, *8*(1), 1–13. doi:10.4018/IJAEIS.2017010101

Loi, N. K., Huyen, N. T., Tu, L. H., Tram, V. N., Liem, N. D., Dat, N. L., Nhat, T. T., & Minh, D. N. (2017). Sustainable Land Use and Watershed Management in Response to Climate Change Impacts: Case Study in Srepok Watershed, Central Highland of Vietnam. In W. Ganpat & W. Isaac (Eds.), *Environmental Sustainability and Climate Change Adaptation Strategies* (pp. 255–295). IGI Global. doi:10.4018/978-1-5225-1607-1.ch010

Londhe, S. (2016). Impact of Climate Change on Agriculture and Food Security. *International Journal of Disease Control and Containment for Sustainability*, *1*(1), 32–46. doi:10.4018/IJDCCS.2016010103

Londhe, S. (2017). Inter Linkages of Water, Climate, and Agriculture. In P. Rao & Y. Patil (Eds.), *Reconsidering the Impact of Climate Change on Global Water Supply, Use, and Management* (pp. 166–194). IGI Global. doi:10.4018/978-1-5225-1046-8.ch010

Londhe, S. L. (2016). Climate Change and Agriculture: Impacts, Adoption, and Mitigation. In S. Dinda (Ed.), *Handbook of Research on Climate Change Impact on Health and Environmental Sustainability* (pp. 393–415). IGI Global. doi:10.4018/978-1-4666-8814-8.ch019

Maftei, C., & Papatheodorou, K. (2015). Mathematical Models Used for Hydrological Floodplain Modeling. In C. Maftei (Ed.), *Extreme Weather and Impacts of Climate Change on Water Resources in the Dobrogea Region* (pp. 240–283). IGI Global. doi:10.4018/978-1-4666-8438-6.ch009

Maharaj, R., Singh-Ackbarali, D., & Sankat, C. K. (2015). Postharvest Management Strategies. In W. Ganpat & W. Isaac (Eds.), *Impacts of Climate Change on Food Security in Small Island Developing States* (pp. 221–254). IGI Global. doi:10.4018/978-1-4666-6501-9.ch008

Mahboob, Q. (2016). Identification of Reliability Critical Items in Large and Complex Rail Electrical Networks. In A. Ahmad & N. Hassan (Eds.), *Smart Grid as a Solution for Renewable and Efficient Energy* (pp. 226–248). IGI Global. doi:10.4018/978-1-5225-0072-8.ch010

Mahmood, W. A., & Azarian, M. H. (2017). Inorganic-Organic Composite Materials from Liquid Natural Rubber and Epoxidised Natural Rubber Derivatives: Prospects and Applications. In T. Kobayashi (Ed.), *Applied Environmental Materials Science for Sustainability* (pp. 128–140). IGI Global. doi:10.4018/978-1-5225-1971-3.ch006

Majumder, J., Shah, P., & Kumar, S. (2016). Heat Stress Vulnerability among Indian Workmen. In S. Dinda (Ed.), *Handbook of Research on Climate Change Impact on Health and Environmental Sustainability* (pp. 61–80). IGI Global. doi:10.4018/978-1-4666-8814-8.ch004

Maximay, S. (2015). The Caribbean's Response to Climate Change Impacts. In W. Ganpat & W. Isaac (Eds.), *Impacts of Climate Change on Food Security in Small Island Developing States* (pp. 33–66). IGI Global. doi:10.4018/978-1-4666-6501-9.ch002

Meldrum, H. M., Szymanski, D., Oches, E. A., & Davis, P. T. (2016). A Picture is Worth a Thousand Words: Commentary of Broadcast Meteorologists on the Visual Presentation of Climate Change. *International Journal of Social Ecology and Sustainable Development*, *7*(4), 1–16. doi:10.4018/IJSESD.2016100101

Mili, B., Barua, A., & Katyaini, S. (2016). Climate Change and Adaptation through the Lens of Capability Approach: A Case Study from Darjeeling, Eastern Himalaya. In S. Dinda (Ed.), *Handbook of Research on Climate Change Impact on Health and Environmental Sustainability* (pp. 455–469). IGI Global. doi:10.4018/978-1-4666-8814-8.ch023

Minea, G., Bandoc, G., & Neculau, G. (2015). Seasonal Statistical Variability of Precipitations in Dobrogea and Danube Delta. In C. Maftei (Ed.), *Extreme Weather and Impacts of Climate Change on Water Resources in the Dobrogea Region* (pp. 1–16). IGI Global. doi:10.4018/978-1-4666-8438-6.ch001

Minhas, D. M., & Hussain, S. (2016). Efficient Control Strategies to Optimize Electricity Cost and Consumer Satisfaction. In A. Ahmad & N. Hassan (Eds.), *Smart Grid as a Solution for Renewable and Efficient Energy* (pp. 69–96). IGI Global. doi:10.4018/978-1-5225-0072-8.ch004

Mohapatra, M., & Baladhandautham, C. B. (2016). Implementation of Improved Control Strategy of DC-AC Converter using Delta-Sigma Modulator. In A. Ahmad & N. Hassan (Eds.), *Smart Grid as a Solution for Renewable and Efficient Energy* (pp. 249–272). IGI Global. doi:10.4018/978-1-5225-0072-8.ch011

Moustache, A. M. (2015). Adaptation to Impacts of Climate Change on the Food and Nutrition Security Status of a Small Island Developing State: The Case of the Republic of Seychelles. In W. Ganpat & W. Isaac (Eds.), *Impacts of Climate Change on Food Security in Small Island Developing States* (pp. 96–129). IGI Global. doi:10.4018/978-1-4666-6501-9.ch004

Mujere, N., & Moyce, W. (2017). Climate Change Impacts on Surface Water Quality. In W. Ganpat & W. Isaac (Eds.), *Environmental Sustainability and Climate Change Adaptation Strategies* (pp. 322–340). IGI Global. doi:10.4018/978-1-5225-1607-1.ch012

Mukherjee, S., & Chakraborty, D. (2016). Does Fiscal Policy Influence Per Capita CO2 Emission?: A Cross Country Empirical Analysis. In S. Dinda (Ed.), *Handbook of Research on Climate Change Impact on Health and Environmental Sustainability* (pp. 568–592). IGI Global. doi:10.4018/978-1-4666-8814-8.ch028

N'Yeurt, A. D., & Iese, V. (2015). Marine Plants as a Sustainable Source of Agri-Fertilizers for Small Island Developing States (SIDS). In W. Ganpat & W. Isaac (Eds.), *Impacts of Climate Change on Food Security in Small Island Developing States* (pp. 280–311). IGI Global. doi:10.4018/978-1-4666-6501-9.ch010

Nersesian, R. L., & Strang, K. D. (2017). Feasibility Approaches to Reduce the Unreliability of Gas, Nuclear, Coal, Solar and Wind Electricity Production. *International Journal of Risk and Contingency Management*, *6*(1), 54–69. doi:10.4018/IJRCM.2017010104

Ngubevana, L. (2017). Sustainable Development Dilemmas of Biofuels Research and Production: A Snapshot in South Africa. *International Journal of Energy Optimization and Engineering*, *6*(2), 24–41. doi:10.4018/IJEOE.2017040102

Nyangon, J., Alabbas, N., & Agbemabiese, L. (2017). Entangled Systems at the Energy-Water-Food Nexus: Challenges and Opportunities. In P. Rao & Y. Patil (Eds.), *Reconsidering the Impact of Climate Change on Global Water Supply, Use, and Management* (pp. 144–165). IGI Global. doi:10.4018/978-1-5225-1046-8.ch009

Onutai, S., Jiemsirilers, S., & Kobayashi, T. (2017). Geopolymer Sourced with Fly Ash and Industrial Aluminum Waste for Sustainable Materials. In T. Kobayashi (Ed.), *Applied Environmental Materials Science for Sustainability* (pp. 165–185). IGI Global. doi:10.4018/978-1-5225-1971-3.ch008

Osmani, A. R. (2016). Greenhouse Gas Mitigation through Energy Efficiency: Perform, Achieve, and Trade (PAT) – India's Emission Trading Scheme. In S. Dinda (Ed.), *Handbook of Research on Climate Change Impact on Health and Environmental Sustainability* (pp. 537–566). IGI Global. doi:10.4018/978-1-4666-8814-8.ch027

Osmani, A. R. (2017). Tipaimukh Multipurpose Hydroelectric Project: A Policy Perspective – Indo-Bangla Priorities, Indigenous Peoples' Rights, and Environmental Concerns. In P. Rao & Y. Patil (Eds.), *Reconsidering the Impact of Climate Change on Global Water Supply, Use, and Management* (pp. 227–251). IGI Global. doi:10.4018/978-1-5225-1046-8.ch013

Ozpinar, A., & Ozil, E. (2016). Smart Grid and Demand Side Management: Application of Metaheuristic and Artificial Intelligence Algorithms. In A. Ahmad & N. Hassan (Eds.), *Smart Grid as a Solution for Renewable and Efficient Energy* (pp. 49–68). IGI Global. doi:10.4018/978-1-5225-0072-8.ch003

Padigala, B. S. (2017). Traditional Water Management System for Climate Change Adaptation in Mountain Ecosystems. In P. Rao & Y. Patil (Eds.), *Reconsidering the Impact of Climate Change on Global Water Supply, Use, and Management* (pp. 9–32). IGI Global. doi:10.4018/978-1-5225-1046-8.ch002

Page, T. (2017). A Feasibility Study in Energy Harvesting from Piezoelectric Keyboards. *International Journal of Energy Optimization and Engineering*, *6*(2), 1–23. doi:10.4018/IJEOE.2017040101

Paul, S., & Roy, P. K. (2016). A Novel Optimization Algorithm for Transient Stability Constrained Optimal Power Flow. In P. Vasant & N. Voropai (Eds.), *Sustaining Power Resources through Energy Optimization and Engineering* (pp. 147–176). IGI Global. doi:10.4018/978-1-4666-9755-3.ch007

Pieroni, A., & Iazeolla, G. (2016). Engineering QoS and Energy Saving in the Delivery of ICT Services. In P. Vasant & N. Voropai (Eds.), *Sustaining Power Resources through Energy Optimization and Engineering* (pp. 208–226). IGI Global. doi:10.4018/978-1-4666-9755-3.ch009

Polprasert, J., Ongsakul, W., & Dieu, V. N. (2016). Improved Pseudo-Gradient Search Particle Swarm Optimization for Optimal Power Flow Problem. In P. Vasant & N. Voropai (Eds.), *Sustaining Power Resources through Energy Optimization and Engineering* (pp. 177–207). IGI Global. doi:10.4018/978-1-4666-9755-3.ch008

Potiyaraj, P. (2017). Poly (Lactic Acid) Generated for Advanced Materials. In T. Kobayashi (Ed.), *Applied Environmental Materials Science for Sustainability* (pp. 106–127). IGI Global. doi:10.4018/978-1-5225-1971-3.ch005

Rale, V., & Tendulkar, P. (2017). Common Duckweeds as a Model System for Climate Change Impact Assessment. In P. Rao & Y. Patil (Eds.), *Reconsidering the Impact of Climate Change on Global Water Supply, Use, and Management* (pp. 364–372). IGI Global. doi:10.4018/978-1-5225-1046-8.ch019

Ramakrishna, A., & Bang, S. (2015). The Impacts of Climate Change on Food Security and Management in Papua New Guinea. In W. Ganpat & W. Isaac (Eds.), *Impacts of Climate Change on Food Security in Small Island Developing States* (pp. 67–95). IGI Global. doi:10.4018/978-1-4666-6501-9.ch003

Rani, S. (2016). Assessment of Annual, Monthly, and Seasonal Trends in the Long Term Rainfall of the Garhwal Himalayas. In S. Dinda (Ed.), *Handbook of Research on Climate Change Impact on Health and Environmental Sustainability* (pp. 222–241). IGI Global. doi:10.4018/978-1-4666-8814-8.ch011

Rao, P., & Patil, Y. (2017). Recent Trends, Issues, and Challenges in Water Resource Development and Global Climate Change. In P. Rao & Y. Patil (Eds.), *Reconsidering the Impact of Climate Change on Global Water Supply, Use, and Management* (pp. 1–8). IGI Global. doi:10.4018/978-1-5225-1046-8.ch001

Ray, S. (2016). A Framework for Understanding Adaptation by Manufacturing Industries. In S. Dinda (Ed.), *Handbook of Research on Climate Change Impact on Health and Environmental Sustainability* (pp. 471–481). IGI Global. doi:10.4018/978-1-4666-8814-8.ch024

Roberts, T. G., & Rodriguez, M. T. (2015). An Overview of Climate Change and Impacts on Food Security in Small Island Developing States. In W. Ganpat & W. Isaac (Eds.), *Impacts of Climate Change on Food Security in Small Island Developing States* (pp. 1–31). IGI Global. doi:10.4018/978-1-4666-6501-9.ch001

Roşu, L., & Macarov, L. I. (2015). Management of Drought and Floods in the Dobrogea Region. In C. Maftei (Ed.), *Extreme Weather and Impacts of Climate Change on Water Resources in the Dobrogea Region* (pp. 403–443). IGI Global. doi:10.4018/978-1-4666-8438-6.ch013

Roşu, L., & Zăgan, R. (2015). Management of Drought and Floods in Romania. In C. Maftei (Ed.), *Extreme Weather and Impacts of Climate Change on Water Resources in the Dobrogea Region* (pp. 345–402). IGI Global. doi:10.4018/978-1-4666-8438-6.ch012

Roy, J., Ghosh, D., Mukhopadhyay, K., & Ghosh, A. (2016). Exacerbating Health Risks in India due to Climate Change: Rethinking Approach to Health Service Provision. In S. Dinda (Ed.), *Handbook of Research on Climate Change Impact on Health and Environmental Sustainability* (pp. 1–25). IGI Global. doi:10.4018/978-1-4666-8814-8.ch001

Roy, P. K. (2016). A Novel Evolutionary Optimization Technique for Solving Optimal Reactive Power Dispatch Problems. In P. Vasant & N. Voropai (Eds.), *Sustaining Power Resources through Energy Optimization and Engineering* (pp. 244–275). IGI Global. doi:10.4018/978-1-4666-9755-3.ch011

Roy, P. K., Dutta, S., & Nandi, D. (2016). Optimal Reactive Power Dispatch Incorporating TCSC-TCPS Devices Using Different Evolutionary Optimization Techniques. In P. Vasant & N. Voropai (Eds.), *Sustaining Power Resources through Energy Optimization and Engineering* (pp. 326–359). IGI Global. doi:10.4018/978-1-4666-9755-3.ch014

Roy, P. K., & Ghosh, M. (2017). Combined Heat and Power Dispatch using Hybrid Genetic Algorithm and Biogeography-based Optimization. *International Journal of Energy Optimization and Engineering*, *6*(1), 49–65. doi:10.4018/IJEOE.2017010103

Samanta, D. (2016). Lack of Land Tenure Security as Challenges to Sustainable Development: An Assessment in the Context of Bihar, India. In S. Dinda (Ed.), *Handbook of Research on Climate Change Impact on Health and Environmental Sustainability* (pp. 348–362). IGI Global. doi:10.4018/978-1-4666-8814-8.ch017

Sasirekha, S., & Swamynathan, S. (2017). Fuzzy Rule Based Environment Monitoring System for Weather Controlled Laboratories using Arduino. *International Journal of Intelligent Information Technologies*, *13*(1), 50–66. doi:10.4018/IJIIT.2017010103

Satoh, M. (2017). Metal Ion Separation with Functional Adsorbents and Phytoremediation Used as Sustainable Technologies. In T. Kobayashi (Ed.), *Applied Environmental Materials Science for Sustainability* (pp. 284–312). IGI Global. doi:10.4018/978-1-5225-1971-3.ch013

Scorza, F. (2016). Towards Self Energy-Management and Sustainable Citizens' Engagement in Local Energy Efficiency Agenda. *International Journal of Agricultural and Environmental Information Systems*, *7*(1), 44–53. doi:10.4018/IJAEIS.2016010103

Sen, S. K., & Pookayaporn, J. (2017). Role of Water-Energy-Waste Inter-Relatedness to Drive Sustainability amid Climate Concerns. In P. Rao & Y. Patil (Eds.), *Reconsidering the Impact of Climate Change on Global Water Supply, Use, and Management* (pp. 195–210). IGI Global. doi:10.4018/978-1-5225-1046-8.ch011

Senapati, S., & Gupta, V. (2016). Impacts of Climate Change on Fish Productivity: A Quantitative Measurement. In S. Dinda (Ed.), *Handbook of Research on Climate Change Impact on Health and Environmental Sustainability* (pp. 243–260). IGI Global. doi:10.4018/978-1-4666-8814-8.ch012

Senapati, S., & Gupta, V. (2016). Vulnerability to Climate Change: Issues and Challenges towards Developing Vulnerability Indicator. In S. Dinda (Ed.), *Handbook of Research on Climate Change Impact on Health and Environmental Sustainability* (pp. 82–104). IGI Global. doi:10.4018/978-1-4666-8814-8.ch005

Serban, C., & Maftei, C. (2015). Using Grid Computing and Satellite Remote Sensing in Evapotranspiration Estimation. In C. Maftei (Ed.), *Extreme Weather and Impacts of Climate Change on Water Resources in the Dobrogea Region* (pp. 145–173). IGI Global. doi:10.4018/978-1-4666-8438-6.ch006

Shanmuganathan, S., Narayanan, A., & Medagoda, N. P. (2016). Temporal Data Analysis and Mining Methods for Modelling the Climate Change Effects on Malaysia's Oil Palm Yield at Different Regional Scales. In S. Dinda (Ed.), *Handbook of Research on Climate Change Impact on Health and Environmental Sustainability* (pp. 482–513). IGI Global. doi:10.4018/978-1-4666-8814-8.ch025

Singh, R. K. (2017). Impact of Climate Change on the Retreat of Himalayan Glaciers and Its Impact on Major River Hydrology: Himalayan Glacier Hydrology. In P. Rao & Y. Patil (Eds.), *Reconsidering the Impact of Climate Change on Global Water Supply, Use, and Management* (pp. 70–83). IGI Global. doi:10.4018/978-1-5225-1046-8.ch005

Singh-Ackbarali, D., & Maharaj, R. (2017). Mini Livestock Ranching: Solution to Reducing the Carbon Footprint and Negative Environmental Impacts of Agriculture. In W. Ganpat & W. Isaac (Eds.), *Environmental Sustainability and Climate Change Adaptation Strategies* (pp. 188–212). IGI Global. doi:10.4018/978-1-5225-1607-1.ch007

Siwe, A. T., & Tembine, H. (2016). Energy Cost Saving Tips in Distributed Power Networks. In A. Ahmad & N. Hassan (Eds.), *Smart Grid as a Solution for Renewable and Efficient Energy* (pp. 26–48). IGI Global. doi:10.4018/978-1-5225-0072-8.ch002

Srivastava, N. (2016). Climate Change Mitigation: Collective Efforts and Responsibly. In S. Dinda (Ed.), *Handbook of Research on Climate Change Impact on Health and Environmental Sustainability* (pp. 427–439). IGI Global. doi:10.4018/978-1-4666-8814-8.ch021

Stennikov, V., Barakhtenko, E., Sokolov, D., & Oshchepkova, T. (2016). Problems of Modeling and Optimization of Heat Supply Systems: New Methods and Software for Optimization of Heat Supply System Parameters. In P. Vasant & N. Voropai (Eds.), *Sustaining Power Resources through Energy Optimization and Engineering* (pp. 76–101). IGI Global. doi:10.4018/978-1-4666-9755-3.ch004

Stennikov, V., Oshchepkova, T., & Stennikov, N. (2016). Problems of Modeling and Optimization of Heat Supply Systems: Methods to Comprehensively Solve the Problem of Heat Supply System Expansion and Reconstruction. In P. Vasant & N. Voropai (Eds.), *Sustaining Power Resources through Energy Optimization and Engineering* (pp. 26–53). IGI Global. doi:10.4018/978-1-4666-9755-3.ch002

Stennikov, V., Penkovskii, A., & Khamisov, O. (2016). Problems of Modeling and Optimization of Heat Supply Systems: Bi-Level Optimization of the Competitive Heat Energy Market. In P. Vasant & N. Voropai (Eds.), *Sustaining Power Resources through Energy Optimization and Engineering* (pp. 54–75). IGI Global. doi:10.4018/978-1-4666-9755-3.ch003

Stennikov, V. A., & Postnikov, I. V. (2016). Problems of Modeling and Optimization of Heat Supply Systems: Methodological Support for a Comprehensive Analysis of Fuel and Heat Supply Reliability. In P. Vasant & N. Voropai (Eds.), *Sustaining Power Resources through Energy Optimization and Engineering* (pp. 102–126). IGI Global. doi:10.4018/978-1-4666-9755-3.ch005

Stone, R. J. (2017). Modelling the Frequency of Tropical Cyclones in the Lower Caribbean Region. In W. Ganpat & W. Isaac (Eds.), *Environmental Sustainability and Climate Change Adaptation Strategies* (pp. 341–349). IGI Global. doi:10.4018/978-1-5225-1607-1.ch013

Swain, M. (2016). Vulnerability to Local Climate Change: Farmers' Perceptions on Trends in Western Odisha, India. In S. Dinda (Ed.), *Handbook of Research on Climate Change Impact on Health and Environmental Sustainability* (pp. 139–155). IGI Global. doi:10.4018/978-1-4666-8814-8.ch007

Swain, M., & Swain, M. (2016). Evolution and Efficacy of Drought Management Policies and Programmes: The Case of Western Odisha, India. In S. Dinda (Ed.), *Handbook of Research on Climate Change Impact on Health and Environmental Sustainability* (pp. 176–194). IGI Global. doi:10.4018/978-1-4666-8814-8.ch009

Takahashi, Y. (2017). Eco-Friendly On-Site Water Analyses for Ultra-Trace Harmful Ions. In T. Kobayashi (Ed.), *Applied Environmental Materials Science for Sustainability* (pp. 313–326). IGI Global. doi:10.4018/978-1-5225-1971-3.ch014

Taokaew, S., Phisalaphong, M., & Newby, B. Z. (2017). Bacterial Cellulose: Biosyntheses, Modifications, and Applications. In T. Kobayashi (Ed.), *Applied Environmental Materials Science for Sustainability* (pp. 255–283). IGI Global. doi:10.4018/978-1-5225-1971-3.ch012

Tauch, S., Liu, W., & Pears, R. (2016). Measuring Cascading Failures in Smart Grid Networks. In A. Ahmad & N. Hassan (Eds.), *Smart Grid as a Solution for Renewable and Efficient Energy* (pp. 208–225). IGI Global. doi:10.4018/978-1-5225-0072-8.ch009

Trang, T. T. (2017). Study on the Use of Biomass Polymer Sheets in Water/Alcohol Pervaporation as a Sustainable Source of Alcohol Energy. In T. Kobayashi (Ed.), *Applied Environmental Materials Science for Sustainability* (pp. 234–254). IGI Global. doi:10.4018/978-1-5225-1971-3.ch011

Tsiaras, S. (2017). Exploring the Impact of Tourism to the Sustainable Development of Mountain Regions: Implications of the Climatic Conditions. *International Journal of Agricultural and Environmental Information Systems*, *8*(1), 14–28. doi:10.4018/IJAEIS.2017010102

Tugjamba, N., Yembuu, B., Gantumur, A., & Getsel, U. (2016). Policy Provisions and Teachers' Needs on Climate Change Education for Sustainable Development in Mongolia. *International Journal of Asian Business and Information Management*, *7*(4), 36–48. doi:10.4018/IJABIM.2016100103

Tyukhov, I., Rezk, H., & Vasant, P. (2016). Modern Optimization Algorithms and Applications in Solar Photovoltaic Engineering. In P. Vasant & N. Voropai (Eds.), *Sustaining Power Resources through Energy Optimization and Engineering* (pp. 390–445). IGI Global. doi:10.4018/978-1-4666-9755-3.ch016

Uddin, Z., Shah, N., Ahmad, A., Mehmood, W., & Alam, F. (2016). Signal Processing Techniques in Smart Grids. In A. Ahmad & N. Hassan (Eds.), *Smart Grid as a Solution for Renewable and Efficient Energy* (pp. 273–297). IGI Global. doi:10.4018/978-1-5225-0072-8.ch012

Ventrapragada, E. A., & Rayavarapu, N. (2017). Climate Change and Agriculture: Time for a Responsive and Responsible System of Water Management. In P. Rao & Y. Patil (Eds.), *Reconsidering the Impact of Climate Change on Global Water Supply, Use, and Management* (pp. 326–363). IGI Global. doi:10.4018/978-1-5225-1046-8.ch018

Wang, Q., & Liu, H. (2017). Optimized Base Station Sleeping and Renewable Energy Procurement Scheme Using PSO. *International Journal of Swarm Intelligence Research*, *8*(1), 54–73. doi:10.4018/IJSIR.2017010103

Wong, J., & Lim, Y. S. (2016). Revolution of Energy Storage System in Smart Grids. In A. Ahmad & N. Hassan (Eds.), *Smart Grid as a Solution for Renewable and Efficient Energy* (pp. 181–206). IGI Global. doi:10.4018/978-1-5225-0072-8.ch008

Wu, Y., Tan, X., Qian, L. P., Tsang, D. H., Song, W., & Yu, L. (2016). Management of Scheduling and Trading in Hybrid Energy Trading Market. In A. Ahmad & N. Hassan (Eds.), *Smart Grid as a Solution for Renewable and Efficient Energy* (pp. 123–148). IGI Global. doi:10.4018/978-1-5225-0072-8.ch006

Xiang, M., Liu, W., Bai, Q., & Al-Anbuky, A. (2016). Dynamic Trust Elective Geo Routing to Secure Smart Grid Communication Networks. In A. Ahmad & N. Hassan (Eds.), *Smart Grid as a Solution for Renewable and Efficient Energy* (pp. 323–343). IGI Global. doi:10.4018/978-1-5225-0072-8.ch014

Zăgan, S., & Chiţu, M. (2015). The Influence of Air Temperature on the Quality Parameters of the Black Sea Coastal Waters. In C. Maftei (Ed.), *Extreme Weather and Impacts of Climate Change on Water Resources in the Dobrogea Region* (pp. 174–204). IGI Global. doi:10.4018/978-1-4666-8438-6.ch007

Zharkov, S. (2016). Assessment and Enhancement of the Energy Supply System Efficiency with Emphasis on the Cogeneration and Renewable as Main Directions for Fuel Saving. In P. Vasant & N. Voropai (Eds.), *Sustaining Power Resources through Energy Optimization and Engineering* (pp. 1–25). IGI Global. doi:10.4018/978-1-4666-9755-3.ch001

About the Authors

Dmitry Strebkov graduated from the faculty of electrification of the Moscow Institute of Mechanization and Electrification of Agriculture in 1959. D.S. Strebkov worked as an engineer at the Electromechanical Workshop of Mosselenergo (1959-1960), Senior Engineer, Senior Researcher, Sector Head, Laboratory Head, Head of Department, Deputy Chief Designer of the VNII Current Sources Institute (VNIIT) NPO Kvant (1960-1987), worked as director of the All-Russian Research Institute for Electrification of Agriculture (VIESH) from 1987 to 2015, from 2015 – scientific director of VIESH. D.S. Strebkov worked part-time as a senior lecturer, associate professor, professor of the Fundamentals of Radio Engineering and Television Department of the All-Union Correspondence Polytechnic Institute (1967–1987), head of the Renewable Energy and Rural Electrification department of the Moscow State Agrarian University. V.P. Goryachkina (2004–2014). From 2003 to 2012, D.S. Strebkov worked as Chairman of the Expert Council of the Higher Attestation Commission of the Ministry of Education of the Russian Federation on agroengineering specialties. In 1967, without a break from production, D.S. Strebkov graduated from the Faculty of Mechanics and Mathematics of Moscow State University M. V. Lomonosov specialty Mathematics, in 1971 D.S. Strebkov graduated from the correspondence postgraduate school at VNIIT and defended PhD-dissertation, in 1983 – doctoral dissertation, in 1985 D.S. Strebkov received the title of professor of the department «Fundamentals of radio engineering and television». In 1991 was elected a corresponding member of the Academy of Agricultural Sciences (VASHNIL), in 1993 – a corresponding member of the Russian Academy of Agricultural Sciences, in 1997 – an academician of the Russian Academy of Agricultural Sciences, in 2013 – an academician of the Russian Academy of Sciences. In 2008, D.S. Strebkov awarded the honorary title Deserved Scientist of the Russian Federation. D.S. Strebkov heads research in the Department of Agricultural Sciences of the Russian Academy of Sciences in the field of electrification of

agriculture and renewable energy. Under his leadership, 26 graduate students and 3 doctoral students defended their dissertations. D.S. Strebkov published over 1000 scientific papers and received 490 USSR author's certificates and patents of the Russian Federation, including 60 foreign patents. D.S. Strebkov since 1992 has been the Chairman of the Russian Section of the International Society for Solar Energy, and since 2002 he has been the Deputy Chairman of the Russian Committee on the Use of Renewable Energy Sources. D.S. Strebkov is a member of the doctoral dissertation council of the FSBSI FSAC VIM, as well as the head of the UNESCO Department of Renewable Energy and Rural Electrification and the head of the working group of the European Bureau for Solar Energy Education.

Natalya Filippchenkova is a candidate of Technical Sciences (2018). In 2013, N.S. Filippchenkova graduated summa cum laude from Volgograd State Agrarian University with a degree in Electrical supply, in 2013 she was enrolled in the graduate school of the GNU VIESH in the specialty 05.14.08 «Power installations based on renewable energy types». She worked as an engineer in the laboratory of solar energy VIESH (2013–2016), engineer, senior engineer, lead engineer of the Department of the perspective development of the power system of the city of Moscow in the JSC Institute ENERGOSETProekt (2013–2017), currently she is working as a lead design engineer in Troitsky and Novomoskovsky electric network area of JSC United Energy Company. She is also the author of 30 published works and 5 patents of the Russian Federation for inventions.

Anatoly Irodionov, born October 24, 1950 in Moscow. In 1974, A.E. Irodionov graduated from the Moscow Energy Institute with a degree in Nuclear Power Plants and Installations. After distribution, A.E. Irodionov worked at the Krasnaya Zvezda Scientific and Production Association, since 1979 at the Research Institute of Current Sources (VNIIT) of the Kvant Scientific and Production Association. From 1988 to 2018, A.E. Irodionov worked at the All-Russian Scientific Research Institute of Electrification of Agriculture (VIESH). A.E. Irodionov – Candidate of Technical Sciences, author of 60 scientific papers and more than 20 inventions in the field of solar technology.

Index

R

S

T

Z